TECHNICAL PERFORMANCE AND STABILITY ANALYSIS OF ESKOM POWER NETWORK USING 600KV, 800KV, AND 1000KV HVDC

UNIVERSITY OF
KWAZULU-NATAL

INYUVESI
YAKWAZULU-NATALI

Oluwafemi Emmanuel ONI

IN FULFILMENT OF MASTER OF SCIENCE DEGREE IN ENGINEERING

COLLEGE OF AGRICULTURE, ENGINEERING AND SCIENCE

UNIVERSITY OF KWAZULU-NATAL

July 2016

Supervisor: Prof. I.E Davidson

Industrial Mentor: Mr. N. Parus (Eskom)

DECLARATION 1 – PLAGIARISM

I, Oluwafemi E. Oni, declare that:

1. The research reported in this thesis, except where otherwise indicated, is my original research.

2. This thesis has not been submitted for any degree or examination at any other university.

3. This thesis does not contain other persons' data, pictures, graphs or other information, unless specifically acknowledged as being sourced from other persons.

4. This thesis does not contain other persons' writing, unless specifically acknowledged as being sourced from other researchers. Where other written sources have been quoted, then:

a. Their words have been re-written but the general information attributed to them has been referenced

b. Where their exact words have been used, then their writing has been placed in italics and inside quotation marks, and referenced.

5. This thesis does not contain text, graphics or tables copied and pasted from the Internet, unless specifically acknowledged, and the source being detailed in the thesis and in the References sections.

6. A modified section of Eskom network was used by permission from Eskom and well acknowledged for the research project.

Signed: …… Date ……

Oluwafemi E. Oni.

As the candidate's supervisor, I agree to the submission of this thesis.

Signed: …… Date……..

Prof. I.E. Davidson

DECLARATION 2 – PUBLICATIONS

The following publications emanated from this research investigation, namely:

[1] K N I Mbangula, O E Oni and I E Davidson, "The Impact of HVDC Schemes on Network Transient Rotor Angle Stability". *In Proceedings of the 24th South African Universities Power Engineering Conference*, 26-28 January 2016, Vereeniging, South Africa, pp. 461 – 466.

[2] O. E. Oni, K.N.I. Mbangula and I.E. Davidson, "Voltage Stability Improvement of a Multi-Machine System using HVDC," Proceedings of the *Clemson University Power Systems Conference (PSC)*, March 8-11, 2016, Clemson University, Clemson, SC, USA.

[3] O E Oni, K N I Mbangula and I E Davidson, "Dynamic Voltage Stability Studies using a Modified IEEE 30-Bus". *Proceedings of the 16th IEEE international Conference on Environment and Electrical Engineering*, Florence, Italy, 7-10 June 2016, pages 129-134.

[4] O.E. Oni, K.N.I. Mbangula and I.E. Davidson, "A Review of LCC-HVDC and VSC-HVDC Technologies and Applications". *Proceedings of the 16th IEEE international Conference on Environment and Electrical Engineering*, Florence, Italy, 7-10 June 2016, pages 135-141.

[5] O E Oni, K. N. I. Mbangula and I E Davidson, "Dynamic Voltage Stability Studies using a Modified IEEE 30-Bus". *Transactions on Environment and Electrical Engineering*, vol. 1, No 3. Sept. 2016, pp. 41-49.

[6] O.E. Oni, K.N.I. Mbangula and I.E. Davidson, "A Review of LCC-HVDC and VSC-HVDC Technologies and Applications". *Transactions on Environment and Electrical Engineering*, vol. 1, No 3, Sept. 2016, pp 68-76.

[7] O.E. Oni, N. Parus and I. E. Davidson, "Static Voltage Stability Analysis of Eskom Eastern Grid', *accepted at 5th IEEE International Conference on Renewable Energy Research and Application, Birmingham*, United Kingdom. 20-23 November 2016.

[8] O.E. Oni, and I E Davidson, "Harmonic Distortion of LCC-HVDC and VSC-HVDC Link in Eskom's Cahora-Bassa HVDC Scheme', *accepted at 5th IEEE International Conference on Renewable Energy Research and Application*, Birmingham, United Kingdom. 20-23 November 2016.

[9] O.E. Oni, N. Parus and I. E. Davidson, "Dynamic Analysis of Eskom Eastern Power Grid". Submitted to *25th South African Universities Power Engineering Conference*, 30 Jan-1 Feb 2017, Stellenbosch, South Africa.

Signed: …… Date: ……

Oluwafemi E. Oni

ACKNOWLEDGEMENTS

Firstly, I give God the glory for the opportunity given to me for this breath of life. I am just a mortal and clay, but with His infinite mercy, he granted me wisdom, gave me courage, and made me to stand among equals. I could not have done this if not for your love. All glory and adoration to HIS name.

I would also like to appreciate my supervisor for all his contribution and support. I cannot imagine the success of this program without him. His criticism and scrutiny have thus help a lot. You did turn a better person out of me through your generous support and guidance.

I would also want to appreciate Eskom Power Plant Engineering institute EPPEI for their financial support throughout this studies.

I want to appreciate the effort of all my colleagues, Kamati Mbangula, Stacey Mwale, Gilbert and others, which space will not allow me to mention for the innumerable input to the successful completion of this research studies. I cannot but also mention our dear administrator Jay Gama, thank you for your help.

My warm gratitude also goes to my parent, Mr and Mrs Oni, my brother, Olusola Mike, and my dear friend Nnadozie Deborah for their support. You all did stood by me. I am indeed grateful. Men of honour, household of DLCF, UKZN community are well appreciated for their indispensable support. I am indeed indebted to you all. One love bind us together. Thanks.

ABSTRACT

In designing electric power networks or implementing major expansions to existing networks, a number of the key issues regarding the technical performance of the network at both transmission and distribution level must be ascertained, namely: voltage regulation, voltage fluctuations, electrical losses, transmission/distribution plant loading and utilization, fault level, generation stability, harmonics, phase balancing, supply availability and system security. System studies and analysis conducted from time to time to ascertain the operating state of a network, taking into account, load growth projections for the future. Undue stresses on the system or anticipated problems are determined from power flow analysis or during operation and maintenance. Using a modified Eskom network (KwaZulu-Natal sub-grid) as a case study, the technical and stability analysis for different high voltage direct current (HVDC) transmission voltages: 600kV, 800kV and 1000kV were carried out using DIgSILENT PowerFactory engineering software tool, as an alternative for bulk power transfer using high voltage alternating current (HVAC) link along the major corridors. Static analysis using PV and QV curves; dynamic analysis using RMS time domain and electromagnetic EMT analysis were carried out. Dynamic analyses were performed to determine the system fault levels and critical fault clearing time. Results obtained from this investigation show that 600kV and 800kV HVDC transmission systems have greater power capacity than equivalent HVAC line. HVDC delivery systems were observed to have lower electrical losses, better voltage profile, increase fault clearing time, enabling robust protection schemes to be installed. Voltage distortion due to harmonic content and imperfect current waveform in Cahosa-Bassa LCC-HVDC link were also investigated, and re-engineering with the use of VSC-HVDC technology has been proposed. This option provides reduced harmonic content, excellent sinusoidal waveform and minimal vulnerability to commutation failure. A financial and economic analysis of a 500kV HVAC double circuit and ±600kV HVDC transmission network were compared. HVDC system was proposed the most suitable scheme for bulk transmission of electric power over long distances due to high efficiency and better economics.

TABLE OF CONTENT

LIST OF FIGURES

LIST OF TABLES

LIST OF ABBREVIATIONS

HVAC	High Voltage Alternating Current
HVDC	High Voltage Direct Current
AC	Alternating Current
DC	Direct Current
ROW	Right of Way
PSSs	Power System Stabilizers
IEEE	Institute of Electrical and Electronics Engineers
DIgSILENT	Digital Simulation and Electrical Network calculation program
US/USA	United State/United State of America
P-V	Active Power - Voltage
Q-V	Reactive power - Voltage
CCT	Critical Clearing Time
CIT	Critical Isolating Time
rms	Root Mean Square
TV	Television
PIV	Peak Inverse Voltage
IGBTs	Insulated Gate Bipolar Transistors
OLTC/ULTC	On-Load Tap Changers/Under-Load Tap changers
XLPE	Cross-Linked Polyethylene Insulation
TUF	Transformer Utilization Factor
LCC	Line Commutated Converter
CCC	Capacitor Commutated Converter
VSC	Voltage Source Converter
ETT	Electrical Triggered Thyristors
LTT	Light Triggered Thyristors
UHVDC	Ultra-High Voltage Direct Current
GTO	Gate Turn On
PWM	Pulse Width Modulation
CEA	Constant Extinction Angle
CIA	Constant Ignition Angle

CC	Constant current
VI	Voltage - Current
VDCOL	Voltage Dependent Current order Limiter
IPC	Individual Phase Control
EPC	Equidistance Phase control
PFC	Pulse Frequency control
PPC	Pulse Phase Control
VORD	Voltage Order
IORD	Current Order
AVR	Automatic Voltage Regulator
SVC	Static Var compensator
STATCOM	Static Synchronous Compensator
NRLF	Newton-Raphson Load Flow
RMS	Real time simulation
EMT	Electromagnetic transient simulation
P.F.	Power Factor
ESCR	Effective Short Circuit Ratio
TDP	Transmission Development Plan
OPGW	Optical Ground Wire
NBTA	New Build Transmission Article
ACSR	Aluminium conductor Steel Reinforced
ACCR	Aluminium Conductor Composite Reinforced
ACSS	Aluminium Conductor Steel Support
HTLS	High Tensile Low Sag
WECC	Western Electric Coordinating Councils
BLM	Bureau Land Management
AFUDC	Allowance for Fund Used During Construction and Overhead Cost
IREQ	Research Institute D'hydro-Québec
NIIPT	Scientific - Research Institute for transmission by direct current high voltage
SECs	Sealing End Compounds
FACTs	Flexible AC Transmission System
SGCC	State Grid Corporation of China

LIST OF SYMBOLS AND UNITS

α	converter firing angle (alpha)
β	converter ignition angle (beta)
π	pi (3.143)
Ω	Ohms
γ	converter extinction angle
μ	overlap angle
GW/MW	gig watt (10^9)/ megawatt (10^6)
kV	kilovolt (10^3)
km	kilometre
ms	milliseconds (10^{-3})
ppb	part per billion
kA	kilo-ampere
p.u	per unit

CHAPTER 1: INTRODUCTION

1.1. Research Questions

An attempt to have a more stable power network in order to meet the ever-increasing energy demand and totally eradicate power failure in South Africa brings about the construction of new power station like Medupi, coal 2 and coal 3 power station, which will give a gross nominal capacity of 30 GW by 2030. Integration of these power stations into the grid could be either through High Voltage Alternating Current (HVAC) or High Voltage Direct Current (HVDC) transmission line. Transmitting using AC lines has concerns such as, the thermal limit, corona loss, skin effect, Ferranti effect, economics of transmission, reliability, cascading problem, and finally the network Right of Way ROW [1]. Now the questions that this research seeks to answer are; can the existing AC transmission line be upgraded to a DC line, what benefit does it offer as compared to the existing AC line with respect to the power output and losses? If the transmission line voltage is increased to 600kV and then to 800kV, what effect does it has on the system stability of the entire networks compared to HVAC line of equivalent rating.

A current carrying conductor has I^2R losses that lead to a heating effect. This can limit the amount of electric power that can be transmitted. Thus, heat losses cause the metallic conductors to expand resulting in a sag, which leads to reduced clearance from the conductor to the ground. Transmission of high voltages exceeding the rated installed capacity also causes electricity to flashover, rather than travel along the line. It also causes corona discharge, which leads to systems instability [2]. Is it possible to develop a strategy for upgrading the transmission line by either increasing the voltage or current or even both or still have a well-stabilized transmission network and solve all these constraints? To what extent is HVDC immune to fault current, that is, how fast does it takes to clear a fault, and the systems restored to its original state?

Eskom has only one HVDC network installation, transmitting 1920MW power at a voltage level of ±533kV from hydroelectric generation station located at Cahora-Bassa Dam in Mozambique to Johannesburg. How will an HVDC line be incorporated into Eskom power network and stabilizes its performance, and what converter technology bring about highest power output, enhanced stability, immunity to commutation failure and finally reduce harmonic content?

1.2. Definitions

Power system stability is defined as the ability of power system to preserve its steady stability or recover the initial steady state after any deviation of the system's operation due to disturbances or fault [3, 4]. The major importance of studying the stability of a transmission network is to avoid interrupted power supply from the generating stations to the load centres, which may lead to blackout

or power outage. One example is the loss of generation, which causes a mismatch between production and load. Another example is an overload of the transmission system caused by congestion, forcing an overloaded power line to trip, causing increased loading of other lines, consequently leading to a voltage collapse due to the high impedance in the weakened grid. Faults do occur in power systems. A system is said to be stable if after subjected to either short or long disturbances or fault, rapidly disconnect the faulty part, have the ability, speed and intelligence to remain the healthy part and still able to regain its perfect operational state or condition.

Southern Africa has experienced electric power deficits over the last decade due to a combination of factors, such as member countries' inadequate electrical power supply system; load growth in areas which were not adequately planned for; high population growth and rapid economic expansion. South Africa has also experienced these major power outages due to rapid economic growth and expansion, which have contributed to a diminishing generation reserve capacity against an increasing growth in demand. Outages have also occurred due to technical and operational challenges. Power outages and poor quality of supply are often the result of insufficient generation capacity or poor operation of the power system [5, 6].

To mitigate these problems, Eskom embarked on implementation of some new power projects. One of such project is the Medupi power station, a coal-fired power plant project located west of Lephalale, Limpopo Province, South Africa. This comprises of 6-units of 800MW each, and a total install capacity of 4800MW. The new Medupi was integrated mainly via the 400kV network to Rustenburg and Polokwane. However, one of the lines was built at 765kV but operated at 400kV in the interim. This gives Eskom the flexibility of upgrading to 765kV in future.

However, due to substantial annual load growth, load shifts and step loads in the recent past, it has become necessary for Eskom to reinforce the existing electrical infrastructure through the establishment of new electricity transmission capacity. As part of its capacity expansion and grid-strengthening programme, Eskom transmission needs to adopt transmission of HVDC because of the numerous advantages it offers.

High Voltage Direct Current Transmission (HVDC) offers several operation advantages over HVAC transmission systems. HVDC transmission lines have no frequency, and hence minimal problems of harmonics, oscillations or transients; they actually damp out transients. Using power electronic switching devices (FACTS controllers), precise and fast power control in either direction is easier to achieve in HVDC than HVAC systems as dc power is minimally affected by reactance. The ease of power flow control in HVDC lines makes it easy to achieve the maximum power and thermal capacity of transmission lines. It is also simple to control active power transfer at a predetermined level or even to modulate this to improve system damping. For weak AC grids, voltage source converter (VSC) based HVDC systems offer better controllability and grid flexibility for integrating intermittent

renewable energy sources such as: wind and solar-power. HVDC systems offer special technical advantages: all angular stability problems disappear and even connection of systems at different frequency is feasible. The problems of cable charging current are eliminated. Thus, cables can readily be used for underwater crossings. Hitherto, HVDC transmission has been perceived as an alternative to overcome the limitations of HVAC transmission, but it is now the established technology of choice for long distance transmission, subsea electrical transmission systems and interconnection of asynchronous AC grids. HVDC technology is expected to grow beyond its traditional position as a complement to AC transmission and play a leading role in modernization of the electric power system (Smart Grids), emergence of medium and low voltage DC distribution networks and renewable energy integration into the grid. These emerging trends are important to Eskom as they are posed to shape the local electricity industry in South Africa. Eskom has an HVDC system in its infrastructure pool, which is the Apollo Converter Station near Johannesburg.

Such as long distance transmission with little loss compared to contemporary AC lines, because in overhead lines above 200km, most of AC voltage is needed to overcome the inductance of the lines [7]. For long underground or submarine cables (less than 50km long), most of AC current is needed to charge and discharge the capacitance of the cable [8]. It allows power transmission between unsynchronized AC distribution systems. Power flow on an HVDC transmission line is set using the control systems of converter stations. Power flow does not depend on the operating mode of connected power systems. Unlike HVAC ties, HVDC intersystem ties can be of arbitrarily low transfer capacity, eliminating the "weak tie problem," and lines can be designed on the basis of optimal power flows. Reduction in the Right-of-Way (ROW) is another advantage because it provides a safety margin between the high-voltage lines and surrounding structures and vegetation. The ROW also provides a path for ground-based inspections and access to transmission towers and other line components during repairs or maintenance. Failure to maintain an adequate ROW can result in dangerous situations, including ground faults. Reduced line cost, since HVDC transmission requires fewer conductors; for example, two for a typical bipolar HVDC line compared to three for three-phase HVAC. HVDC technologies still have some drawbacks, namely:

- The high cost of converter stations at the beginning and end of the HVDC line
- Challenges of suitable DC circuit breaker technology for protection from faults
- In contrast to AC systems, designing and operating multi-terminal HVDC systems is complex.

However, all these disadvantages can be eliminated with new techniques aimed at improving the performance of HVDC technology [9]. Nevertheless, as electricity demand grows rapidly and expansion in transmission and generation is restricted by the limited availability of resources and the strict environmental constraints. Most power utilities thus operate near stability limits. Generator

controller did provide system improvement with its Power System Stabilizers (PSSs). This assist in maintaining system stability and improving dynamic performance by providing a supplementary signal to the excitation system.

Recently HVDC systems have greatly increased. They interconnect large power systems offering numerous technical and economic benefits. These result from functional characteristics and performance such as non-synchronous interconnection, control of power flow and enhanced system stability. Eskom currently has only one HVDC power transmission line linking a hydroelectric generation station at the Cahora-Bassa Dam in Mozambique to Apollo Converter station in Johannesburg, South Africa. It transmits 1920MW at a voltage level of ±533kV. This research work is therefore aimed at investigating the technical performance and stability of Eskom power network when fed with HVDC ranging from 600-1000kV from a bulk power generated at Medupi power station via Massa substation to Eskom Eastern grid (Invubu or Hector substation)**.**

1.3. Problem Statement

The need for more power generated output and more stable and reliable networks bring about the transmission of electric power using HVDC lines. The electric power transmitted along transmission lines is a function of voltage and current, that is, the direct product of current and voltage. For a specific power generated, mode of transmission is either alternating current AC or direct current DC.

$$P_{ac} = V_{ac} I_{ac} \cos\theta \tag{1.1}$$

$$P_{dc} = V_{dc} I_{dc} \tag{1.2}$$

For a constant power output, as voltage increases, the current drops, and vice versa. The most common mode of transmitting bulk electric power is through a constant voltage alternating current. This method was adopted because of ease to transform from different voltage level using a transformer. Easy direct connection to a load without any mode of conversion is another reason for its wide usage. However, as time goes on, generating stations are located far away distance from the load center, which brings about long transmission lines. The inherent losses along the line due to leakage current, partial discharge and so on make it disadvantageous in using the common HVAC transmission line.

The transmission of the new Medupi power station, which is to generate a total power capacity of 4800MW, which will be transmitted using an HVAC lines. This will eventually bring about corona, and hysteresis losses as well as eddy current losses. Also, the I^2R power loss is another factor. All these losses result in a reduction of power output delivered. Controllability, cascading problem, stability problem, and increase in ROW, number of conductors' bundles etc. are all key concerns of AC lines.

This research proposes a better way of transmitting the bulk power generated from Medupi power station to Eskom Eastern grid.

1.4. Aims and Objectives

This research investigation aimed to achieve the following:

1. Investigating the effect of grid planning applications such as increasing in transmission lines loading capacity near their steady state, short time and dynamic limits on Eskom power network's stability and performance.
2. Upgrading better transmission lines either by increasing the voltage, current capacity or both.
3. Evaluating the technical performance and the stability of Eskom power network when fed with 600, 800, and 1000kV HVDC along Limpopo transmission network to Eskom Eastern grid.

In order to achieve the aim of this project, an Eskom Eastern transmission network was modelled using Digital Simulation and Electrical Network Calculation Program (DIgSILENT) PowerFactory software. A technical examination of its performance was then carried out on the network.

1.5. Methodology

An extensive literature survey was carried out on:

- HVAC and HVDC transmission networks; advantages and disadvantages
- Recent HVDC transmission network technology and mode of operation.
- Line performance assessment of HVAC and HVDC lines.
- Stability and technical performance of HVDC transmission line on HVAC networks.

1.6. Delimitation

This research was carried out on Eskom Eastern grid located in KwaZulu-Natal Province, South Africa.

CHAPTER 2: LITERATURE REVIEW

2.1. Introduction to HVDC Systems

The use of electricity can be dated back to the late 1870s, with the invention of dc dynamo generator, and incandescent light [10]. Thomas Edison, the first inventor of electric power systems that consist of a generator, transmission cable, a fuse, and load. This system was commissioned and operated at Pearl street station, New York in the year 1882 [11]. DC underground cable system was used with 110V rating, mainly used for incandescent lamps to supply an area of 1.6 km radius. This new development brings about the adoption of DC generators driven by steam engines to be used by central district of the largest city for electricity generation. DC generator was used because AC generator has not then been invented [12].

Soon in 1886, the limitation of DC systems became apparent, which involve voltage drop and high power loss for a long distant usage. Voltage transformation is required in solving this problem which is obviously not possible with DC systems [13]. Transformation of voltage to higher voltage levels suitable for transmission of electric power over long distances was made possible with the invention of AC systems by Nikola Tesla [14]. In 1889, the first AC transmission system was commission in the USA between Willamette falls and Portland, Oregon, consisting of one phase, with 4kV line voltage through 21km distance [15]. With this, DC systems slowly fade away and AC systems become popular. Moreover, Westinghouse starts the gradual development of AC systems. Controversy arose in the 1890s on whether industries should standardize AC or DC systems, Edison advocated DC and Westinghouse AC. Nevertheless, AC becomes more feasible because it is possible to increase the voltage, with simpler and cheaper generators and motors. This new development of AC systems paves the way for the first 3-phase power system operated in 1893 with 2.4kV at California through 30km distance [15].

A French engineer Rene Thury designed HVDC transmission system in 1889, it was observed that at high voltage, there is minimal losses and minimum drop in this system. Thury systems made used of DC-series generator operated in a constant current mode. But in 1938, all the Thury systems were dismantled because there were several problems like safety problem, maintenance and the cost of the series generator becomes a problem [16]. With this, AC systems were seen again as a better way of power transmission [17].

Transverter, electrolytic, and the atmospheric-arc converter are some of the most serious attempts to develop a converter suitable for DC transmission. The transverter was never used commercially, the electrolytic cannot withstand high voltage application because of low breakdown voltage and the risk of electric shock, while the latter consumes electrode periodically, which require replacement. But in

1950, Mercury arc valve was designed and developed [18]. With this, conversion from AC to DC was made possible. This brings about the first HVDC transmission line built in 1954, between Sweden and Gotland Island by 70km overhead cable. This begins the usage of HVDC systems [19].

2.2. Features of HVDC Delivery Systems

The invention of modern semiconductor devices for HVDC converter made HVDC transmission systems to be widely adopted for different application such as electrical and electronic power distribution systems, micro grids and super grids for renewable energy integration. Few reasons are listed below to why HVDC systems should be more encourage and adopted in electric energy transmission.

2.2.1. Power carrying capability

For HVAC and HVDC system with an equal current rating of $I_{ac}=I_{dc}$, same insulation length in each conductor, as well as the same number of conductors, double circuits of three-phase HVAC system with six conductors, will generate three-bipolar HVDC system. With these constant values (K_1, K_2, and K_3), it shows HVDC overhead line can transmit 1.5 to 2.1 times power than the AC overhead line and 2.9 to 3.8 times the power for the underground cables than the equivalent AC line. This shows that HVDC systems can transmit more bulk of power from high generating capacity to the point where there are high loads of demands than AC system. More so, the two conductor of DC transmission tends to reduce the transmission losses to about two third of the comparable AC systems. This ability of HVDC systems to operate at a voltage higher than AC systems brings about the high power capability, with voltage rating up to 1600kV (±800kV) in service and ±11000kV ongoing project in china [20-22]. The first highest known commercialized AC lines was 1200kV on the line connecting Russia to Kazakhstan, which came into operation in 1988 and later, was dismantled by 1996 and then operated at 500kV. China is now the first country to introduce 1000kVAC transmission line to be operated at full rated voltage. The 650km line has a power carrying capacity of 5000MW.

$$P_{ac} = 6EI_{ac}\cos\theta \tag{2.1}$$

$$P_{ac} = 6V_{dc}I_{dc} \tag{2.2}$$

$$\frac{P_{dc}}{P_{ac}} = K_1\frac{K_2}{K_3} \tag{2.3}$$

E= phase voltage and ϕ=power factor

K_1= relationship between ac and dc maximum conductor voltage. This value for overhead lines ranges between 1- 1.41 and 2-3 for underground cable

K_2= relationship between ac insulation voltage of the conductor and the rated conductor voltage. Values range is from 2.5-3.

K_3= relationship between dc insulation voltage of the conductor and the rated conductor voltage. The value for k_3 ranges from 1.7 – 2.0.

AC line capability reduces with increasing transmission length: This graph in Figure 2.1 show a 1000 kV line with 70 percent maximum compensation and 30^0 angle between terminals. It could be seen how the power transferred reduced after line distance of 1200km.

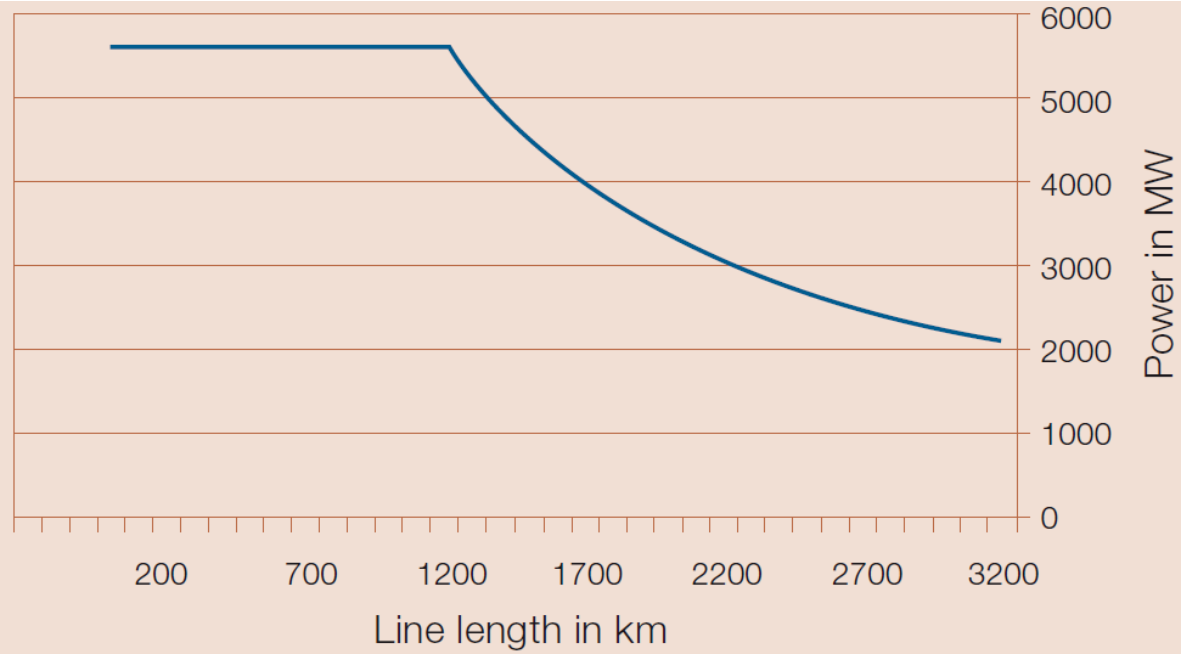

Figure 2.1: Transmission capacity on 1000kV AC (ABB review 2007)

2.2.2. Span and right of way

This is the potential difference between the overhead conductors, the earth, and the space-charge clouds. This further cause an electric field on the conductor surface. The highest electric field is felt directly under the conductors. This field is mostly affected by weather, seasonal variation, and relative humidity. DC lines have less electric field problem than AC lines being two conductors, whereas the AC lines comprises of three and more circuit are even needed to transmit higher power. This means that DC lines require lesser insulating materials, cheaper, smaller overhead towers, and small ROW than the AC transmission of comparable rating. Transmitting 5000MW using 765kV AC lines requires a double circuit of AC lines as shown in Figure 2.2 below. These make HVDC lines to be 30% cheaper than its contemporary HVAC of the same rating [23].

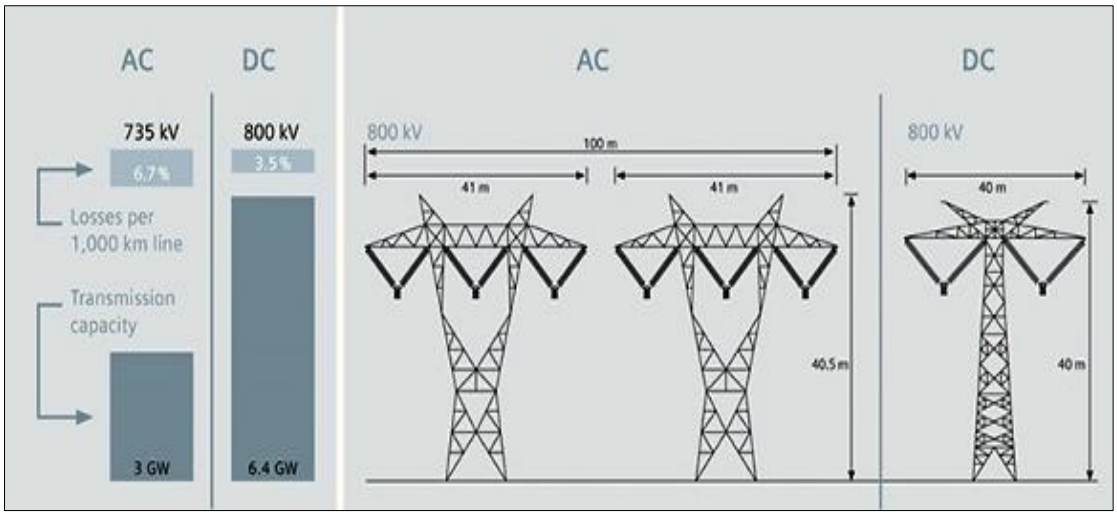

Figure 2.2: Transmission line clearance for both AC and DC (HVDC Siemen)

2.2.3. Transmission distance and cost

HVDC transmission encourages a more bulk power transmission for a long distance as opposed to HVAC transmission. Research has it that once the length of transmission line exceeds a certain limit called the breakeven distance, then HVDC transmission lines will be preferable and economical than HVAC transmission lines. This distance ranges from 500-700km for overhead lines, and from 40-50km for underground or submarine cables. This makes HVDC more preferable than HVAC for long distance bulk power transmission or for underground cable connection [23, 24]. The cost comparison can be seen in Figure 2.3.

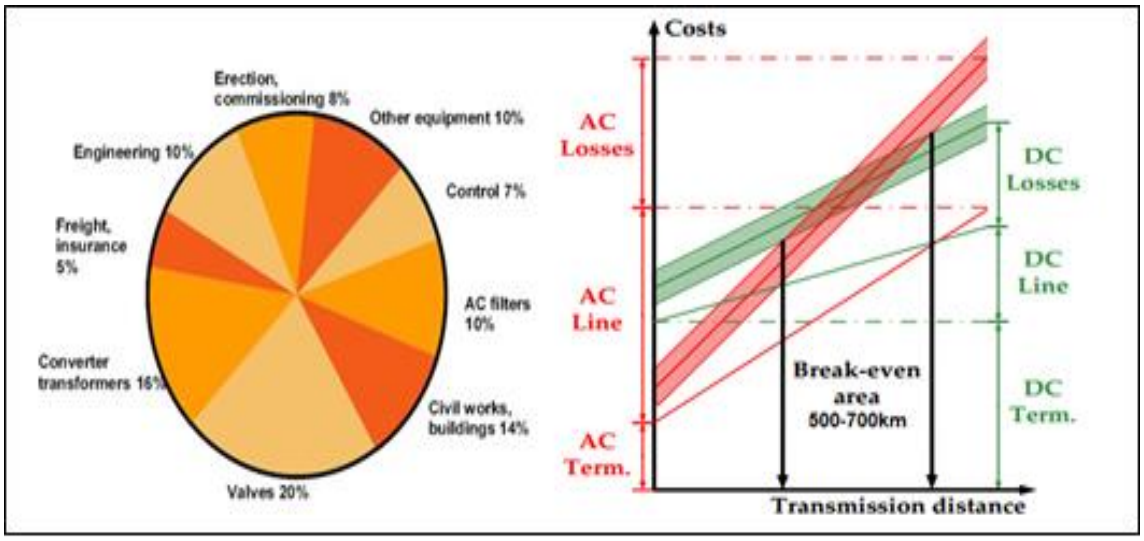

Figure 2.3: Cost comparison of DC and AC system

2.2.4. Stability of HVDC system

As AC transmission power and distance increases, the angle difference also increases, and the power transferred is limited. The load angle needs to be kept at relatively low values under normal operating conditions because any disturbance in the power flow will cause large oscillations in the load angle and tend to swing out of stability without power controllability. Therefore, an AC lines need some

reactive power compensator such as series capacitor, shunt reactors, synchronous condenser, and static VAR compensators to help increased the voltage profile, alleviate the problem of line charging and help reduce stability limitations of the AC systems. The approximate power equation that represents the sending and the receiving end transmitted power shown in Figure 2.4 is given by equation 2.4 and 2.5. Where U is the rms voltage, X is the series reactance of the line and $\delta_S - \delta_R$ is the relative phase shift of the voltage [25-29].

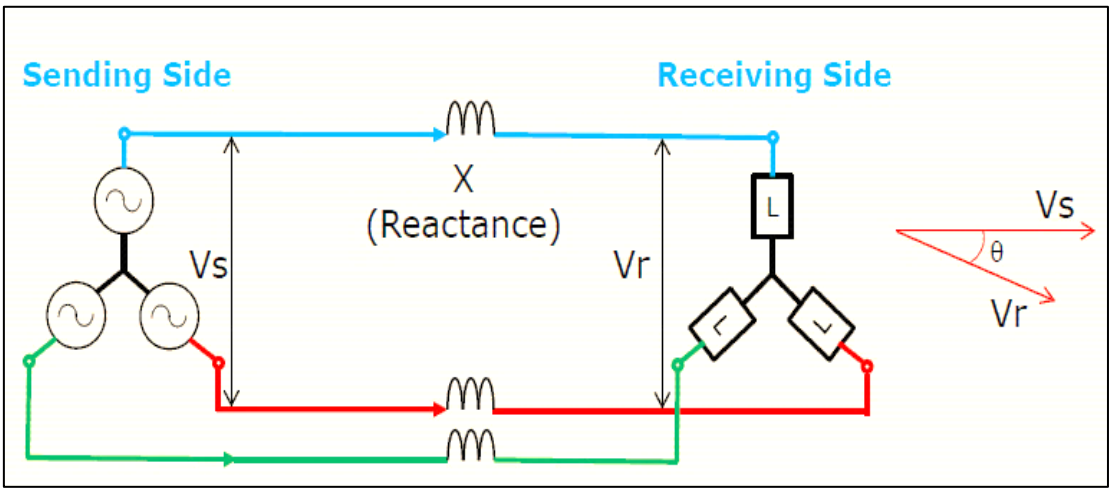

Figure 2.4: Power Flow in AC systems

$$P_{SR} = \frac{U_S U_R}{X}(\delta_S - \delta_R) \text{ Governed by reactance law} \qquad (2.4)$$

HVDC line in Figure 2.5 under steady state conditions has a transmission distance that is not affected by the inductance and the capacitances of the DC lines. Thereby, not affected with all the AC difficulties mentioned above. The DC systems need no switching stations or compensating equipment save only converter stations (converters and AC filters).

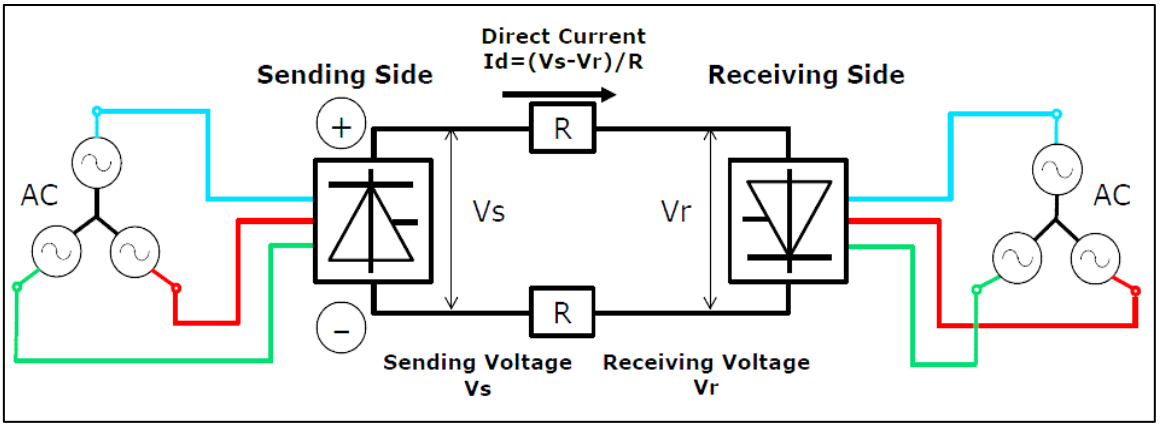

Figure 2.5: Power Flow in DC systems

$$P = \frac{V_S(V_S - V_R)}{R} \text{ governed by ohms' law.} \qquad (2.5)$$

2.2.5. Asynchronous link capability

Interconnecting two AC systems using tie lines requires both systems to be coordinated in using the same system voltage and frequency. However, such interconnections are subjected to some operational problems in control coordination such as large oscillations that may lead to equipment tripping and cascading problem (transmission of disturbance from one system to another). Not all these problems are in HVDC systems, in that it is insensitive to frequency changes. Thereby increasing its usage for asynchronous interconnection as in the case of Itaipu in Brazil [28-30].

2.2.6. AC stability improvement

HVDC link has fast and accurate power flow control which help in isolating systems disturbances and increase the transient stability of an AC system [4]. After a specific disturbance in the AC power system, HVDC controls helps in controlling the DC power flow along the link in order to restore steadiness between generation and load on both sides of the AC systems. Converters control also help to provide reactive power and voltage support to the AC systems to aid transient stability [31].

2.2.7. Less corona loss and radio interference

Corona effects on the surface of high voltage overhead transmission lines are the major source of radiated noise. This ionization during corona discharge contributes to ozone production. Approximate of 50 ppb (part per billion) natural concentration of ozone are in the clean air but has a high value up to 150 ppb in the city/urban areas. With 180-200 ppb being the highest level, a person can withstand before prone to risk. Lower ozone productions of about 10 ppb make HVDC lines an environment-friendly transmission systems [32]. Electromagnetic shielding of the valve hall and the use of filtering circuits help reduced radio, TV and telephone interference in HVDC transmission lines to a minimal level compared to that of the HVAC overhead transmission lines. Ferranti and skin effect is a phenomenon that occurs majorly in an AC line when there is non-uniform in current distribution in the power carrying conductors. Most of the current are found in the outer layers of the conductors, which cause an increased in resistance of the conductors and thereby result in higher transmission losses. HVDC systems do not suffer from these effects being that the current is constant, which brings about higher efficiency of power transmission [33].

2.2.8. Cable transmission

Difficulty in making an overhead line path due to high population density in the urban area brings about the use of underground cables while submarine cables are used for offshore interconnections. Using AC cables for long distance power transmission produce large amounts of reactive power and high dielectric loss in the cable. This makes the transmission capacity to decreases sharply as transmission distance increases. However, DC cables do not suffer from capacitive charging or leakage current, save the I^2R loss on the cable resistance. As shown in Figure 2.6, this advantage makes DC cables preferable as the best option in conveying power to load centres via underground

cable. Moreover, with the increase in wind farms that are located far away from shore, DC submarine cables are the best option.

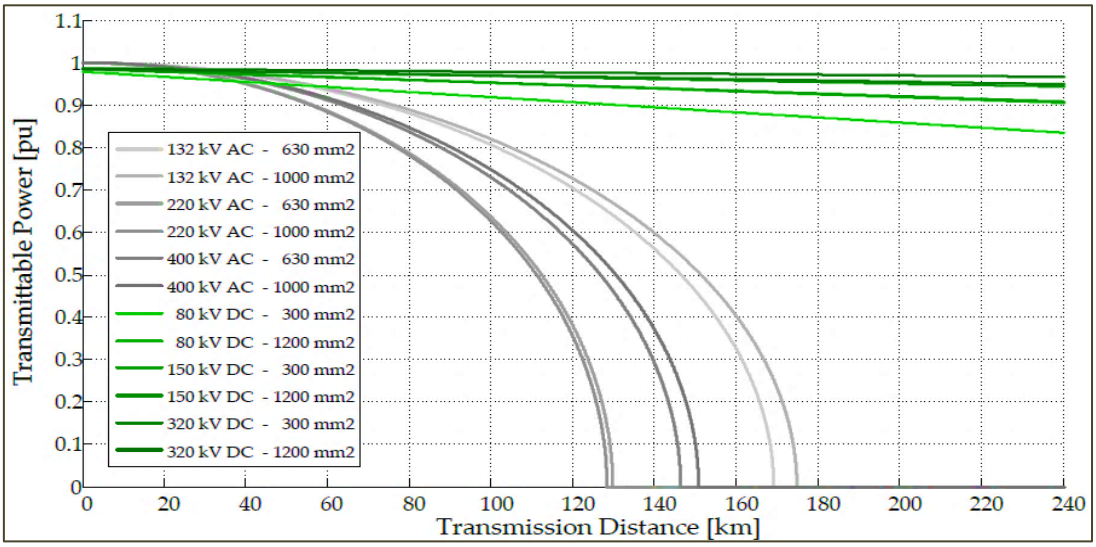

Figure 2.6: AC and DC cable transmittable power vs transmission distance [34].

2.3. Component of HVDC Systems

HVDC systems consist majorly of the converter valves, converter transformer, AC and DC filters, transmission lines, earth electrodes etc. Figure 2.7 show the component of HVDC scheme as presented in Siemen's HVDC setup.

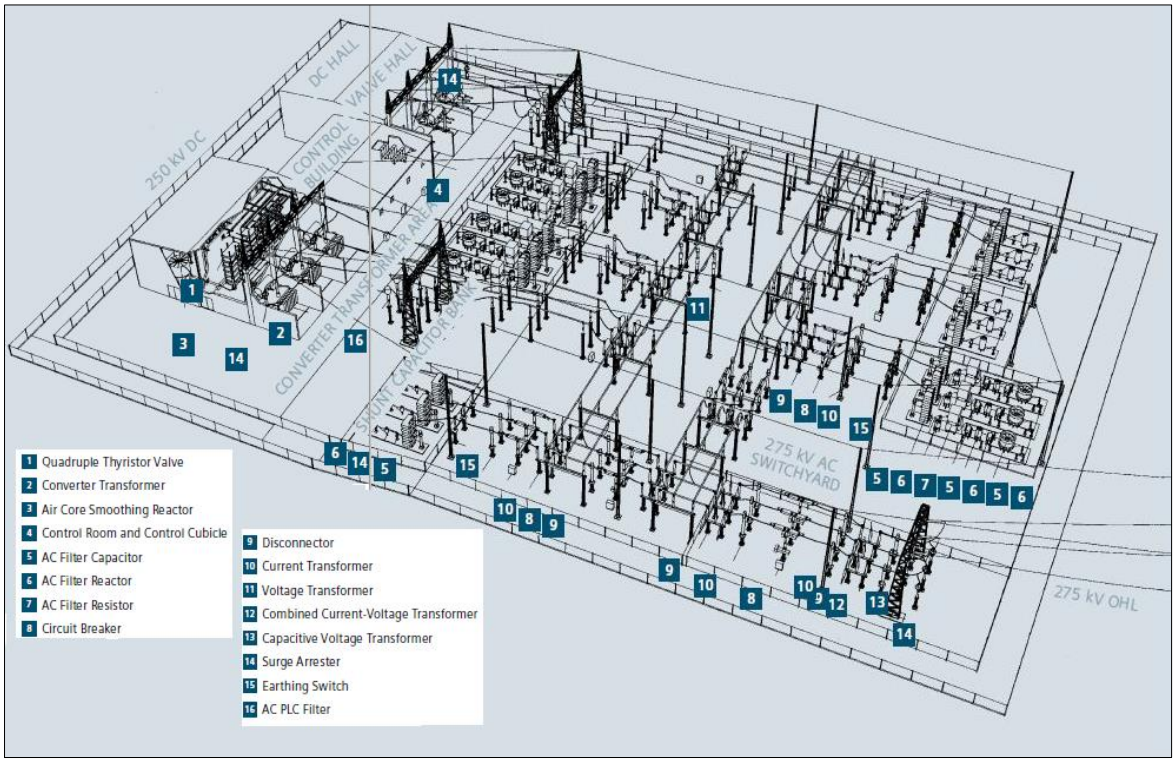

Figure 2.7: Siemen HVDC layout [35].

2.3.1. Converter valves

The converter is the most important part of HVDC systems. It is the component responsible for AC to DC conversion and vice-versa. A good converter valves should not only allow current flow with low voltage drop across the valve during its conducting phase, but also offer high resistance during the non-conducting phase. It should as well be able to withstand high peak inverse voltage (PIV) during the non-conducting phase. Furthermore, allow reasonable short commutation margin angle during inverter operation and smooth control during both conducting and non-conducting phases. Traditionally, thyristors valves that are air insulated, water cooled and suspended indoors are used for HVDC transmission. The need for better performance and good power controllability brings about the emergence of Insulated gate bipolar transistor (IGBT) [36-38].

2.3.2. Converter transformer

The converter transformer transforms the AC voltage to the required converter rating. 12-pulse converter configuration are normally used per pole in HVDC systems. This commonly use two 3-phase converter transformers with phase shift of 30^0. This is achieved by setting the vector groups of each transformer to Yy0 and Yd5. This type of transformer is different from the conventional AC transformer because of its characteristics such as short-circuits impedance, on load tap changers (OLTC), and DC-magnetization. It also has a winding that is not used close to yoke because the winding voltage connections depend on the conducting valves. This makes the entire winding to be completely insulated. Other configurations that a converter transformer can adopt are shown in Figure 2.8 below.

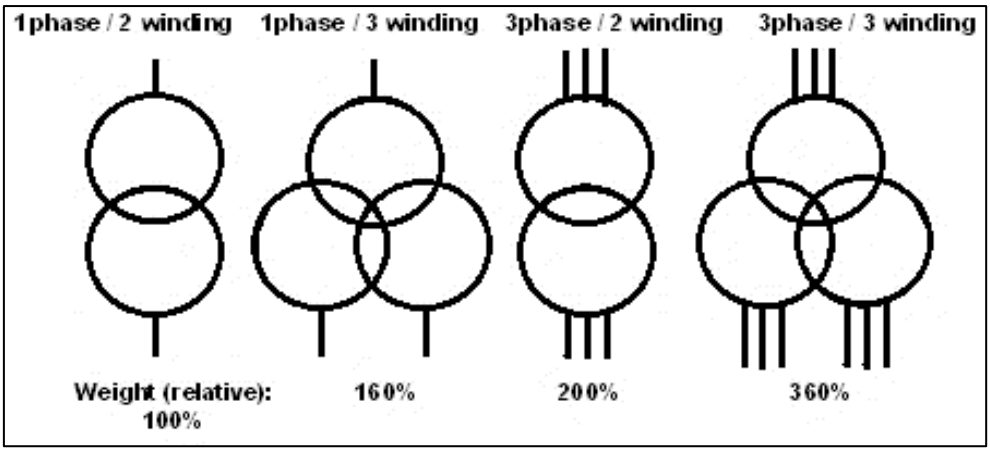

Figure 2.8: Transformer phase(s) connection

2.3.3. Smoothing reactors

Smoothing reactors are a large inductive element with little or no resistance that is used for prevention of intermittent increase of DC current that can damage the converter due to over-voltage. Reactors are also used to prevent resonance effect caused by DC switching yard or DC lines fault from entering into the valve hall, as well as to limit telephone interference. Air-insulated dry-type with magnetic shield reactors or braced disc oil type windings can be used for HVDC systems. The former has the

advantage of easy maintenance and less expensive spare unit but cannot provide large inductance with one unit. Also, in a place where there is space limitation or in a region prone to the earthquake (seismic region), the latter is most preferred [35].

2.3.4. Harmonic filters

Harmonics can either be characterized (i.e. follow the same pattern) or uncharacterized. Harmonics generated by the converters are of two order (np±1) in the AC side and (np) on the dc side, where p is the number of pulse and n is an integer. The filters were used to provide a low impedance path to the ground for the harmonic current thereby preventing the harmonic currents generated by the converter from entering the connected AC systems. However, it is impossible to protect all the harmonics from entering AC systems, but the filters help in reducing their magnitudes and thus reduce their effect in the AC network. Secondly, it also serves as reactive power support for AC network and the converter. Figures 2.9 and 2.10 below show DC transformer, DC filters and AC filters with their harmonic order [39].

Figure 2.9: Oil insulated and air insulated smoothing reactor [35].

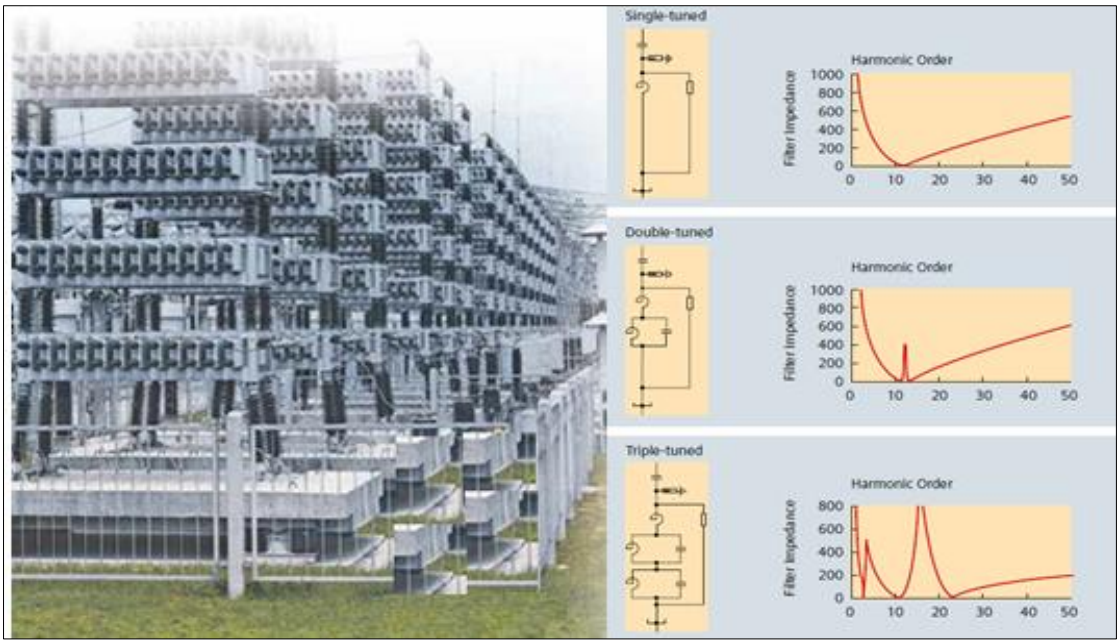

Figure 2.10: AC filter and harmonic order [32].

2.3.5. Transmission lines

HVDC power can be transferred via overhead lines or cable. The choice of which mode of transmission to adopt depends on the converter locations, rating of the line (power and voltage), line route terrains, the population density of the route, and so on. Both AC and DC overhead lines have a similar mechanical design. Only differs in their conductor configuration, insulation design, and electric field requirement. DC cables are mostly used for transmission systems that are crossing sea area. These cables are preferred than the AC cables for distances above 50km and transmission capacities from several hundred to more than thousand MW for bipolar systems. Special cables with DC current and voltage is required for submarine transmission. These cables are [11, 40-43]:

- Mass impregnated, this has a nearly unlimited transmission length with installation depth up to 1km under sea level. It has a voltage rating up to 500kV, 800MW capacity in one cable. Nevertheless, it suffers from overload capabilities due to conductor temperature.
- Oil-filled cable is insulated by paper impregnated with low-viscosity oil with a longitudinal duct that permits oil flow along the cable. High rating up to 600kV with greater sea depths, but limited transmission distance of below 0.1km. Prone to oil pollution due to leakage.
- The cross-link polyethylene, XLPE is another cable used in HVDC to overcome the disadvantages of those two cables.
- Better future cable is the lapped thin film insulation with ability to sustain up to 60% higher electrical strength, making it useful for very long and deep submarine interconnections.

2.4. HVDC Links Configuration

HVDC interconnections can be configured in different forms to suit different desired performance and operational requirements [39], namely, as presented in Figure 2.11:

- **Back to back connection**: This has both the inverter and the rectifier in the same location, and the valves are normally in the same building. It, therefore, has a short dc line of few meters located inside the same environment [44].
- **Monopolar connection**: This has both converters separated by a single dc pole line, either positive or negative voltage. The ground is used as a current return path. Most submarine cable connections use monopolar systems.
- **Homopolar connection**: This has two or more dc line of the same polarity connected to the converters. Negate polarity is normally used for less corona and reactive power loss. The ground is used as the return path. It works as a monopole when one pole develops a fault. The disadvantage of high cost make it unpopular and seldom used [45].
- **Bipolar connection**: This is the most popular method of HVDC interconnection of converters. It is similar to the homopolar connection, but it has different polarities. Each pole is independent, that is, it can operate with a single pole with ground used as return path [36].
- **Multi-terminal connection**: This has more than two sets of converters operating independently. Each converter can operate as a rectifier or an inverter [36, 46]

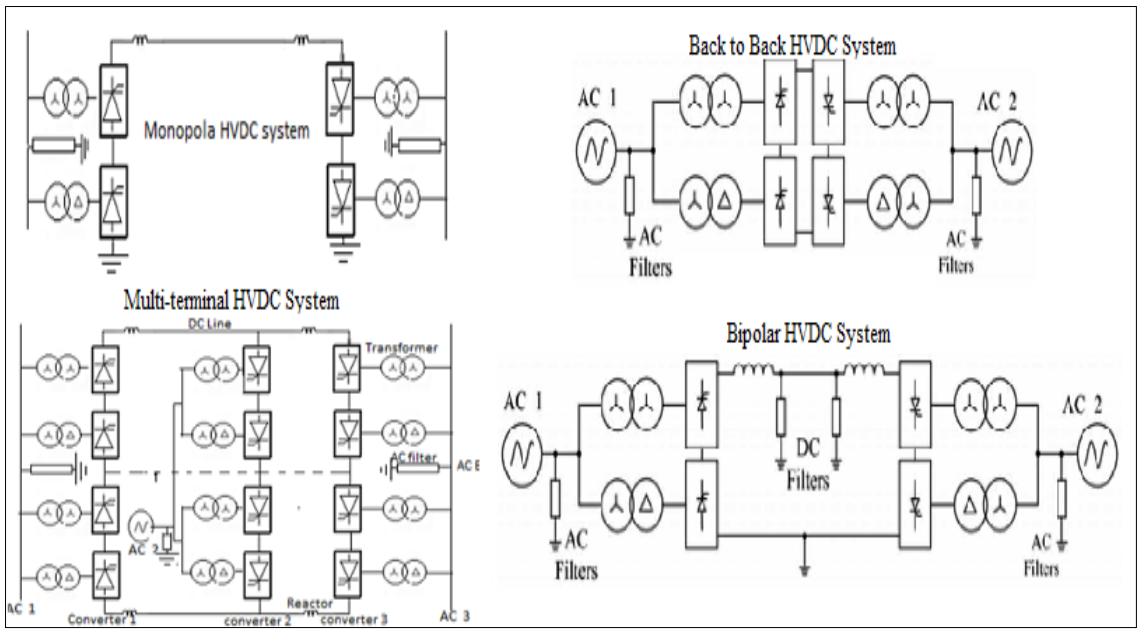

Figure 2.11: HVDC link configuration

2.5. Converter Technology

HVDC systems have been an alternative method of transmitting electric power from one location to another with some inherent advantages over AC transmission systems. The efficiency and rated power carrying capacity of direct current transmission lines highly depends on the converter used in transforming the current from one form to another (AC to DC and vice versa). Most commonly used AC/DC converter is the three-phase two-way or three-phase bridge circuits also called the Greetz

rectifier circuit. This type of circuits uses the same transformer to feed two one-way rectifiers of opposite connections. This, in turn, doubles the output dc voltage, but the PIV remains the same, and the pulse becomes six, this makes it useful for high-voltage direct current applications. The desired features of good converter circuits include [17, 39, 47-50]:

- High pulse number reduces harmonic content. Converter high pulse number is developed out of two 6-pulse circuits that are connected to two transformers. First with the star-star connection, and the second with the star-delta connection. This is done to generate a phase shift of 30^0 which tends to double the dc output voltage once again. Waveform of a 12-pulse converter can be seen in Figure 2.12.

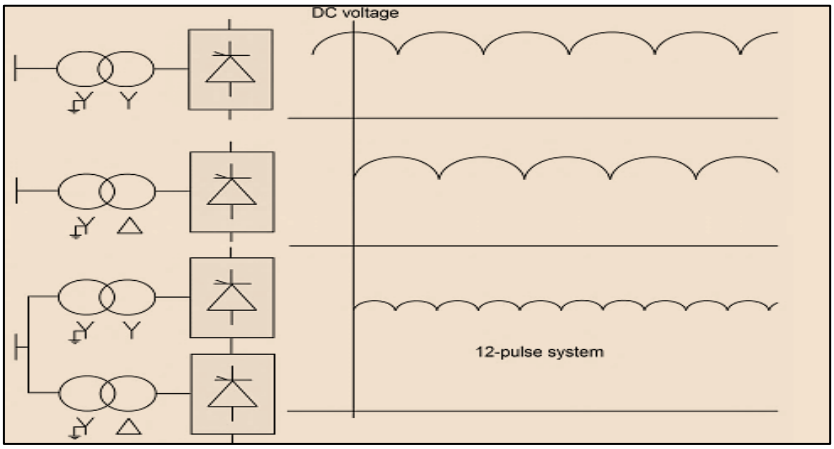

Figure 2.12: Voltage waveform of 12-pulse LCC converter

- The ration of PIV to the no load dc voltage must be as low as possible
- Ratio of no load dc voltage to the AC voltage should be as high as possible
- Finally, the transformer utilization factor (TUF) should be near to zero.

A well-configured converter reduces harmonics; increases power transfer capabilities, and reliability in that it offers high tolerance to fault along the line. Different HVDC converter topologies have been proposed, built and utilized all over the world. The well pronounced out of these technologies are the line-commutated converter LCC, capacitor commutated converter CCC and the voltage source converter VSC. However, LCC and VSC are the most dominant out of these three technologies.

2.5.1. LCC-HVDC

LCC, also known as a current source converter CSC uses a thyristors base technology for its converter switching. The thyristors is a silicon semiconductor device with four layers of negative and positive type material acting as bi-stable switches, triggered on with a gate pulse and stayed in that on condition until the next current zero crossing [51-56]. The thyristor can be triggered on by either injecting electrons, Electronic triggered thyristors (ETT) or photons of light, Light Triggered Thyristors (LTT) into the gate. The ETT requires a lot of components in its electronic circuits for

converting light signals into an electrical pulse, the special microcomputer for information processing, and during faulty or under-voltage condition, the ETT suffer a lot of setback in generating gate their pulse. Unlike the ETT, the invention of LTT reduces thyristor valve component up to 80%, which results in simplicity and availability of the transmission system. Less power requirement and usage of direct light make it useful for black start capability and during under-voltage or faulty conditions. Six inches UHVDC thyristor and its wafer can be seen in Figure 2.13. In order for LCC to commutate, the converters require a very high synchronous voltage source, thereby limiting its use for a black start operation. In addition, the lagging power factor in which the converter-firing angle operate makes it to consume a large amount of reactive power. Despite all these demerits, LCC still has the highest current rating reaching up to 6250A and blocking voltage of 10kV [57-60]. This account to why LCC-HVDC has the highest voltage and power rating level of all the HVDC schemes as shown on Table 2.1. Recent application of LCC-HVDC can be seen on Table 2.2.

Table 2.1: Semiconductors ratings

Features	**Thyristors**	**GTO**	**IGBT**
Max. Voltage rating (V)	8000	6000	1700
Max. current rating (A)	6250	6000	800
Voltage blocking	Sym/Asym	Sym/Asym	Asym
Gating	Pulse	Current	Voltage
Conduction drop (V)	1.2	2.5	3
Switching frequency (KHz)	1	5	20
Development target maximum voltage rating (kV)	10	10	3.5
Development target maximum current rating (KA)	8	8	2

Figure 2.13: Six inches UHVDC thyristor and its wafer

Table 2.2: Topology, application, and manufacturer.

Project Name	**Location**	**Characteristic**			
		(MW)	(kV)	Year	(km)
UK- Netherlands		1000	±400	2011	260
Jinping – Sunan	China	7200	±800	2012	2093
Mundra – Haryana	India	2500	±500	2012	960
Rio – Madeira	Brazil	800	100	2012	B-B
Rio – Madeira	Brazil	2x3150	±600	2013	2375
Xiluodu – Guangdong	China	6400	±500	2013	1251
Nuozhadu – Guangdong	China	5000	±800	2013	1451
Southern Hami – Zhengzhou	China	8000	±800	2014	2200
Biswanath – Agra	India	6000	±800	2014	1728
Xiluodu- Zhejiang	China	8000	±800	2014	1688
Zhundong – Sichuan*	China	10000	±1100	2015	2600

2.5.2. CCC-HVDC

The capacitor commutated converter also consist of a three-phase, full wave bridge rectifier circuits just like the LCC as shown in Figure 2.14 below, only that it has an additional series capacitor connected on the AC side. The current flowing through each capacitor during forward or reverse direction charges the capacitors, which result in aiding the commutation process. The capacitive region to which the converter operates tends to compensate for the reactive power consumption that

occurs in the LCC system. Also, an increase in commutation voltage provided by the capacitor charge reduces the risk of commutation failures even in weak AC systems. Although there was a lack of interest in its commercial usage due to complex control and protection scheme, but it starts to gain recognition again in the 1990s with the first commercial application used in Argentina and Brazil 1100MW back to back asynchronous tie in the year 2000 [61].

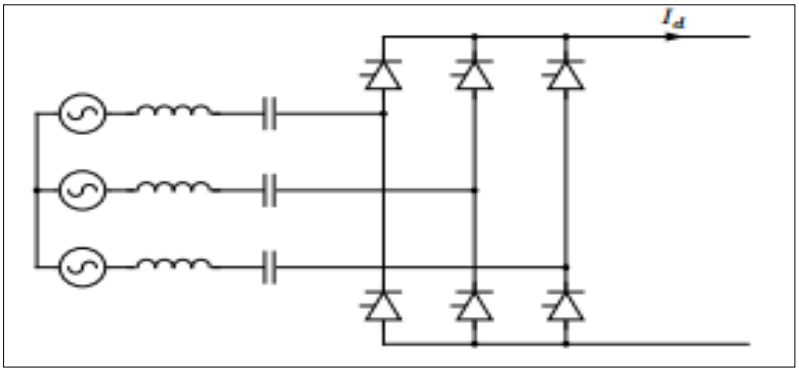

Figure 2.14: CCC Thyristor Bridge

2.5.3. VSC-HVDC

Voltage source converter uses IGBT technology. The current in this technology can both be switched on and off at any time independent of the AC voltage, that is, it creates its own AC voltages in case of black start [62]. Its converters operate at a high frequency with pulse width modulation PWM that allows simultaneous adjustment of the amplitude and phase angle of converter while keeping the voltage constant [63-65]. VSC has a high degree of flexibility with an inbuilt capability to control both its active and reactive power, which makes it more useful in urban power network area [37, 66-68].

This technology was developed in the 1990's with the first project commissioned 1997 by ABB [19, 69], . But due to its capacity limits, VSC-HVDC has not been able to make much edge over its contemporary LCC scheme due to low device rating, high power losses and high dielectric stress on equipment insulation [70], [68]. Its application is approaching 1800MW, 500kV. An example is the 1400MW, ±525kV Nordlink that interconnect 623km Statnett grid in Norway and TenneT in Germany [71]. A lot of research is ongoing to override this limitation [72], and to have the ability to ride through fault [73, 74]. VSC control, modeling, simulation and stability analysis in power systems was well explained in [75, 76] and .

VSC-HVDC topology starts with a two-level converter, which is the basic building block of the VSC-HVDC technology [23, 77, 78]. It is like a six-pulse bridge in which IGBT with inverse-parallel diodes replaced the thyristors, and the DC smoothing reactor of LCC is replaced by DC capacitor as shown in Figure 2.14. It derives its name from the fact that it has switching devices that are complementarily operated to generate two levels of voltage ($+V_{dc}/2$ and $-V_{dc}/2$) at the AC output terminal of the converter as shown in Figure 2.15. This complementary operation only allows one

switching devices to operate at a time, and the other is turned off. Simultaneous turning on of both two switching devices will lead to short circuit of the capacitor across the DC link which may destroy the converter switches due to over-current [79]. With this topology, each semiconductors switch withstands the full voltage stress that is flowing in the link.

Prevention of the DC voltage from changing polarity is done by the diode that is connected in parallel to the IGBT, since the diode can only conduct when forward biased, thereby discharging the DC circuits. But the current flows in both direction, passing through either the IGBT or the diode [80].

It adopts the PWM techniques to control the gate switching frequency of the IGBT, and to reduce the harmonic distortion generated by the converter. Due to high switching losses in the IGBTs as a result of the PWM which is switched on and off many times in cycles, the overall transmission efficiency of a two-level converter is very poor compared to the LCC converter [81, 82]. Another major setback is that high levels of electromagnetic interference occur when the two-level converter is used for HVDC operation [83, 84].

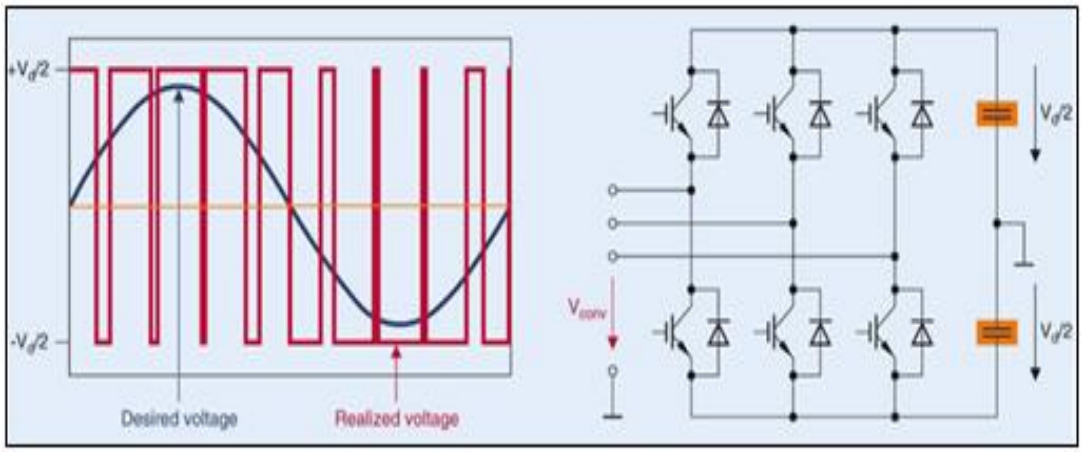

Figure 2.15: DC waveform of VSC-HVDC

An attempt to reduce the poor harmonic distortion and to have a high efficient in VSC brings about multi-level converter (which start from the three-level converter with three discrete voltage level). It synthesizes more than two voltage level at the AC terminal of each phase. Several types of multilevel converter have been mention and analysed in the literature [85-95], such as the diode clamped, where diodes are used as clamped and the DC output is subdivided into switches by capacitors. With n-levels, there will be n+1 capacitors, and n-1 switch pair is required to work in a complementary manner to generate the output dc voltage [96-98]. High efficiency for switching at the fundamental frequency, low cost and a lesser number of components are some of its merits [98]. However it suffers a setback as its less attractive for high voltage transmission due to difficulty in charging and discharging of its dc capacitor, lack of a modular index and large inductance stray in the clamping path which has an effect on the converter switching characteristics [99, 100]. Flying capacitors multilevel converter is another type that made use of a pre-charged capacitor [101-104]. Unlike the

diode clamped, two or more switch can synthesize an output voltage at the AC output terminal of the converter, and has a phase redundancy, which allows specific choice of the capacitor to be charged or discharged for voltage balancing across different levels. It has the ability to control real and reactive power flow, and to ride through fault and voltage sag because of its large number of capacitors. Nevertheless, as the level increases, so does the size of the capacitors, as it becomes bulky. Also, the control to track the voltage for all the capacitor becomes complicated as it requires high-frequency switches [105]. The single-phase full bridge is the building block for the cascaded H-bridge multilevel link. It has four switches connected to an isolated capacitor (separate dc source). Each H-link generates three voltage levels [106]. Easy modularized layout package for the series H-bridges makes it cheaper and quick to fabricate. It also has a possible voltage levels output than the DC source. Good for reactive power compensation with good voltage balancing capability through adaptive control action [107]. However, cascaded H-bridge conversion is not suitable for HVDC application because it H-bridge requires the use of many isolated DC sources in series.

Recently, a new alternative to VSC-HVDC circuits was proposed in 2003, at the University of Bundeswehr in Munich, Germany, by Prof. Rainer Marquardt [108, 109]. This converter topology is based on series-connection of several sub-modules of two semiconductor switches and a capacitor. This topology is known as a modular multilevel converter (MMC or M2C). The converter, can either adopt the half bridge cascaded or full-bridge connections for the arrangement of each submodule. The half-bridge modular multilevel (HB-MMC) addresses some of the limitation encountered in the conventional VSC-converter. Reduction in the magnitude of the transient dc fault current, converter scalable to the highest transmission voltage through addition of more levels, great reduction in the harmonic content and elimination of low-order harmonics which usually requires large filters, and losses reduced to approximately 1% per converter are well taken care of [65]. All these features made HB-MMC to be widely adopted in recent years. But the HB-MMC freewheeling diodes is unable to stop AC grid contribution to the dc fault current which makes it in need of fast acting DC circuit breaker [107, 110, 111], else the excessive current stresses may damage the freewheeling diode [112]. The recent technology that overrides the overcurrent fault condition of the HB-MMC is the full bridge multilevel converter (FB-MMC) [113-115]. Though, this technology increases semiconductor losses but the important feature of dc fault reverse blocking capability was achieved by the converter by blocking current flow in the converter switches during DC faults, thereby disallowing both active and reactive power exchange that may want to occur between the DC systems and the AC grid [106, 116].

Other recent HVDC converter topologies with intrinsic dc fault ride-through capabilities are alternative arm modular multilevel (AA-MMC) converters and hybrid cascaded multilevel converter with AC side H-bridge cells. These converters achieve dc fault reverse blocking capability in order to eliminate AC grid contribution to dc side faults, but has little footprint and conversion losses compared to the H-bridge modular multilevel converter[87, 107].

Table 2.3 Application of VSC-HVDC

Project Name	Location	Characteristics			
		(kV)	Year	(MW)	(Km)
Borwin 1	Germany	±150	2009	400	200
Caprivi link	Namibia	±350	2010	300	951
Transbay	USA	±200	2010	400	85
EWIC	UK	±200	2012	500	261
Inelfe	France	±320	2013	1000	65
Skagerrak 4	Norway	±500	2014	700	244

Table 2.4 VSC compare to LCC HVDC

LCC	**VSC**
Thyristor base technology	IGBT base technology
The semiconductor can withstand voltage in either polarity	Withstand current in either direction
Constant current direction	Current direction changes with power
Energy is stored inductively	Store energy as a capacitor
Turned on by a gate pulse but rely on external circuit for its turn off	Both turn on and off is carried out without the help of an external circuit
High power capability	Lower power capability
Good overload capability	Has weak overload capability
Requires stronger AC systems for excellent performance	Operate well in a weak AC systems
Requires additional equipment for black start operation	Possesses black start capability
Requires AC and DC harmonic filters for removal of distortion and harmonics	Requires no filter because it generates an insignificant level of harmonics
Poor in reactive power control	Good reactive power control
Large site area, dominated by harmonic filters	A more compact site area
Requires converter transformer	Conventional transformer is used
Lower station losses	Higher station losses
More mature technology	Still at its infancy

Reversal of power is done by reversing the voltage polarity	Power is reversed by changing the current direction
Higher voltage capability of over 1000kV	Lower voltage capability of almost 600kV
Mostly used to transmit bulk power for a long distance	Used for transmitting power from remote area with renewable energy
Suffers commutation failures because of a sudden drop in the amplitude or phase shift in the AC voltage, which results in dc temporal over-current. Though, the effect has no significant impact on the AC systems as it's a self-clearing effect within a few power frequency cycles	Ability to turn on as well to be turned off of VSC makes it immune to any voltage dips or transient AC disturbance, therefore, it does not suffer commutation failure [117].
Change in dc polarity is needed when converter wants to change from rectifier to inverter mode, making its converter be more problematic to adopt in a multi-terminal HVDC system. The reason for a low number of LCC base technology for multi-terminal HVDC.	Suitable for multi-terminal HVDC systems because it does suffer from commutation failures, has independent, multi-directional power flow, and operate with the same voltage polarity.
During short circuits on the dc line, control of the firing angle of the thyristors valves stops the increase of dc fault current. This converter control and protections reduce the damage caused by the fault current. In cases of overhead lines fault, power transmission is stopped for arc de-ionization, after which power transmission resumed.	Continuous conduction in the diode will cause an increase in dc fault current even when the IGBTs are turned off. The AC circuit breakers at both VSC HVDC ends must be opened to stop the diode conduction. The converter link must be re-started after a fault has been removed.

2.6. Challenges of HVDC Systems

- Converter stations are much expensive
- Valves switches generate harmonics which result in systems interference and noise
- HVDC converters require reactive power compensation.
- HVDC Control functions become cumbersome as the number of terminal increases.
- During a case of large disturbance, the DC lines might add to a voltage collapse during the swings that might come due to high reactive power consumption.

However, the use of HVDC controller with active and reactive power modulation technique reduces such effect. Furthermore, the currents and voltages rating of the valves can be increased with emergence of new semiconductors technology. Multi-pulse operation of converter (6-pulse, 12-pulse). Use of forced/self-commutated converter for high reliability and controllability also reduces both characteristics and the uncharacteristic harmonic current in the convectional LCC systems. Finally, the use of fast components like fiber optics, digital signal processing, digital computers in the converter control.

The resulted improvements after using the advanced technologies have minimized the cost of power conversion and improved the reliability of the HVDC line. Additionally, the advanced technologies opened the way for the modern HVDC technology. For example, the HVDC light is now in the operation and it reduced the cost of reactive power compensation at the HVDC terminals [42, 118-121].

CHAPTER 3: METHODOLOGY

3.1. Research Approach

The purpose of this research is to analyze and observe the effect of HVDC link on Eskom Eastern grid transmission network. However, being that there are many interconnected element on this network, the author limited this research to investigate key elements such as the busbar voltage profile, transmission lines, compensating devices, generators and different network controllers. This result will give the author a good idea of the stability margin of the network under investigation. The variables that are to be analyzed in this research are the busbar voltage profile (both steady state and dynamic analysis), transmission line loadings (steady state), rotor angles of the generators with reference to the reference machine angle (dynamic analysis), and the rotor speed of the generators.

The main purpose of analyzing the behavior of the system variables in Eastern grid is to determine the critical fault clearing times (CCT) of different interconnected element in the system. The numerical value of the obtained critical fault clearing times will then be analyzed and compared to set standards, in order to allow conclusions to be drawn on the machine transient stability, by determining whether the machine transient stability meets the requirements as set out by the national grid code for system operation [122]. The ultimate aim is to compare the critical fault clearing time for various study cases and network operation scenarios and observe how HVDC technologies based transmission schemes in the power system affect the values of this critical fault clearing times.

3.2. Research Procedure

Two bus network, multi-machine network, IEEE 30-bus network and Eskom Eastern Power grid were the four network used to carry out this research study. In addition, different HVDC configurations of voltage rating from ±600kV to ±800kV were used as an alternative means of power transmission in these networks. This is to investigate the impact of each HVDC scheme on the overall systems stability and performance of each test network used.

The two-bus network used consists of an external grid connected to a 400kV busbar (Bus 1) which is linked to another bus (Bus 2) via double circuit (400km and 300km) overhead lines. While the multi-machine network is a four-area network supplied by DIgSILENT during their stability-training program. This network consists of 24 buses divided over four geographical areas that is interconnected by a number of tie lines. The third network used for this study is the modified IEEE 30 bus test network. This network diagram represents a portion of the American Electric power system (in the Midwestern US) as of December 1961. Few modifications were made on the model parameters and generator ratings. The fourth network is that of the Eastern grid located in the KwaZulu-Natal province. It was modelled out of the original Eskom main transmission network of

the South African power grid as dated back to third, March 2014. Few upgrades were also done based on Eskom transmission development plan for 2016-2025 [10]. Chapter 4 and 5 give more emphasis on these networks design and modelling.

Steady state load flow calculation-tool on DIgSILENT was used. This Load flow calculation follows the Newton-Raphson iterative equation. During this steady state, a bar plot showing the bus voltage, active and reactive power generated, load demand, as well as different elements percentage loading, was observed to ensure compliance with regulated standards. During this steady state, DIgSILENT P-V, and Q-V script are used to generate the simulation graph displayed in this study. This script uses series of load flow simulation base on Newton-Raphson iterative method to plot the graph. P-V curves show how an increase in power in a particular area causes a reduction in bus voltage of the connecting busbar, while Q-V curve relates the amount of reactive power needed to be injected/absorbed to keep a system stable at an acceptable voltage level.

Dynamic analysis with the use of time-domain simulations was carried out to examine the system critical clearing time (CCT) or critical isolating time (CIT) for transmission lines. This method used in power system stability analysis involve the use of real-time dynamic analysis to calculate, for a given defined fault, the maximum allowable clearing period in which the system can remain stable. This period gives the allowance to which the fault must be cleared or isolated from the rest of the system for it to remain in a stable state. If the fault, however, stays longer than this period, the power system will definitely become unstable. The result of this analysis is depicted on a graph. These graphs consider the voltage stability of the entire system. A situation whereby the entire system will still be rotor angle stable, but the bus voltage will be below appreciable limit was encountered. Thereby, whenever the bus voltage is below or above (± 0.5%) the stipulated grid code, the system is thus tag to be unstable.

3.3. Research Instrument

This project made used of DIgSILENT PowerFactory for its network modelling and simulations. The control features and all iterative components were also modelled using DIgSILENT simulation Language DSL. RMS time domain simulation with electromagnetic EMT simulation are the flexible tools offered by this software. The product broad range includes static analysis using DIgSILENT Programming Language (DPL) script, 3-phase short circuits, radial and meshed network simulations, AC/DC load flow and dynamic simulations, modelling of low, medium and high voltage networks, and distributive generating system with penetration of high renewable energy. Error debugging was much easier on this software as it is equipped with output window where network conditions are depicts [123].

DIgSILENT PowerFactory is well equipped with various IEEE controller models, namely; generator prime movers, automatic voltage regulators (AVR) and power system stabilizers (PSS). However,

major DC controller models are not on this software, leaving the users to define and model such controllers where applicable.

Different fault analysis can be carried out on this software using different standards. Various fault conditions can be define by user and thereby analyse the behavioural condition with respect to all others interconnected components.

3.4. Research Layout

Organising this research study involve the use of set out goals and defined activities. Technical performance of Eskom eastern grid with respect to voltage stability study using HVDC network is the major task of this research. The steps taken to meet the research deliverables are highlighted below:

An extensive literature review was carried out on meshed HVDC system on HVAC networks. This is to get a broad base knowledge of the network performance and impact of HVDC link on HVAC networks. Modelling and controlling of HVDC technologies, principle of operations, topologies, different configurations and applications were researched for better understanding of this research work. Based on the acquired knowledge from the literature review, expert technical contribution were made to industry (Eskom) in other to define a definite area of research and to identified a major score of study. Identification of system pre-set conditions using load flows study and RMS simulation study was the next inline task. This process helps to pre-determine the original condition of the system element and components before faults conditions. Analysis of critical elements were carried out using different contingencies studies to prioritise network element in terms of outage of faults conditions. Controller actions were modelled and tuned to alleviate the effect of fault conditions on this Eastern gird network. However, this does not override the original system condition of the Eskom Eastern grid.

3.4.1. Steady state and static analysis

Newton Raphson load flow model is used to analysis this Eskom Eastern grid during steady state condition. Under this activity, the percentage loading of several element such as the transformer, transmission lines, and generators checked to see that they complied with grid code of value below 80%. Active and reactive power consumed by the load and generated by the generators are also looked into. All these are observed on a bar-subplot during load flow analysis of the network. Static voltage analysis using active Power-Voltage (PV) curve and Reactive power-Voltage (QV) curve was also analysed. These activities predict the effect of load changes/increase on busbar voltage profile, and the reactive power required to maintain the voltage at acceptable limit of ±5% of the rated voltage.

3.4.2. Time-domain simulations

Dynamic analysis was carried out on the Eastern grid using RMS/EMT Time-domain simulations using DIgSILENT PowerFactory software. During this period, the system critical condition and the

network stability levels were determined. Variables to be analysed are defined and insert into a subplot, then a pre-fault conditions is determined by running load flow. Fault is then applied on any critical location or element on the network, the initial conditions are first calculated, and then the simulation is carried out to determine the dynamic analysis of the network for both short and long of term period. The defined variables are plotted on a graph against the simulation time. A multiple element can also co-plotted on the same graph based on user specification a similarities of variable to be analysed. Conclusions are drawn based on the result from all these different subplots during both steady states and dynamic analysis of the network.

CHAPTER 4: HVDC MODELING AND CONTROL

4.1. HVDC System Equivalent Circuit

The major advantage of a HVDC system is the ease of flexibility and controllability of the transmitted power by controlling the firing angles of the converter circuits. Modern controllers are not only fast but also reliable and serve as means of protecting HVDC converters during line or converter fault. HVDC controls are quite complex especially with increasing number of terminals. High-speed microprocessors are mainly deployed for monitoring and supervisory control functions.

A two terminal DC scheme equivalent circuit shown in Figure 4.1. This gives a better understanding of HVDC converter model for voltage calculation at both the rectifier and inverter stations using sequential load flow model, equation (4.1 – 4.7). While Figure 4.2, represent HVDC equivalent circuits. To maintain safe commutation margin, γ is used as control variable at the inverter side instead of β. Power control in two terminal dc links is desirably done by having current control in one converter and voltage control in the second converter. While power reversal, is done by changing the voltage polarity for an LCC systems. Increasing power in the link can be achieved either by:

- Reducing α which will also improve the power factor or,
- Increase γ or β which will worsen the power factor and higher loss in the valve snubber circuit

It is, therefore, better to operate the inverter at minimum extinction angle (γ), and the rectifier at constant current control. This mode of operation is good for voltage regulation than operation with minimum α at rectifier and current control at the inverter. Constant Extinction Angle (CEA) control mode is a best economical way to operate inverter in order to avoid commutation failure. However, negative resistance characteristic of the converter is the main problem with CEA control. This makes it difficult to operate stably if connected with weak AC system. Under normal condition, rectifier operates at Constant Current (CC) control and inverter at CEA control. Increasing the rectifier voltage will cause the current in the link to be increased. To control the current at the rectifier end, the controller will increase the delay angle α while inverter end controller will maintain CEA. Decrease in α value will worsen the power factor, hence, it is generally controlled up to some fixed value and tap changer is thereafter used.

Increase in inverter voltage will caused current in the link to be reduced and to maintain the constant current in the link, delay angle α will be reduced up to α-min. This is the required for the complete firing of the valve. If the current in the link is still less than the reference current, the tap changer is to be operated to increase the AC voltage at the rectifier. Decrease in inverter voltage: dc current in the link will be increased, the rectifier-end controller will increase the delay angle α. Decrease in α will worsen the power factor and generally α is controlled up to a certain angle and thereafter tap

changer is used. Decrease in converter voltage will cause a decrease in the DC current, to maintain this current, α is to be decreased but to a limited value α-min and then tap changers is to be used to increase the current. If further decreased, rectifier characteristic falls below, and CEA characteristic will not intersect and I_d will be zero, therefore, the inverter is also equipped with constant current control [53, 124, 125].

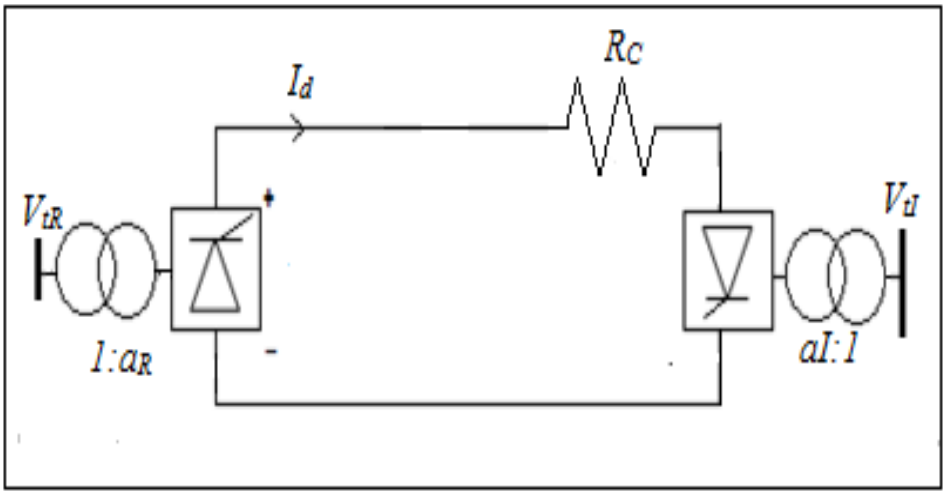

Figure 4.1: HVDC circuit for sequential power flow calculation

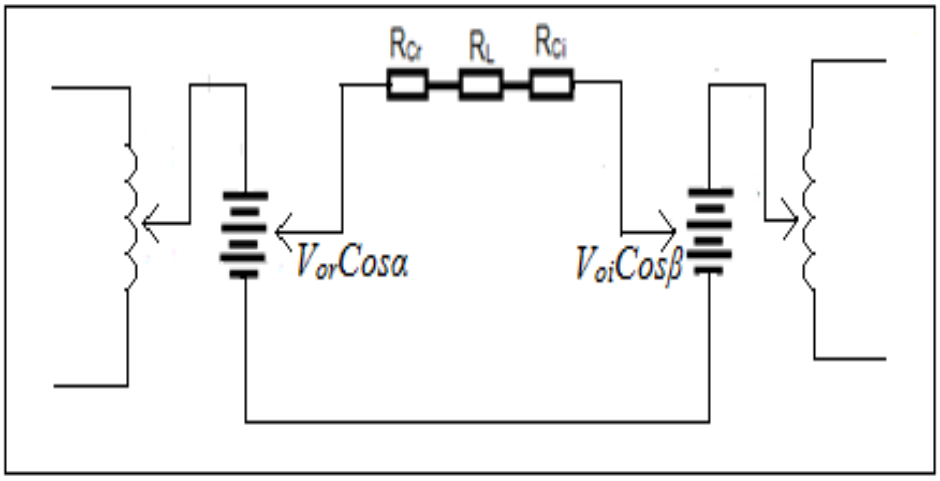

Figure 4.2: HVDC equivalent circuits

$$V_{dR} = \frac{3\sqrt{2}\alpha_R V_{tR} \cos\gamma_R - 3X_C I_D}{\pi} \tag{4.1}$$

$$V_{dI} = \frac{3\sqrt{2}\alpha_I V_{tI} \cos\gamma_I - 3X_C I_D}{\pi} \tag{4.2}$$

$$P_{dR} = V_{dR} I_d \tag{4.3}$$

$$V_{dR} = V_{dI} + R_d I_d \tag{4.4}$$

$$I_{ac} = \frac{3K\sqrt{2} I_{dc}}{\pi}, K \approx 0.995 \tag{4.5}$$

$$P_{dI} = V_{dI} I_d \tag{4.6}$$

HVDC equivalent circuits' equation is given by equation 4.7

$$I_d = \frac{V_{dor} \cos\alpha - V_{doi} \cos\beta \cos\gamma}{R_{cr} + R_L \pm R_{ci}} \tag{4.7}$$

V_{tI}	-	AC terminal voltage, inverter side,
V_{tR}	-	AC terminal voltage, rectifier side
I_d	-	DC current
R_d	-	DC line resistance
A_I	-	Inverter transformer ratio
a_R	-	Rectifier transformer ratio
V_{dR}	-	DC voltage, rectifier side
V_{dI}	-	DC voltage, inverter side
α_R	-	rectifier firing angle
X_c	-	Commutation reactance
P_{dR}	-	Rectifier power
P_{dI}	-	Inverter power
R_c	-	Commutation resistance

- **Line modelling**

The line can be represented either as a Pi model or as T-model. T-model is often used to represent DC line model for system dynamics. Figure 4.3 shows this model diagram with equations 4.8 to 4.10 showing the mathematical representation [126]. Simple calculation of instantaneous power from the line to each converter station can thus be calculated with equation 4.11

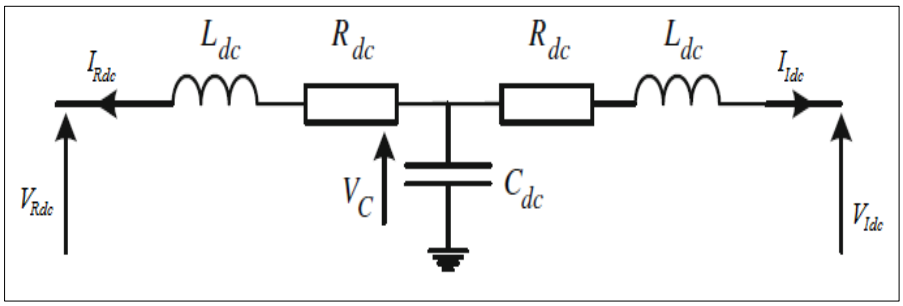

Figure 4.3: T-model of transmission line

$$\frac{d}{dt} I_{Rdc} = \frac{1}{L_{dc}} (V_c - V_{Rdc} - R_{dc} I_{Rdc}) \tag{4.8}$$

$$\frac{d}{dt} I_{Idc} = \frac{1}{L_{dc}} (V_c - V_{Idc} - R_{dc} I_{Idc}) \tag{4.9}$$

$$\frac{d}{dt}V_C = \frac{1}{C_{dc}}(-I_{Rdc} - I_{Idc}) \tag{4.10}$$

$$P_{dc} = V_{dc}I_{dc} \tag{4.11}$$

4.2. HVDC Link Controls Characteristic

For adequate power flows through an HVDC link, proper control measures of the converter need to be implemented. Adoption of these control features help in coordinating the performance and behaviour of the rectifier and the inverter. These tend to prevent overcurrent in the DC link, maintain 1.0pu value of the DC voltage, and help reduce the occurrence of commutation failure at the inverter side.

HVDC systems are basically operated by a constant-current control by varying the voltage to control the power output of the line. Table 4.1 shows the difference in the two control mode in which an HVDC can be operated on. The current control is the most preferred because it prevents the DC link from shutting down during AC-system fault.

Table 4.1: HVDC control mode

Functions	Voltage control	Current control
Connection of Loads	Parallel	Series
Load replacement	Without delay or problems.	Needs isolation of circuits before replacement or a bypass
I^2R Losses in the line	Losses changes as load changes	Constant losses irrespective of load
During fault conditions	The circuit breaker trips the fault. And shut down the systems	Being a constant current, whatever happen during faults, the current must not exceed I_d.

4.2.1. VI characteristics

In a simple two terminal DC network, the normal operation holds that the rectifier varies the firing angle α, but the rectifier passes to constant ignition angle CIA when α reaches its minimum and thereby permitting no further increase in voltage. The voltage-current (VI) characteristic of a converter is represented in Figure 4.4. The constant current CC mode is represented by section BC for the rectifier and section DF for the inverter, and AB represents the rectifier CIA mode. The normal operating point of the converter is located somewhere between point B and C (CEA mode). During the normal condition, both rectifier and inverter characteristic intersect at E. However, the rectifier CIA would follow the dotted-dash line A'B' when there is an increase in its voltage. To bring about normal operation, the inverter is also equipped with CC mode, which tries to reduce the current order in the inverter than that of rectifier and brings about new normal operating section DF. The current margin is the difference between the inverter and rectifier current orders, usually 10-15% of the rated value [127].

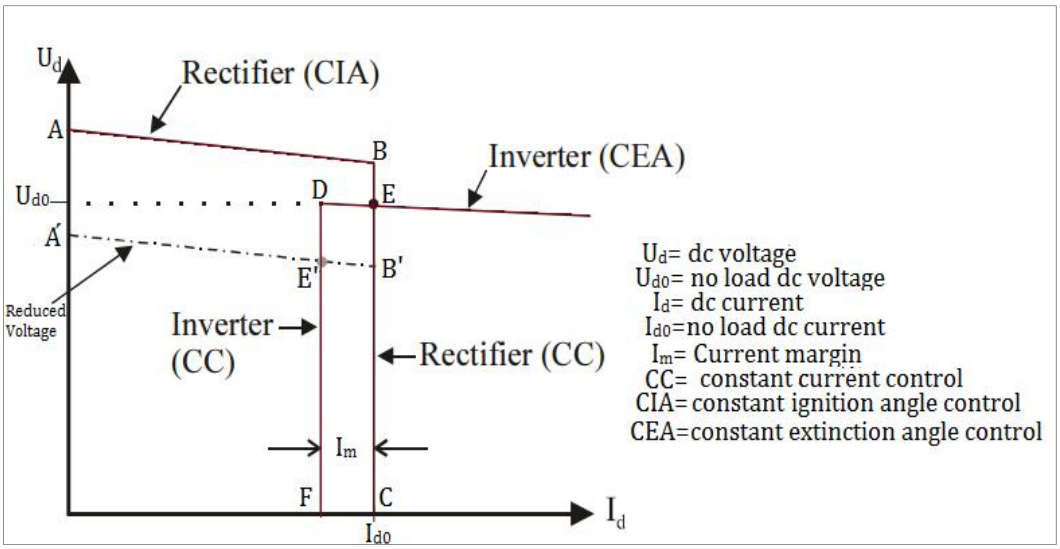

Figure 4.4: Converter VI characteristics

Most HVDC systems are operated in a bi-directional power flow in that both converters can serve either as inverter or as rectifier. This is accomplished by equipping each converter with combine control characteristic of both inverter and rectifier as shown in Figure 4.5.

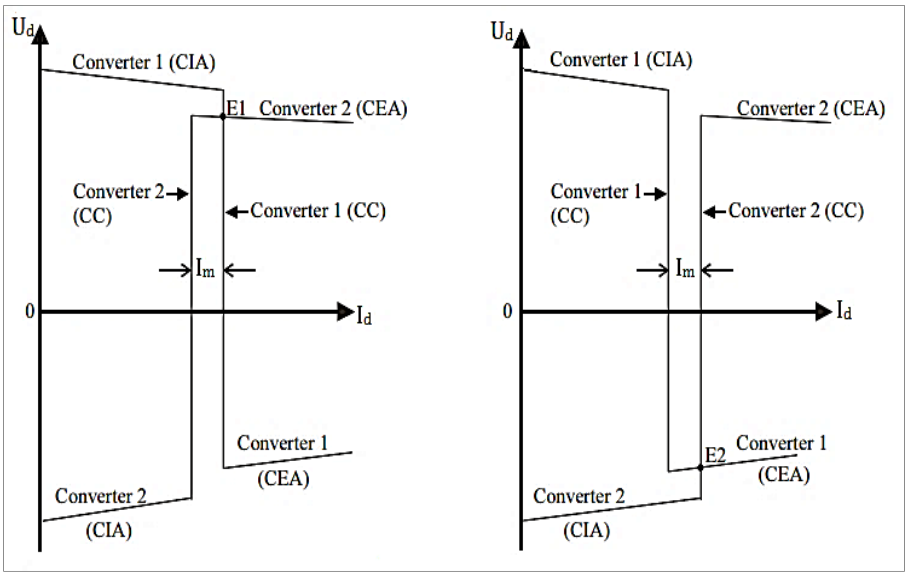

Figure 4.5: Bidirectional power flow characteristic

4.2.2. Control schemes

All HVDC control schemes aim toward proper firing of the converter circuits. The CC or CEA controller output if fed into the gate pulse generator in turns determines the instance of gate pulse generation for each valve. Nevertheless, in a situation where all the control characteristics are exhausted, then the On-load tap changer (OLTC) is used in such an extreme condition. There are two types of firing controls schemes, which are [126]:

- **Individual Phase Control (IPC)**: this is an outdated control mode when each valve determines the phase position of each control pulse separately, which is directly related to the zero crossing of the commutation voltage. This control uses six parallel delay circuits, which

caused it to have many uncharacterized harmonics that is generated because of using different firing angle for each pulse circuits.

- **Equidistance Pulse Control (EPC)**: this control is used in the modern day HVDC systems. Generation of the pulse has no synchronization with the zero crossing of the AC voltage, thus making it to generated gate pulse at an equal interval of (1/fp, f=frequency, p=pulse). Although it gives low DC output, but very useful in weak AC systems. The EPC control could either be of Pulse Frequency control PFC or Pulse Phase Control PPC.

4.2.3. HVDC controls

HVDC control as set up on DIgSILENT PowerFactory software can be divided into three hierarchical levels: power control, pole control and the converter control as depict in Figure 4.6. A block definition that defines the transfer function in the form of graphical block diagrams and equation is first created for each of the control, and then a composite block frame is created for the overall control. This consists of the entire overview diagram showing all the slots interconnections and which object should be assign to a slot. After a common model is created from the block definition, they are then added into the composite model. Figures 4.7 and 4.8 from Ref. [128] give a simple overview diagram of the controller as connected to the converter. These diagrams are all fully shown in Appendix (APP 1) as it was modeled on DIgSILENT. The functions of these major controllers of HVDC converter are explained below.

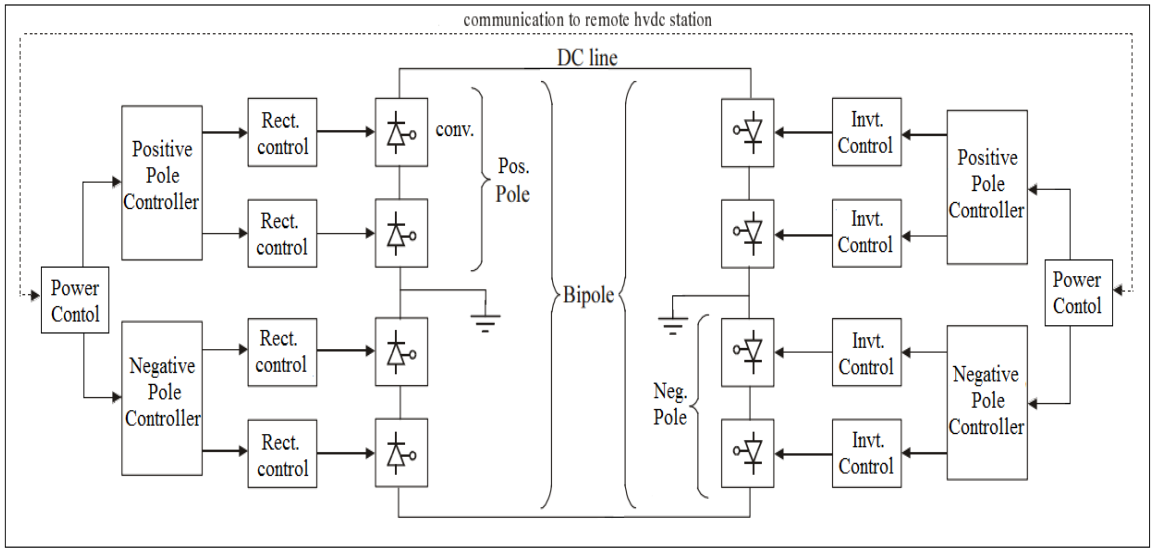

Figure 4.6: HVDC hierarchical control block

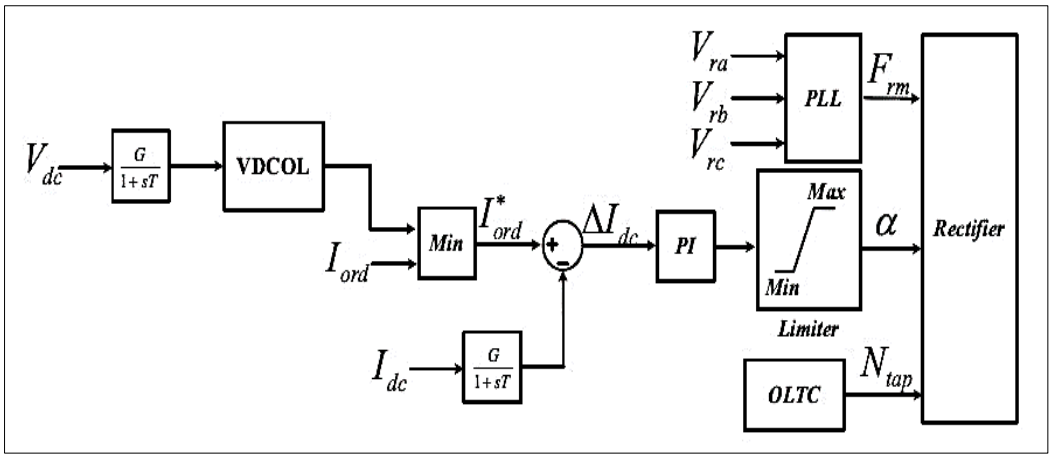

Figure 4.7: Rectifier Controller

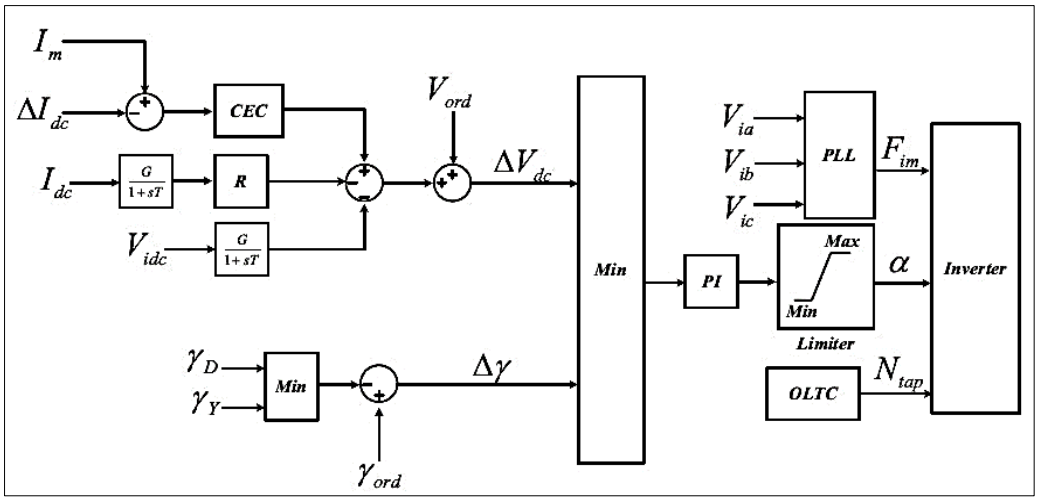

Figure 4.8: Inverter Controller

- **Voltage-Dependent Current Order Limiter (VDCOL):** VDCOL function is to reduce the current order value when there is a disturbance that causes a reduction in the DC voltage. The converter looks up the current order on the table based on the filtered DC voltage as shown in Figure 4.9. This control prevents a high rate of reactive power consumption and reduces voltage stress in the valve thereby facilitating the recovery of the converter after disturbance.

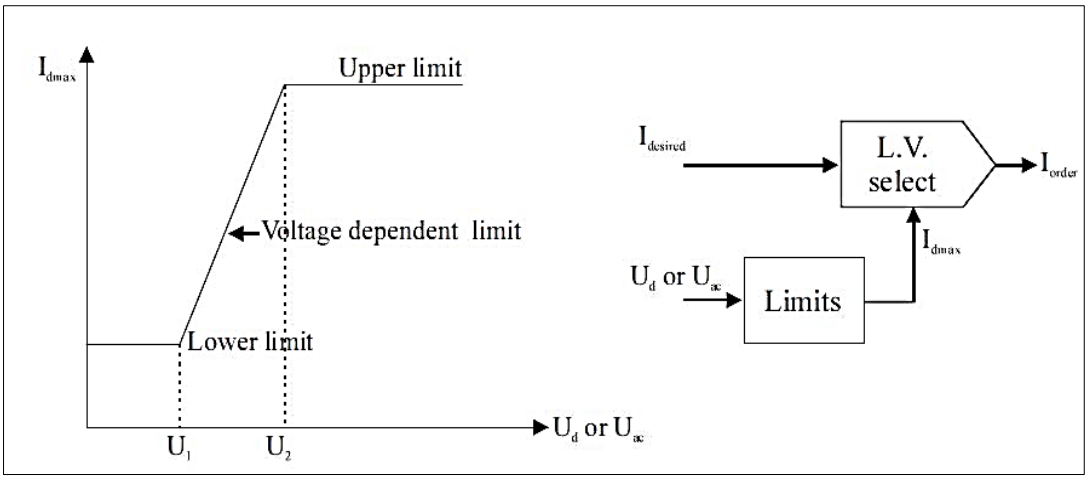

Figure 4.9: Voltage-dependent current order limiter

- **Gamma Controller**: also know has extinction angle controller. This controller ascertains that the commutation finishes well before the polarity of the voltage across the valve turns positive during an inverter operation of the converter. The firing angle order used in gamma controller is gotten from a Proportional and Integral (PI) regulator that takes the differences between the commutation margin γ (delay between the valve extinction and the voltage of the valve just before turning positive) and a fixed set point. During a situation when the margin is larger than necessary, the PI controller stops at the α-max. Else, the firing angle is reduced until γ equal the set value.

- **Current Controller**: this controller filtered the actual direct current measured and then calculates the difference from the reference signal, and fed the current error into a PI controller, which outputs the firing angle order. The rectifier always operates as a current controller while the inverter due to the minimum value selector uses the gamma controller.

- **Converter Controller:** the firing pulse generator, this controller generates each valve firing pulse by comparing the reference signal from the PLL.

- **Power Controller:** this serves as the master controller that coordinates and oversees the overall control actions of the systems. It determines the current order signals for each pole of the converter.

4.3. HVDC Systems Fault and Protection

HVDC schemes in power systems are practically not immune to a fault despite all their control actions. In fact, faults on AC busbar, DC line or cable faults, and converter faults frequently occur. Thus, have some negative impact on the HVDC system operation. This might result in the systems going out of operation if proper control action is not put in place within timely range. Nonetheless, the major benefit in HVDC systems is that most of its fault are self-cleared or cleared through proper

converter control action, which makes it not like the AC systems that require relays and circuit breaker to isolate/trip the faulty lines or network until the fault is cleared.

4.3.1. Types and nature of faults

- **AC System Fault:** the AC fault could occur either at the inverter or at the rectifier end. During fault at any of the converter end, there is a reduction in the converter current. This is to reduce output power transfer across the link. Sometimes, these faults often lead to commutation failures at the inverter end.

- **DC system Fault:** this fault mostly occurs on the line or cable as the line to ground faults as bipolar faults are rare to come by. Even, the line to a ground fault has little impact on the AC systems compare to AC lines fault. Bipolar HVDC system fault on one pole only limits it to operate as monopolar system, meaning the power at the faulty pole are blocked by control action and the other pole left unaffected.

- **Commutation Failure:** This very frequent fault occurs mostly at the inverter end during AC/DC systems disturbance. During this fault, the current passing through the converter rises to about 1.5 – 2.5pu of the rated value. Weak receiving AC network increases the occurrence of commutation failures during disturbance due to reduced commutation voltage. However, this type of fault is self-clearing by multiple β-control and VDCOL action.

4.3.2. Experimental viewpoint

The HVDC configuration used in this research study is based on the IEEE CIGRE benchmark modelled using DIgSILENT PowerFactory. Figure 4.10 shows the single line diagram of the HVDC system. It is a ±600kV, 3000MW with transmission length of 1300km. The bipolar HVDC system is based on LCC technology. Each pole consists of twelve-pulse thyristors with an inbuilt transformer on both sides of the converter. More details about the HVDC link are shown in Table 4.2.

Verifying the stability of the HVDC system and its controller actions involve the use of the time-domain electromagnetic simulation (EMT) tool on DIgSILENT to obtain a graphical illustration of the step response to a system fault. Two case studies were considered; in case study 1, three-phase short circuit fault of 30Ω fault reactance was applied at the rectifier AC bus for 200ms time duration. Study case 2 is also as study case 1**,** only that the three-phase short circuit with 10Ω fault reactance was applied on the AC bus at the inverter side for 200ms. After running the (EMT) simulation, the response of the positive pole of the HVDC signals and variables and its controller's signals are depicted on a graph. Positive pole was used for the graphical representation being that both positive and negative pole uses the same controller, only differ VDCOL pole polarity.

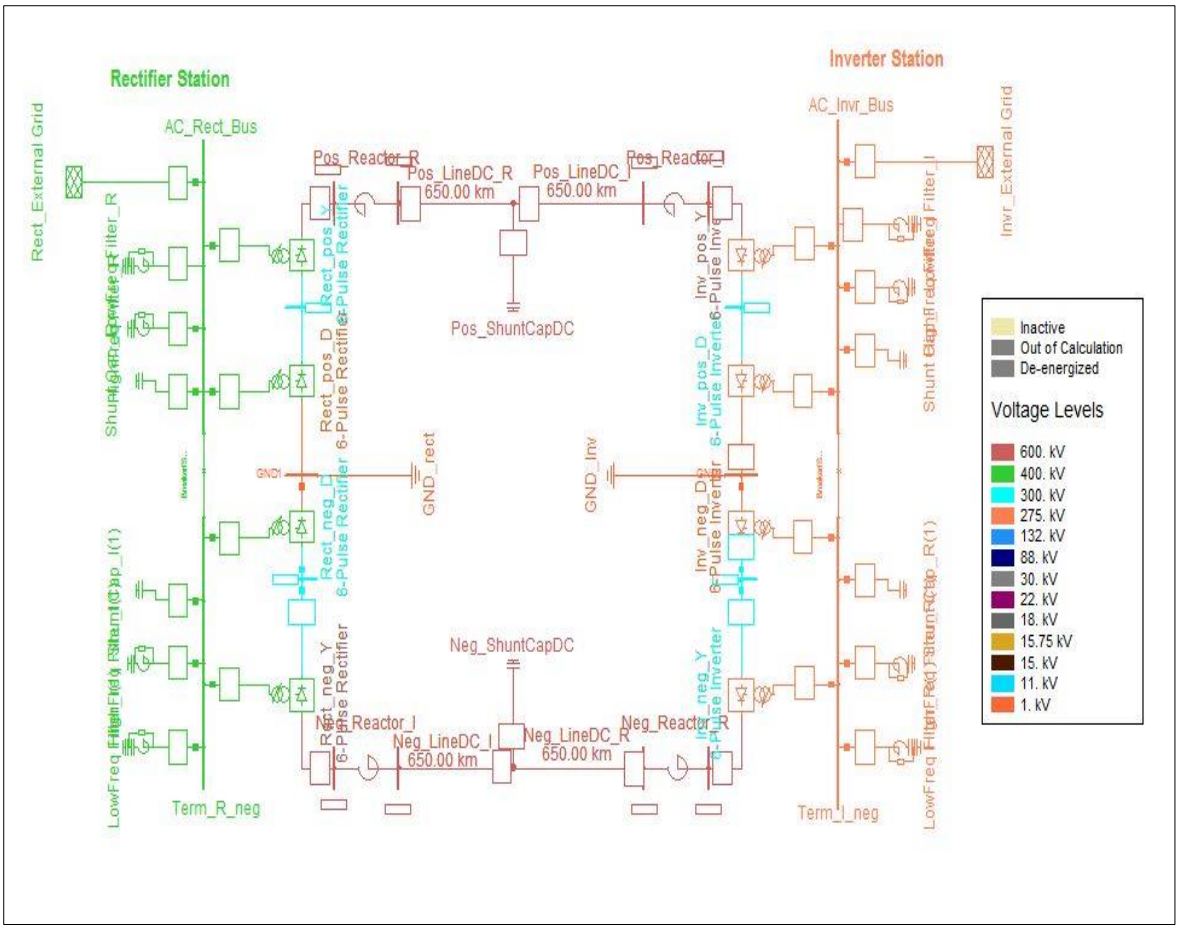

Figure 4.10: HVDC model

Table 4.2: HVDC converter data

		Rectifier	**Inverter**
Rated AC voltage		400 kV	275 kV
Rated DC voltage		309 kV	301 kV
Rated DC current		3 kA	3 kA
Rated power		929 MW	904 MW
Control mode (set point)		Current (2KA)	Voltage (0.99p.u)
Transformer	Min. turns ratio	0.7	0.9
	Max. turns ratio	1.4	1.3
Rect. Firing angle/ Inv. Extinction angle		15 degrees	20 degrees
Tap control mode		Alpha-control	Gamma-control

Table 4.3: HVDC transmission line data

Rated voltage	600 kV
Rated current	3 kA
Length	1300 km
Smoothing reactor	650.8 mH

- **Study case 1: Rectifier fault**

Figures 4.11 to 4.18 show the response of HVDC controllers when a three-phase fault of 30Ω was applied at the AC terminal of the rectifier station for 200ms fault duration. This is to test the reliability of HVDC scheme and to observe the contribution of each control parameters to systems fault.

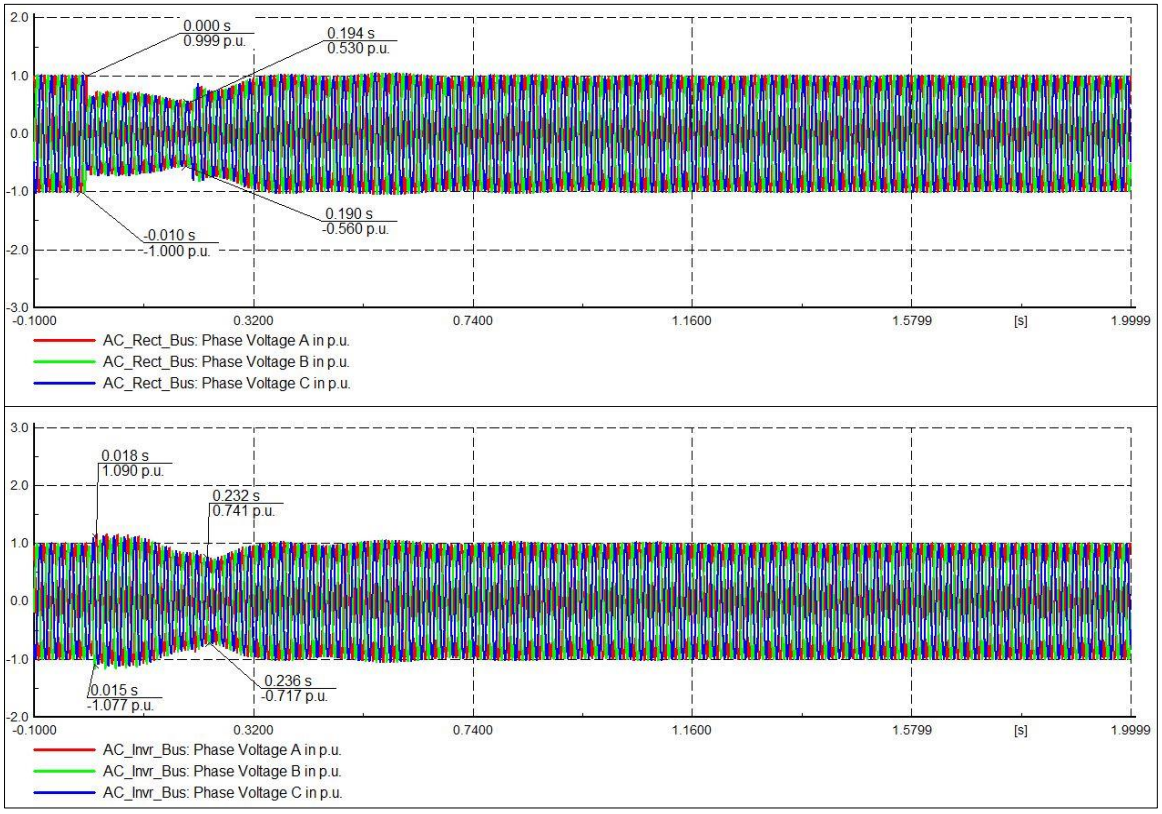

Figure 4.11: Inverter and rectifier busbar voltage

It can be seen from Figure 4.11 that the voltage profile at both AC side of the converter station retains their steady states value of 1.0p.u before the fault. More impact is felt at the rectifier side of the station being that the fault occurs there. It can be seen that the voltage went as low to about 0.5p.u. at AC rectifier bus. In order to maintain constant power flow at the instant of fault, the inverter AC voltage rose to about 1.09p.u, which later came down to about 0.7p.u. This depict minimal power transfer during a fault. The systems return to their steady state pre-fault value after that the fault is cleared. The converter AC current is shown in Figure 4.12; it can be observed that the current dips down to about 0.37kA during the fault which latter rose to about 2.1kA due to increasing in firing angle to keep the system back to its steady state value. The converter reverted to its pre-fault value after that the fault is cleared. There is no case of commutation failure from the converter current waveform.

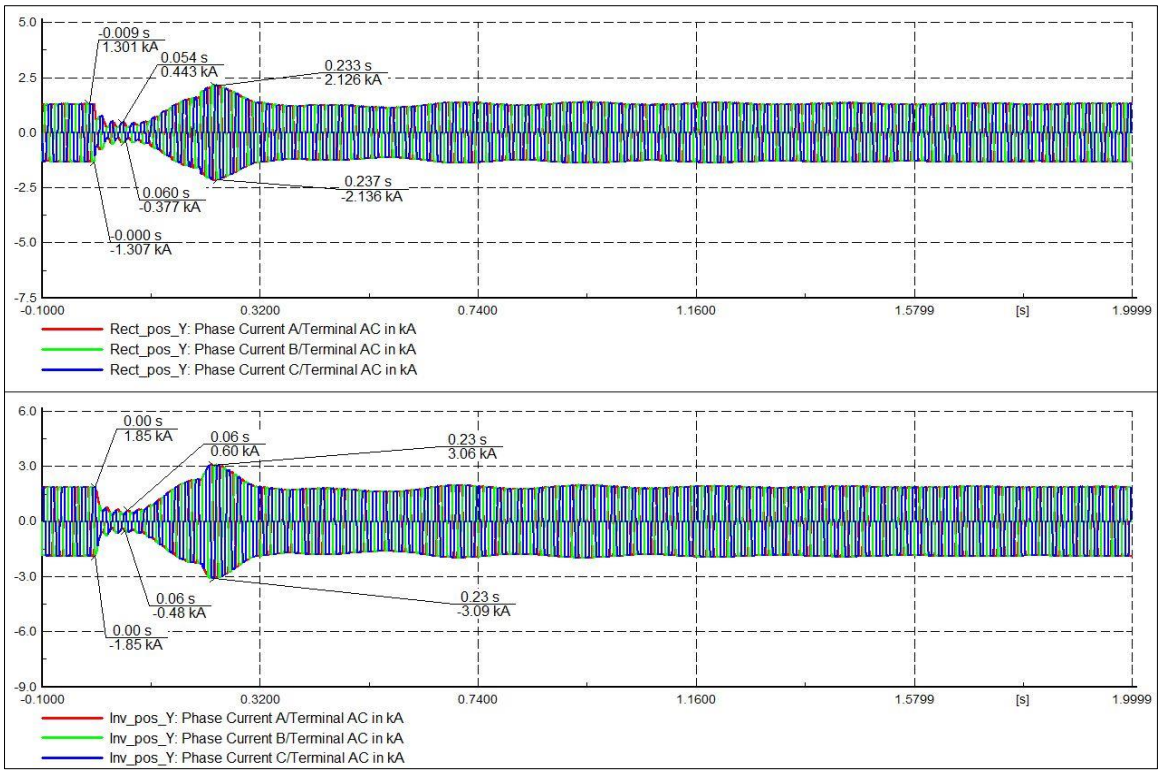

Figure 4.12: Inverter and rectifier converter AC current waveform

Shown in Figures 4.13 to 4.17 are the responses of HVDC major control signals to the three-phase fault at the rectifier station. Figure 4.13 shows the converter voltage and current taken at the reactor terminal of the HVDC scheme. This value area measured using an appropriate transducer and then passed through a necessary filter before usage for controller actions. These parameters are very important as it main aim is to give feedback to each of the converter controllers. Its value depicts the state of the system.

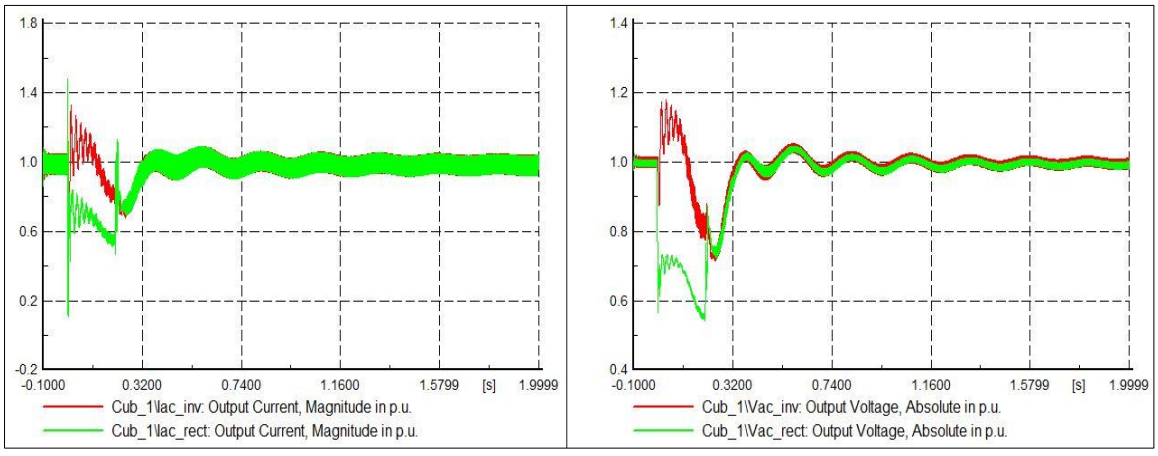

Figure 4.13: Inverter and rectifier DC voltage and current measure

Figure 4.14 and 4.15 shows the current and voltage (VDC, IDC), which is input into a filter to give (VDC_Filtered, IDC_Filtered) respectively. It can be seen from this graph that the filtered curves are much smoother than the measured curves. Each of the measured signals has a pre-set reference value

(IORD, and VORD); this value is always constant except in the case of a severe fault. The filtered signals can always take after their reference value after a fault.

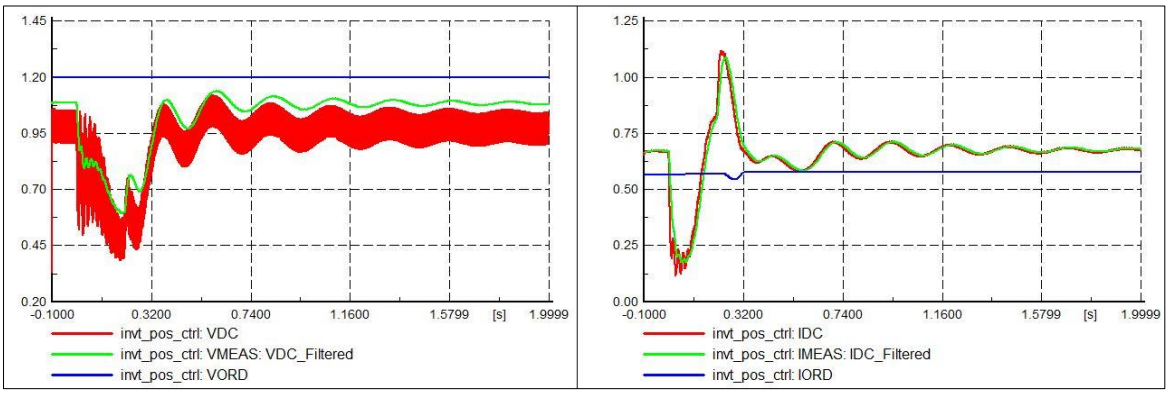

Figure 4.14: Inverter voltage and current control signal

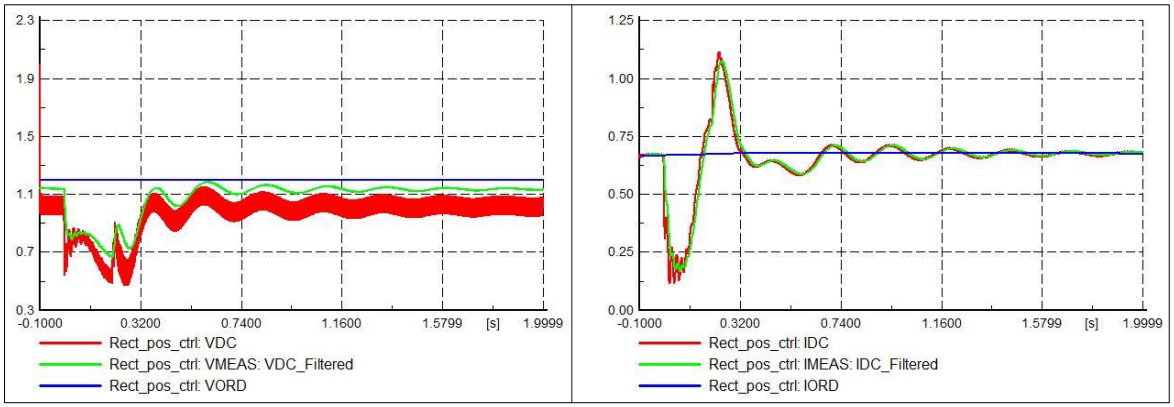

Figure 4.15: Rectifier voltage and current control signal

Figure 4.16 illustrates the rectifier firing angle and its mode selection at the inverter side. During a fault, the firing angle is supposed to be 15^0, but dips down to about 3^0, the inverter thereby activates VDCOL selection mode. This VDCOL is always activated when the firing angle is excessively high or too low. It can be observed from the graph as the firing angle recovers from 3^0 to 15^0 (as it recovers from the faults to its normal operating range) that the inverter switched to current control mode and later back to VDCOL mode when the firing angle was increased to about 27^0. When the fault was successfully cleared, the converter switches back to its normal current control (IDC Control) mode. The VDCOL functions as earlier stated are to look up the current order on the table based on the filtered DC voltage. This is to prevent the high rate of reactive power consumption and reduce voltage stress in the valve.

At the inverter side, Figure 4.17 shows the inverter extinction angle and its mode selection at the rectifier side. It could be seen how the value went up to about 61^0 during a fault, but later retain is the pre-fault value after the fault has been cleared at the rectifier station.

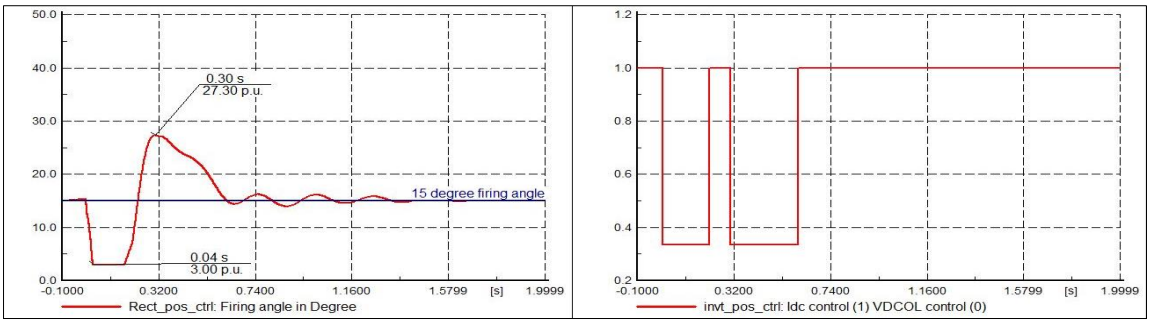

Figure 4.16: Rectifier firing angle and inverter mode selection

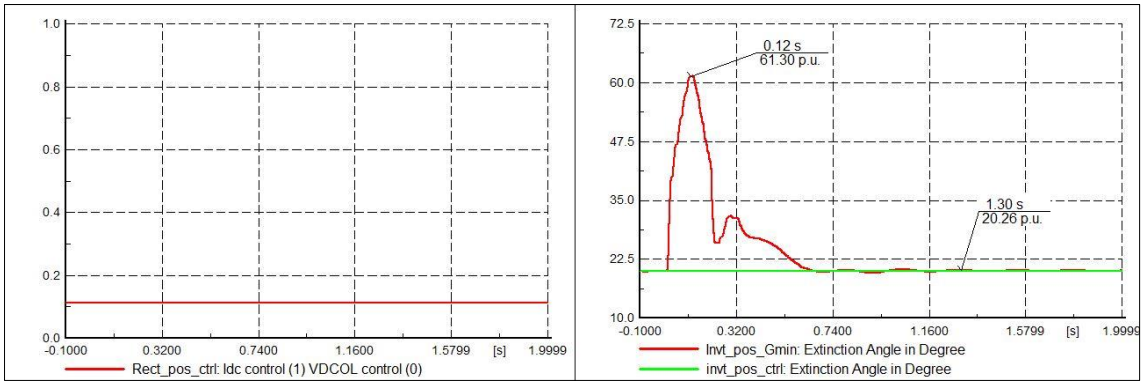

Figure 4.17: Inverter extinction angle and rectifier mode selection

Figure 4.18 finally explains the DC voltage magnitude for both positive and negative pole of the converter. This is to justify the fact that, both poles respond to fault in a similar manner, only polarity difference. The value being ±1.0p.u. dips down to about ±0.5p.u. during a fault, and after the fault is cleared, it maintained back its pre-fault value of ±1.0p.u.

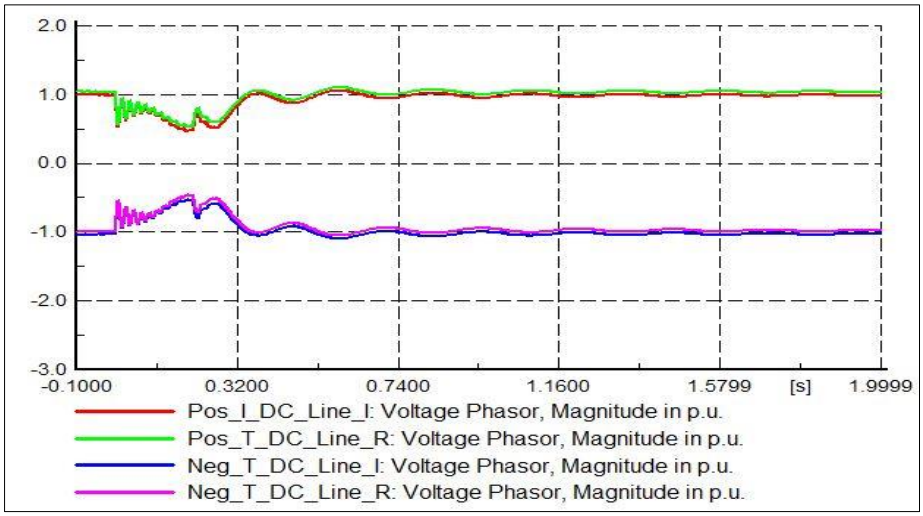

Figure 4.18: Voltage magnitude for positive and negative pole

- **Study case 2: Inverter fault**

The fault location for the second case study is at the inverter station. A three-phase fault reactance of 10Ω is applied at the inverter AC busbar for 200ms. This is to observe the controller action of HVDC

scheme as this will help instability assessment purposes of HVDC system. The graphs gotten from this study are illustrated in Figures 4.19 to 4.26.

Figure 4.19 shows the phase voltage for the AC busbar of the converter. This fault causes the voltage profile to dips down to about 60% of its original value. The controller action when deployed, in an attempt to stabilize the systems first made the voltage shoot up and later return to the steady state value of 1.0p.u when the fault was cleared. The converter phase current is shown in Figure 4.20. From this graph, a case of commutation failure can be seen at the inverter end. It was observed that, there was no current transfer during this fault period. This hinders commutation process at the inverter end, which eventually lead to outage, or zero power transfer along the link until the fault was cleared. This conclude the fact that inverter faults are more severe than the rectifier fault. Reason has been that more impact is felt on inverter side than rectifier side during a fault. Therefore, adequate control measures are required at the inverter station of HVDC system.

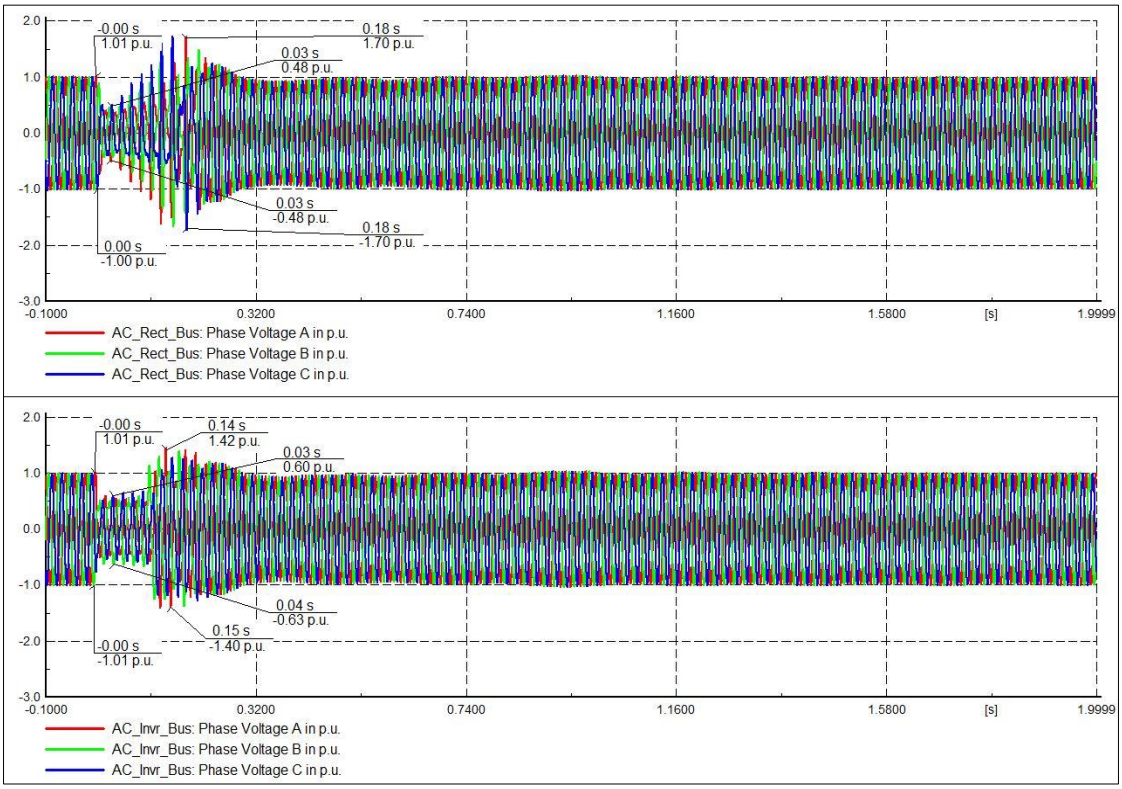

Figure 4.19: Inverter and rectifier busbar voltage

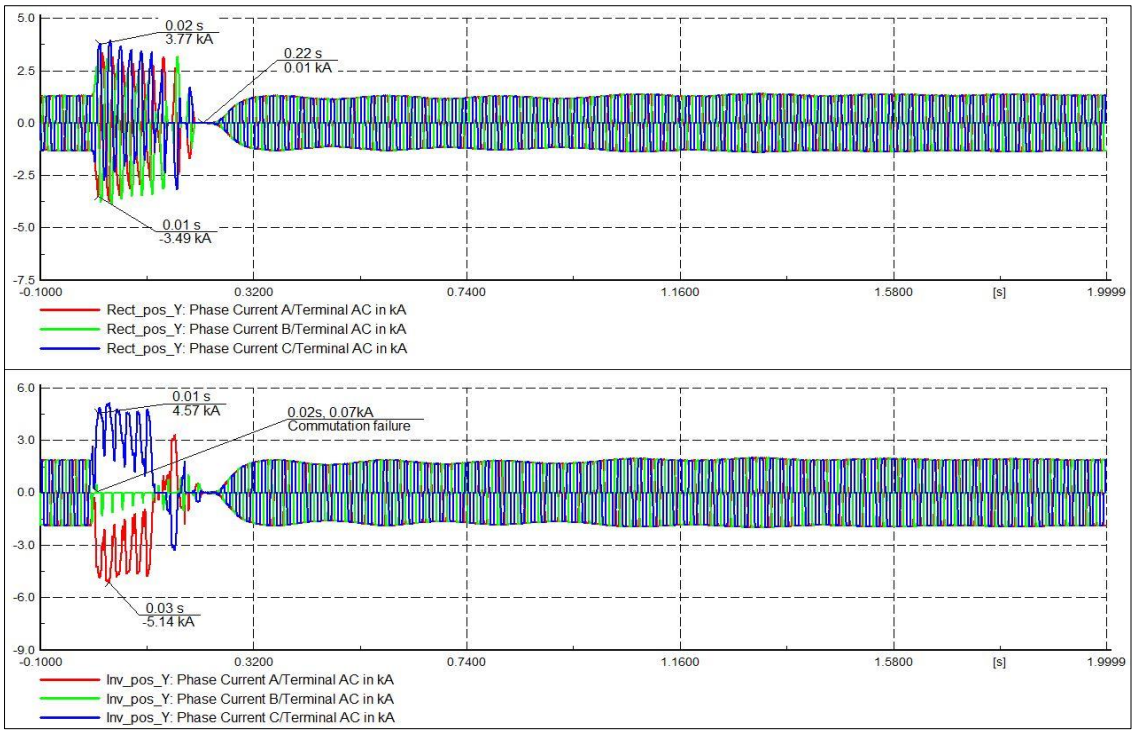

Figure 4.20: Inverter and rectifier converter AC current waveform

The response of HVDC major control signals to the three-phase fault at the inverter station are depicted in Figures 4.21 to 4.25. Converter voltage and current taken at the reactor terminal are shown in Figure 4.21. It main aim is to give feedback to each of the converter controllers. Its value depicts the state of the system.

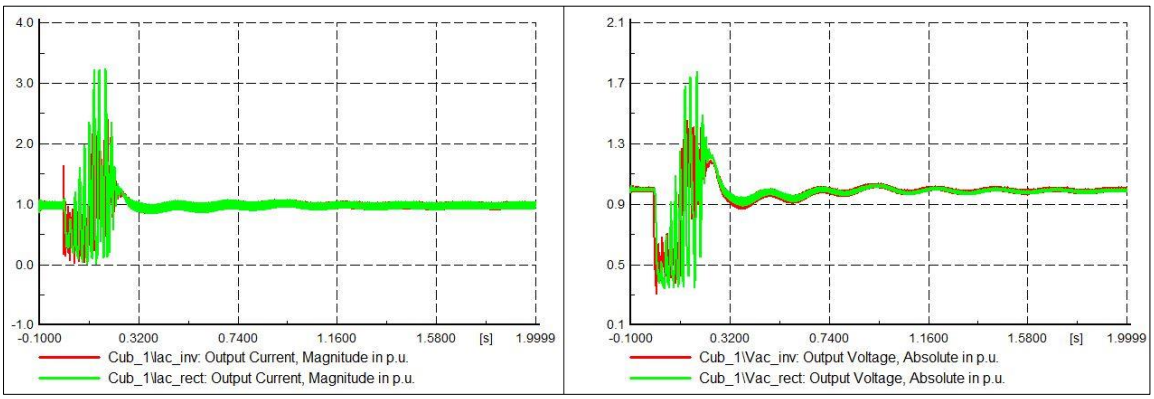

Figure 4.21: Inverter and rectifier DC voltage and current measure

Figure 4.22 and 4.23 shows the current and voltage (VDC, IDC), which is input into a filter to give (VDC_Filtered, IDC_Filtered) respectively. This can be seen from the graph that the filtered curves are much smoother than the measured curves. Each of the measured signals has a pre-set reference value (IORD, and VORD), and so the filtered signals can always take after their reference value after a fault. This could be readily seen from the graphs.

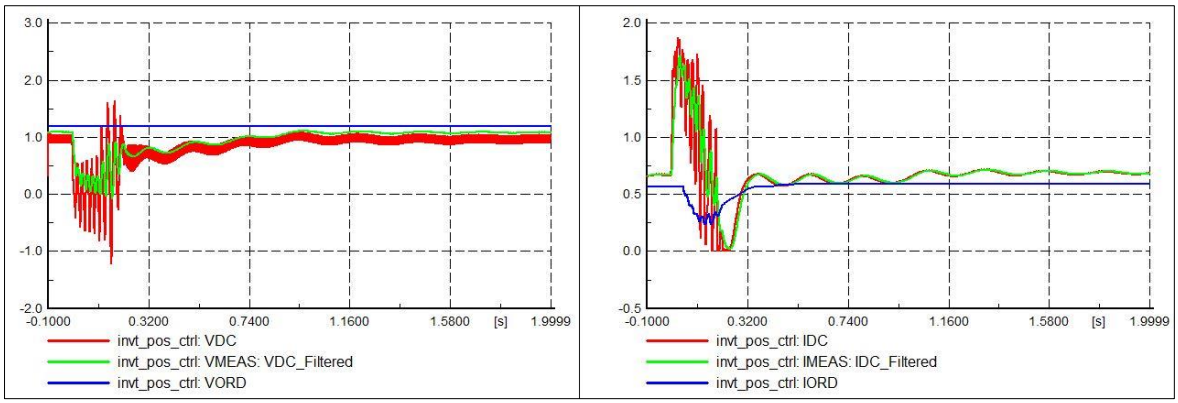

Figure 4.22: Inverter voltage and current control signals

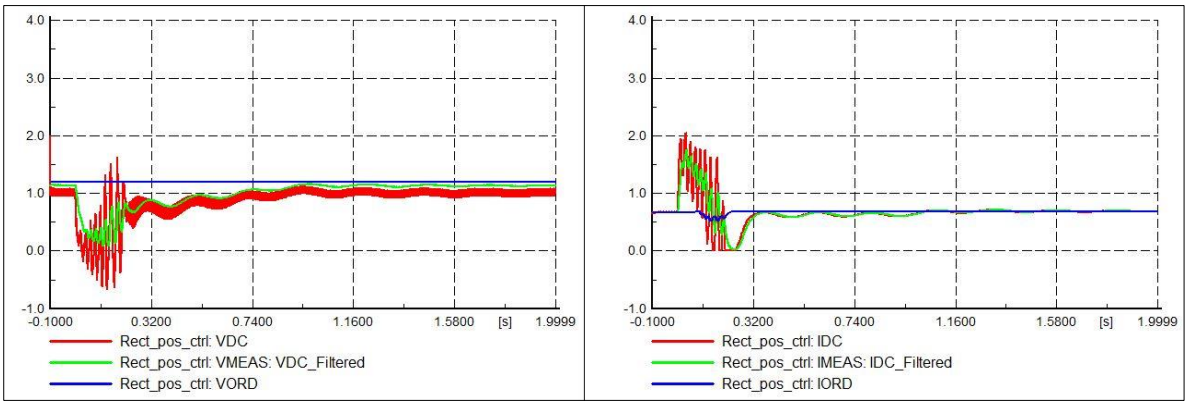

Figure 4.23: Rectifier voltage and current control signal

Figure 4.24 illustrates the rectifier firing angle and its mode selection at the inverter side. During a fault, the firing angle that is supposed to be 15^0 increased to about 89^0, VDCOL selection mode is thereby activated at the inverter side, after the disturbance, the converter switches back to its normal current control (IDC Control) mode.

At the inverter side, Figure 4.25 shows the inverter extinction angle and its mode selection at the rectifier side. It could be seen how the extinction angle slightly reduced from its operating range of 20^0 and then went up as high as 55^0 during a fault, but latter retains its pre-fault value after the fault has been successfully cleared at the inverter station.

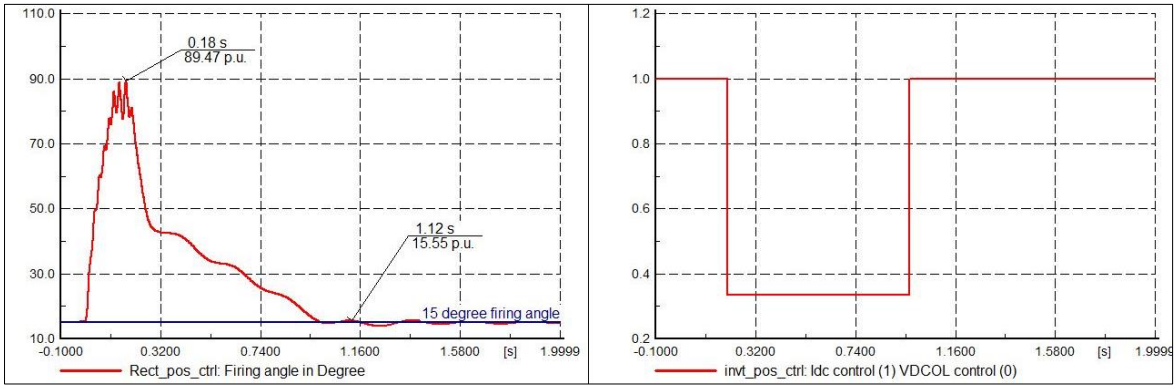

Figure 4.24: Rectifier firing angle and inverter mode selection

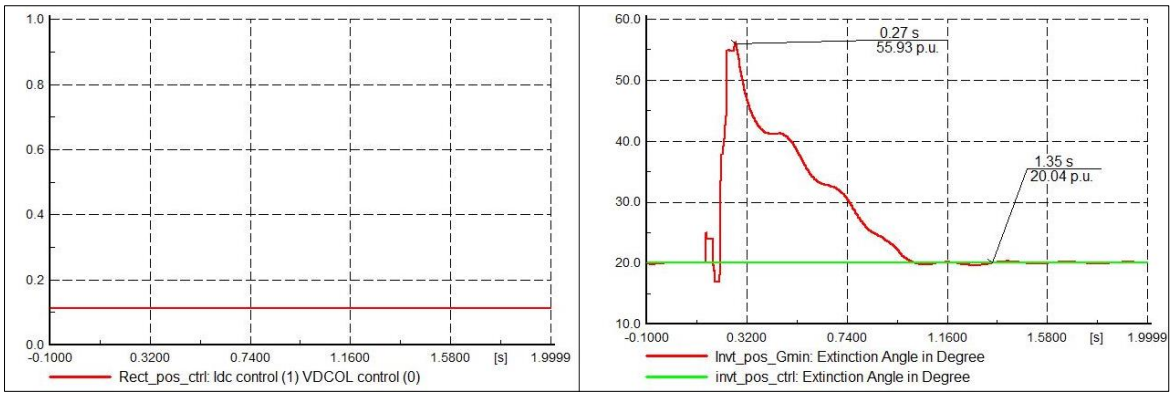

Figure 4.25: Inverter extinction angle and rectifier mode selection

Also shown in Figure 4.26 is an illustration that the DC voltage magnitudes for both positive and negative pole of the converter are the same. This justifies the fact that both poles respond to a fault in a similar manner. The only difference was change polarity. The value being ±1.0p.u before fault, dips down to about ±0p.u during a fault, and to a high value of ±1.8p.u. The pre-fault value of ±1.0p.u was maintained back after the fault was successfully cleared at the inverter AC bus.

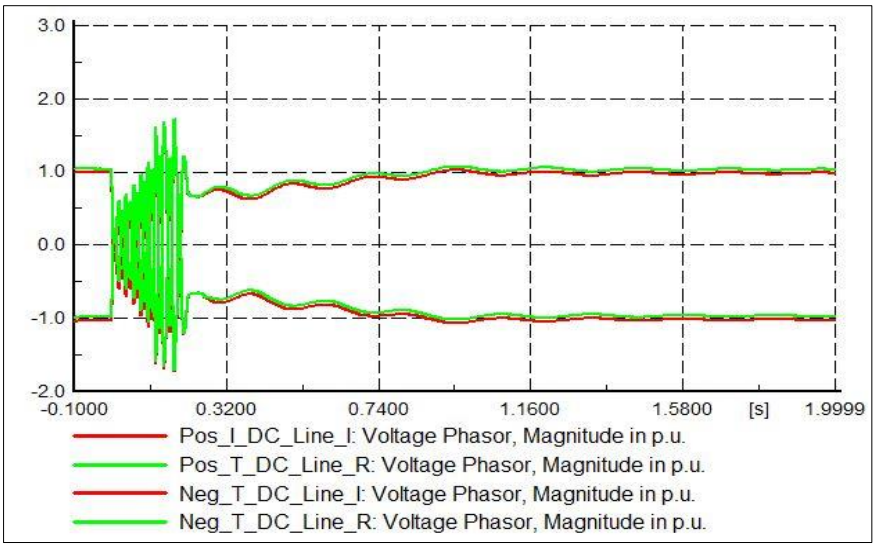

Figure 4.26: Voltage magnitude for positive and negative pole

4.4. Influence of AC System Strength on HVDC Systems

AC network strength extremely has a high impact on the AC/DC system interactions of an HVDC link capacity. AC system weakness can be because of a low inertia or high impedance. Short Circuit Ratio (SCR) which is the ratio of the MVA short circuit of the AC system (Ssc) to the MW rating of the DC converter (Pdc) is used in measuring the strength of an AC/DC system. Effective Short Circuit Ratio (ESCR) index measures the strength of AC systems considering the effect of HVDC systems connected with the controls that play a vital role in stimulating the AC systems against instability. ESCR index above 3 means the AC systems has high strength, recorded low strength if falls between 2 and 3, but very low if below 2. The AC systems become more unstable when connected with HVDC systems with ESCR value less than 2. Such system with low ESCR are likely to suffer from problems

like high dynamic overvoltage. This can eventually lead to voltage instability due to of excess reactive power at the HVDC terminal and loading sensitivity of the HVDC systems. Continuous switching of various compensating devices like the shunt capacitors, filters and reactors also caused voltage flickering which results in resonance on the AC voltage network. The use of a synchronous condenser, static VAR compensators, and very good HVDC link controller can improve the HVDC performance against system with low ESCR [81, 129, 130].

CHAPTER 5: AC NETWORK STABILITY USING HVDC SYSTEM

5.1. Power System Stability

Power systems stability is defined by Kundur 1994, as the ability of a power system that enables it to remain in a stable equilibrium state under normal operating conditions and to regain an acceptable stable state after being subjected to a disturbance [126]. Also defined by IEEE/CIGRE group as the ability of an electric power system, for a given initial operating condition, to regain a state of operating equilibrium after being subjected to a physical disturbance, with most system variables bounded so that practically, the entire system remains intact [4]. ’

A system is said to be secure if it has the ability to meet its load requirement even during disturbances and protect its network variables from straying away from their normal operating range. Power systems stability is classified based on these options as shown in Figure 5.1;

- Resulting instability physical nature.
- Disturbances size.
- The time span, processes or devices.
- Method used in the stability calculation and prediction.

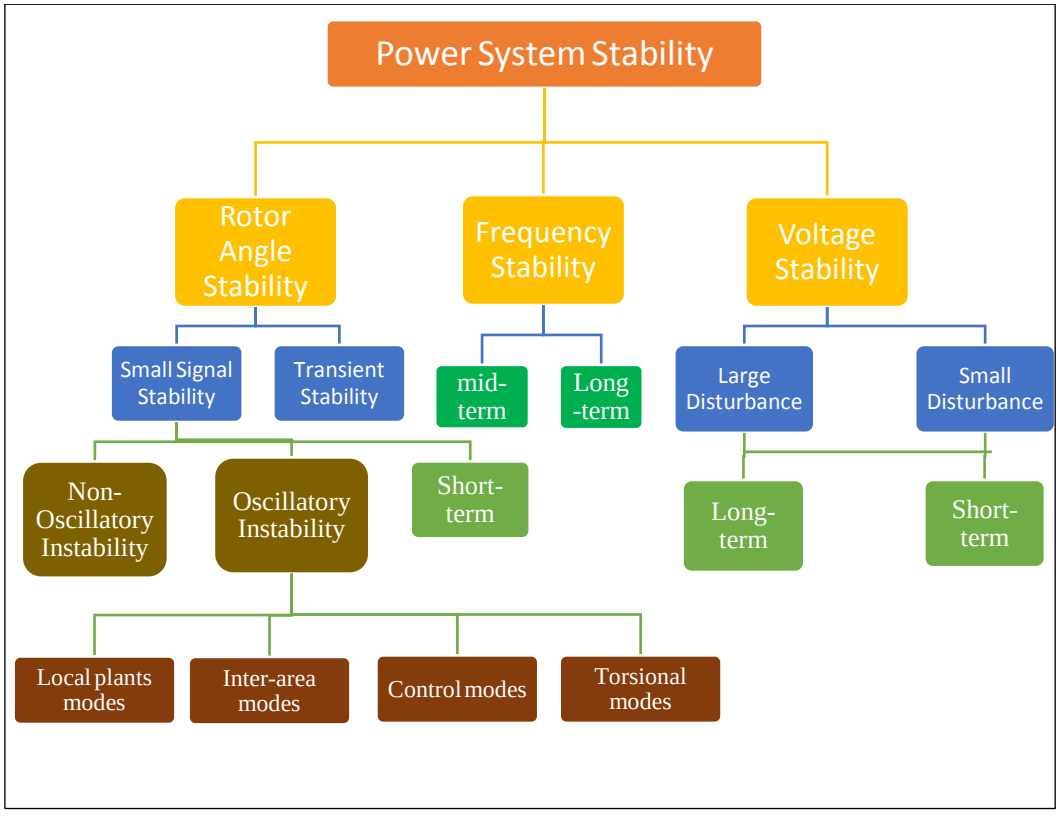

Figure 5.1: Power system stability

5.2. Voltage Stability

Voltage stability is the ability of a power system to be able to maintain an acceptable voltage profile at all buses in the power network when operated under healthy conditions or when subjected to systems disturbance. Oftentimes, power systems are always stressed beyond their stability limit. Increase in load demand, reduced generating capacity due to fault like loss of synchronization of large power plant, tripping of load and/or sudden fault on a transmission line can results in cascading effect. This caused interconnecting systems to lose their stability by not meeting active/reactive power demanded and acceptable voltage at each systems busbar. Voltage stability can be either large disturbance or small disturbance voltage stability. The former occurs when a system can control its voltage profile after being hit by a large fault, such as loss of generator or tripping of major transmission lines. While the latter occurs, when the systems still maintain appreciable voltage level at all busbar after being subjected to small disturbance like change in load.

The state of voltage instability can further lead to voltage collapse when all the voltage profile after disturbance is bellow acceptable limit in an important part of power systems such that the different part of the systems controller lost their control because they have reached their operational limit. Although, voltage stability and rotor angle stability can sometimes be linked to each other, however, the latter deals with load stability while the former manage generator stability. A lot of factors contribute to voltage instability/collapse, few which are mentioned are;

- The level of power transfer and transmission network strength.
- Generator field current characteristics.
- Voltage dependence of the load.
- Reactive power characteristic of compensating devices.
- Transformer voltage controller (under load tap changers ULTC).

The generator has an automatic voltage regulator AVR, through the help of the field and armature current windings. During normal operation, the terminal voltage of the generator is maintained constant by the field current, which gets reduced during a disturbance in order to avoid overloading of the generator. This aims at maintaining synchronism between the generator and the grid. Some loads characteristics do have an effect on voltage stability because their active and reactive power is voltage dependence. Since reactive power flow to the area of low voltage, during a situation of low voltage condition, the load absorb reactive power more. This tends to drop the voltage profile further.

Reducing the occurrence of voltage stability brings about compensating device likes the shunt capacitor, regulated shunt capacitor, and series capacitor.

- **Shunt Capacitor**: this is one of the most inexpensive means of improving voltage profile in a power system. Only suffers setback during a condition of low voltage as its VAR support drops because it is proportional to the square of the voltage. This situation further compounds voltage instability problem.
- **Static VAR compensation (SVC)**: also improve voltage profile within its operational limit, but becomes a simple capacitor when stressed beyond its limit.
- **Static Synchronous condenser (STATCOM)**: this is the best method of providing reactive power support to systems. It provides the VAR support to the system even during a relatively low voltage. This is because it has an internal voltage source.
- **Series capacitor**: since its reactive power supplied is proportional to the square of the line current and independent of the bus voltage, therefore, self-regulate the reactive power supplied base on the systems demand.

5.2.1. Two terminal network

A simple two-terminal transmission network shown in Figure 5.2 can be used to study the behaviour of voltage stability, with E representing the sending end voltage at the generator side and V representing the voltage at the load end. Current flowing in the network is calculated according to equation 5.1 – 5.5. As the load demand increases by decreasing load impedance, the load power PR increases rapidly, reaches its maximum at (Z_{ld}=Z_{ln}=1), and then start to decrease. More increase in load demand beyond the critical point can eventually result in system collapse. This was well represented on Figure 5.3. [126]:

$$I = \frac{E_S}{\sqrt{\left(Z_{\ln}\cos\theta + Z_{ld}\cos\phi\right)^2 + \left(Z_{\ln}\sin\theta Z_{ld}\sin\phi\right)^2}} \tag{5.1}$$

$$I = \frac{1}{\sqrt{F}}\frac{E_S}{Z_{\ln}} \tag{5.2}$$

$$F = 1 + \left(\frac{Z_{ld}}{Z_{\ln}}\right)^2 + 2\left(\frac{Z_{ld}}{Z_{\ln}}\right).\cos\left(\theta - \phi\right) \tag{5.3}$$

$$V_R = Z_{id}.I \tag{5.4}$$

$$P_R = V_R.I\cos\phi = \left(\frac{Z_{ld}}{F}\right)\left(\frac{E_S}{Z_{\ln}}\right)^2\cos\phi \tag{5.5}$$

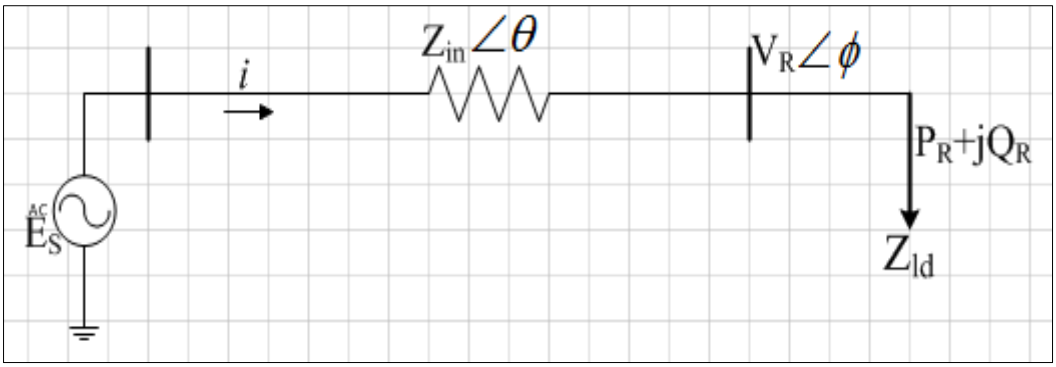

Figure 5.2: Two terminal network

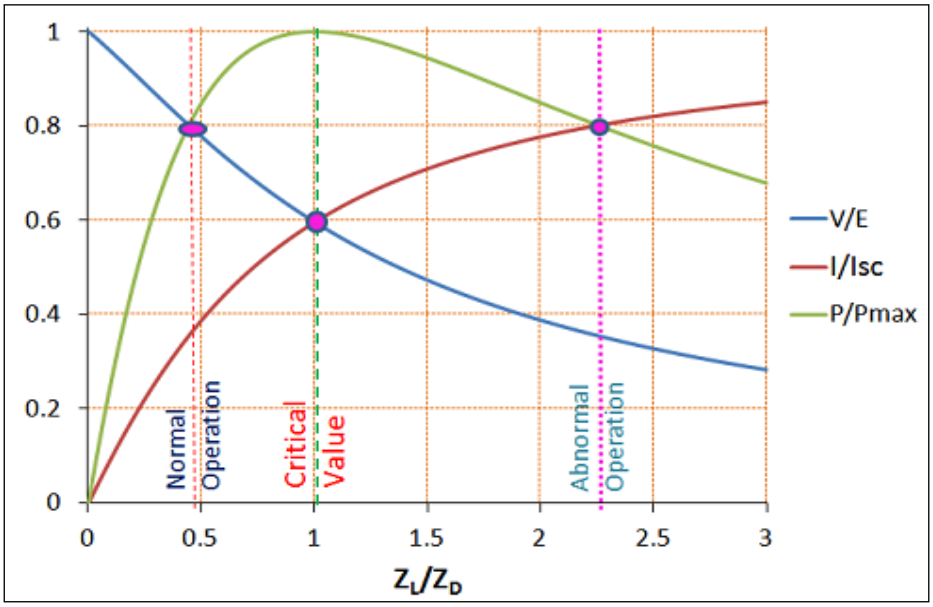

Figure 5.3: Receiving and power, current and voltage as a function of load impedance [126].

5.2.2. V-Q sensitivity analysis

Static analysis of voltage stability in [131-133] uses reduced Jacobian matrix to analyse the voltage sensitivity of a particular bus to change in reactive power in that bus while the active power is kept constant (5.6 – 5.9)

$$\begin{bmatrix}\Delta P\\ \Delta Q\end{bmatrix}=\begin{bmatrix}J_{P\theta} & J_{PV}\\ J_{Q\theta} & J_{QV}\end{bmatrix}\begin{bmatrix}\Delta\theta\\ \Delta V\end{bmatrix} \tag{5.6}$$

Let ΔP=0, then

$$\Delta Q=\left[J_{QV}-J_{Q\theta}J_{P\theta}^{-1}J_{PV}\right]\left[\Delta V\right] \tag{5.7}$$

$$\Delta Q=J_R\Delta V \tag{5.8}$$

$$\Delta V=J_R^{-1}\Delta Q \tag{5.9}$$

Where; ΔP is Incremental change in bus real power

ΔQ is Incremental change in bus Reactive Power

$\Delta\theta$ is Incremental change in bus Voltage phase angle

ΔV is Incremental change in bus voltage magnitude

J_R^{-1} is called the V-Q sensitivity as it value determines how stable the system is. A positive value indicates a stable system while a negative value indicates an unstable system. For a positive value, the smaller the sensitivity value, the more stable the system becomes, meaning as load increases, the value tends towards infinity signifying an unstable system condition.

5.2.3. Modal analysis

For the modal analysis that explains different snapshot of voltage sensitivity to reactive power, this is given in equation (5.10 – 5.14).

$$J_R = \xi\Lambda \tag{5.10}$$

$$J_R^{-1} = \xi\Lambda^{-1}\eta \tag{5.11}$$

$$\Delta V = \xi\Lambda^{-1}\eta.\Delta Q \tag{5.12}$$

Since $\xi^{-1}=\eta$, i.e. an identity matrix.

Therefore,

$$\eta\Delta V = \Lambda^{-1}\eta.\Delta Q \tag{5.13}$$

$$v = \Lambda^{-1}q \tag{5.14}$$

($v=\eta\cdot\Delta V$) is the vector for the modal voltage variations and ($q=\eta\cdot\Delta Q$) is the modal of reactive power variations.

5.2.4. Load flow analysis

Load flow analysis is a means of finding out the operating condition of a network but establishing the bus voltage, elements loading, active and reactive power at different bus and nodes of a power transmission network. This helps gives the steady state of a network. It also helps engineers to make adequate plans for any foreseeable load changes or for proper forecasting. Different methods for load flow calculation have been developed by researchers such as Newton-Raphson method (NRLF), Gauss-Seidel, decoupled and fast-decoupled method. All these methods are used for AC load flow calculation as well as DC load flow. Although, each method have a different approach with different parameters, but NRLF has been well adopted in this research study for power flow calculation because it has some HVDC parameters such as the firing angle and control measures adapted into its equations. This method is adopted by DIgSILENT PowerFactory. It solves a set of simultaneous nonlinear equation iteratively. More about a method for calculating load flow in power system are well discussed in [134-137].

5.2.5. P-V and Q-V curve

P-V curve is a static analysis approach used in determining the voltage stability of a radial or large meshed network. The curve shows how the voltage V of a particular area decreases with a step increase of power. The critical position is reached when a further increase in loads brings about a drastic drop in the bus voltage. Figure 5.4 shows PV curve for a simple two-terminal network of Figure 5.2. P represent the point of maximum loading (maximum power transfer). At this point P, the load flow solution will not converge. This means a point of instability. Below point P signify near instability operation of power systems. This exposed the system to a large scale of collapse or blackout at point Q. Point XY shows the satisfactory operating condition that gives rooms for power stability margin.

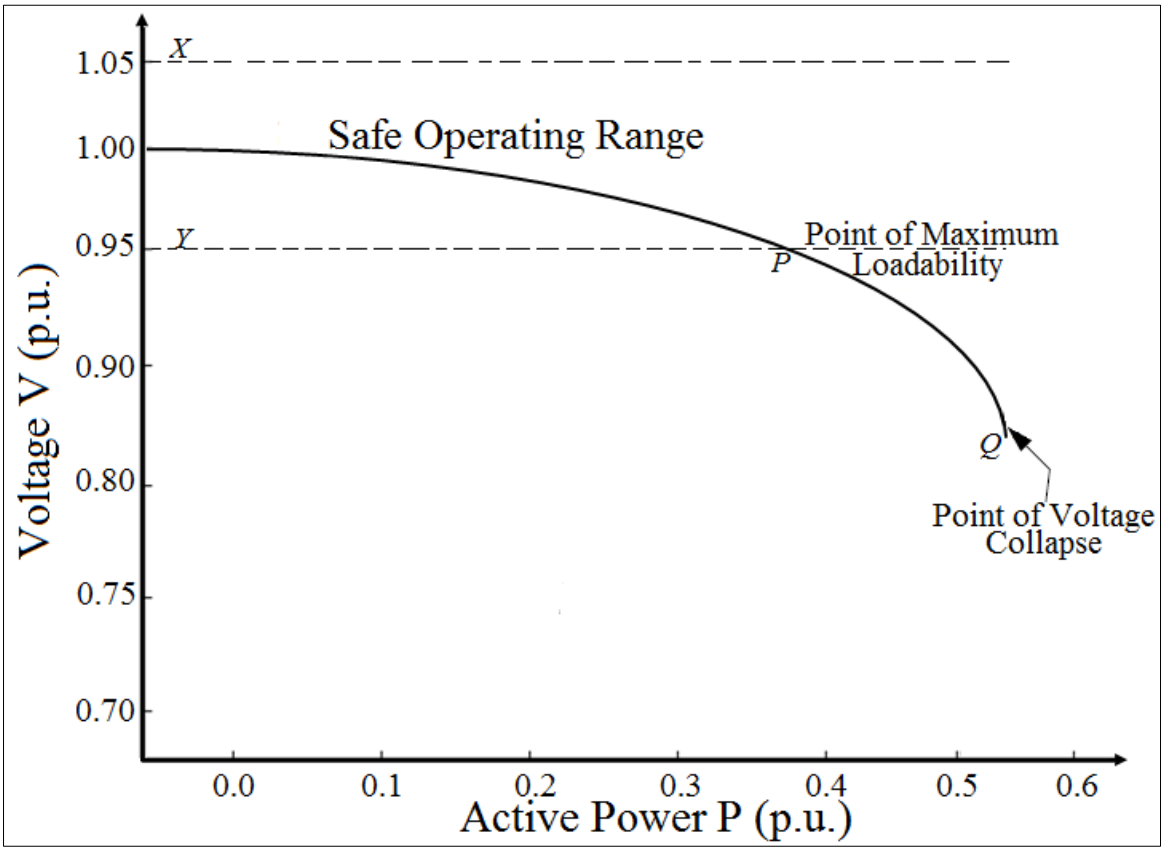

Figure 5.4: The PV-curve in per-unit

Q-V curve gives the relationship between the bus voltage and the reactive power support for a different value of active power transfer. As shown in Figure 5.5, the stability of the network at different load level P_{L1} or P_{L2} depends on the amount of reactive power injected. Point A to B show the stable region when there is no reactive power support at the load end. While B, C and D show the unstable region. The systems become more stable as more reactive power (negative Q) are injected at the load end.

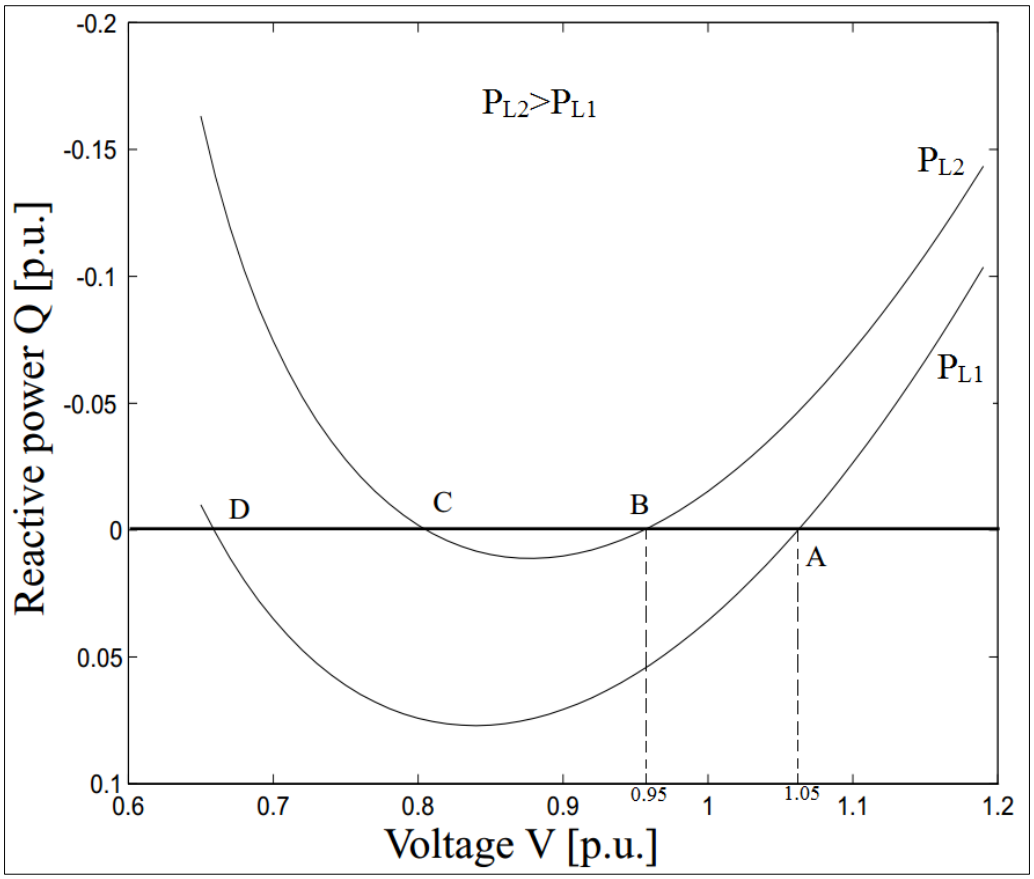

Figure 5.5: The QV curve in per-unit for two different active loads [138].

5.3. Simulation of Three Test Networks

The test networks used for this investigation are the; two-bus network, multi-terminal networks and the IEEE 30-bus network. The following subsequent sections will give full details about their models. More information as regards the network parameters can be seen in Appendix (APP 2).

5.3.1. Test network 1 (Two-bus network)

A small test network shown in Figure 5.6 was used for better understanding of the effect of load increase on voltage stability. The test network consists of an external grid connected to a 400kV busbar that is linked to another 400kV transmission line via a two circuit (400km and 300km) overhead line. A load of 800MW, 0.9P.F. is connected to it. P-V and Q-V curves are used to analyse the voltage stability of the network. The former shows how an increase in power in a particular area causes a reduction in bus voltage while the latter shows the amount of reactive power needed to be injected/absorbed to keep a system stable at an acceptable voltage level for different load levels. DIgSILENT P-V and Q-V script were used to generate the simulation graph displayed in this study. This script uses series of load flow simulation on Newton-Raphson iterative load flow equation to plot the graph.

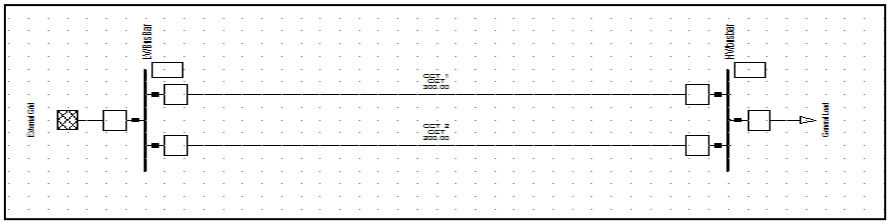

Figure 5.6: Two-bus network

Figures 5.7 is a P-V curve showing the allowable power that can be transferred for different power factors before the receiving end voltage falls below 0.95p.u while its Q-V curve as shown in Figure 5.8 illustrates the amount of reactive power needed to keep the busbar voltage profile at 0.95 – 1.05p.u.

A scenario that the longest transmission line tripped because of a fault on the line will result in heavy loading of the other line. The fault will lead to increase in reactive power absorbed by the load that will eventually lead to minimal power transfer along the healthy line. A fault that is unattended to, in an important part of a power system, can eventually lead to a system collapse if adequate measures are not put in place.

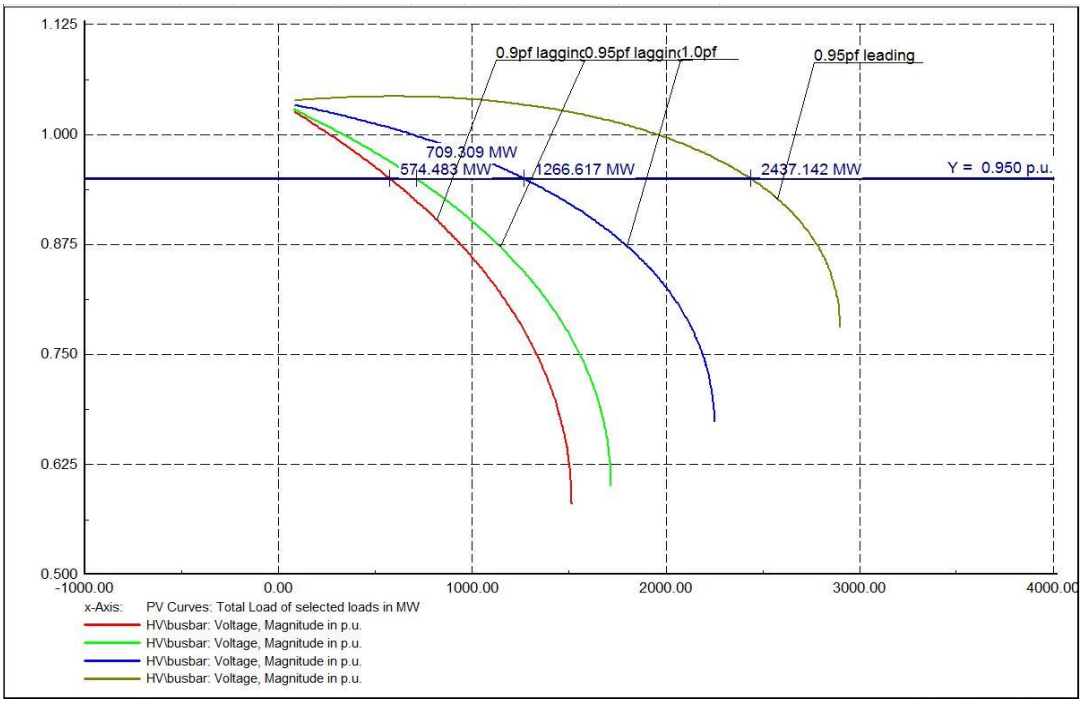

Figure 5.7: P-V Curve for different power factor.

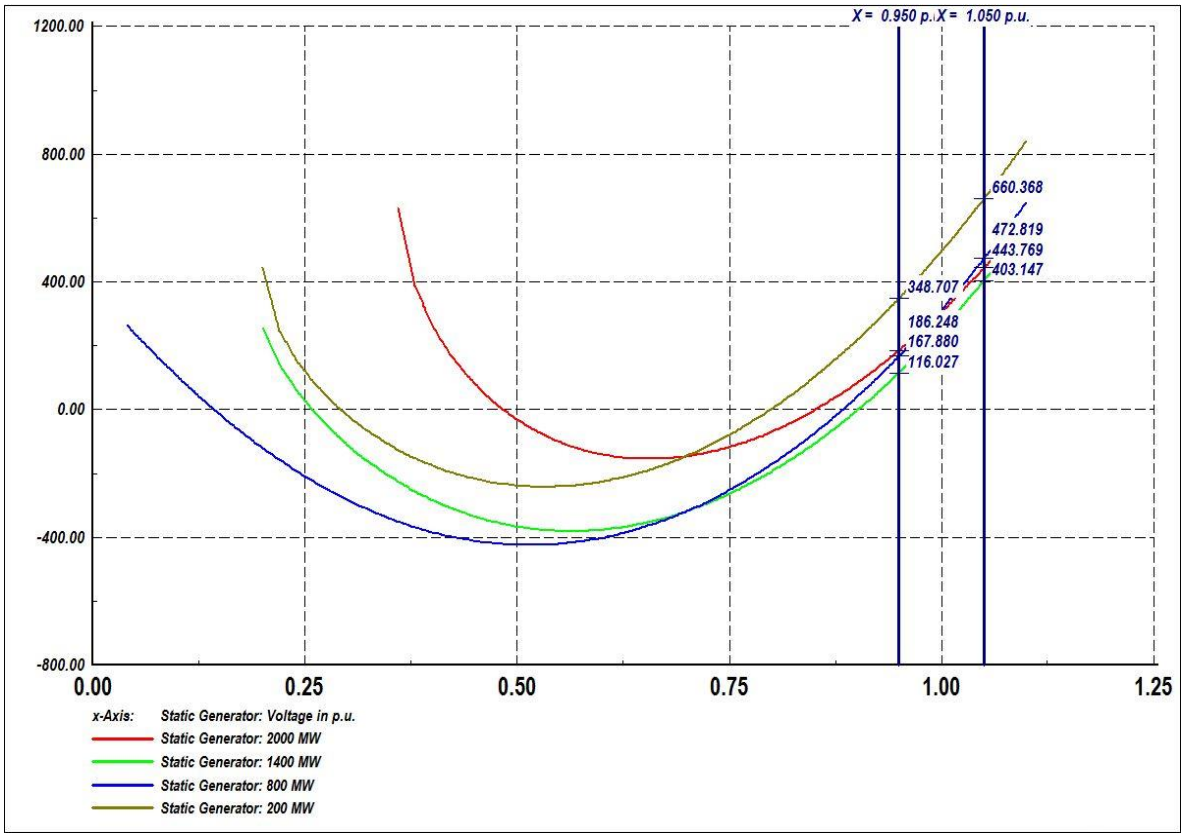

Figure 5.8: Q-V Curve for different power level.

5.3.2. Test network 2 (Multi-machine network)

For a better understanding of this project, a larger system of 24 buses was used to implement the little experience gotten from the small test network. The network is divided into four geographical area interconnected by a number of tie lines as presented in Figure 5.9. Area Northwest, Southwest and Northeast are connected closely with short tie lines, whereas the area Southeast is loosely connected to the rest of the systems via two circuits of 600km tie lines, (the longest line in the network). The Southeast area is selected for this voltage stability study because it is loosely connected to the rest of the network and prone to voltage instability upon an increase in load demand.

The Southeast has 6 generators with total installed capacity of 1664MW supplying a load of 2300MW and 20MW of motor load. Due to a shortage of generating capacity, the Southeast area depends solely on the power coming from Northeast area via the Southeast border interconnection. Voltage stability of the critical busbar (bus SS16.2/BB2) was used as the reference bus. Different series of load flow scenario were taken, to investigate to what extent the area is stable.

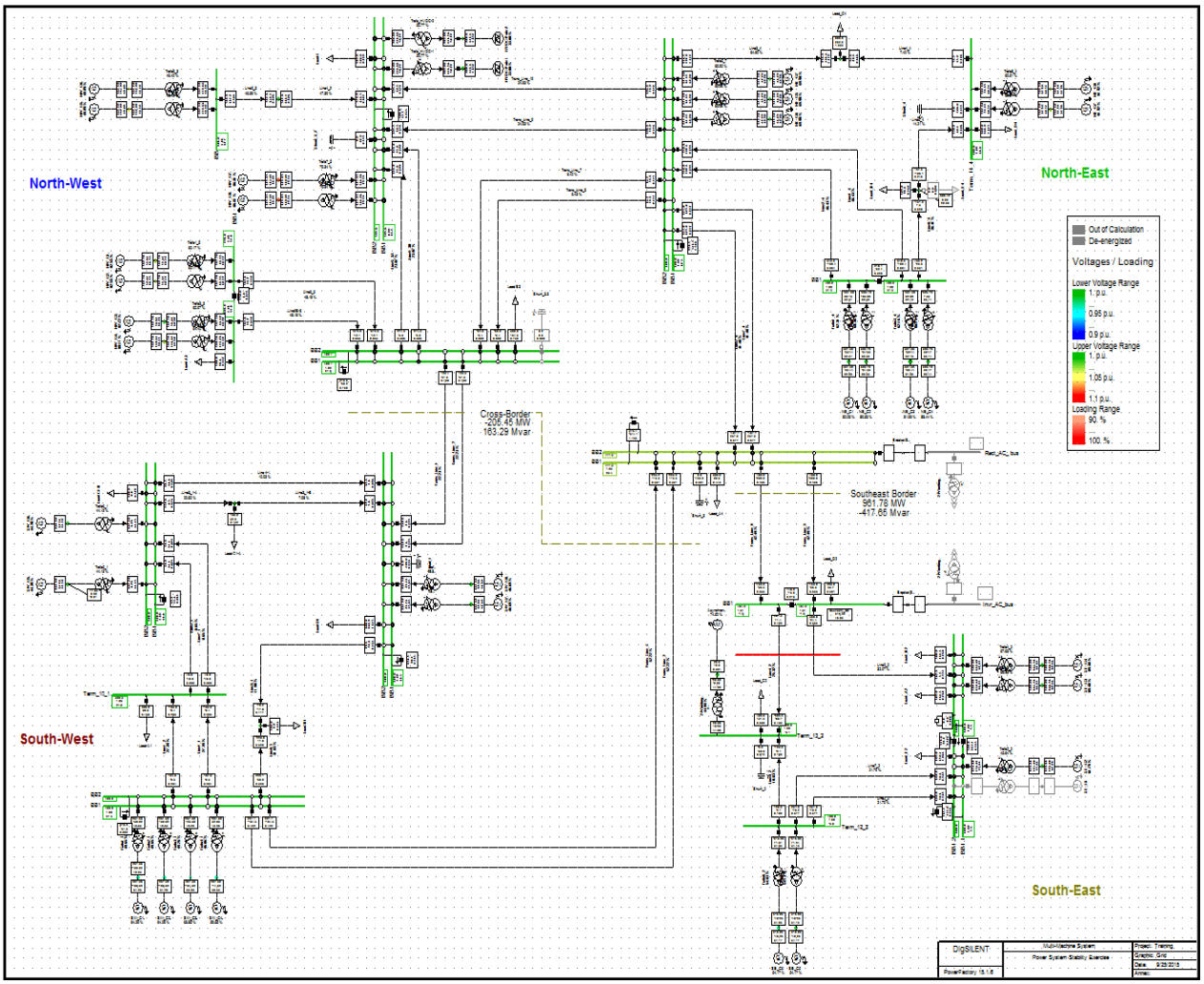

Figure 5.9: Four area multi-machine network

A scenario whereby the existing AC tie line was replaced with an HVDC line was carried out and its effect on voltage stability of the area. The results are compared to see if an HVDC network increases the voltage stability of the area upon load increase at the critical bus and in the Southeast area.

The two methods used in the P-V curve diagram is to first increase the load connected to the critical busbar step by step, and the voltage level of the bus is plotted against load power. The second approach is to look into the amount of load the Southeast area can withstand before instability occurs. This is done by increasing all the load in the area Southeast, then plotting the voltage against total load increase.

All the busbars in the southeast area were first selected and different scenarios were carried out on it. The aim is to get the busbar that is more prone to voltage instability upon load increase. There it was found out to be bus SS16.2/BB2 (critical busbar) as shown in Figure 5.10. All other busbars still maintain their voltage limit even after being subjected to different load increase and disturbances due to nearness to a generating plant. But the critical bus SS16.2/BB2 was found to be the major bus that fails to restored to its stable region even during small load increase or disturbance.

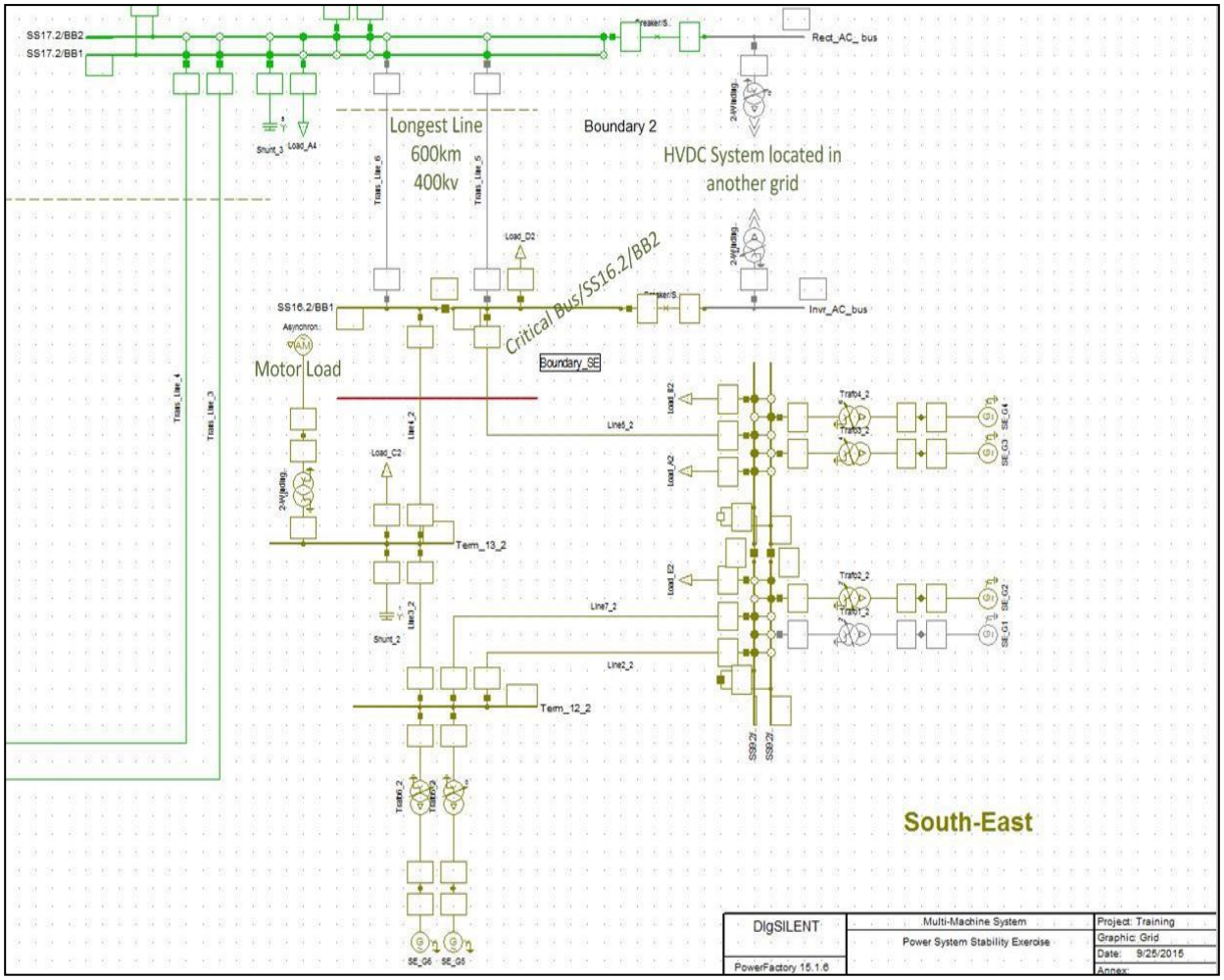

Figure 5.10: Southeast region of the multi-machine network

Hence, the reason why voltage analysis becomes a serious issue to be considered in this multi-machine network. Figure 5.11 shows the maximum load power that can be connected to the critical bus when using AC lines of different power factor for the load. It can be seen from the diagram that the load could only be increased to 664MW, 704MW and 786MW for 0.9, 0.95 and 0.95 power factor respectively before the voltage level drops below 0.96p.u. (The region where the system rate of entering voltage collapse increases). Figure 5.12 shows the relationship between the load and the critical bus voltage when HVDC line was used. It can be seen that the load can accommodate an approximate double of the power in AC lines for different power factors before the voltage level falls below the acceptable limit. Figures 5.13 and 5.14 show the power that can be transferred from Northeast area to Southeast area before voltage instability occurs at Bus 'SS16.2/BB2' for AC and HVDC lines respectively. It can be seen that HVDC line offers higher power transfer capacity before instability occurs as compared to the conventional AC lines. Reason being that HVDC line is well equipped with good control action that tends to keep the voltage constant even during a fault or a situation when there is rapid increase of load.

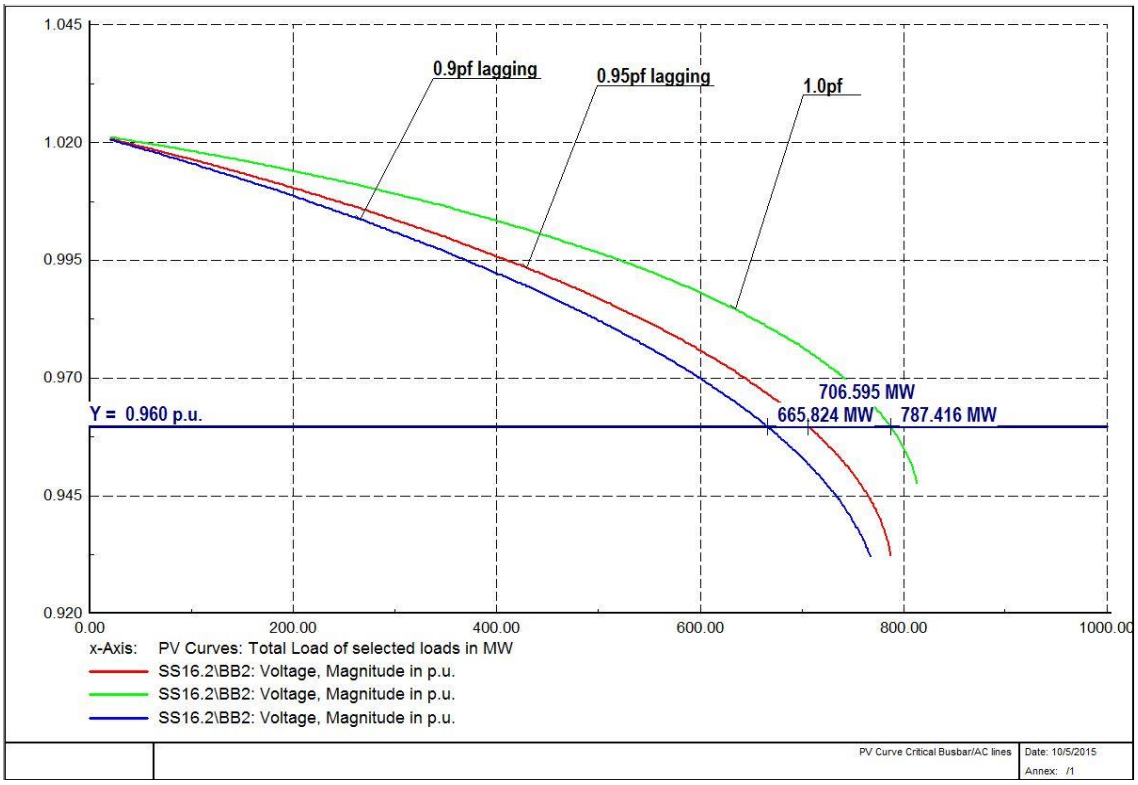

Figure 5.11: P-V curve for critical Bus when fed with AC line.

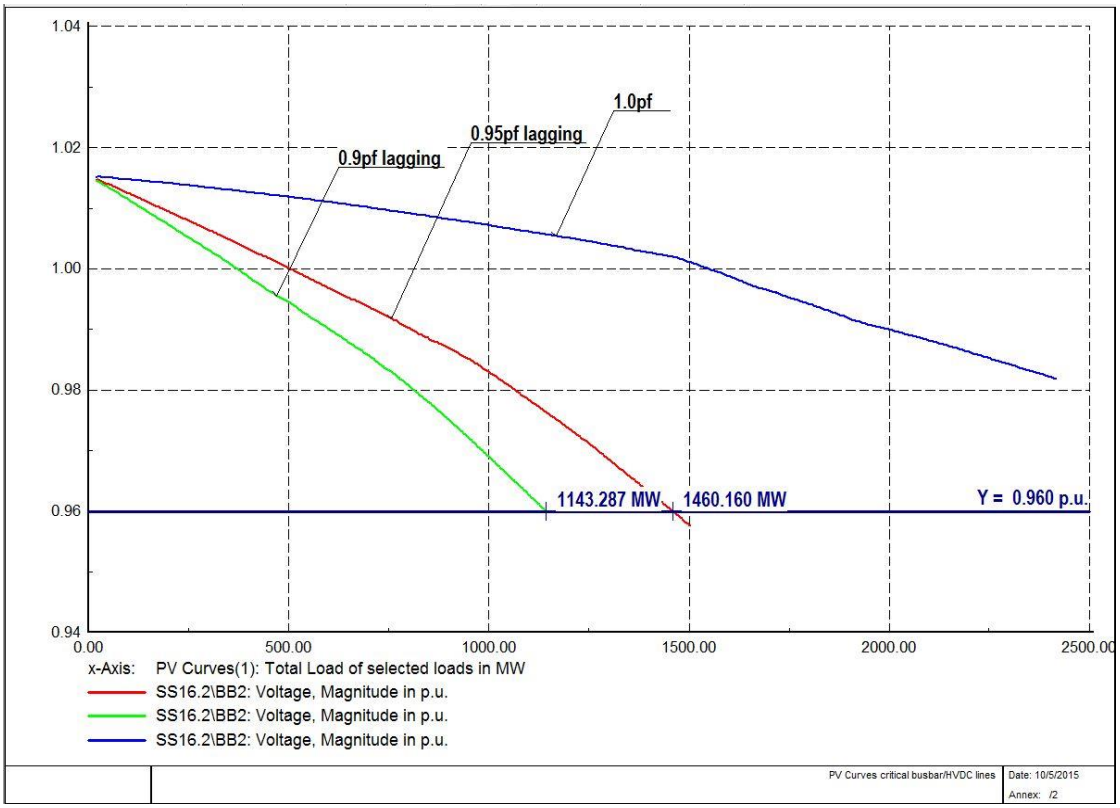

Figure 5.12: Curve for Critical Bus when fed with HVDC Lines

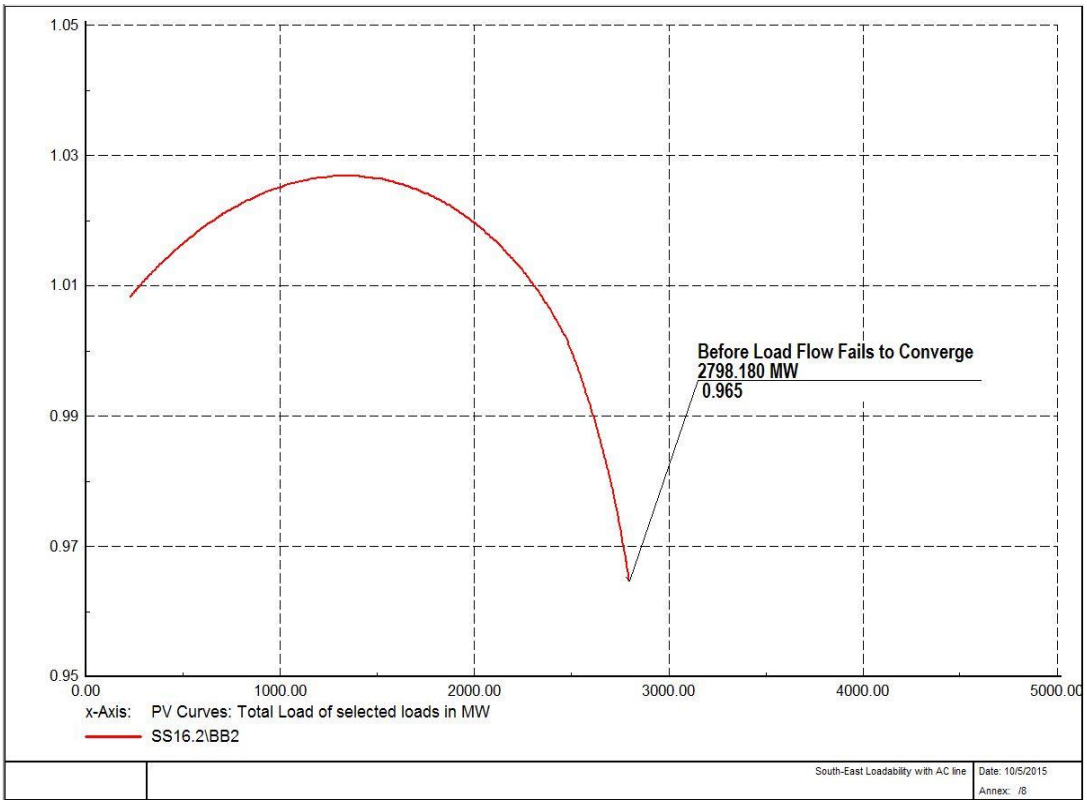

Figure 5.13: Loadability of South-East Area with AC lines.

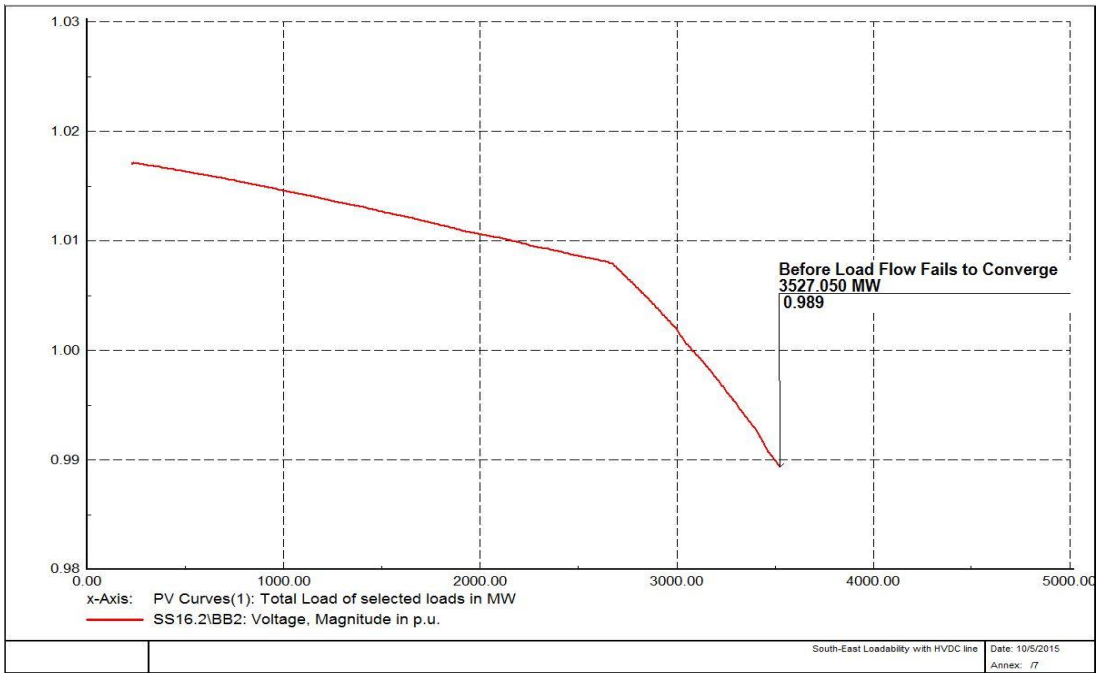

Figure 5.14: Loadability of South-East Area with HVDC line.

5.3.3. Test network 3 (IEEE 30-bus network)

A modified IEEE 30 bus test network was used for this study. The test network is a representation of a portion of the American electric power system (in the Midwestern US) as of December 1961. Figure 5:15 show the modified IEEE 30 bus test network as setup on DIgSILENT PowerFactory. The modified network consists of 30 buses, 8 generators, 20 loads, 40 lines, 11 transformers, 1 shunt

capacitor, and 1 shunt reactor. The main voltage level of the network is 400kV (nominal voltage) with nominal transmitting frequency of 50Hz. The 132kV of bus 19, bus 20 and bus 21, and the 11kV of bus 15 and bus 18 were assumed on PowerFactory for this study.

a. Model parameters

The model parameters were based on calculations and use of standard IEEE models, because most data unit were not specified by different online sources for the IEEE 30 bus systems.

- **Load model**

The loads are modeled to be voltage dependent with constant active and reactive power demand for load flow calculation and for stability analysis according to (5.15). The value of Kp is set to be 1 for active power (constant current) and 2 for the reactive power (constant impedance) [15].

$$P + jQ = P_0\left(\frac{U}{U_0}\right)^{kp} + Q_0\left(\frac{U}{U_0}\right)^{kp} \tag{5.15}$$

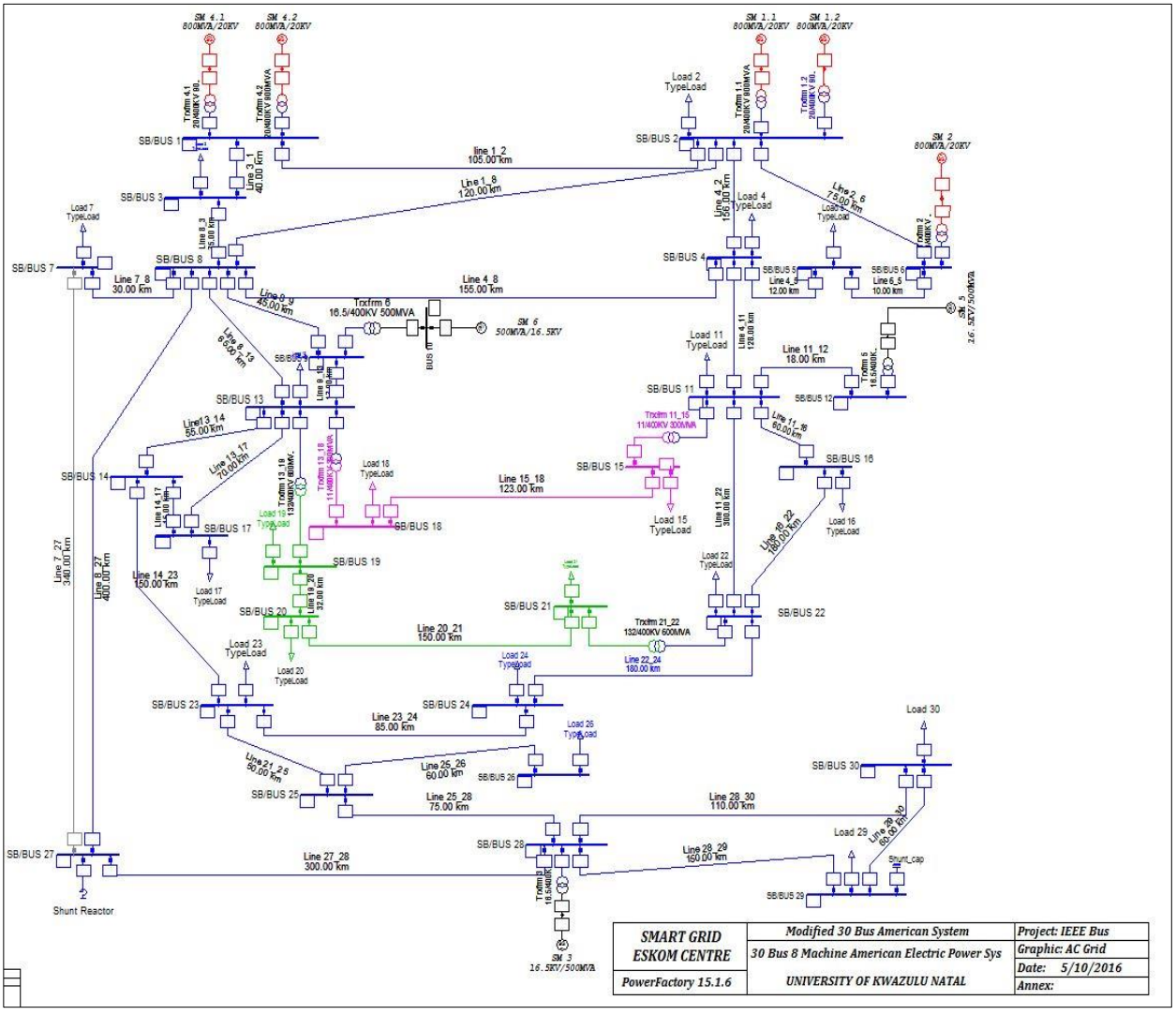

Figure 5.15: Single line diagram of the modified IEEE 30 bus system.

- **Generator model**

All the generators are connected via a transformer. SM (synchronous machine) was used on PowerFactory to name all the generators. SM 1.1 with 0^0 voltage angle and 1.00pu voltage set point were used as the reference machine because it is connected to the bus with the highest fault level. All generators were set to be in voltage control mode.

Two generator types were used, first is the 16.5kV, 500MVA used by SM 3, 5 and 6 and the other synchronous machine uses the 20kV, 800MVA type.

All generators are rated for realistic inertial time constant and modeled using the IEEE controller model on PowerFactory for the automatic voltage regulator, governor control as well as the power systems stabilizer (but the PSS for all the generator are disabled due to set point error). More details about the generator controllers can be seen in Appendix (APP 2).

- **HVDC model**

The HVDC network is modeled as represented in Figure 5.16 with the parameter on Table 5.1. The 1350MW monopolar with 600kV operating voltage transmits power over a distance of 700km. The reliability of the HVDC network was put to test using a three-phase fault at the inverter terminal (fault reactance of 10Ω for 200ms. The result shows a commutation failure at the inverter side of the converter. The voltage dependent current order limiter (VDCOL) was activated because of a reduction in DC voltage. The commutation failure was resolved when the rectifier controller reduces the DC current to allow minimum power across the link during fault conditions. With this, most of the DC faults are self-clearing with the help of a well-equipped controller.

Equations (5.16) and (5.17) show the fundamental law governing the HVDC systems.

$$V_{dI} = \frac{3\sqrt{2}\alpha_I V_{tI} \cos\gamma_I - 3X_C I_d}{\pi} \tag{5.16}$$

$$V_{dR} = \frac{3\sqrt{2}\alpha_R V_{tR} \cos\alpha_R - 3X_C I_d}{\pi} \tag{5.17}$$

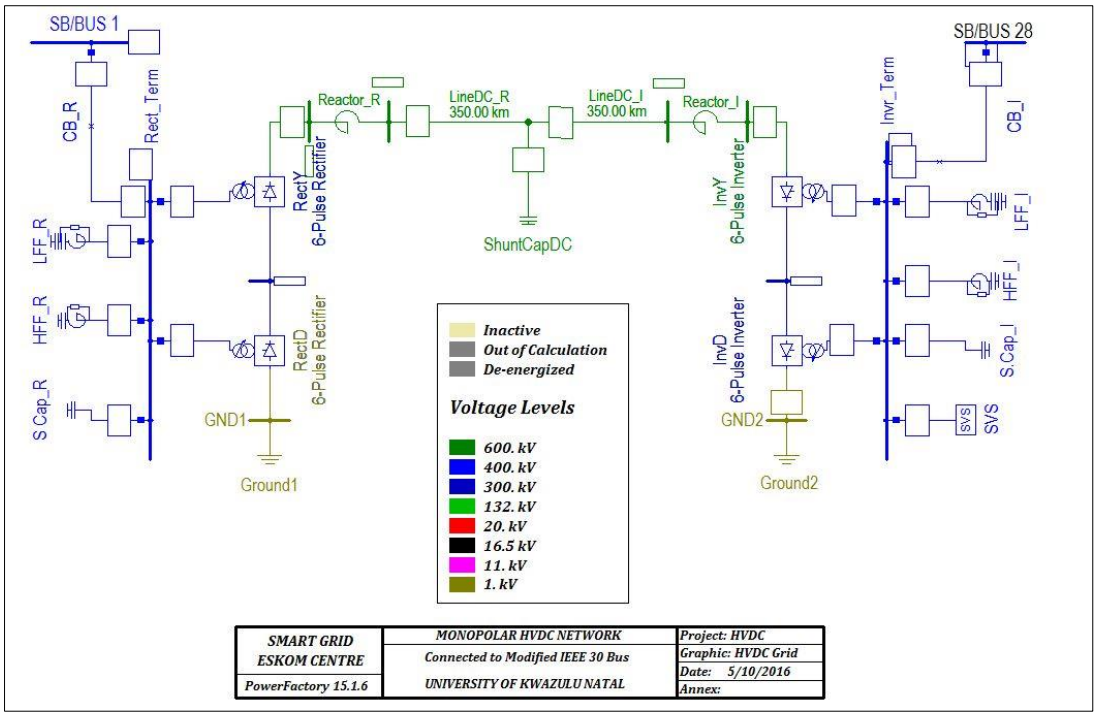

Figure 5.16: Monopolar HVDC model.

Table 5.1: HVDC data

HVDC Parameters		
	Rectifier	**Inverter**
AC Voltage (kV)	400	400
Firing angle control	Current control	Voltage control
Commutation Reactance	13.445Ω	13.445Ω
Tap changer control	α-control	γ-control
Actual winding ratio	0.97	0.97

b. Simulation result

The results consist of both the steady state power flow results, which are depicted in bar graphs, and transient stability analysis results that are configured using the real-time RMS simulation. Two operational scenarios were considered in this study. The first scenario is when the power is being transmitted using AC lines only, and the second scenario is when an existing AC 'line 8_27' is replaced with a monopolar HVDC system shown in Figure 5.16.

- **Steady-state load flow (HVAC/HVDC)**

The steady state load flow results follow the Newton-Raphson iterative equation for power flow calculation. Figures 5.17 to 5.23 show the steady load flow presented in a bar diagram format for the bus voltage magnitudes, generator power (P/Q), the line loading, and load active and reactive power respectively when either AC or HVDC line was used for power transmission. Figure 5.17 show the busbar voltage profile when AC lines only were used for power transfer while Figure 5.18 show the same Busbar voltage when HVDC line was used. Little difference could only be noticed on this bar-

diagram as both subplots meet the require 0.95p.u. voltage profile. The generator active and reactive power also are shown in Figure 5.19 and 5.20.

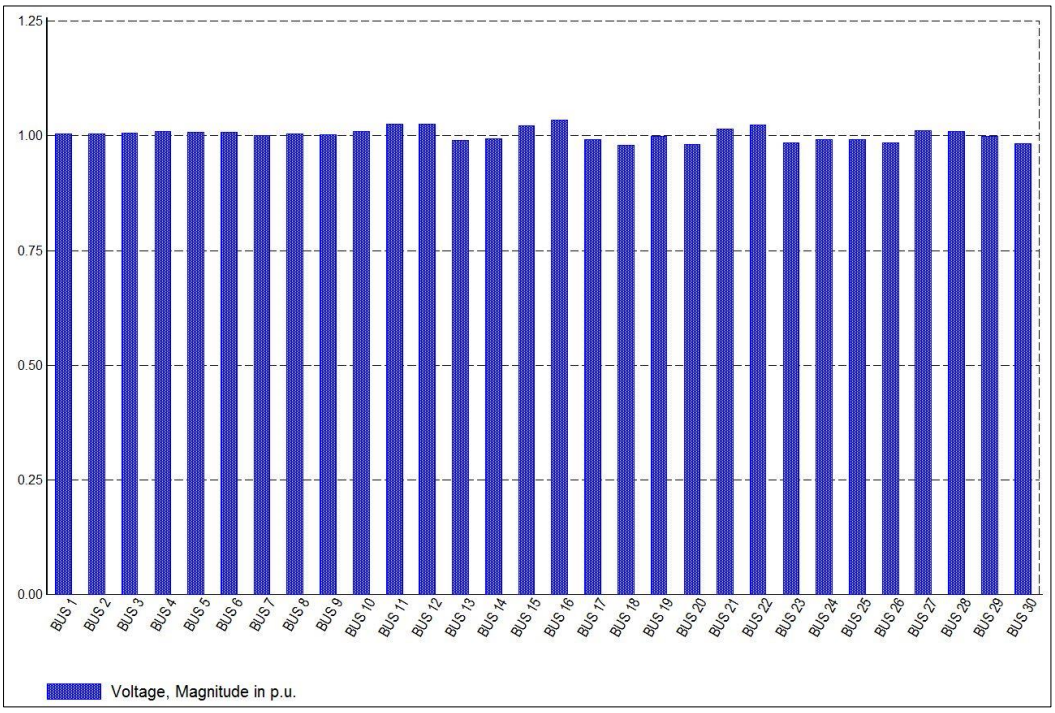

Figure 5.17: Busbar voltage magnitudes (HVAC line only)

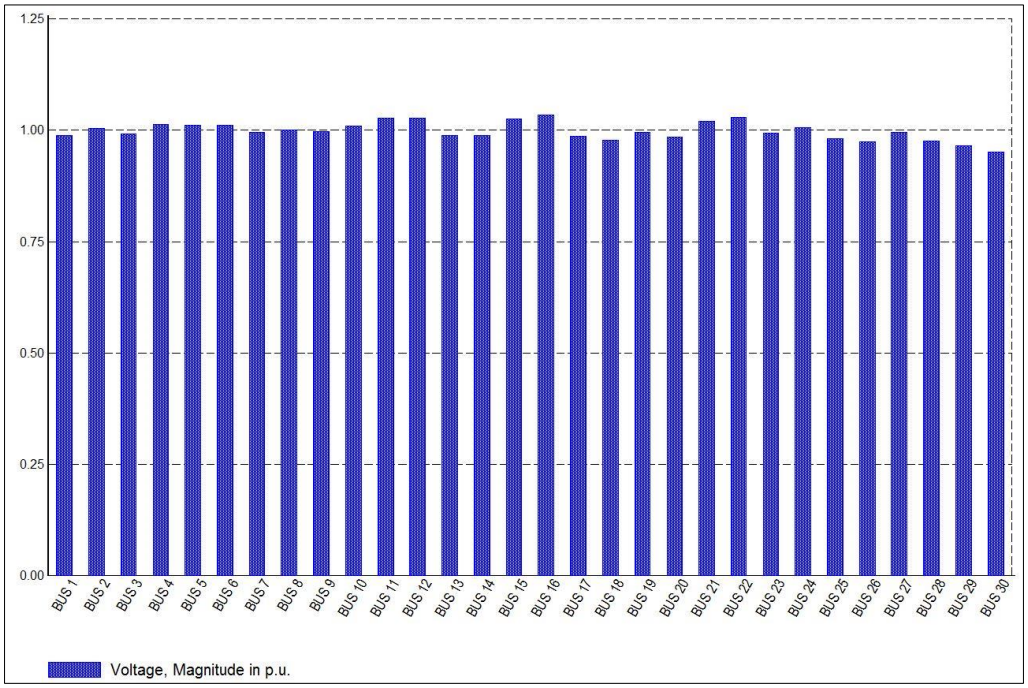

Figure 5.18: Busbar voltage magnitudes (with HVDC line)

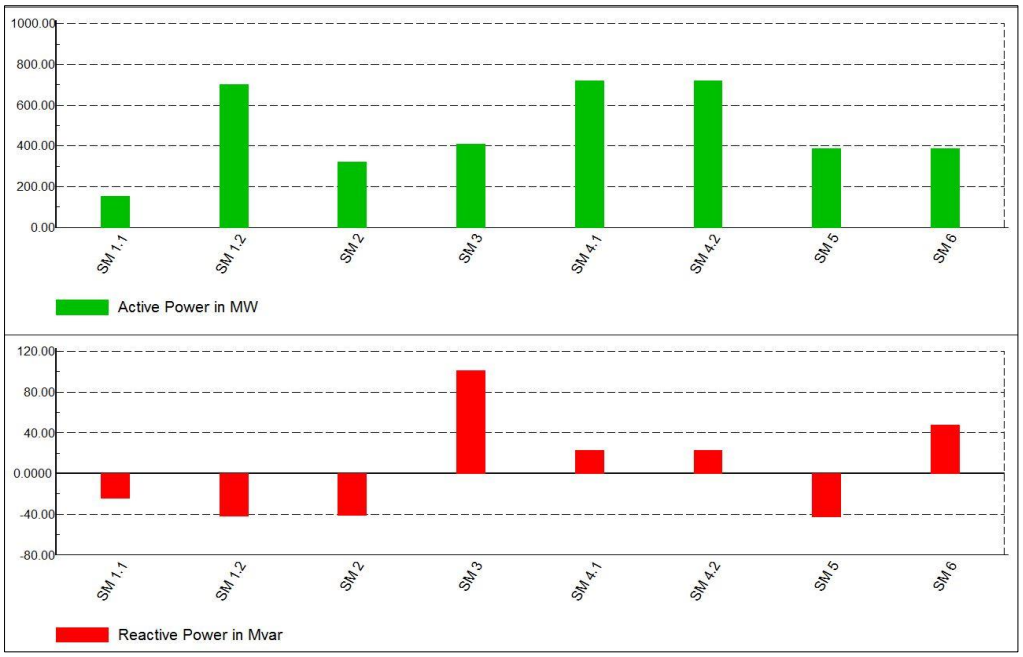

Figure 5.19: Generator active and reactive power (AC line only)

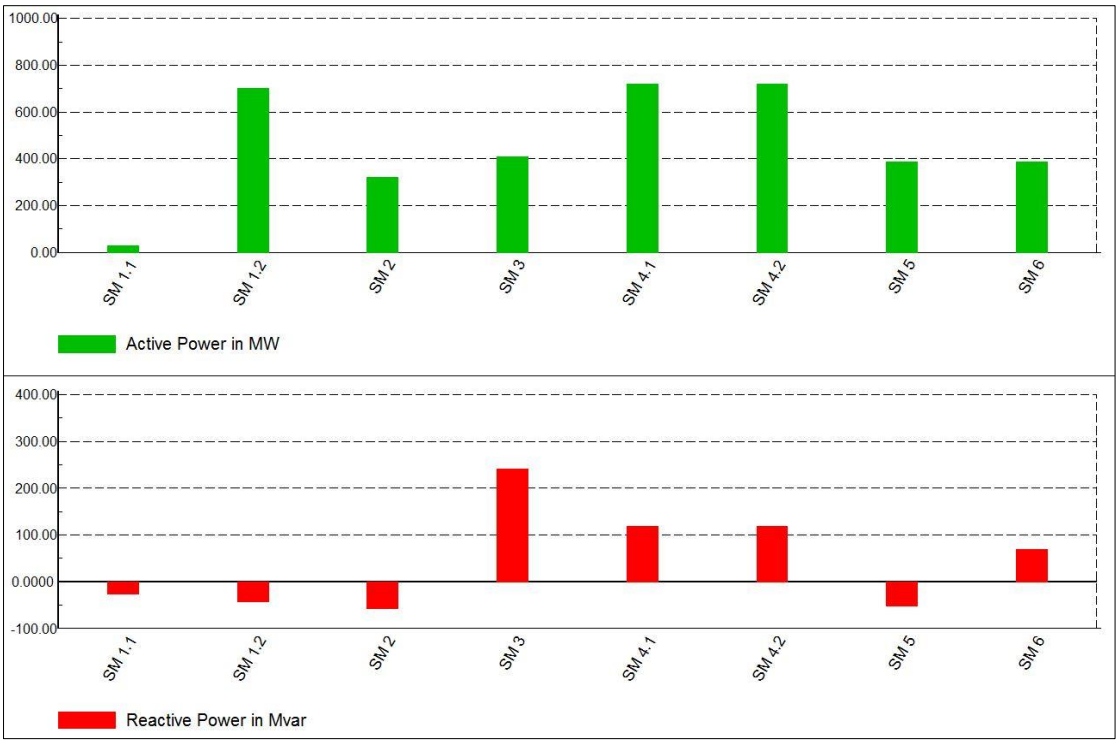

Figure 5.20: Generator active and reactive power (with HVDC line)

From the line-loading diagram in Figure 5.21, the transmission line connecting bus 3 and 1, and the line connecting bus 8 and 3 is already overloaded than their ratings, even line connecting bus 9 to bus 13. However, the HVDC line is out of service, to know the systems state when only AC lines are in operation (meaning HVDC system is out of service). During the second scenario (i.e. using HVDC line), the load flow result for the lines loading as shown in Figure 5.22, with all lines loading within an acceptable range. Load active and reactive power can be seen in Figure 5.23.

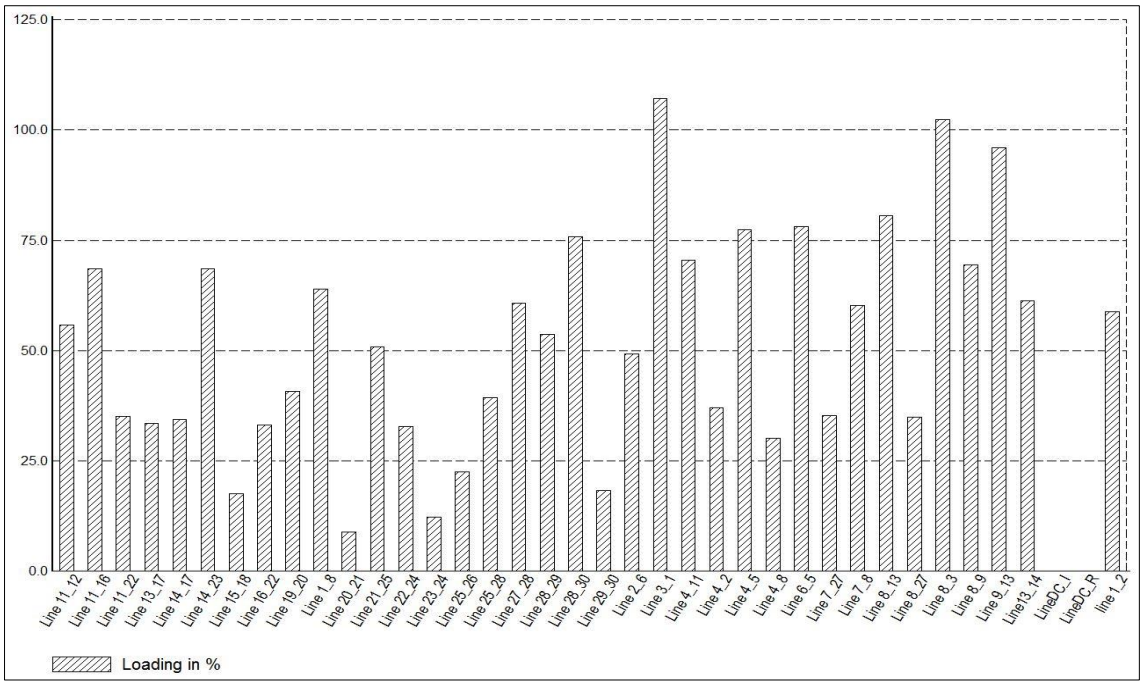

Figure 5.21: Line loading (AC Lines only).

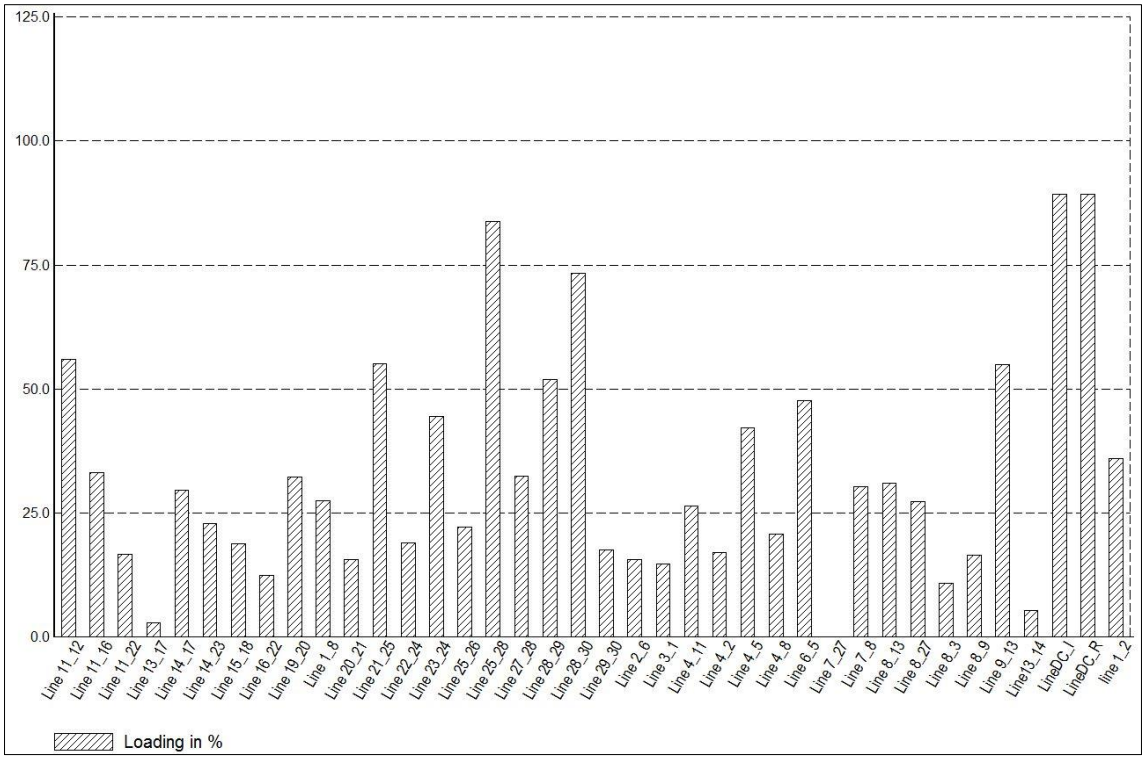

Figure 5.22: Line loading (with HVDC line).

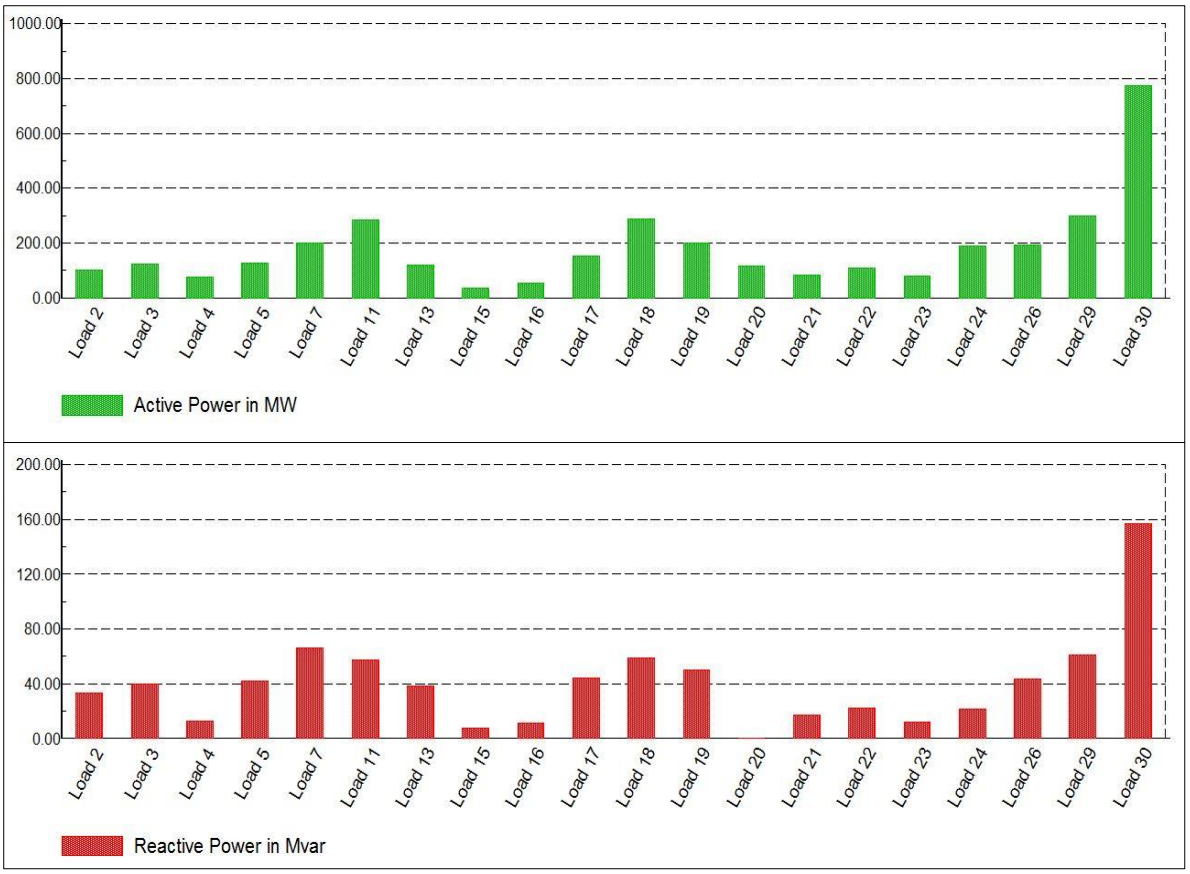

Figure 5.23: Load active power.

- **Time-domain stability simulation**

Two operational scenarios were considered in this study. The first scenario is when the power is being transmitted using AC lines only, and the second scenario is when an existing longest AC line is replaced with an HVDC line and the results are depicted on a graph. Bus voltage and generator excitation current are the main objects of focus for this study. For the bus voltage magnitude graph, specific busbars that are prone to voltage instability was selected rather than use all the 30 buses of the network.

- **The first scenario (without HVDC)**

Different study cases were carried out while using the time domain simulation to investigate the weakest area of the network. This involves the use of critical clearing time to observe the maximum time a fault can stay on each of the element on the network (busbar and lines). Three-phase short circuit fault was placed on each of the busbars once at a time and their CCT was estimated. It was observed that bus 8 has the least critical time. The same process was also carried out on the line (placing the fault at the beginning of the line) and cleared by switching off the line. This process also confirmed line inter connecting bus 1 and bus 3 (Line 3_1) to be the most important line of the network due to its least allowable clearing time after fault. Three-phase short circuit fault on this line can be seen as portrayed in Figure 5.24.

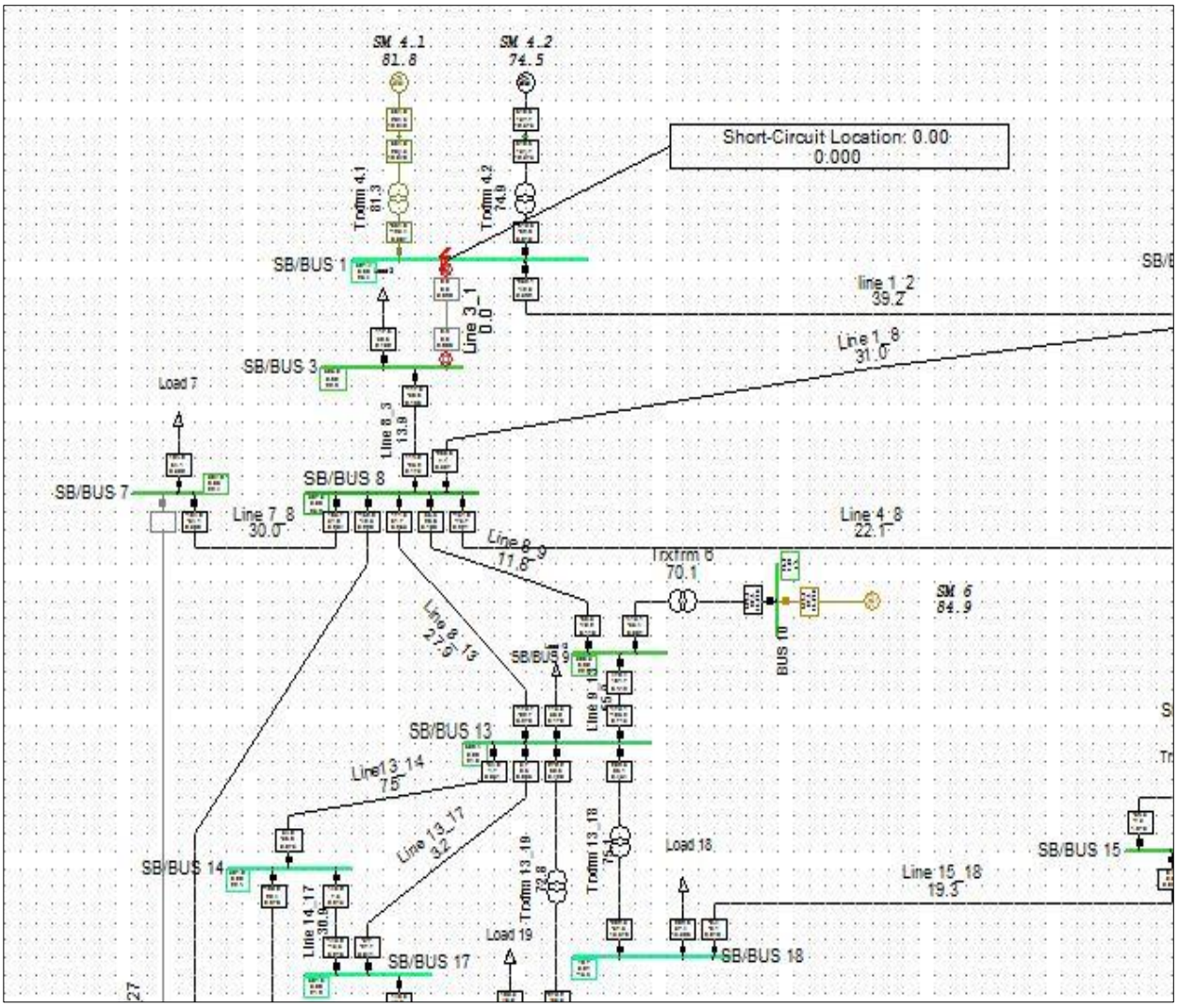

Figure 5.24: three-phase short circuits event on Line 3_1.

Figures 5.25 – 5.27 show the bus voltage magnitude, generator rotor angle and it's excitation current when a three phase fault placed at the beginning of 'line 1_3' was simulated and the fault cleared by switching the line off after 100ms. This is the maximum allowable time the fault can stay on the line for the system to be stable when using only AC lines to transmit power from bus one to bus 3. During the fault, the bus voltage dips down to about 0.11p.u. However, the generator exciter helps to restore the system back to stability by increasing the field current winding of the synchronous generator. Thereby automatically adjust the field current to maintain the required terminal voltage. Figure 5.28 present load active and reactive power during simulation time.

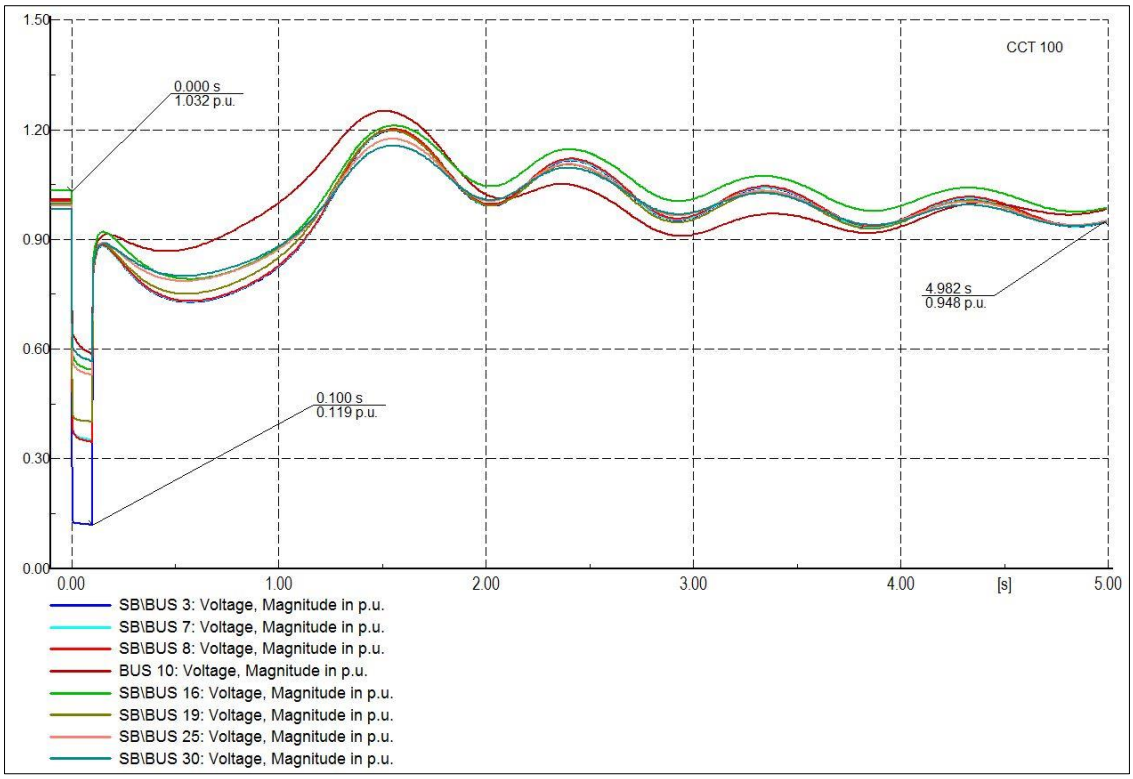

Figure 5.25: Voltage Plot during a fault on 'Line 3_1', cleared by switching off the line after 100ms. (Without HVDC line).

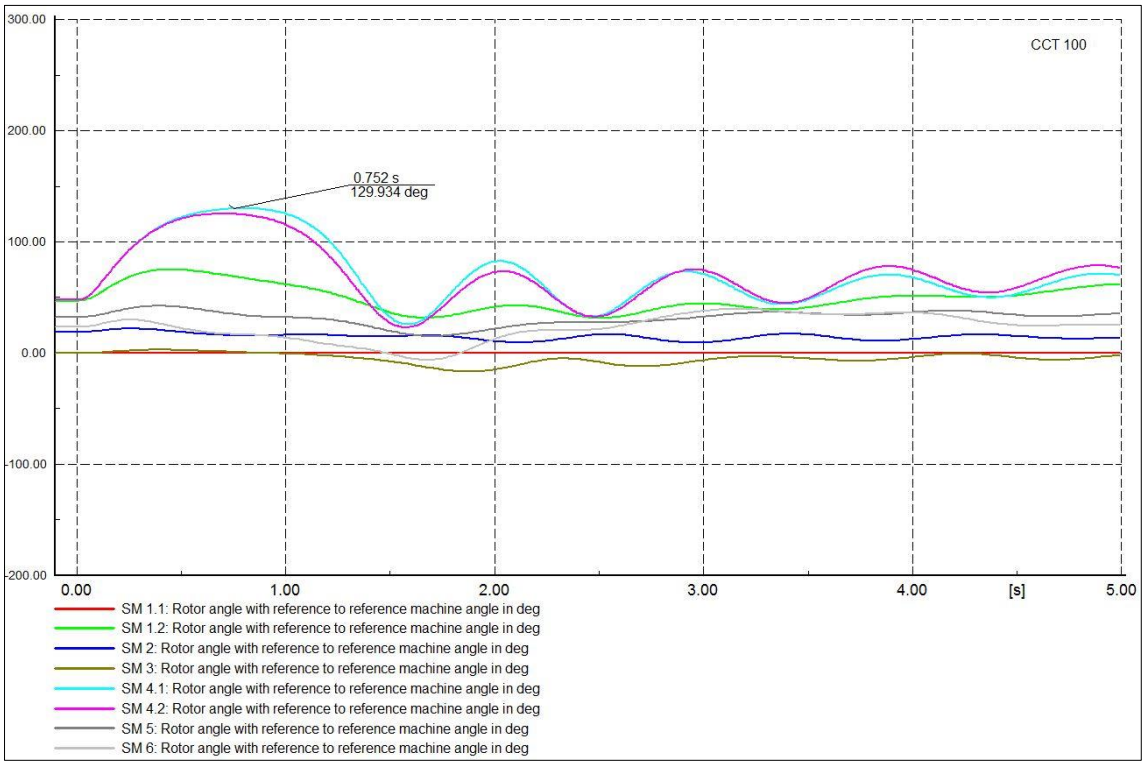

Figure 5.26: Generators rotor angle (Without HVDC line).

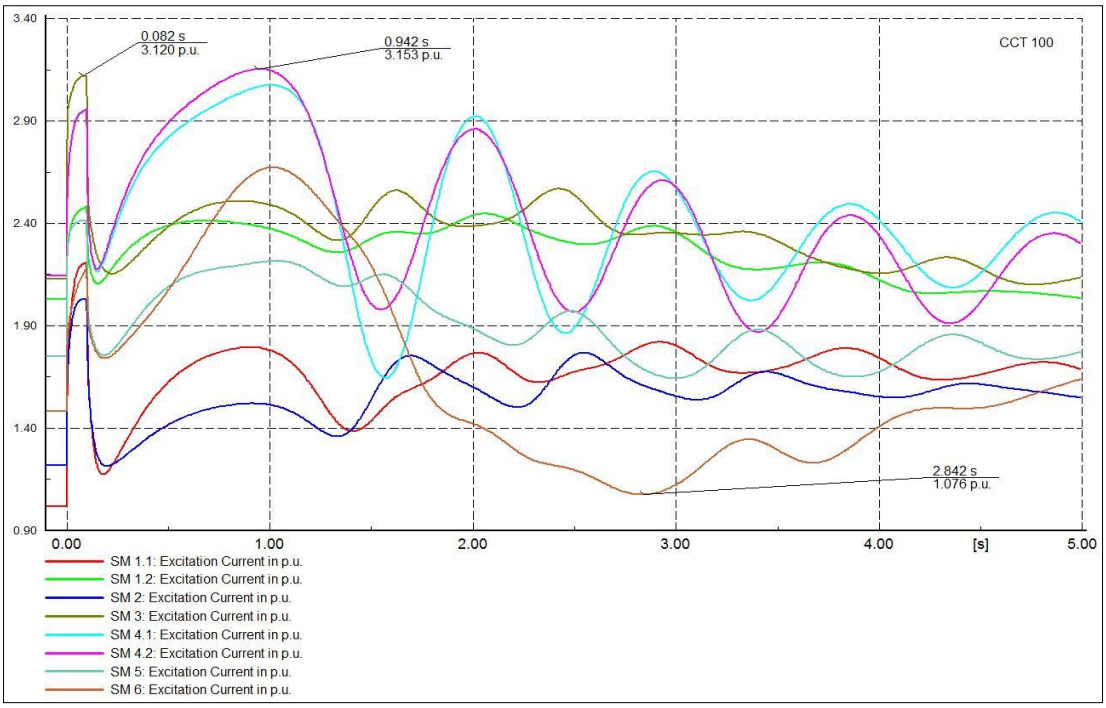

Figure 5.27: Generator excitation current (Without HVDC line).

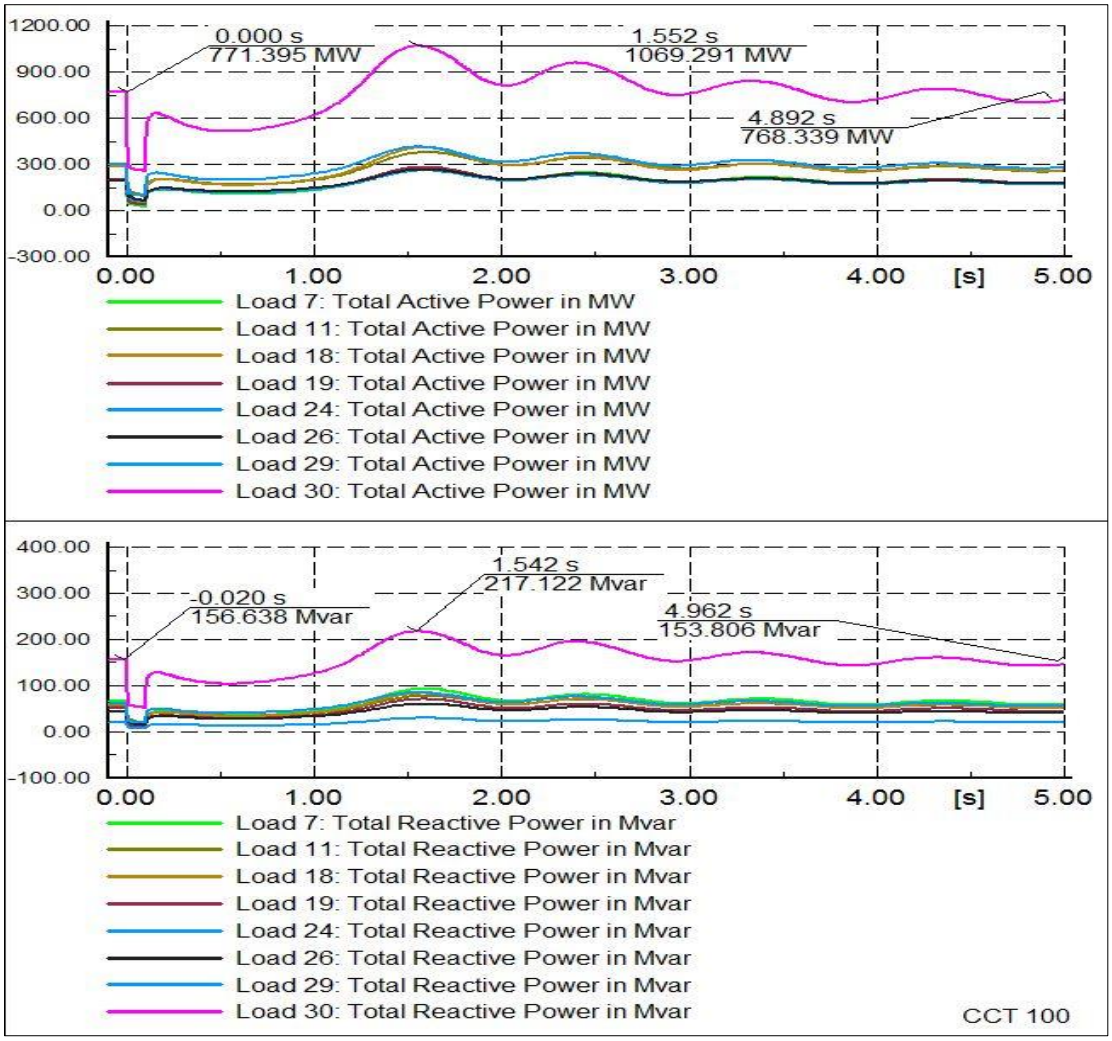

Figure 5.28: Load (P and Q).

Figures 5.29 – 5.31 show a situation whereby the fault stay more than expected time before the circuit breaker of the line was opened (120ms). This caused the generator to have yielded its entire excitation limit and the systems enter instability when the voltage profile of all the buses cannot be met again. This causes the generator angle to swing 360^0 off from the reference machine, a situation caused when the generator pole slipped.

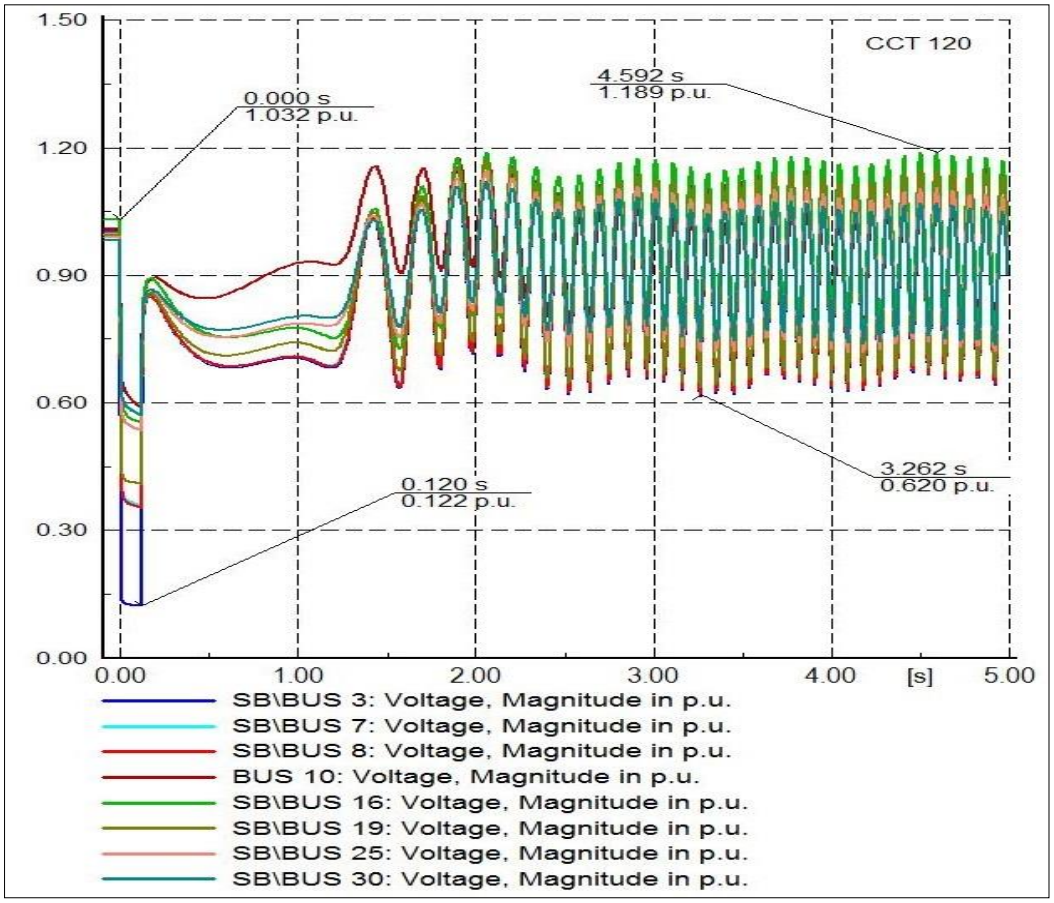

Figure 5.29: Voltage Plot during a fault on 'Line 1_3', cleared by switching off the line after 120ms. (Without HVDC line).

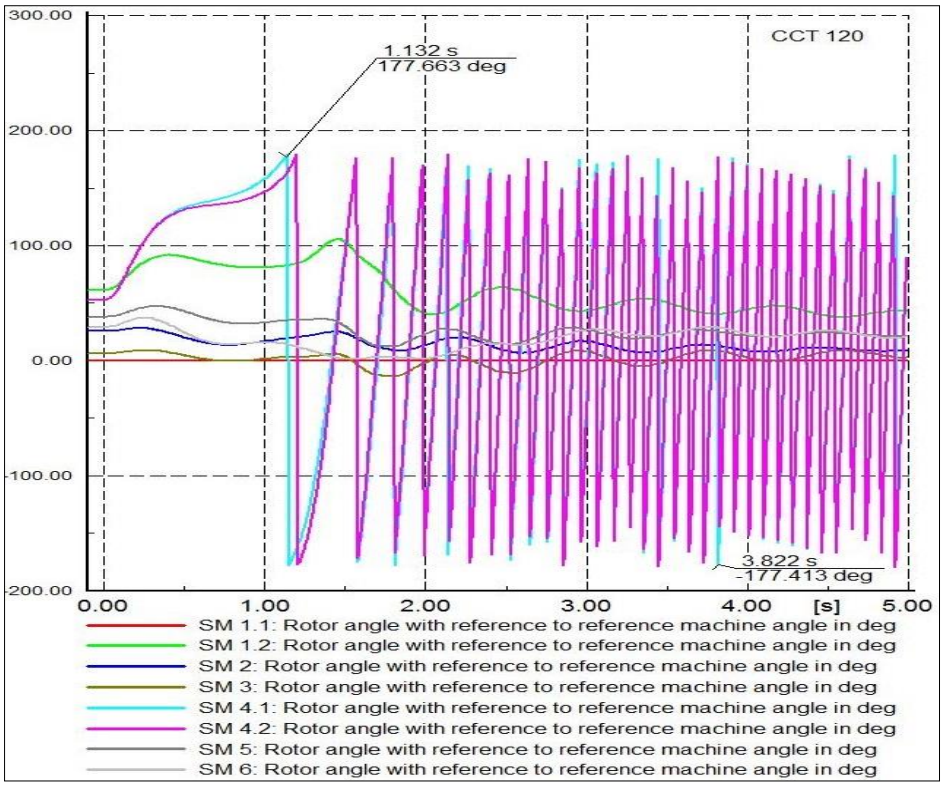

Figure 5.30: Generator Rotor angle fault (Without HVDC line).

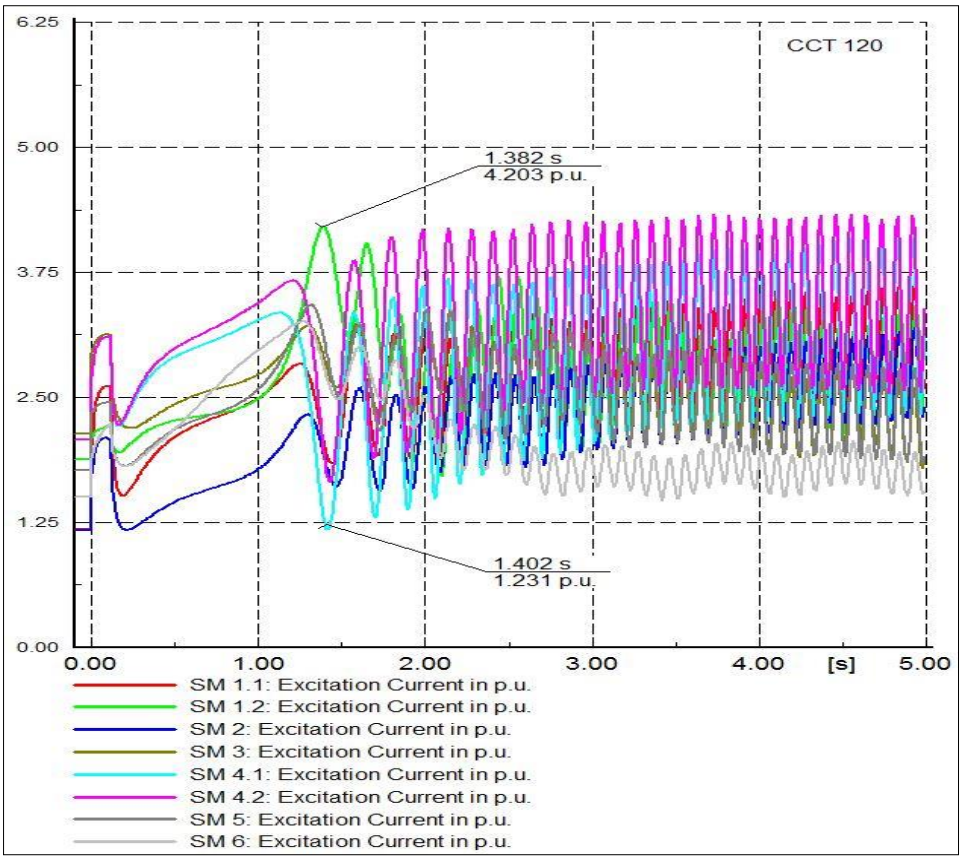

Figure 5.31: Generator Excitation current (Without HVDC line).

- **Second scenario (With HVDC line)**

When existing AC ‘line 8_27’ was replaced with a monopolar HVDC system as shown in Figure 5. 16. Same three phase fault was applied on ‘Line 3_1’ and the fault cleared by isolating the line after 120ms while using HVDC line to interconnect ‘bus 1’ to ‘bus 28’, it was found out that the system was stable even until it reaches a maximum fault isolating time of 150ms. Further increase of fault duration beyond this margin resorted in convergence error. Figures 5.32 – 5.35 show the bus voltage magnitude, generator rotor angle, and excitation current respectively.

A case of commutation failure occurs at the inverter side of the HVDC link during fault period, with the help of the converter selection mode by blocking the fault current from transferring into the HVDC link, the systems were able to maintain stability. HVDC systems thus help to increase the time duration a fault can stay on the line before being isolated from the systems.

All different study cases carried out on the systems prove the efficacy of HVDC link in power systems stability and control during system disturbance.

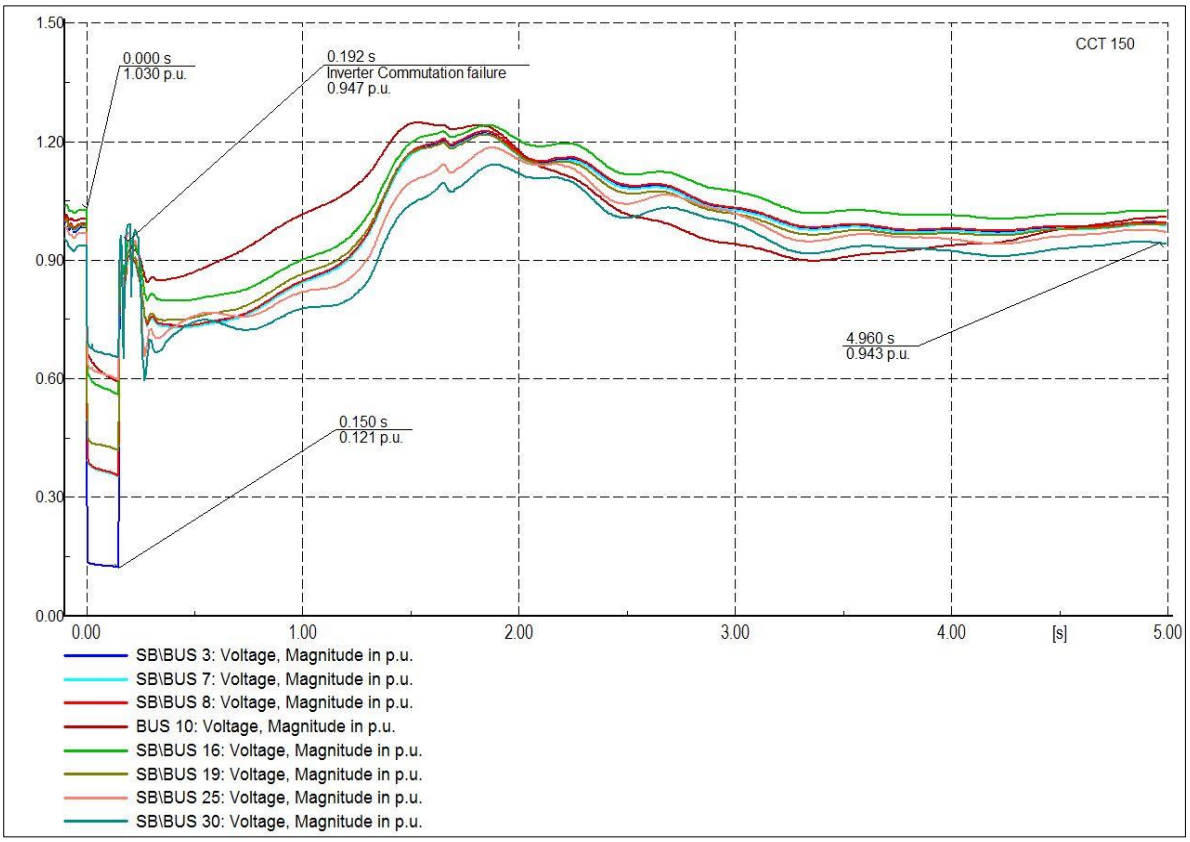

Figure 5.32: Voltage Plot during a fault on ‘Line 3_1’, cleared by switching off the line after 150ms. (With HVDC line).

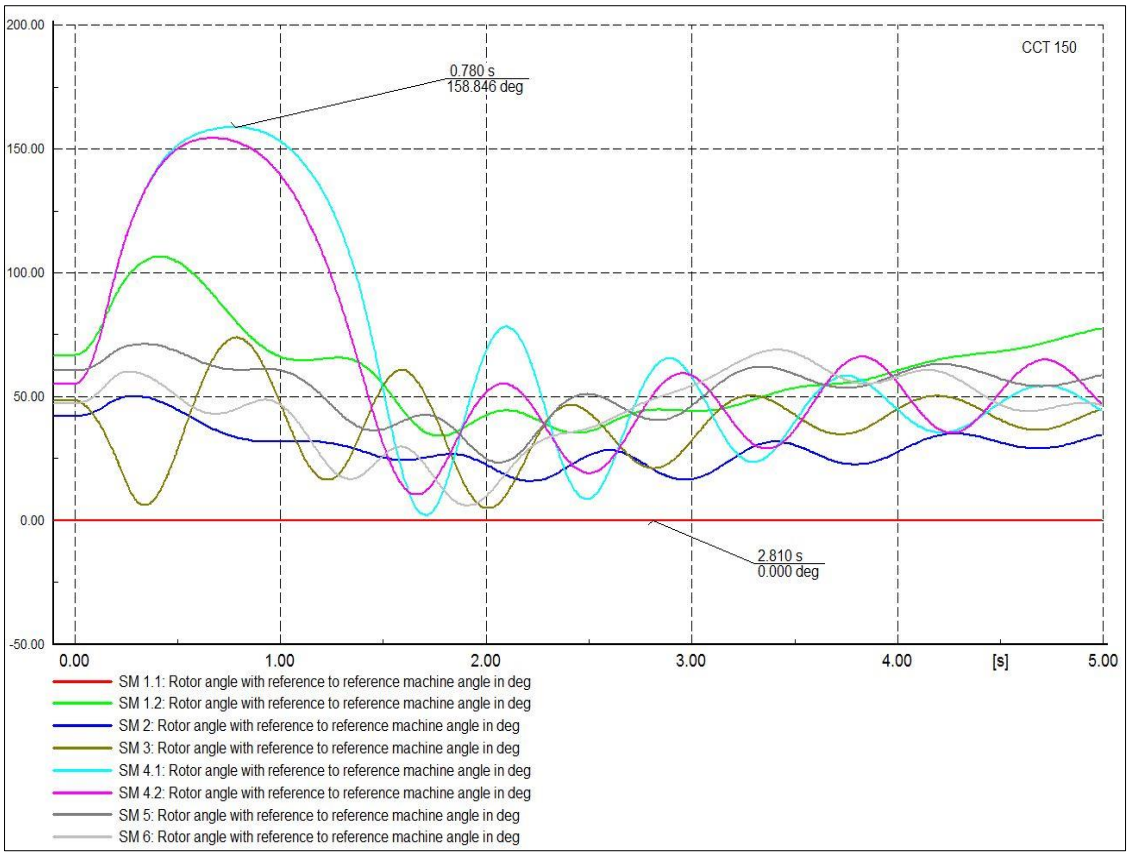

Figure 5.33: Generators rotor angle (With HVDC line).

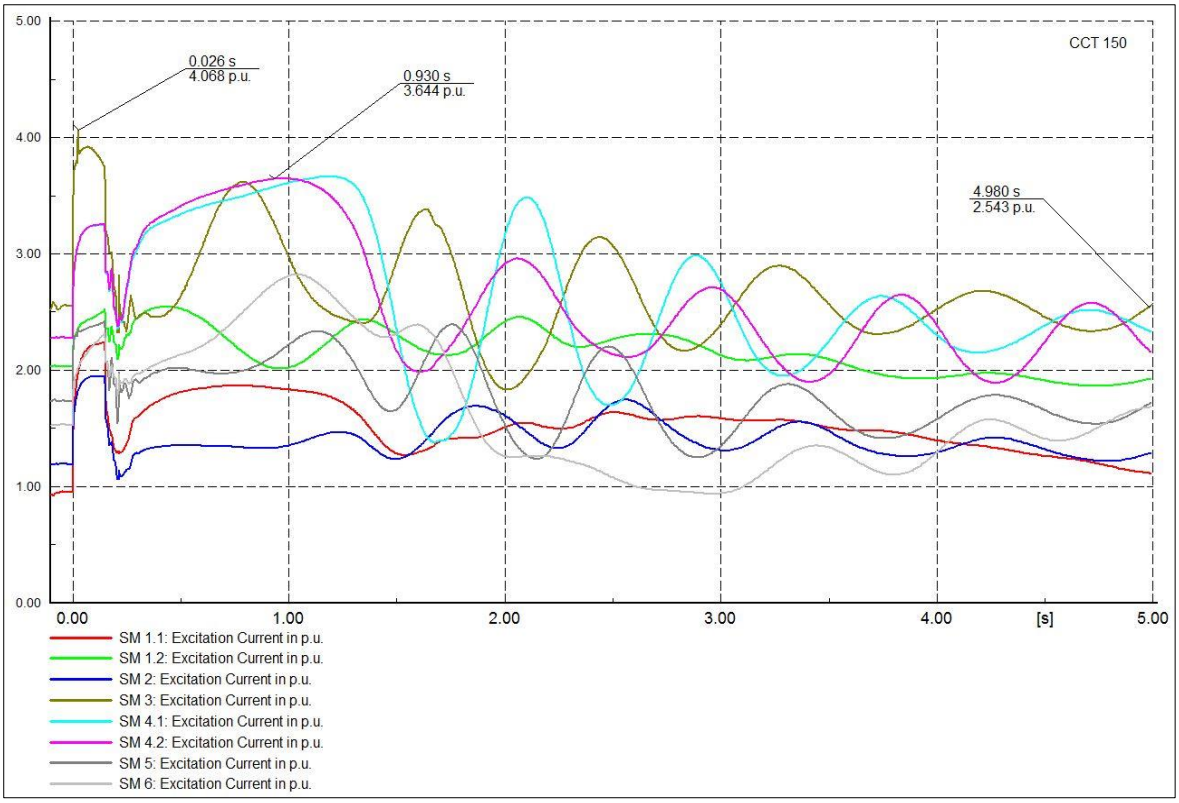

Figure 5.34: Excitation current. (With HVDC line).

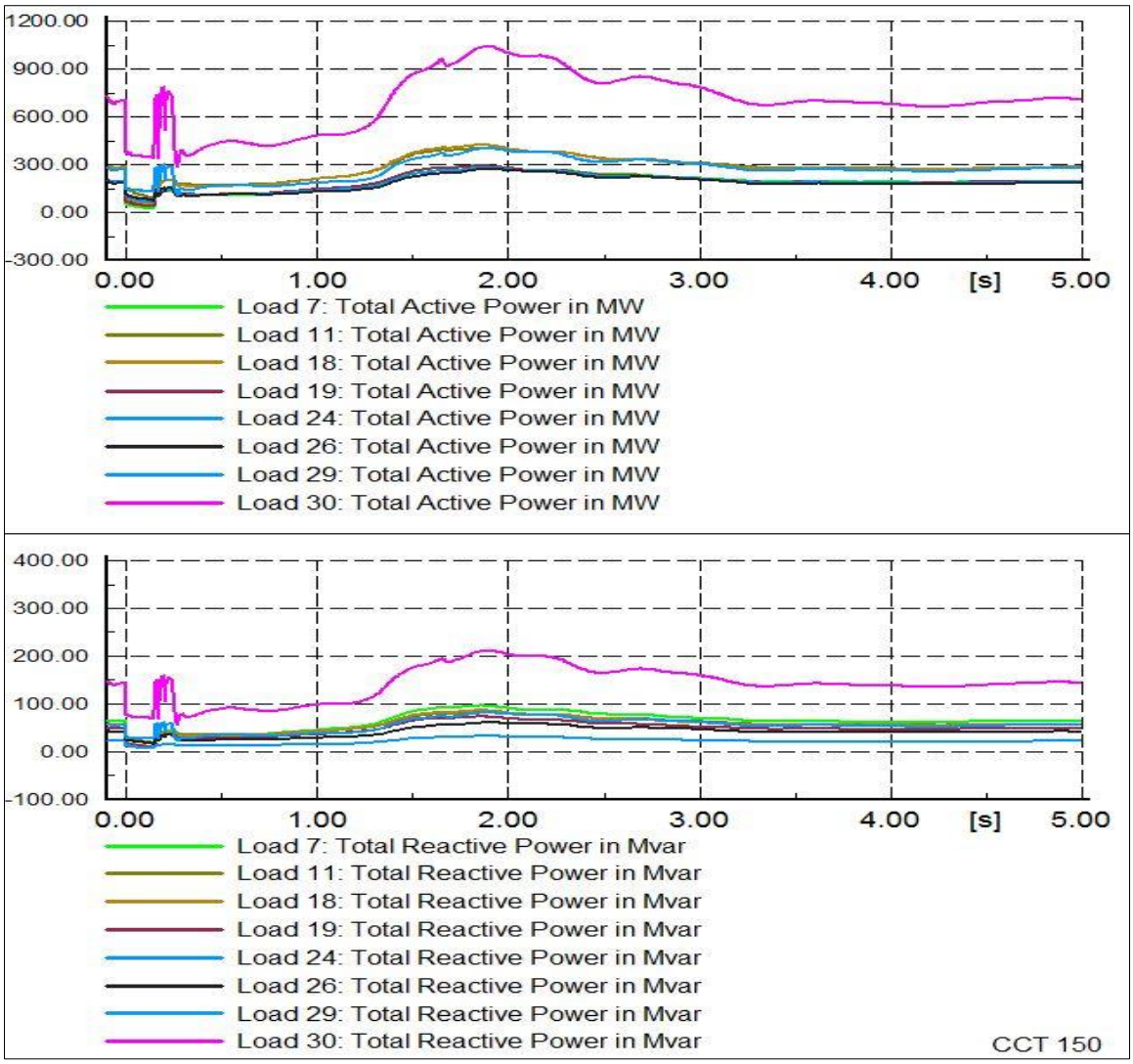

Figure 5.35: Load active and reactive power (with HVDC).

CHAPTER 6: MODIFIED ESKOM NETWORK

6.1. Introduction

Eskom power network has a total installed capacity of over 44 GW as shown in Table 6.1. Eskom generating, transmitting and distributing electric power all over South Africa and its neighbouring country. Its network is divided into 9 grid with each province making one grid [139].

Table 6.1: Eskom's power station

Name of station	Type of station	Sets (MW)	Total Capacity (MW)	Year of Operation
Arnot	Coal		2100	1975
Candem	Coal		1600	1967
Dulva	Coal		3600	1980
Grootvlei	Coal		1200	1969
Hendrina	Coal		2000	1970
Kendal	Coal		4116	1988
Komati	Coal		1000	1961
Kriel	Coal		3000	1976
Lethabo	Coal		3708	1985
Majuba	Coal		4110	1996
Matimba	Coal		3990	
Matla	Coal		3600	1983
Tutuka	Coal		3654	1985
Koeberg	Nuclear	2x960	1920	1984
Gariep	Hydro		360	1971
Vanderkloof	Hydro		240	1977
Drakensberg	Pumped storage		1000	1981
Palmet	Pumped storage		400	1988
Darling	Wind		5.2	2008
Klipheuwel	Wind		3.2	2002
Acacia	OCGT		171	1976
Port rex	OCGT		171	1976
Ankerlig	OCGT		1338	2007
Gourikwa	OCGT		746	2007
Total installed capacity			**44032.40**	

The scope of this study is focused on the Eastern grid located in the KwaZulu-Natal province. This network was modeled out of the original Eskom main transmission network of the South African power grid as dated back to 3rd March 2014. The main power supply comes from Tutuka power station in the Mpumalanga province, and the Drakensberg pumped storage, majorly via a 400 kV transmission lines. The load demand was 6799MW in 2014, but as the demand for electricity in this province increases, the existing transmission infrastructure will be heavily loaded and will eventually reach its full capacity. This demand is expected to increase up to 8045 by 2025 [140]. This load demands are for commercial, mining, industrial, residential, tractions and agricultural purposes. Catering for this anticipated growth over the next couple of years brings about some implementation of several number of different reinforcements for stability and uninterrupted power supply purposes.

Table 6.2 listed few of the ongoing/planned projects that are implemented in this study with few details of the generators and the grid overview shown in Appendix (APP 3). Thus, the methodology approach which was highlighted in chapter 3, and carried out in chapter 5 test networks was also applied on Eskom Eastern grid to analysis the technical performance as regards its steady state performance and dynamic voltage stability analysis of the network.

Table 6.2: Proposed project 2016-2020

SCHEME NAME	**PROJECT NAME**
Greater East London Strengthening - Phase 1	Eros-Vuyani 1st 400 kV line Avon 3rd 250 MVA 275/132 kV transformer
Avon 680MW IPP	IPP OCGT at Avon 275 kV
Ariadne – Venus 2nd 400 kV Line	Ariadne – Venus 2nd 400 kV line (recycle Georgedale – Venus 1 or 2-275 kV line)
Ingula 1320MW Pumped Storage Power Station Transmission Substation Integration	Ingula 400 kV busbar, Loop-in Majuba – Venus 2-400 kV line into Ingula Substation Ingula – Venus 2nd 400 kV line
Incandu 3rd 400/132 kV transformer upgrade	Incandu 3rd 400/132 kV transformer upgrade
Mersey 3rd 250 MVA 275/132 kV transformer upgrade	Mersey Ext 3rd 250 MVA 275/132 kV transformer

Ensuring to meet the N-1 contingencies criterion specified in south Africa grid code and to increase bulk power transmission brings about a proposed project of either using a HVAC or HVDC transmission lines in a new proposed project. Bulk power from pool of generation capacity of Medupi, coal 2 and coal 3 power station (planned PS) from Massa substation in Limpopo province will be transmitted to Hector or Invubu substation in Kwazulu-Natal area via these 1300km overhead lines. These areas are major load centers. Therefore, the need to examine the effect of both lines on the entire systems stability. The Eastern grid and its full network diagrams are shown in Figure 6.1. while its overview diagram are shown in Appendix.

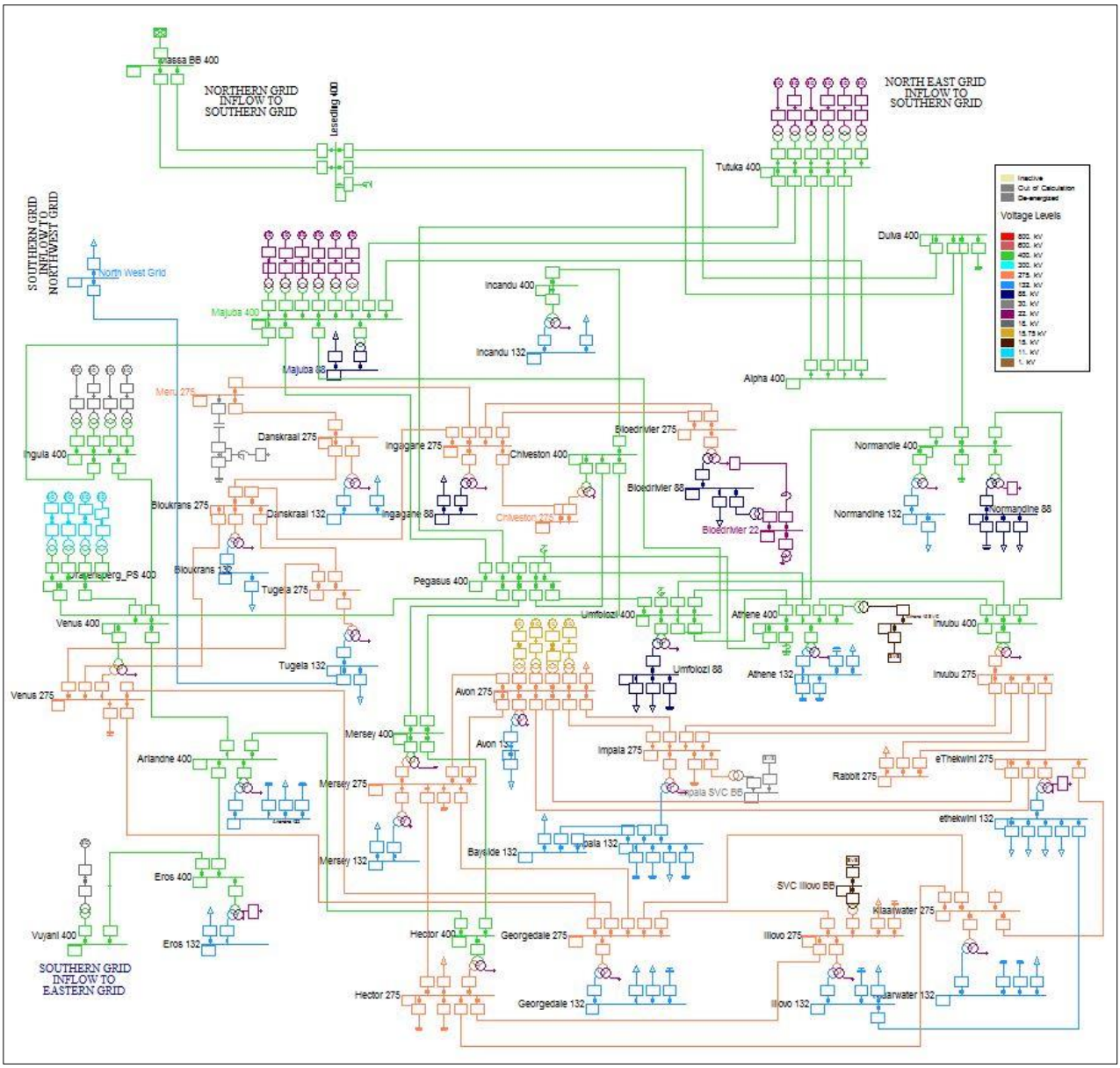

Figure 6.1: Eskom Eastern grid.

6.2. Load Flow Analysis

Load flow analysis was carried out on Eskom Eastern grid to ascertain the system performance and operation. This will give power engineers information about system planning and operation. The result of this load flow which encompasses the element loadings, busbar voltage profile, active and reactive power flow are all depicted using a bar subplot. These subplots are gotten from load flow study on DIgSILENT PowerFactory based on NRFL equation.

Figure 6.2 show the busbar voltage profile during this steady state load flow analysis. From this bar-plot, it could be seen that nearly all the busbar voltage profile are in acceptable limit except Georgedale 132kV and Normandie 400 kV busbar. This is because of lack of reactive power compensation on the transmission line that interconnects these busbars.

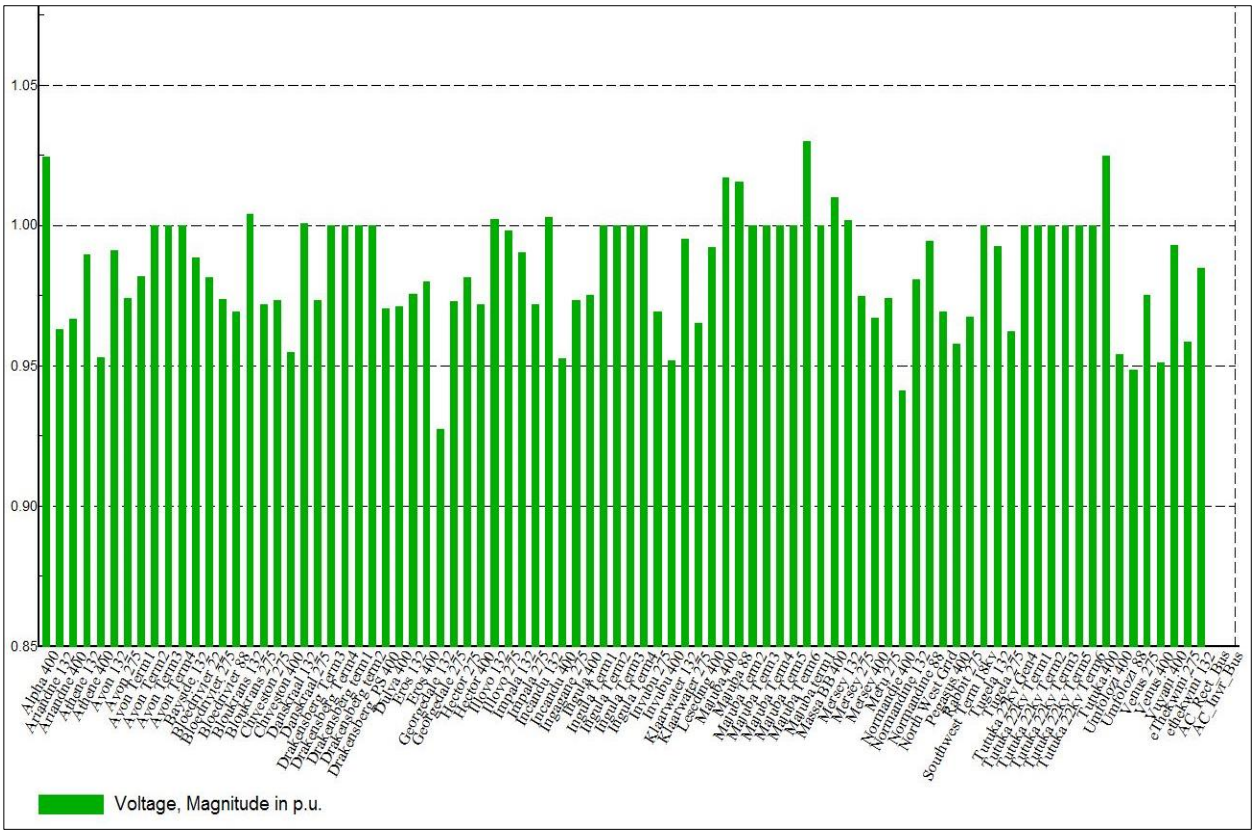

Figure 6.2: Busbar voltage profile.

The transmission loading and losses are shown in Figures 6.3 and 6.4 respectively. Transmission line loading depends majorly on the current rating of the transmission line. This line rating determines the power transfer via the line. Though most of the lines have an acceptable loading limit, yet proper preventive measures needs be taking to either increase the current carrying capacity of those that are almost loaded or construct a new transmission line for proper effectiveness. Either way, the latter is less expensive that the former to implement, but the former gives a better reliability that the latter. Higher transmission losses could be noticed from the new transmission line that was used to transfer bulk power from the northern grid into the KwaZulu-Natal Eastern grid; this is inherent due to the length of the line.

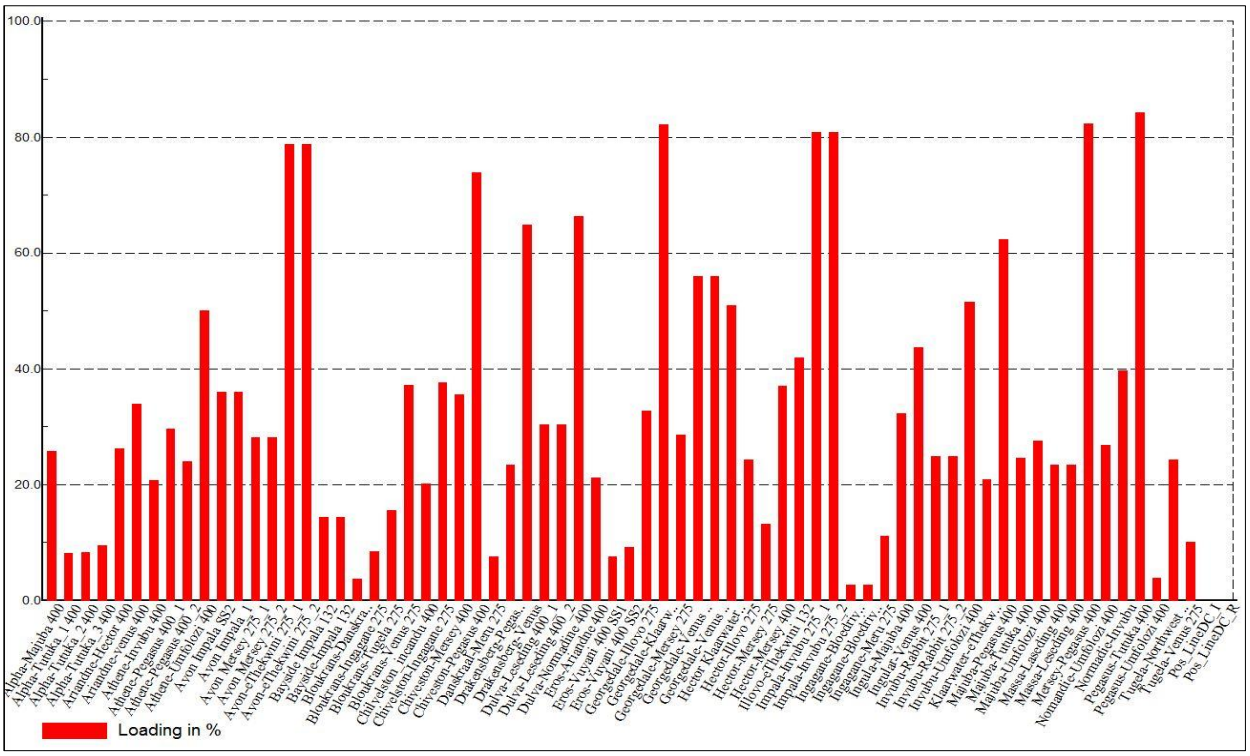

Figure 6.3: Transmission line loadings

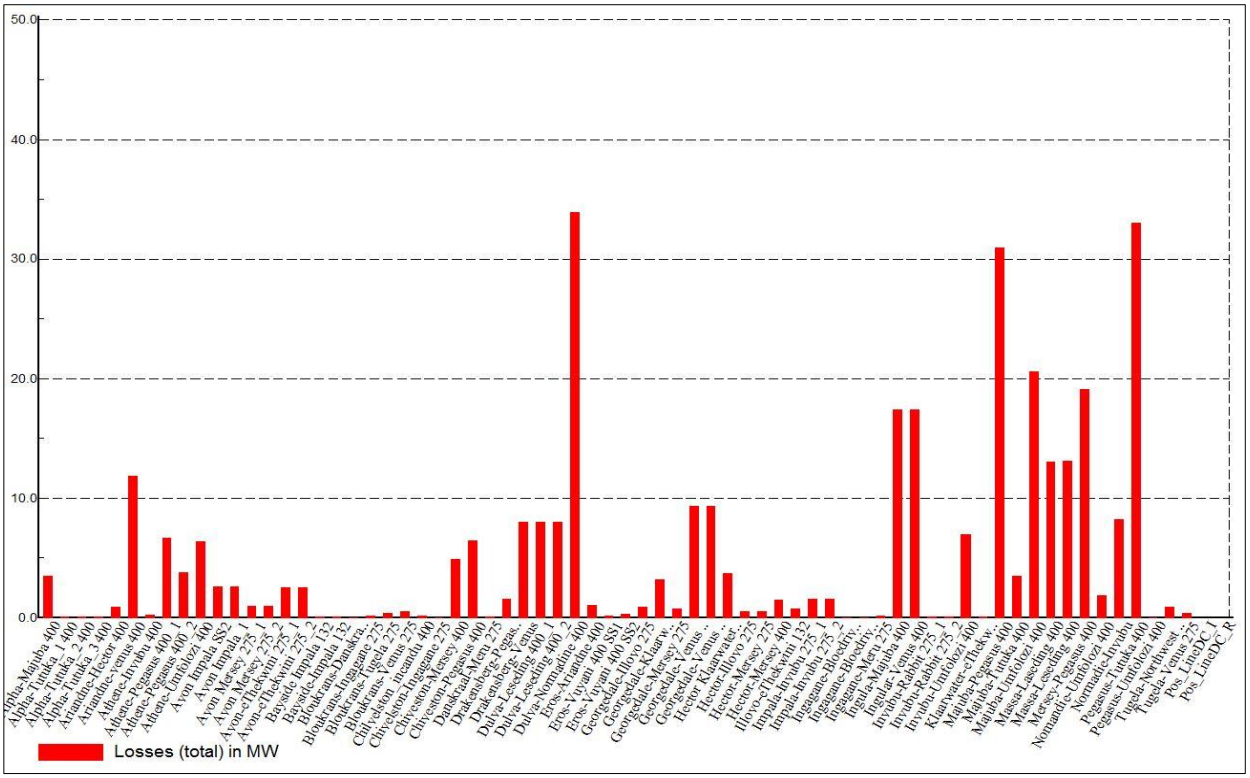

Figure 6.4: Transmission line losses

Figure 6.5 shows the active and reactive power generated into the Eastern grid. Tutuka generator located in the Mpumalanga pumped storage (Northeast province) generated the most, followed by Majuba power station. The percentage loading of these generators can be seen in Figure 6.6. Avon power plant and Drakensberg power station could be seen that they are overloaded more than the

required limit. This boils to the fact that there is a need for more power to be transferred to the Eastern grid to ease the available generator of being overloaded.

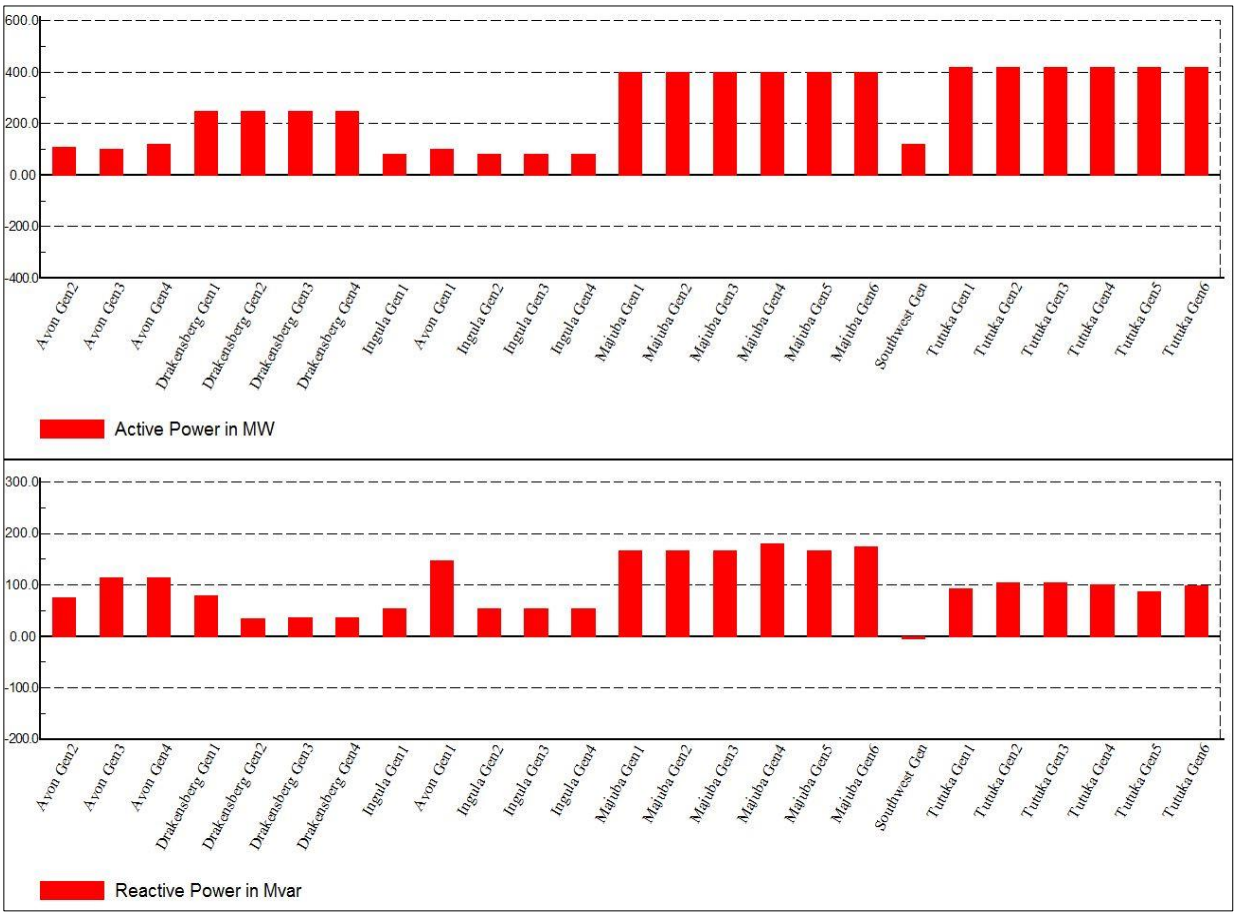

Figure 6.5: Generator active and reactive power

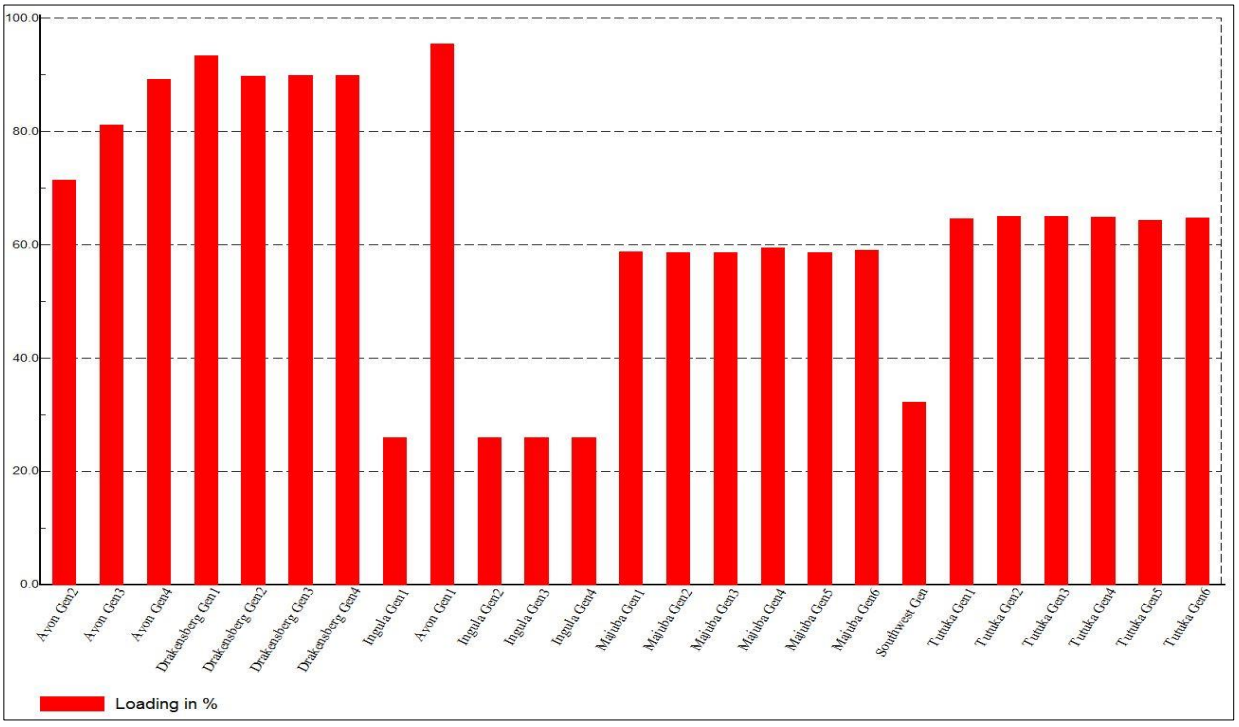

Figure 6.6: Generator loading

Figure 6.7 shows the three-winding transformer loading. These transformers were used in the entire substation to step down to lower voltage levels. While the two-winding transformer loading can be seen in Figure 6.8. The two winding transformers were used to interconnect each of the generators to high-voltage transmission busbar.

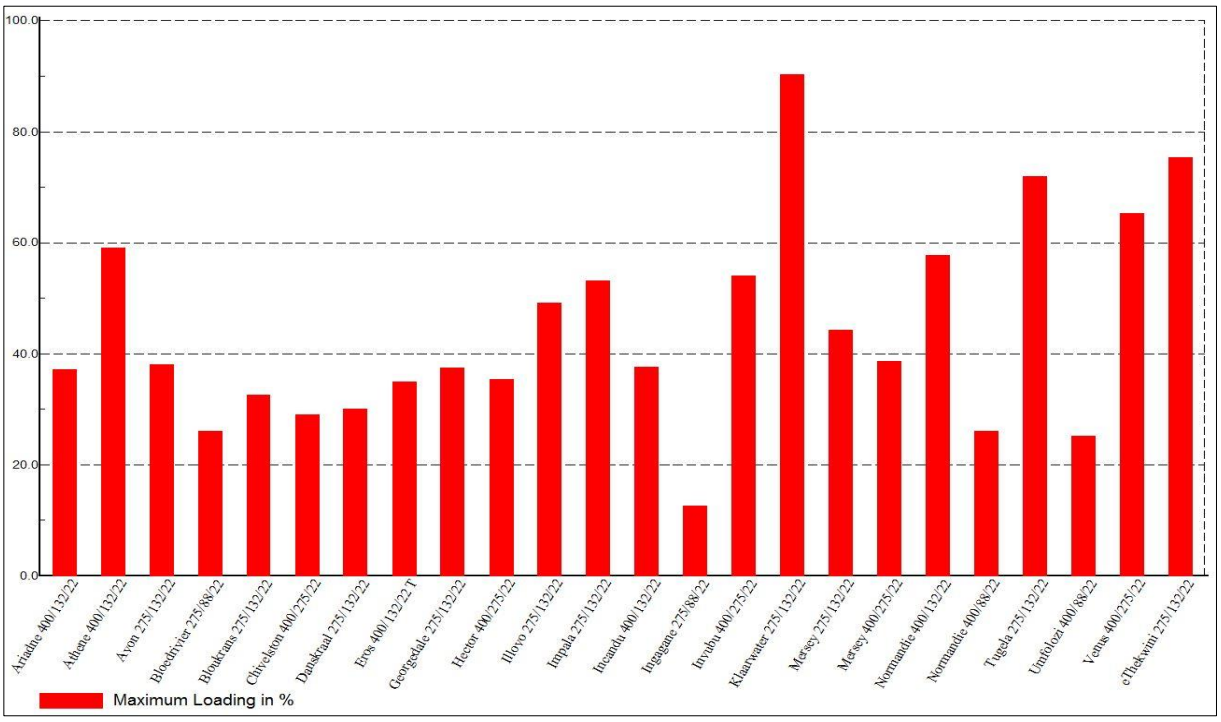

Figure 6.7: Three winding transformer loading

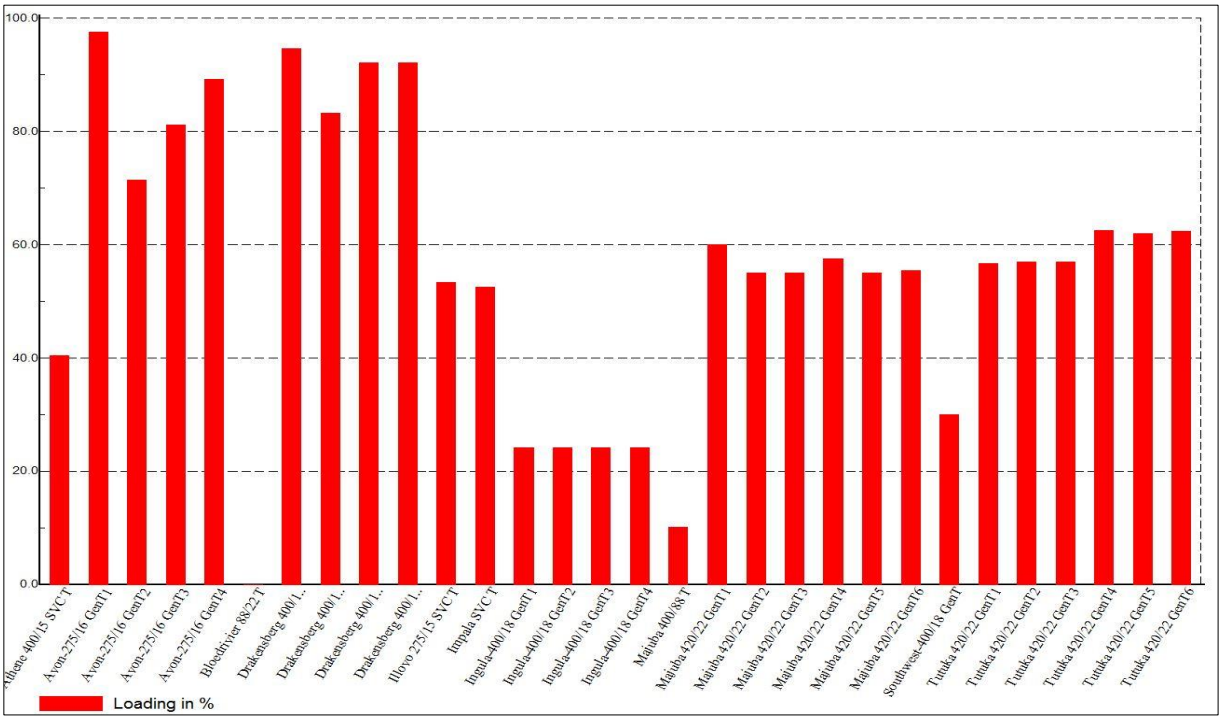

Figure 6.8: Two-winding transformer loading

Active and reactive power of the load can be seen in Figure 6.9. Athene and Klaawater loads are the major urban center with high power usage because it housed most industries.

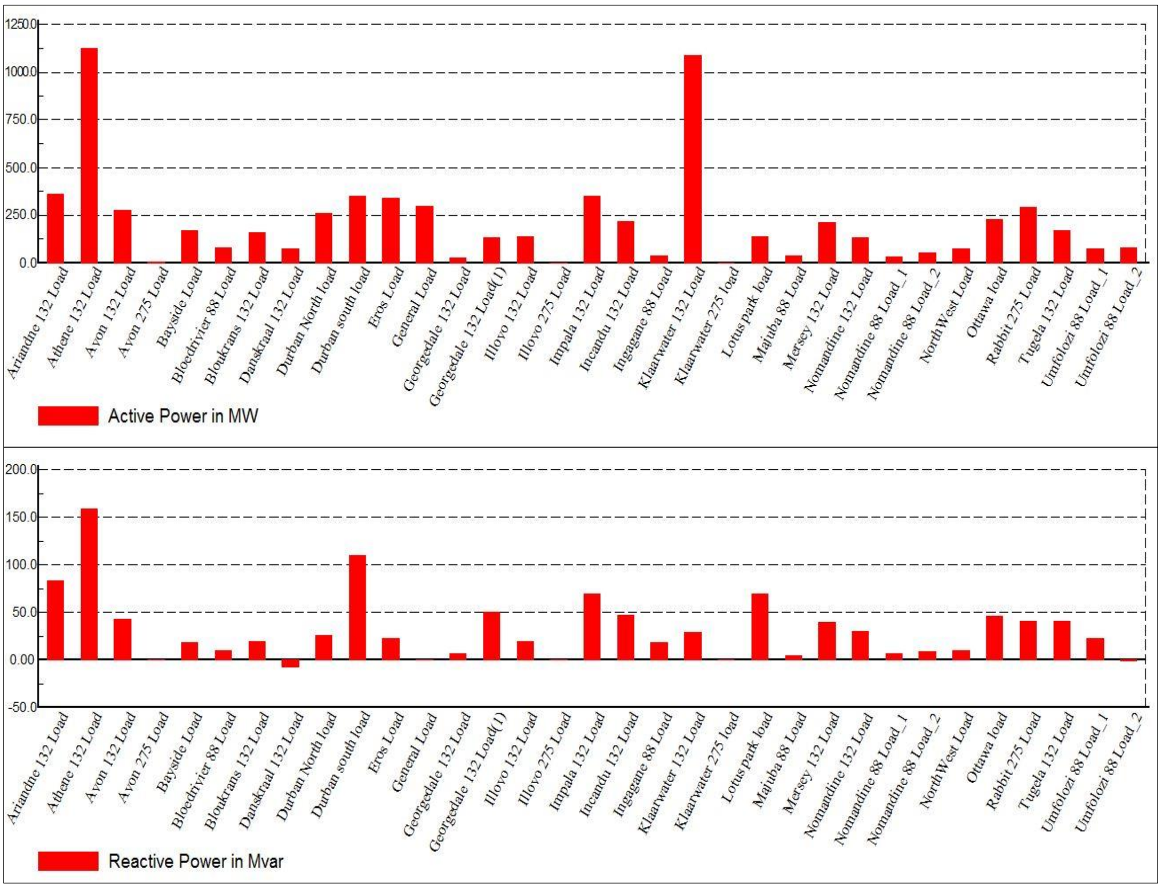

Figure 6.9: Active and reactive power of Eastern grid load

The overall system summary could be seen in Figure 6.10, this Figure highlights the total load, power generated, external infeed from Limpopo province, and the total losses on the grid.

```
-------------------------------------------------------------------------------------------------------------------
|              |                                                          |  DIgSILENT   | Project:                 |
|              |                                                          | PowerFactory |---------------------------
|              |                                                          |    15.1.6    | Date:  5/10/2016         |
-------------------------------------------------------------------------------------------------------------------
-------------------------------------------------------------------------------------------------------------------
| Load Flow Calculation                                                                             Grid Summary |
-------------------------------------------------------------------------------------------------------------------
|    AC Load Flow, balanced, positive sequence              |   Automatic Model Adaptation for Convergence      No        |
|    Automatic Tap Adjust of Transformers          Yes      |   Max. Acceptable Load Flow Error for                     |
|    Consider Reactive Power Limits                Yes      |     Nodes                                          1.00 kVA  |
|                                                           |     Model Equations                                0.10 %    |
-------------------------------------------------------------------------------------------------------------------
-------------------------------------------------------------------------------------------------------------------
| Grid: 1.0 EskomEastern Gri System Stage: 1.0 EskomEaster | Study Case: 2.0 Power_Flow AC        | Annex:        / 1  |
-------------------------------------------------------------------------------------------------------------------
| Grid: 1.0 EskomEastern GridSummary                                                                              |
|                                                                                                                 |
| No. of Substations     57        No. of Busbars        90       No. of Terminals      951      No. of Lines          68  |
| No. of 2-w Trfs.       30        No. of 3-w Trfs.      24       No. of syn. Machines  25       No. of asyn.Machines  0   |
| No. of Loads           33        No. of Shunts         26       No. of SVS            3                                 |
|                                                                                                                 |
| Generation          =    6275.33  MW       2090.31   Mvar     6614.32  MVA                                      |
| External Infeed     =    1000.00  MW       -232.88   Mvar     1026.76  MVA                                      |
| Inter Grid Flow     =       0.00  MW          0.00   Mvar                                                      |
| Load P(U)           =    6935.98  MW       1040.76   Mvar     7013.63  MVA                                      |
| Load P(Un)          =    7211.08  MW       1135.73   Mvar     7299.97  MVA                                      |
| Load P(Un-U)        =     275.11  MW         94.96   Mvar                                                      |
| Motor Load          =       0.00  MW          0.00   Mvar        0.00  MVA                                      |
| Grid Losses         =     339.36  MW       2351.31   Mvar                                                      |
| Line Charging       =                     -3471.69   Mvar                                                      |
| Compensation ind.   =                       196.84   Mvar                                                      |
| Compensation cap.   =                     -1731.48   Mvar                                                      |
|                                                                                                                 |
| Installed Capacity  =   10858.40  MW                                                                            |
| Spinning Reserve    =    4583.07  MW                                                                            |
|                                                                                                                 |
| Total Power Factor:                                                                                             |
|   Generation        =          0.95  [-]                                                                        |
|   Load/Motor        =  0.99 / 0.00  [-]                                                                        |
|-----------------------------------------------------------------------------------------------------------------|
```

Figure 6.10: Eskom Eastern grid load flow summary

6.3. Busbar Fault Levels

IEC 60909 short circuits method was carried out on the entire Eastern grid. This circulation was done on DIgSILENT PowerFactory to investigate the fault currents levels of all the busbar on the network.

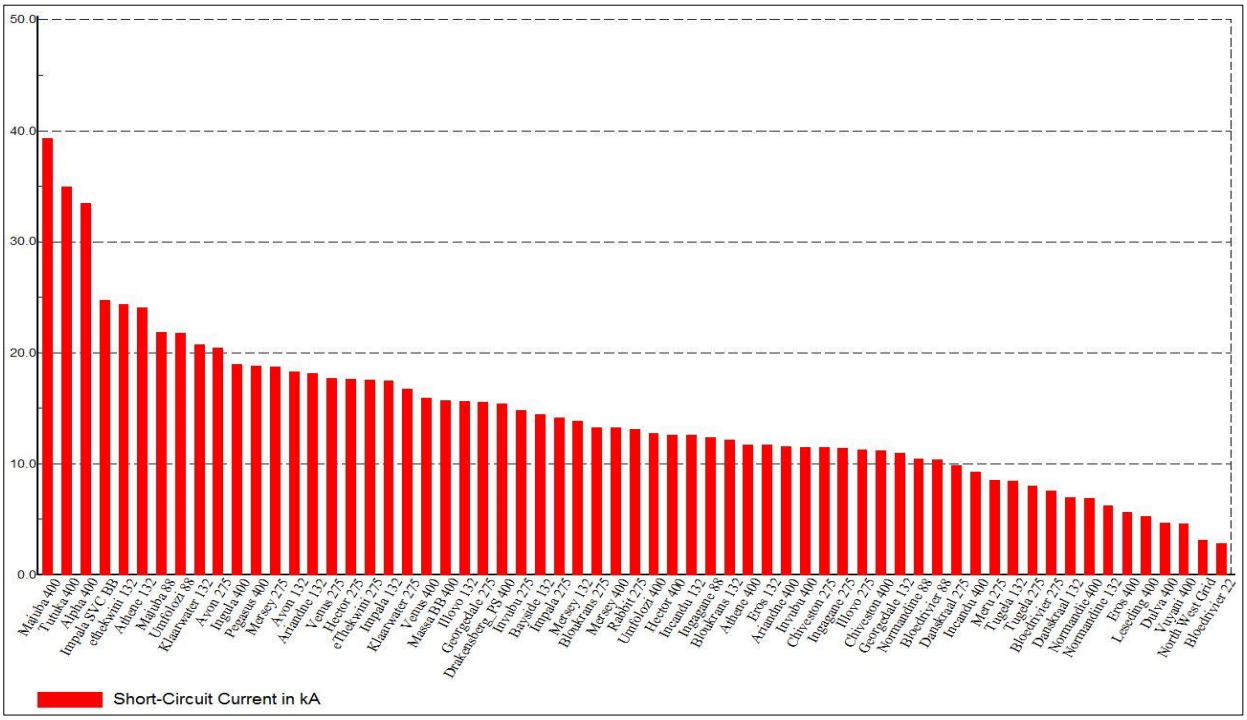

Figure 6.11: Busbar short circuits current

The faults levels of each investigated busbar signify the strength of such particular busbar. High fault current level implies a strong system. The result of this fault current level, represented in Figure 6.11 above helps to determine which busbar or generator should be used as a reference bus/machine i.e. the bus with high fault current level signifies strongest bus and the reference machine should therefore be connected to it.

6.4. Voltage Stability Analysis

Voltage stability analysis of a network can either be determined using a static method with use of PV/QV curve or dynamic analysis with the use of time domain simulation. This analysis aims at analysing the system voltage profile of the network upon load increase, small or large disturbance on the network. A system is said to be voltage stable if all system operating condition can be met after small or large disturbance. Power systems due to fault such as loss of synchronization of a large power plant, tripping of a load and/or sudden disturbance on a transmission line, most times result in a cascading effect. It can lead to voltage instability when the systems fail to meet active/reactive power demanded and acceptable voltage level on all the busbars. This can further cause voltage collapse when all the voltage profile after disturbance is below acceptable limits in an important part of power systems when different part of the systems controllers is stressed beyond their operational limit.

The generator is always equipped with an automatic voltage regulator (AVR) through the help of the field and armature current windings. During normal operation, the terminal voltage of the generator is maintained constant by the field current, which is reduced during a disturbance in order to avoid overloading of the generator. This aims at maintaining synchronism between the generator and the grid. Some load characteristics have an effect on voltage stability because their active and reactive power is voltage dependent. Such loads tend to absorb more reactive power and thereby tends to drop the voltage profile further during fault conditions. This comes to the fact that reactive power flow to the area of low voltage area during a situation of low voltage in power systems.

This section will both investigate the effect of load increase on interconnecting bus voltage by using PV curve as well as the RMS simulation analysis.

6.4.1. Static analysis

PV curve script on DIgSILENT was used to generate all the graphs in this section. This script uses series of load flow simulation base on Newton-Raphson iterative load flow equation to plot the graph. Eskom Eastern grid has its highest load demand in two major areas; the Athene substation in Empangeni area and Klaawater substation in Pinetown area. This substation recorded almost 60% of all the load demand in the Kwazulu-Natal province (TDP 2016-2025). Presented in Figure 6.12 is the expected load growth in Eskom Eastern grid.

Figure 6.13 shows the normal operating condition of the Eastern grid when a DIgSILENT script was used to increase the load in Athene substation. It was observed in Figure 6.13 that the least stable busbar when the transformer tap changers were switced off is eThekwini 132 busbar. It can only allow 955MW power transfer before the bus voltage level falls below 0.95p.u. Nevertheless, when the transformer taps-changers were enabled, the P-V curve in Figure 6.14 turns to a zigzag format, signifying the effect of tap-changers in stabilizing bus voltage further to be able to allow more power transfer before the voltage profile falls below the appreciable limit.

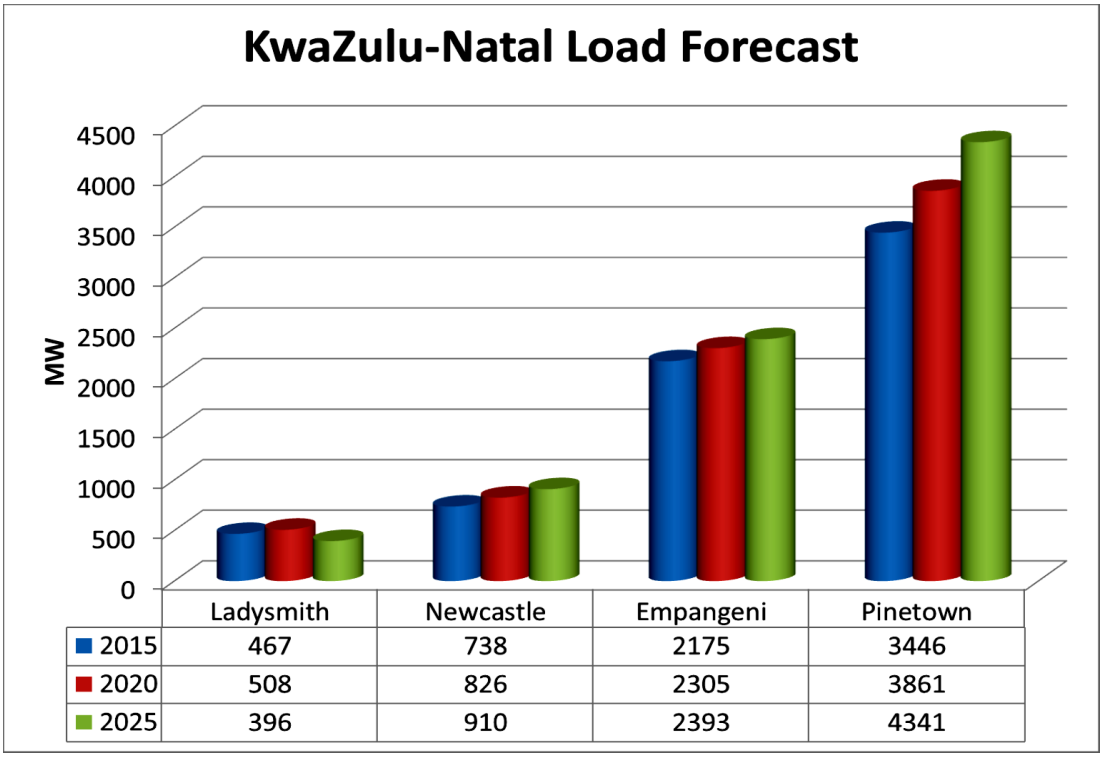

	Ladysmith	Newcastle	Empangeni	Pinetown
2015	467	738	2175	3446
2020	508	826	2305	3861
2025	396	910	2393	4341

Figure 6.12: Load demand in KwaZulu-Natal province (Eskom TDP 2016-2025)

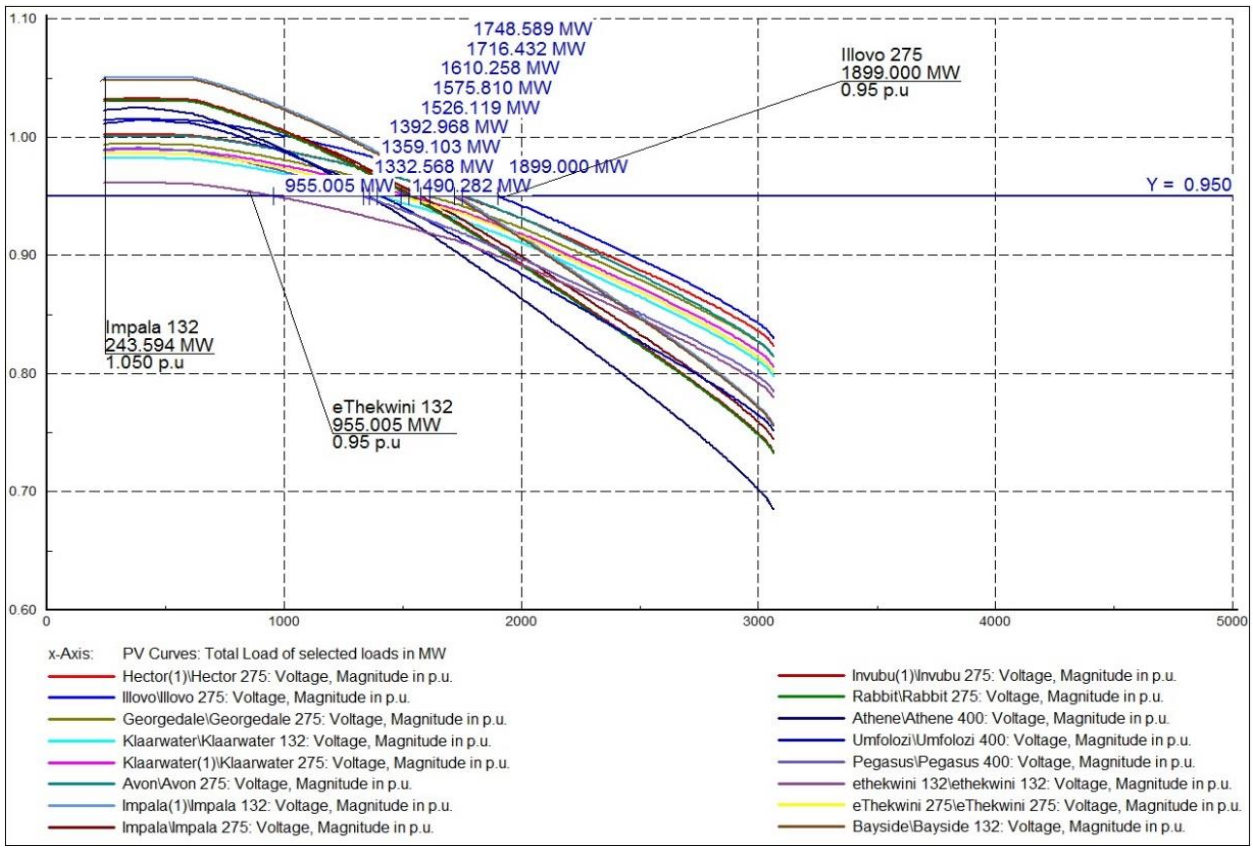

Figure 6.13: PV curve for Athene load (tap changers OFF)

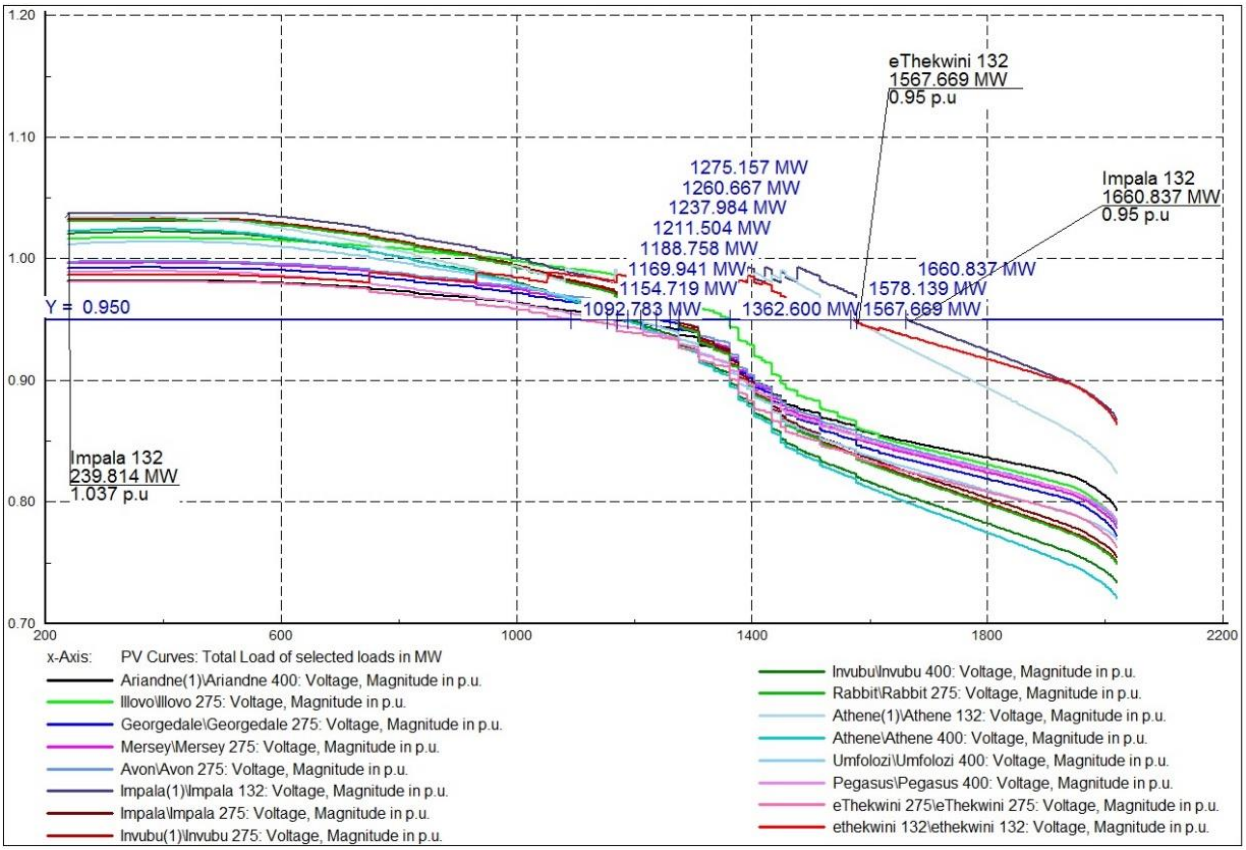

Figure 6.14: PV curve for Athene load (tap changers ON)

6.4.2. PV curve during N-2 contingency analysis

Figure 6.15 shows the PV curve during an N-2 contingences analysis. This N-2 contingences condition is a situation whereby a fault on the Majuba_Umfolozi 400kV line trip due to a fault which later leads to tripping of generating plant unit 6 in Majuba power station. It can be noticed from the graph that eThekwini bus voltage is already below an acceptable limit. This can later lead to system imbalance as eThekwini station hold an important part of the Eastern grid. When the transformer tap changers were enabled, the effect could be seen on the weakest eThekwini bus in Figure 6.16, which later allows 966MW power transmission into the eThekwini bus before voltage falls below 0.95p.u.

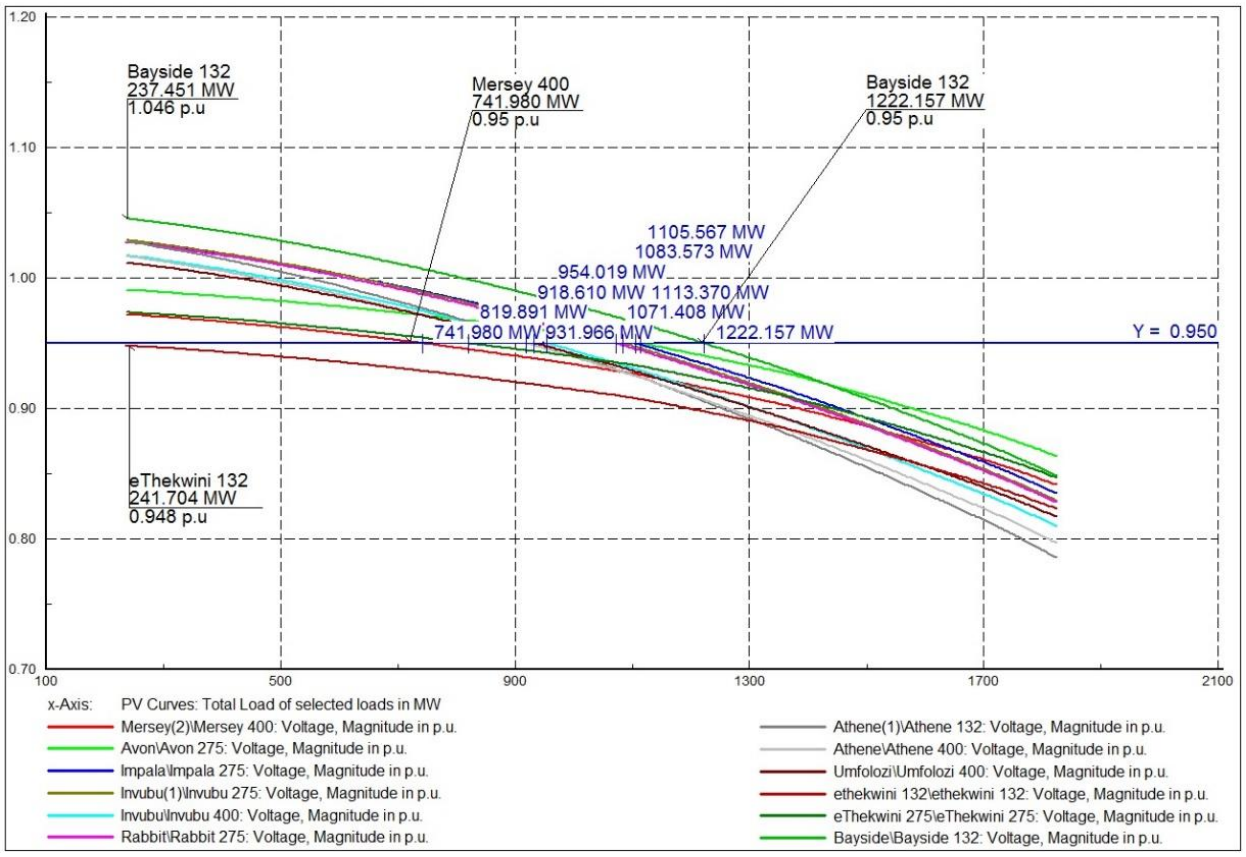

Figure 6.15: PV curve for Athene load during N-2 contingences (tap changes OFF)

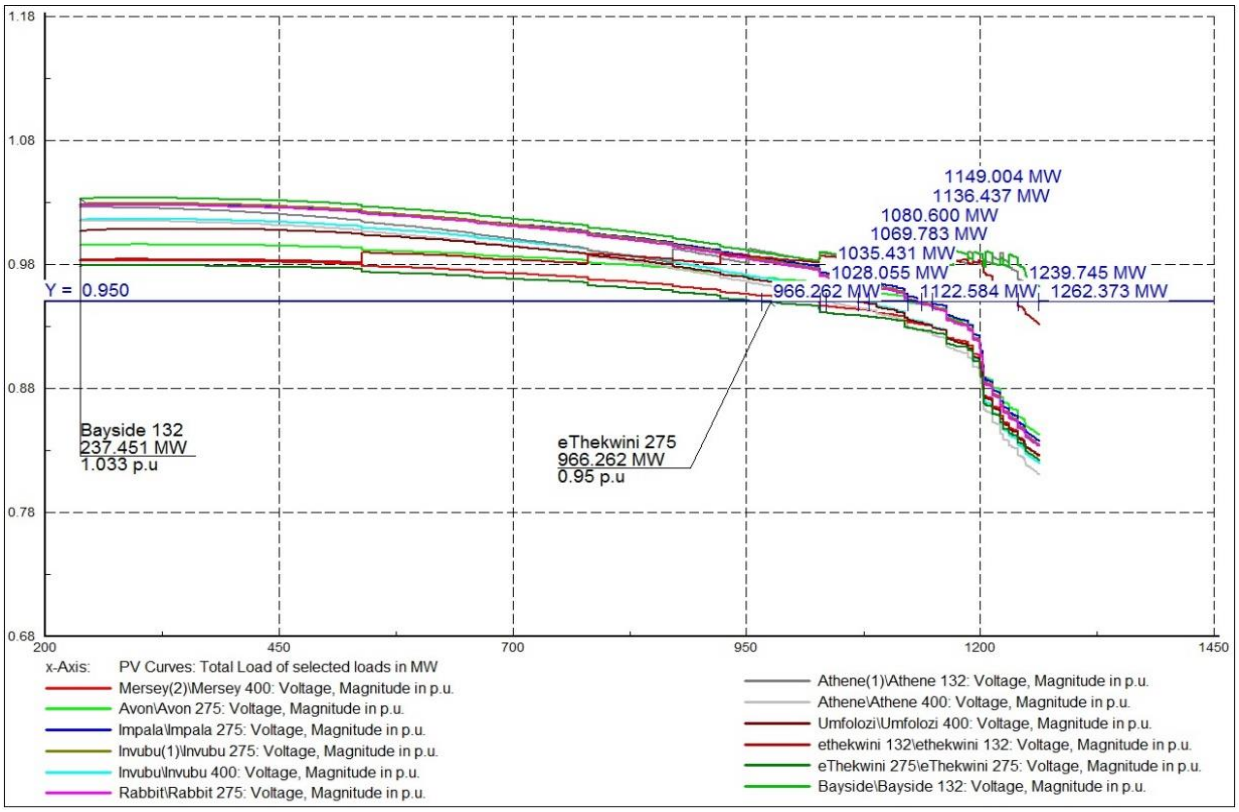

Figure 6.16: P-V curve for Athene load during N-2 contingences (tap changers ON)

6.4.3. Dynamic analysis

Different case studies were carried out while using the time domain simulation to investigate the weakest bus as well as the transmission line on Eskom Eastern grid. These case studies involve applying three-phase short circuits on busbar and transmission line on the network to observe the maximum time the bus/transmission line can withstand three-phase fault applied to it.

Three phase short circuits of 5Ω reactance fault were applied on the transmission line and a switch event was used on DIgSILENT PowerFactory to isolate the faulty lines from the entire systems. The critical isolating time (CIT) was thus recorded. This time, correspond to the maximum allowable time for the fault to remain on the network before instability occurs. A scenario whereby the fault was cleared rather than isolated from the entire system was also investigated. The time corresponding to the critical clearing time (CCT). This procedure was carried out on each transmission line one after the other, and their CIT/CCT was thus recorded. The transmission line with least CIT/CCT corresponds to the weakest line of the network and proper preventive measures needs be taken to avoid fault conditions on such line. In addition, a solid three-phase short circuit of 0Ω fault reactance was applied on the busbar and the CCT was estimated. These simulation results show that 400kV line connecting Majuba and umfolozi was the weakest transmission line of the network. In addition, Majuba 400kV busbar was the weakest bus in the Eastern gird.

The major point of focus for these research study is the busbar voltage profile, generator excitation current generator rotor angle, generator speed, and load active and reactive power.

Figure 6.17 show the busbar voltage profile when a three phase short circuits fault was applied on Majuba 400kV busbar for Fault time t=50ms. This graph shows a situation whereby the busbar voltage dips down to 0p.u. during fault but the system maintains a stable condition after that the fault was cleared. This means that the fault was cleared before instability occurs. The generator rotor angle with respect to reference machine plot can be seen in Figure 6.18. This graph shows how the generator of all the machines in the network undergoes slight oscillations, but the amplitude of these oscillations decreases with increase in time after clearing the fault. These oscillations eventually were damped off after fault and the system maintain back their steady state condition. The generator excitation current is displayed in Figure 6.19. Due to a fault, the value increases to provide for more generator field current. This aimed at maintaining synchronism between the grid and the generator by allowing more power from the generator and maintaining the generator terminal voltage at appropriately rated value. The generator speed is presented in Figure 6.20. This graph still maintains their steady state value as the fault has little impact on the generator speed. Active and reactive power consumed in the Eastern grid during fault analysis was represented in Figure 6.21.

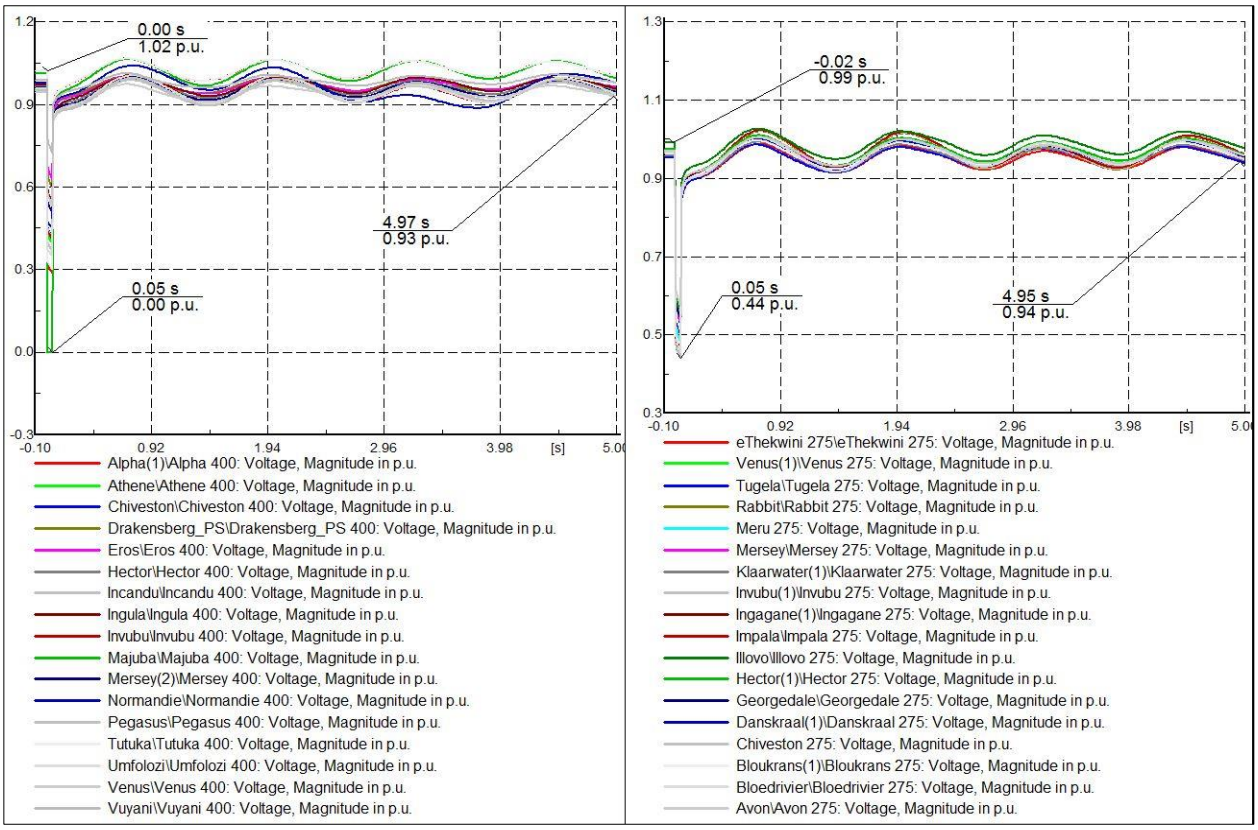

Figure 6.17: Busbars voltage after a three-phase fault on Majuba 400kV bus for t=50ms.

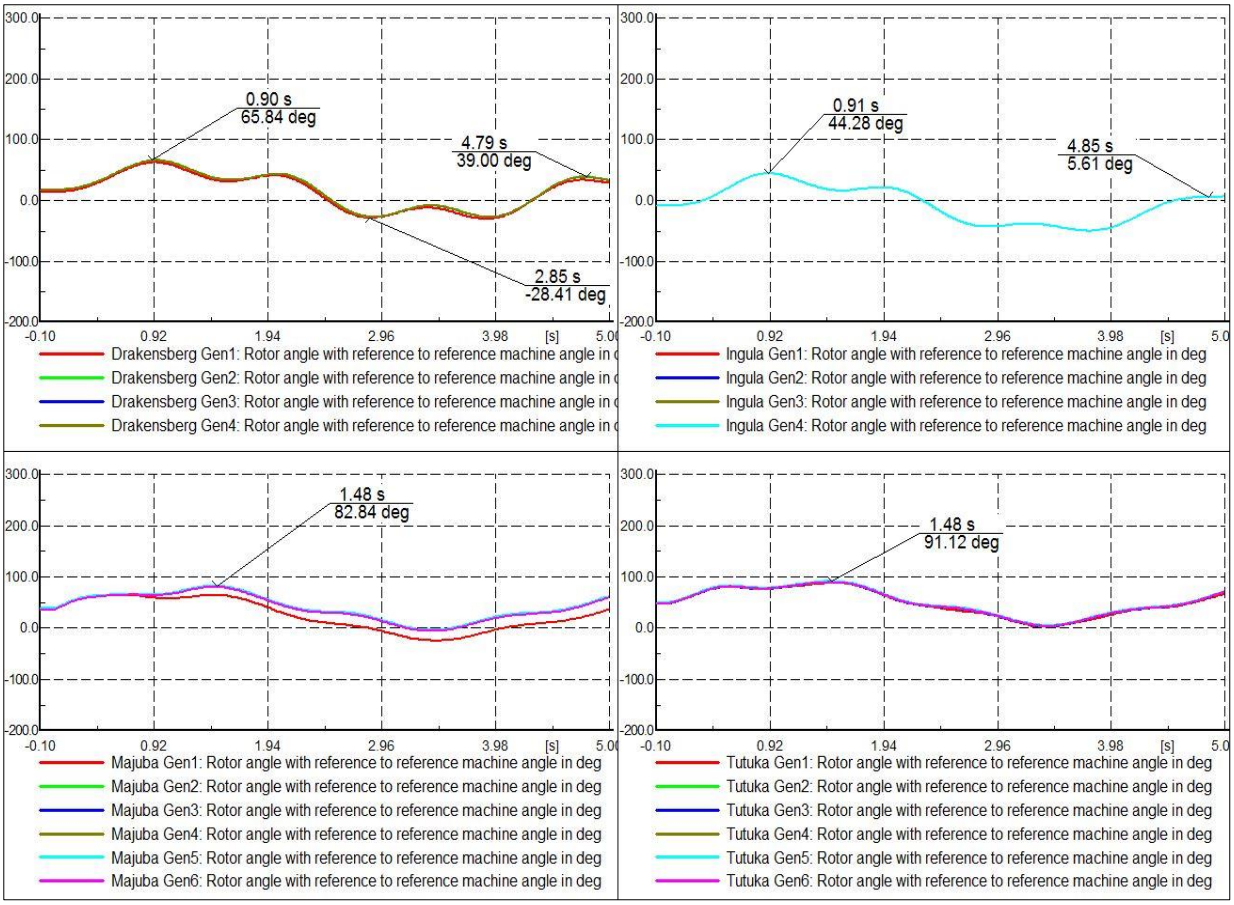

Figure 6.18: Generator rotor angle with respect to reference machine angle

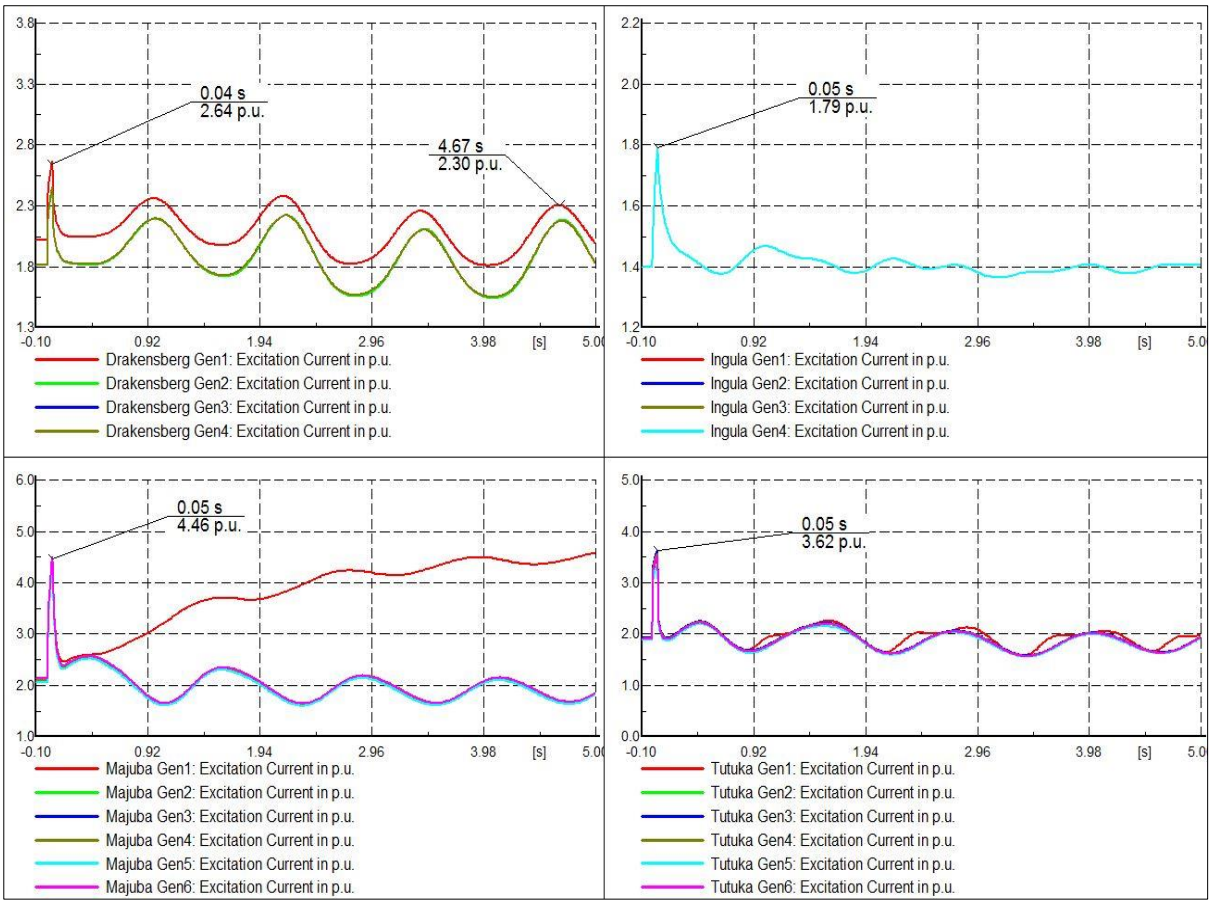

Figure 6.19: Generator excitation current

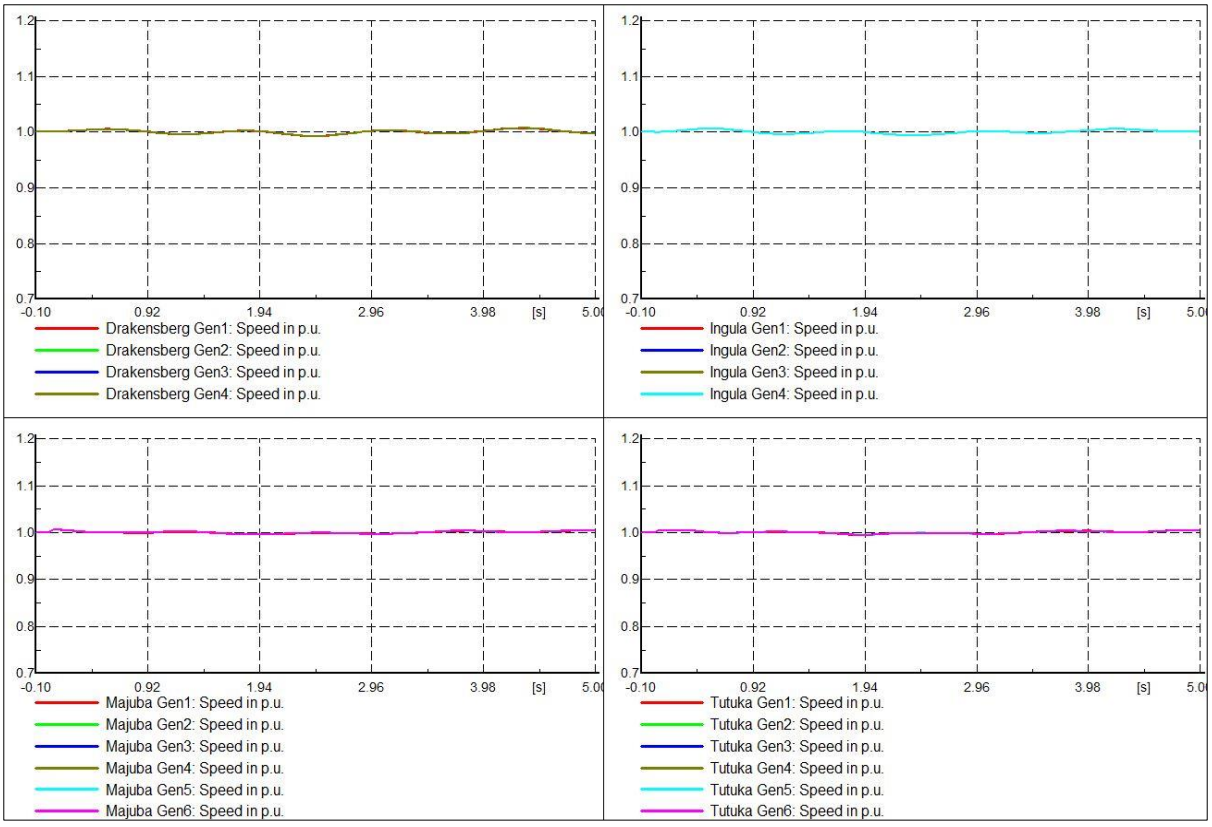

Figure 6.20: Generator speed

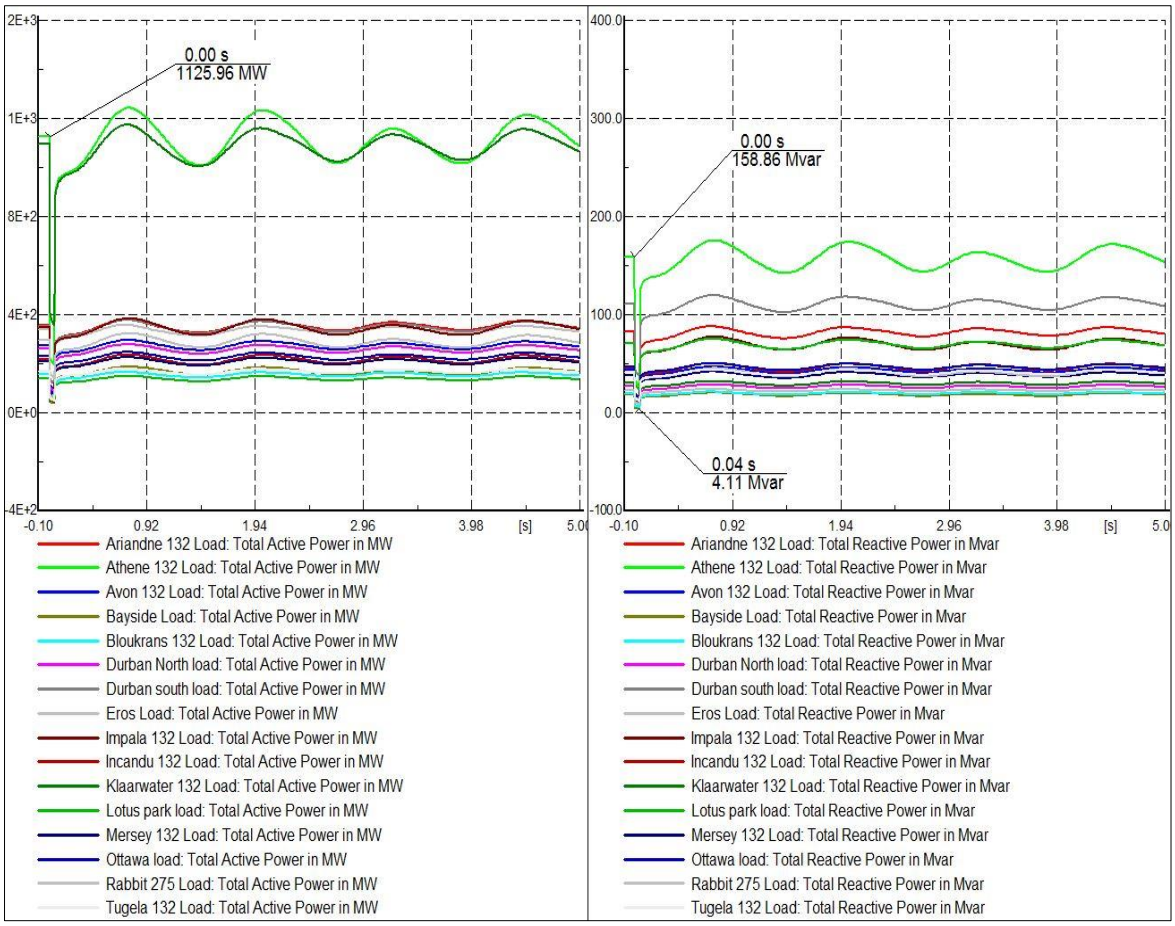

Figure 6.21: Load active and reactive power

When the critical clearing time was increased from t=50ms to t=120ms, the time corresponding to when appropriate breaker action should respond to isolate the fault, Figures 6.22 – 6.26 show the response of the network element to the elongated fault clearing time. Figure 6.22 shows the busbar voltage profile as it continuously oscillates from 0.4p.u. to 1.1p.u. This signifies an unstable condition of the entire system. The same unstable condition can also be noticed from the generators angle in Figure 6.23 as it swings pole to pole (-180 to +180 degree). Generator excitation current is shown in Figure 6.24.

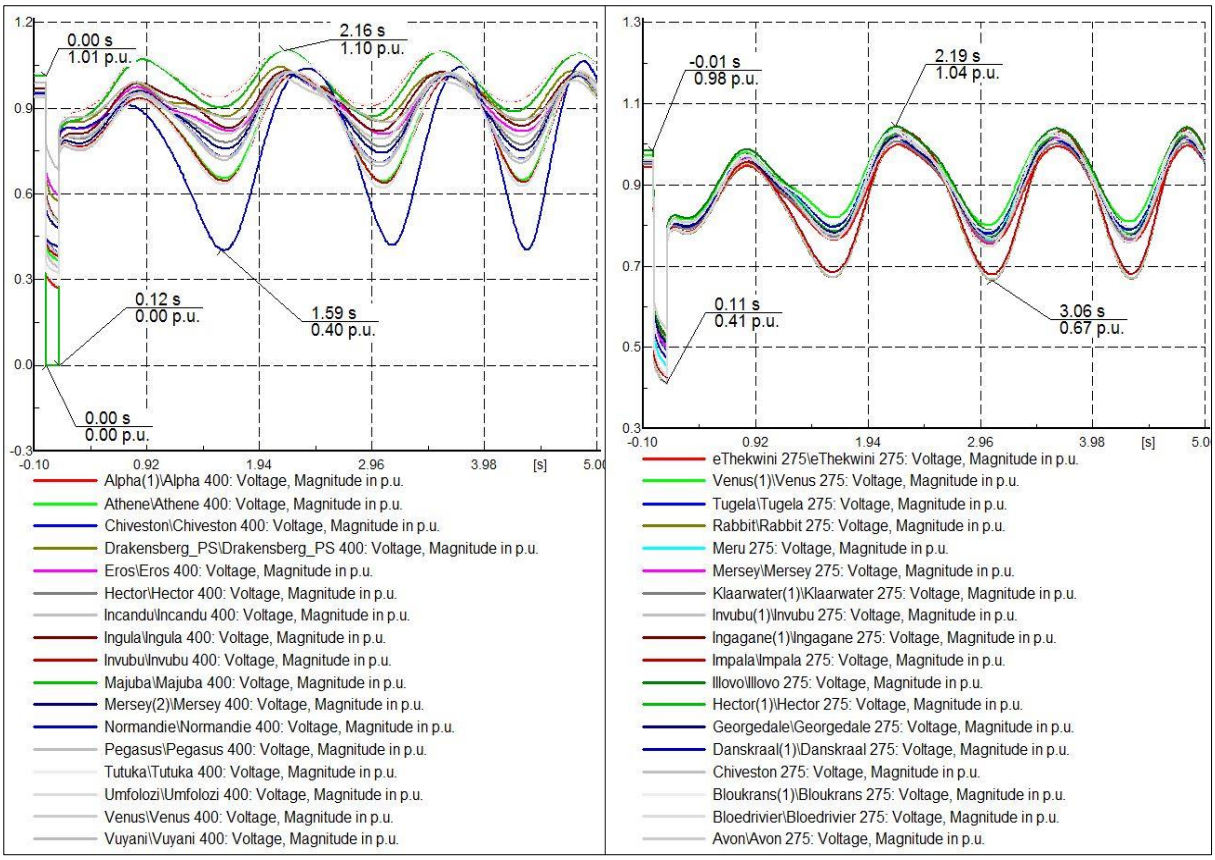

Figure 6.22: Busbars voltage after three-phase fault on Majuba 400kV bus for t=120ms

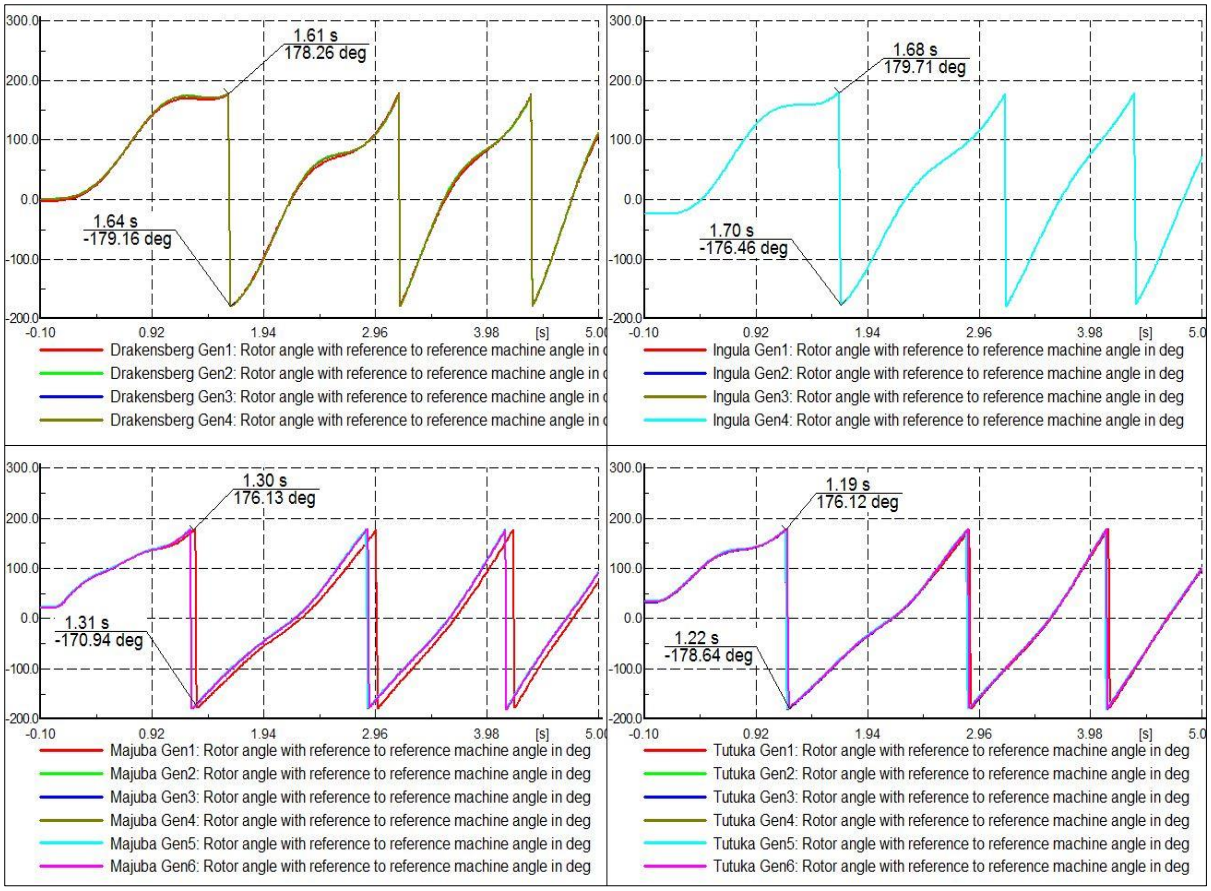

Figure 6.23: Generator rotor angle with respect to the reference machine

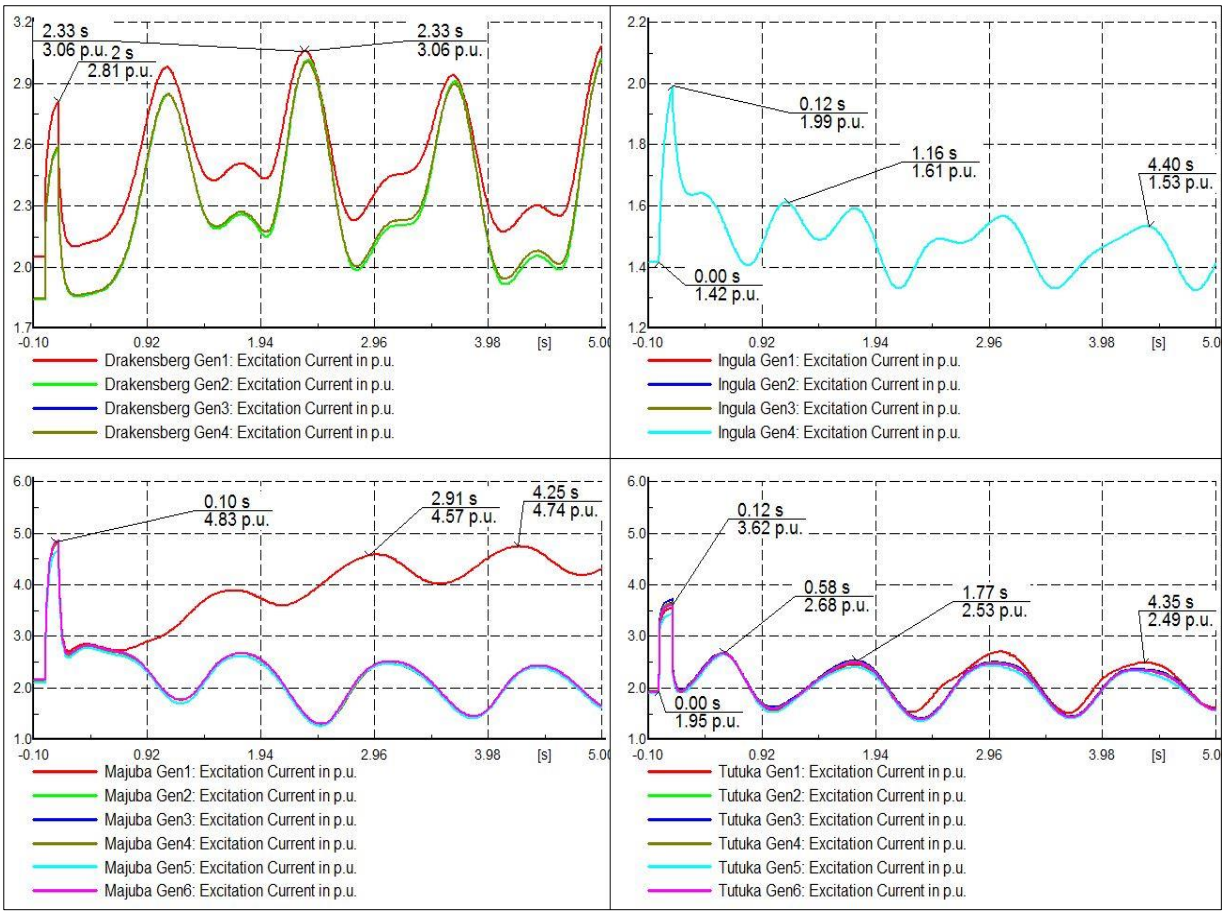

Figure 6.24: Generator excitation current

From Figure 6.25, the generator speed can be observed going out of step as the rotor speed of the entire generator oscillate and increase indefinitely. The same continuous oscillating in the load active and reactive power can be seen in Figure 6.26. Thus, it can be concluded that during a three-phase short circuits fault on Majuba 400kV busbar with fault clearing time of t=120ms, that the system was unable to maintain its steady state as all the field current. PSS and AVR of the generator as well as different compensating devices have yielded all their capacity to hold the system from entering instability condition after fault.

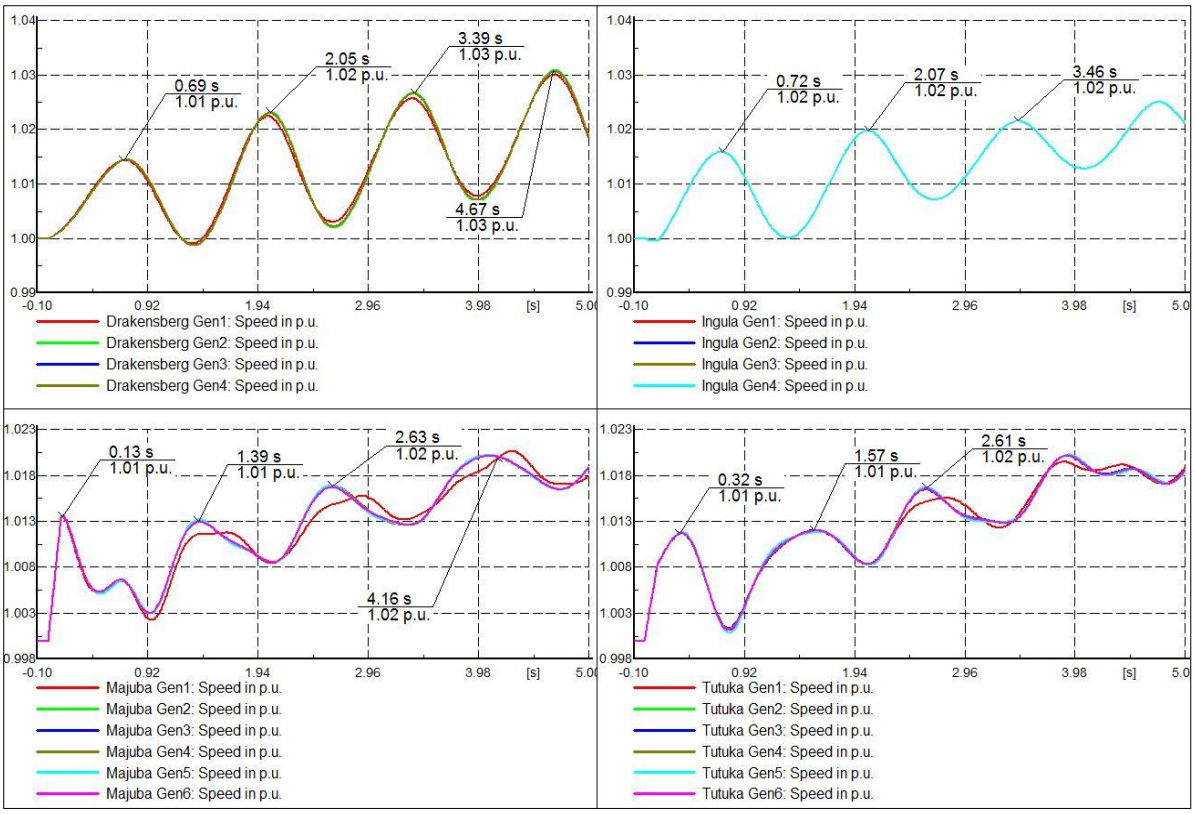

Figure 6.25: Generator speed

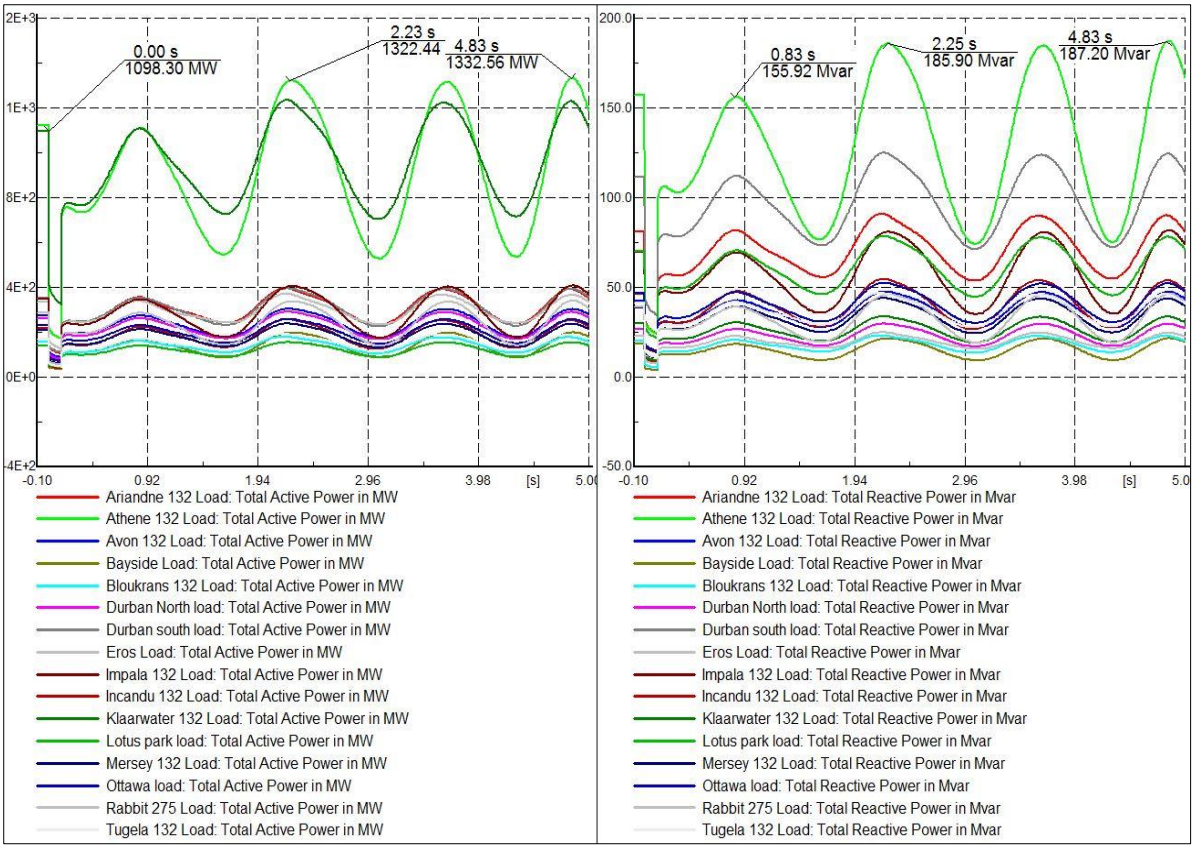

Figure 6.26: Load active and reactive power

6.5. Integration of HVDC Line into Eskom Eastern Grid

Eskom transmission development plan (2016 – 2025) made some plan of using HVDC network to transfer power into the Eastern grid due to yearly increase in the rate of load demand by this province. Constructing a new transmission line depends on many factors; one of such factors is ROW. In order to maximize this ROW, transmit bulk power over a long distance with minimal losses, and to have a transmission line that will improve the stability margin of the entire network, brings about the use of 600kV, 3000MW HVDC line to interconnect Massa substation in Limpopo province to Hector Substation in KwaZulu-Natal province. The rectifier station of this HVDC was planned to be in Massa substation while that of inverter was planned for two substations namely Hector and Invubu substation based on the station with high stability enhancement impact and load growth/demand. Figure 6.27 show the LCC HVDC scheme as modeled on DIgSILENT PowerFactory. More details about the controller modeling, fault analysis, and the step response have been addressed in chapter 3.

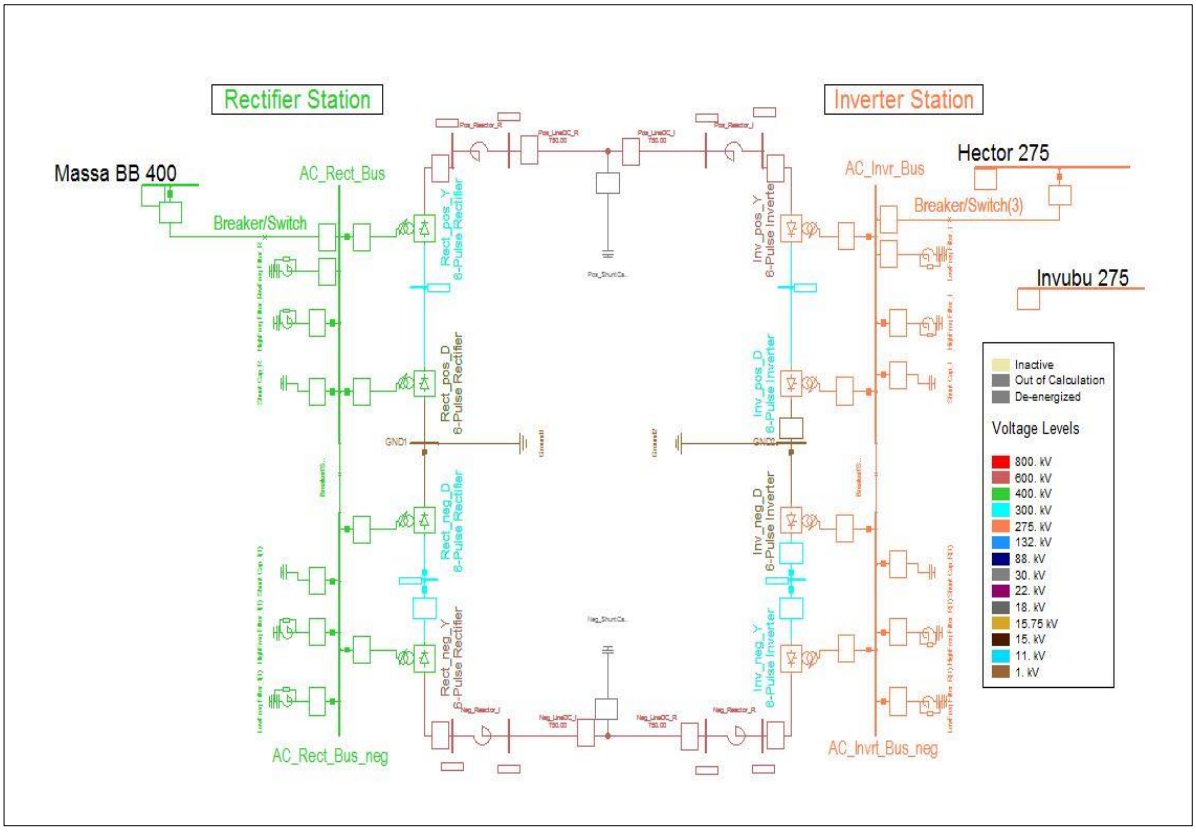

Figure 6.27: interconnection of LCC HVDC model into Eskom Eastern grid

6.5.1. System performance with 600kV HVDC

A load flow analysis was carried out on Eastern grid transmission network whilst using HVDC line to transmit bulk of power into the grid. A bar diagram was used to represent the result of this load flow analysis just as in the case of HVAC lines. This is to compare the load flow result with that of HVAC lines. This is to observe which of the method used for bulk power transmission reduces system loading with minimal losses on the transmission network. The busbar voltage profile, unlike the HVAC lines, has its voltage value above the stipulated 0.95p.u. This can be readily seen in Figure

6.28. This prove the fact that HVDC systems help to raise the busbar voltage profile of the network due to more reactive power that was supplied into the network. Figure 6.29 show the transmission line loading, reduction in this transmission line loading can be observed on this plot except for Hector_Klaawater line that is almost loaded, and the major reason is due to the high load demand in Klaawater station. A significant reduction can be seen from the transmission network losses on Figure 6.30. This was due to a reduction in power transfer along the HVAC lines because HVDC lines were used instead to transmit a chunk of power into the Eastern grid.

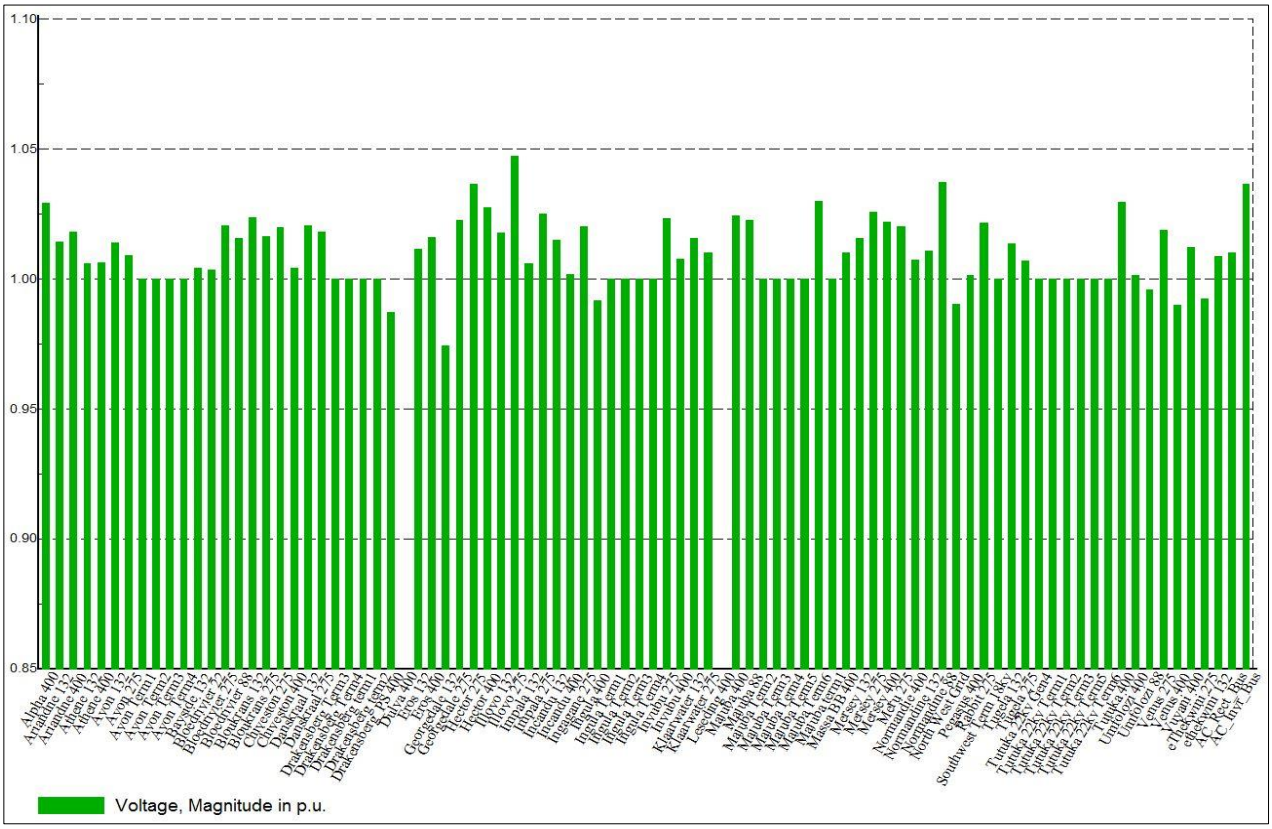

Figure 6.28: Busbar voltage

Figure 6.31 show the generator active and reactive power. Majuba gen 4 could be seen on this plot with a negative value for its active power, this signify a spinning reserve in case of emergency.

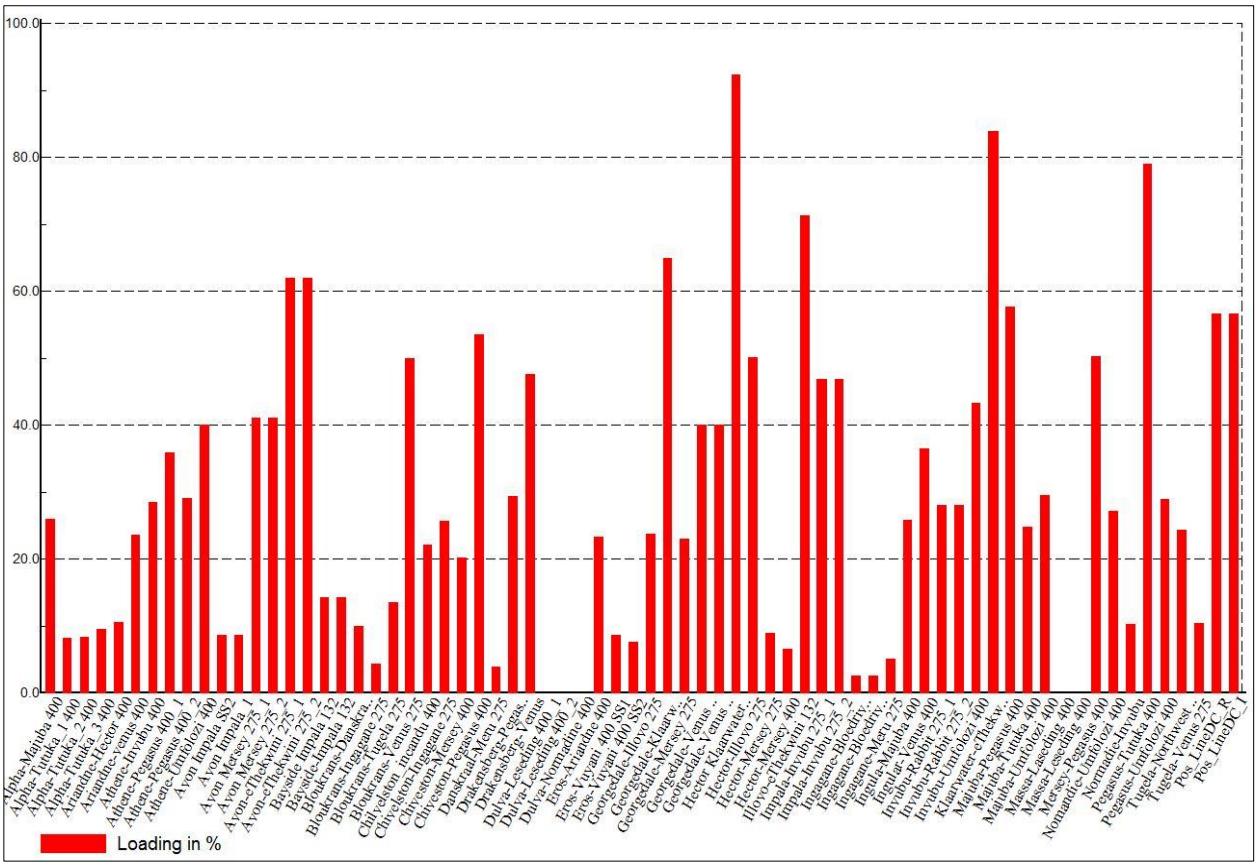

Figure 6.29: Transmission line loading

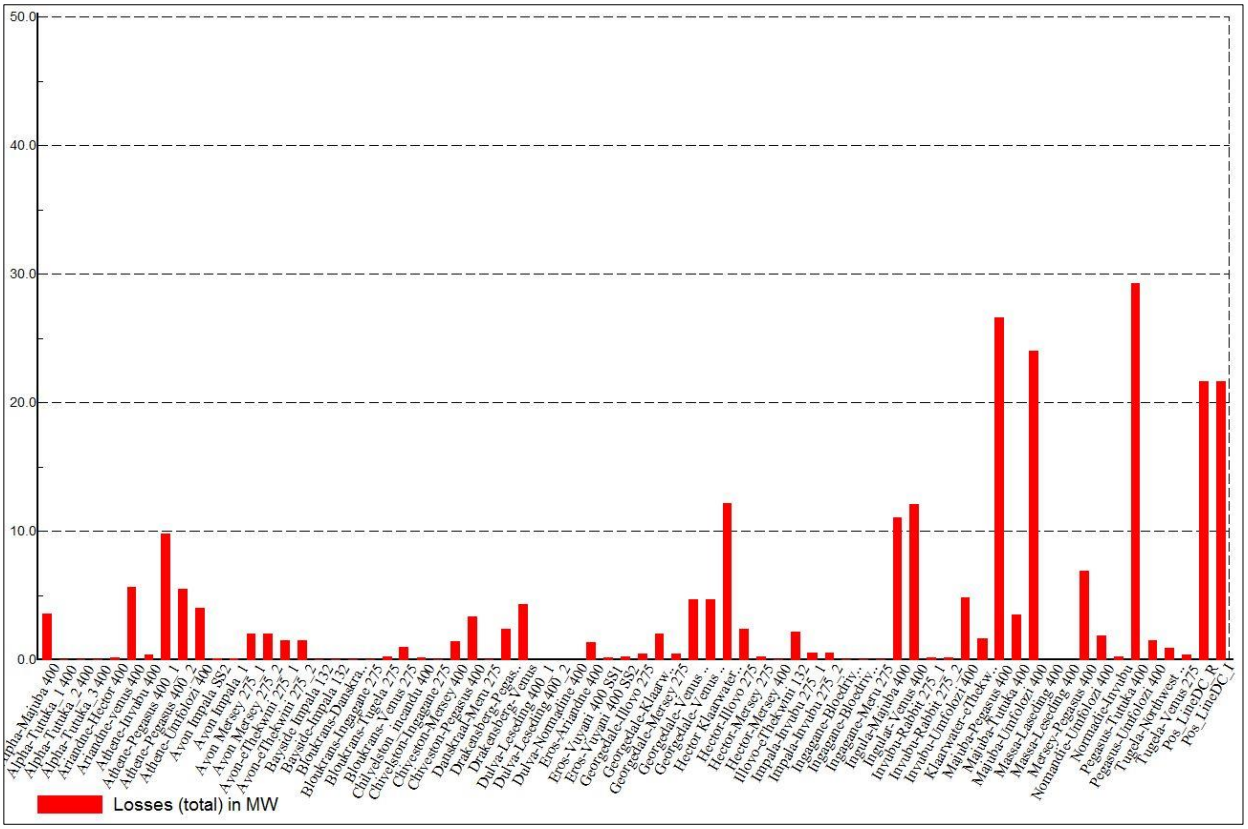

Figure 6.30: Transmission line losses

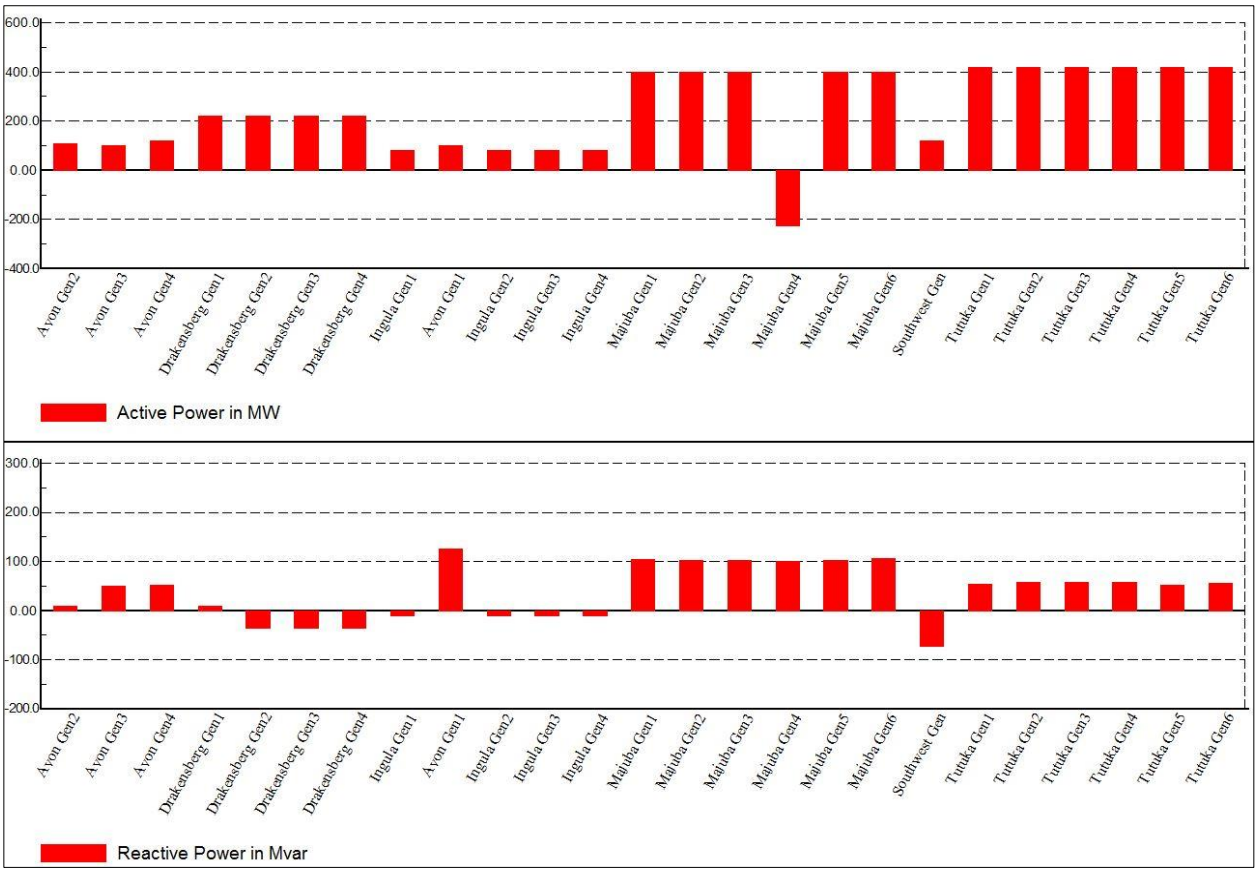

Figure 6.31: Generator active and reactive power

Figure 6.32 show the percentage loading of all the generator on the Eastern grid when HVDC system is in operation, a much relieve could be observed from this diagram as all the generators are below 80% loading except Avon gen1. This was unlike the first scenario when HVAC line was used which resulted in most of the generator to be overloaded pass the required limit.

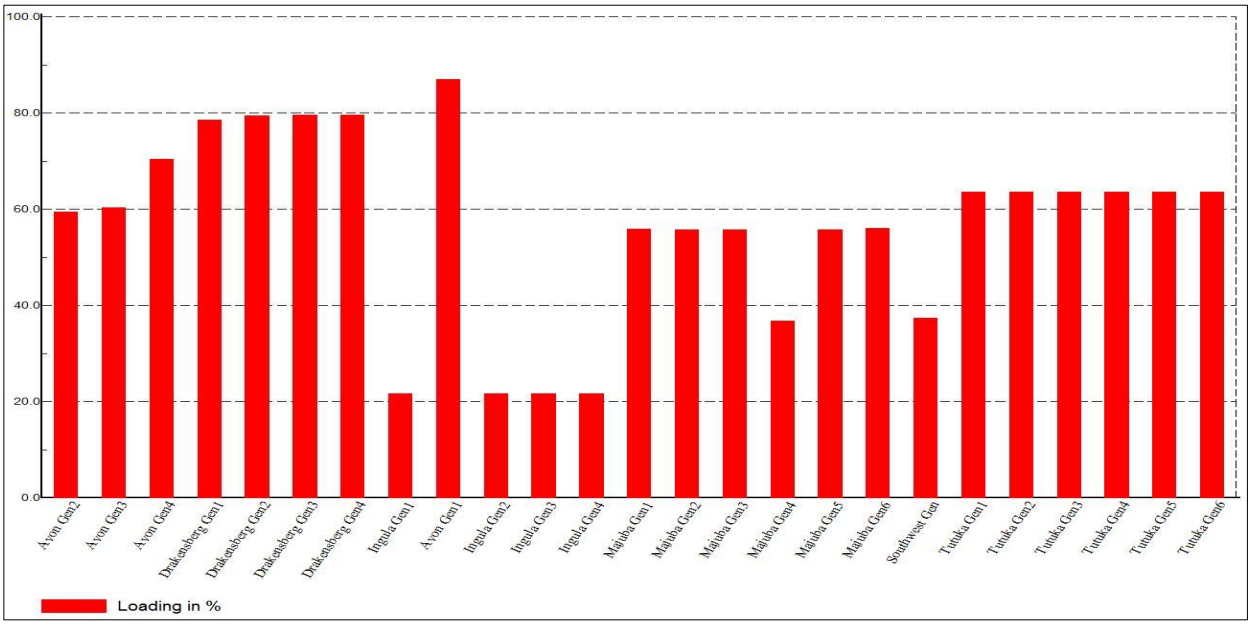

Figure 6.32: Generator loading

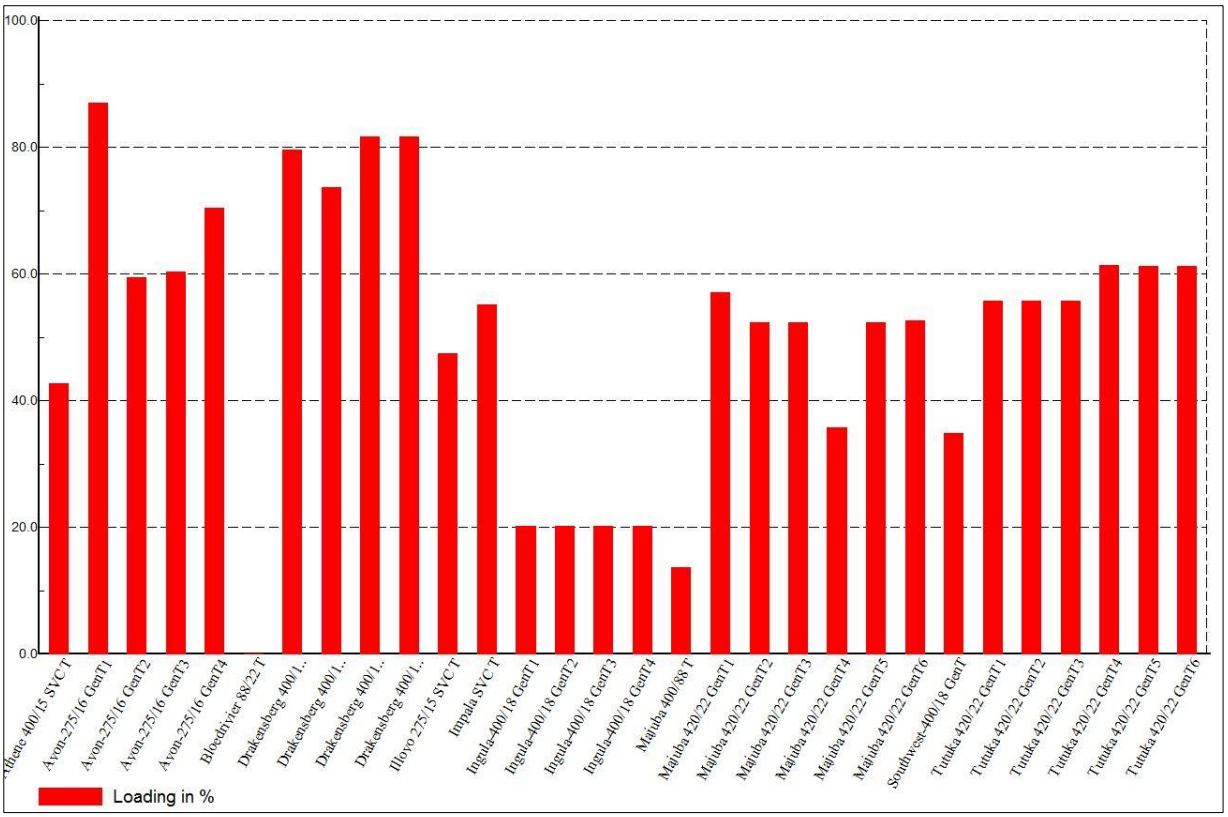

Figure 6.33: Two-winding transformer loading

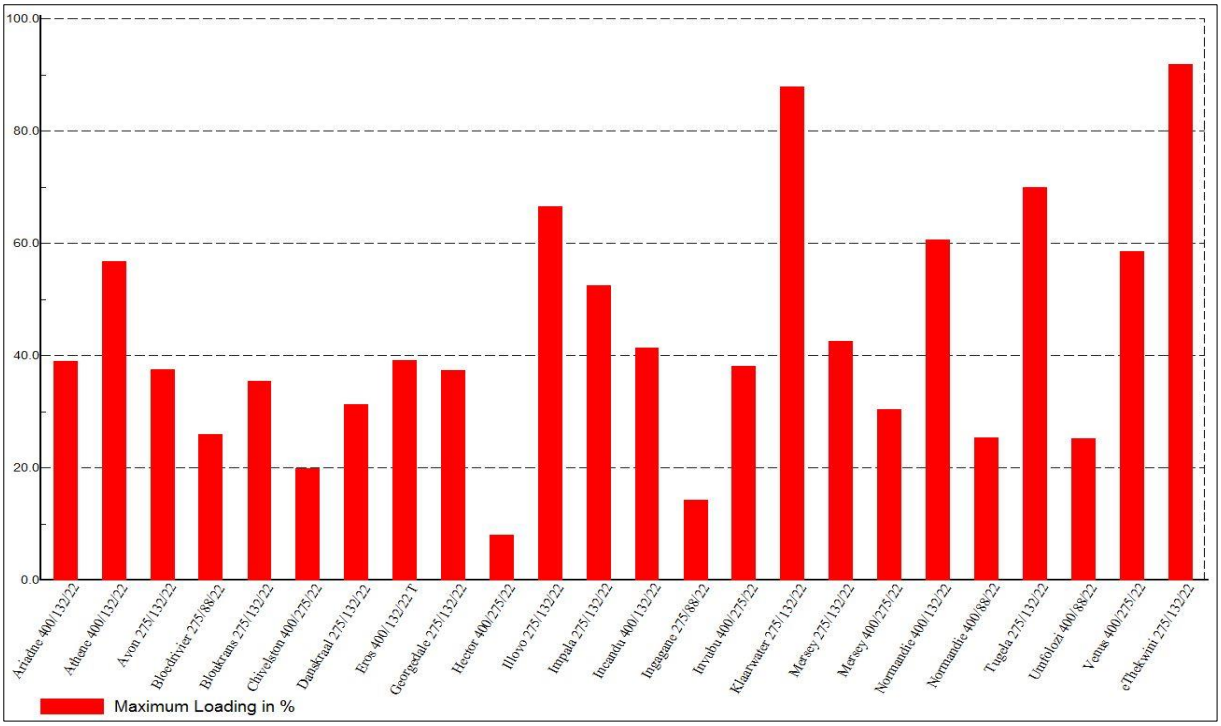

Figure 6.34: Three winding transformer loading

Figures 6.33 and 6.34 show the two-winding and the three-winding transformer loading respectively. This also maintains the fact that when HVDC system are used to transmit power over a long distance, all the network element around the recipient grid get relieved from being overloaded. An overloaded

transformer can lead to fire due to heat that causes all its insulating material/coolant to turn to a conductor.

Figures 6.35 and 6.36 display the network summary for both entire Eastern grid and HVDC grid respectively. It can be observed that the network losses is much lesser compared to the first scenario, and the HVDC network provides a reactive power support for the HVAC system as it only requires only 60% of its active power as reactive power support. Where there is the case of a shortage in AC busbar voltage, the reactive power in HVDC system is then used as compensation for the AC network. These reactive power supports are from capacitors and inductors that are switchable with tap changers. From these summaries, it can even be seen that the power supplied to all the loads are much more than the one when HVAC lines were used, meaning HVDC can work up to 95.75% percent of their rated value with minimal approximate losses of 4.24% per pole per transmission distance.

							DIgSILENT PowerFactory 15.1.6	Project:			Date: 5/10/2016
Load Flow Calculation											Grid Summary
AC Load Flow, balanced, positive sequence					Automatic Model Adaptation for Convergence						No
Automatic Tap Adjust of Transformers		Yes			Max. Acceptable Load Flow Error for						
Consider Reactive Power Limits		Yes			Nodes						1.00 kVA
					Model Equations						0.10 %
Grid: 1.0 EskomEastern Gri System Stage: 1.0 EskomEaster					Study Case: 2.1 Power_Flow AC with 600						Annex: / 1
Grid: 1.0 EskomEastern GridSummary											
No. of Substations	57		No. of Busbars	90		No. of Terminals	951		No. of Lines	63	
No. of 2-w Trfs.	30		No. of 3-w Trfs.	24		No. of syn. Machines	25		No. of asyn.Machines	0	
No. of Loads	33		No. of Shunts	23		No. of SVS	3				
Generation	=	6017.22	MW	977.79	Mvar	6096.15	MVA				
External Infeed	=	2139.79	MW	23.16	Mvar	2139.92	MVA				
Inter Grid Flow	=	173.11	MW	25.15	Mvar						
Load P(U)	=	7776.79	MW	1177.51	Mvar	7865.43	MVA				
Load P(Un)	=	7859.20	MW	1212.19	Mvar	7952.14	MVA				
Load P(Un-U)	=	82.42	MW	34.68	Mvar						
Motor Load	=	0.00	MW	0.00	Mvar	0.00	MVA				
Grid Losses	=	207.11	MW	1453.53	Mvar						
Line Charging	=			-2537.11	Mvar						
Compensation ind.	=			0.00	Mvar						
Compensation cap.	=			-1655.23	Mvar						
Installed Capacity	=	10858.40	MW								
Spinning Reserve	=	4841.18	MW								
Total Power Factor:											
Generation	=	0.99	[-]								
Load/Motor	=	0.99 / 0.00	[-]								
Inter Grid Flow to											
600 HVDC ctrl	=	173.11	MW	25.15	Mvar						
Total	=	173.11	MW	25.15	Mvar						

Figure 6.35: Eastern grid summary

		DIgSILENT	Project:
		PowerFactory	
		15.1.6	Date: 5/10/2016

Load Flow Calculation — Grid Summary

AC Load Flow, balanced, positive sequence		Automatic Model Adaptation for Convergence	No
Automatic Tap Adjust of Transformers	Yes	Max. Acceptable Load Flow Error for	
Consider Reactive Power Limits	Yes	Nodes	1.00 kVA
		Model Equations	0.10 %

Grid: 600 HVDC ctrl | System Stage: 600 HVDC ctrl | Study Case: 2.1 Power_Flow AC with 600 | Annex: / 2

Grid: 600 HVDC ctrl — Summary

No. of Substations	0	No. of Busbars	20	No. of Terminals	0	No. of Lines	4
No. of 2-w Trfs.	0	No. of 3-w Trfs.	0	No. of syn. Machines	0	No. of asyn.Machines	0
No. of Loads	0	No. of Shunts	12	No. of SVS	0		

Generation	=	0.00 MW	0.00 Mvar	0.00 MVA	
External Infeed	=	0.00 MW	0.00 Mvar	0.00 MVA	
Inter Grid Flow	=	-173.11 MW	-25.15 Mvar		
Load P(U)	=	0.00 MW	0.00 Mvar	0.00 MVA	
Load P(Un)	=	0.00 MW	0.00 Mvar	0.00 MVA	
Load P(Un-U)	=	0.00 MW	0.00 Mvar		
Motor Load	=	0.00 MW	0.00 Mvar	0.00 MVA	
Grid Losses	=	86.70 MW	2084.53 Mvar		
Line Charging	=		0.00 Mvar		
Compensation ind.	=		0.00 Mvar		
Compensation cap.	=		-2059.38 Mvar		
Installed Capacity	=	0.00 MW			
Spinning Reserve	=	0.00 MW			
Total Power Factor:					
Generation	=	0.00 [-]			
Load/Motor	=	0.00 / 0.00 [-]			

Inter Grid Flow to			
1.0 EskomEastern Gri	= -173.11 MW	-25.15 Mvar	
Total	= -173.11 MW	-25.15 Mvar	

Figure 6.36: 600kV HVDC grid summary

6.5.2. Loadability using PV curve with 600kV HVDC line

A case of static analysis using PV curve was also investigated while using HVDC lines to interconnect Massa and Hector substation. The PV curve was plotted to determine the amount of active power that could be transferred via the lines before the busbar voltages fall below 0.95p.u. This process has been well explained in chapter four with a 2-bus network. Results show that the busbar voltages reduce as load demand from constant source increases. It could be observed in Figure 6.37 that with HVDC line, Athene load could allow more power up to 1839MW before the busbar voltage falls below 0.95, even when the tap changers were disabled. This can be compared to the first senario of HVAC line of Figure 6.13 with 955MW load-ability when the tap changers were switched OFF and 1092MW of Figure 6.14 when the tap was ON. This shows that HVDC line enhances system stability and help to maintain busbar voltage since its transmission lines are like a pure resistive load.

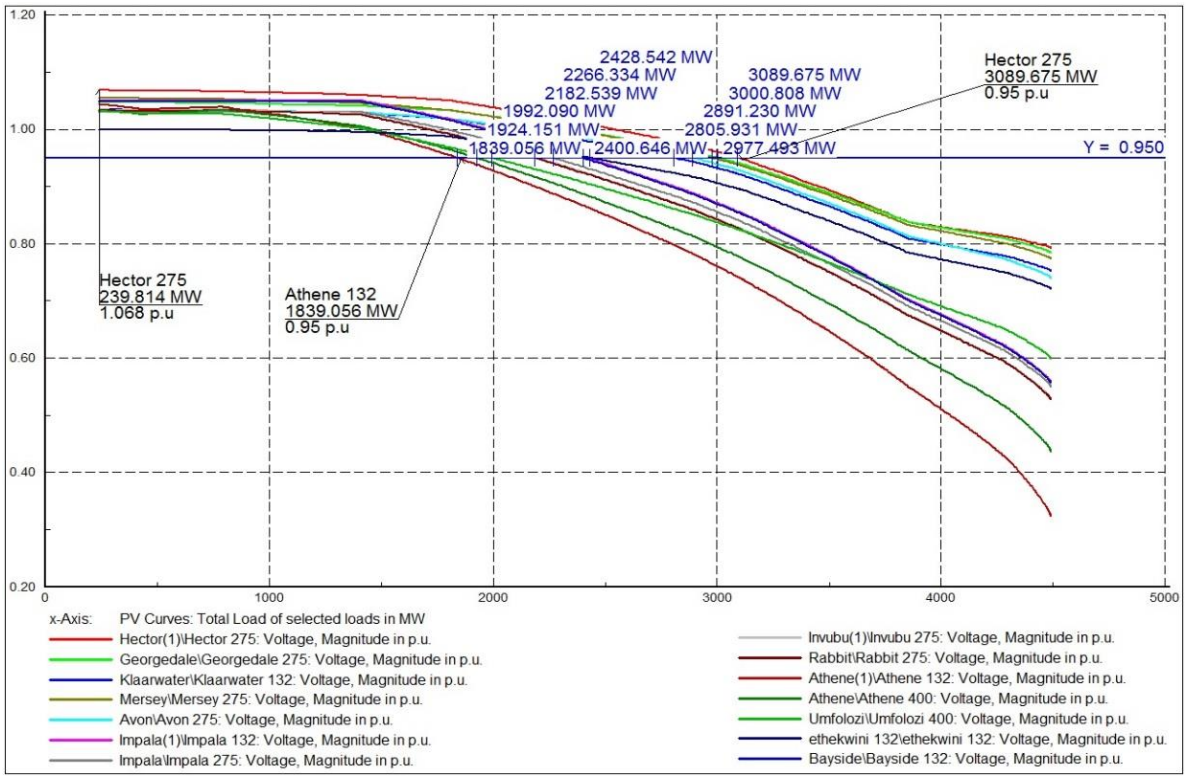

Figure 6.37: PV curve for Athene load (with HVDC line)

6.5.3. N-2 contingences analysis with HVDC line

Figure 6.38 shows the PV curve during N-2 contingences analysis. This scenario is the same as the one stated in section 6.4.2. Whereby system fault in Majuba busbar result in both a generator (Majuba gen 6) and a transmission line (Majuba_Umfolozi) to trip. It can be summarized from this curve that the power transfer capability increases before voltage profile falls below 0.95p.u. in Athene station. The 1440MW power transfer can be compared to 214MW of Figure 6.15 and 966MW of Figure 6.16. This implies that, during system fault when HVAC system requires more reactive power support in order to maintain the busbar voltage between an acceptable range of 0.95 – 1.05p.u. However, it was still unable to meet such reactive power support. This can originate from many reasons, such as shortage in the generator field current or shortage of reactive power compensator from available capacitor bank or SVC. Therefore, HVDC system helps to sustain the network by reducing the loss on the line with improved power transfer to most of the load centres. This is due to the effective controller at each converter station of the HVDC system.

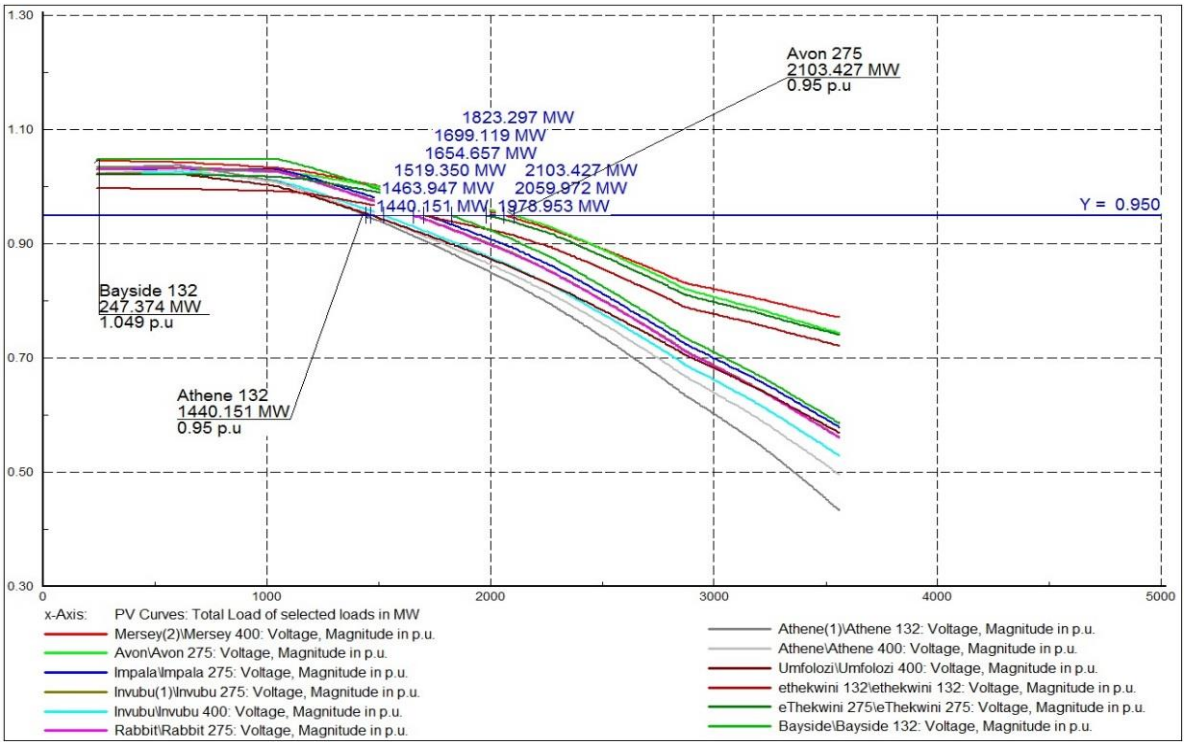

Figure 6.38: PV curve for Athene load during N-2 contingencies (with HVDC line)

6.5.4. Dynamic analysis (with HVDC line)

RMS Dynamic analysis with the use of time domain simulation was also carried out on the Eastern grid when 600kV HVDC line was used to interconnect Massa substation with Hector substation. Since the weakest bus was investigated to be Majuba 400K busbar, a three-phase short circuit fault was also applied on this Majuba 400kV bus just as in the case of the HVAC system in section 6.4.3. The following results that are represented in Figures 6.39 to 6.42 show the system response to this fault analysis whilst using HVDC scheme on Eskom HVAC network. Figure 6.39 show the busbar voltage, during a fault, the voltage dips down to 0p.u. at 0sec simulation time. At 0.418 sec, a commutation failure was recorded at HVDC inverter station hence more reason for voltage distortion at this simulation time. System restoration can be noticed after 1.296sec simulation time. Although, voltage waveform experiences some slight oscillations, but the amplitude of these oscillations decreases with increase in simulation time after the fault has been successfully cleared. Slight increase in the generator excitation current during fault can be seen in Figure 6.40. Majuba gen 4 (reference machine) recorded the highest excitation current of 6.3p.u, this is to keep the entire system in synchronism. However, the system maintained its steady state condition with increased simulation time.

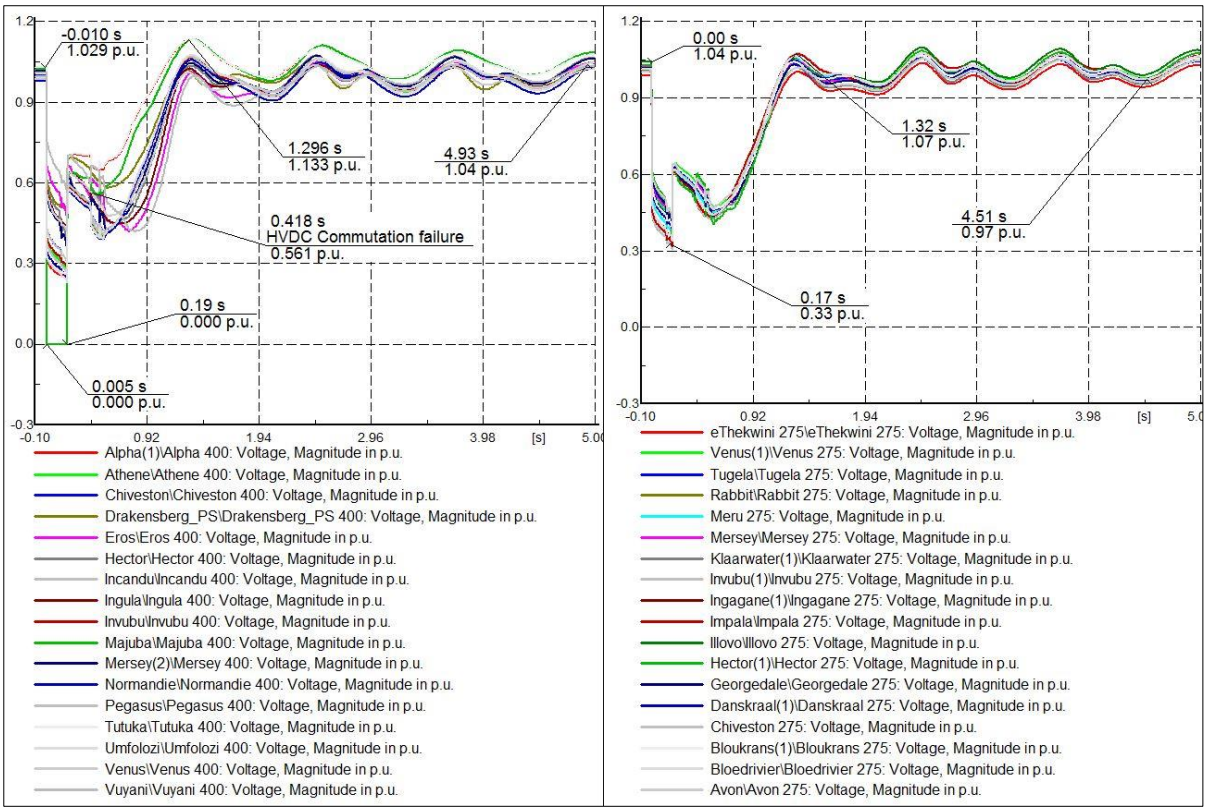

Figure 6.39: Busbars voltage after three-phase fault on Majuba 400kV bus for t=190ms

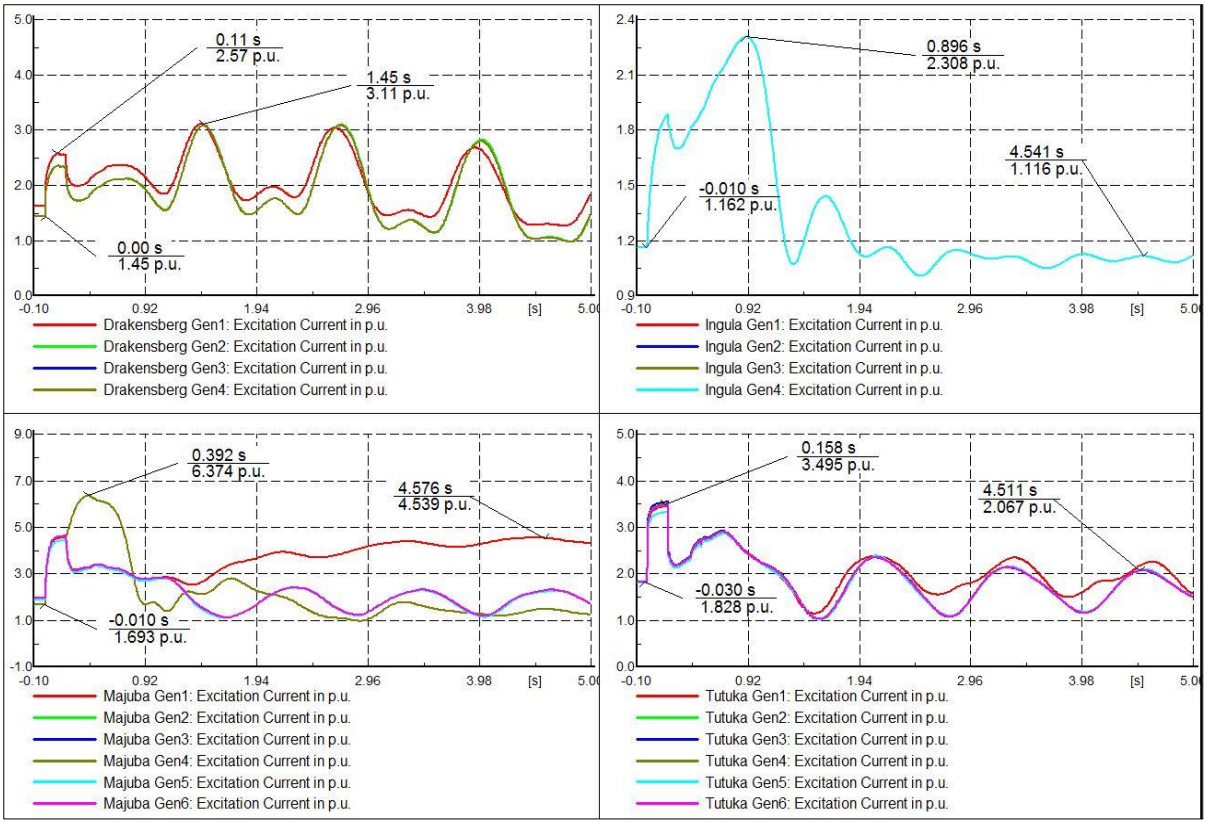

Figure 6.40: Generator excitation current

Generator rotor angle can be seen in Figure 6.41, Drakensberg and Ingular generator responded the same by the shape of their waveform, and this can be attributed to being located few kilometers from

each other. Their angles swing between 67^0 and -142^0 in Ingula station, this phenomenon was also observed at Drakensberg station with -50^0 to 76^0. The amplitude of these swings reduce as simulation time increases. This signifies a stable network condition. Majuba and Tutuka power station are also both few kilometres apart near Mpumalanga area. This justifies the reason for having the same curve. The case of pole slip when the generator swings out of step between an angle of 179^0 and -174^0 was recorded at 0.282secs simulation time. This was just after the fault was cleared, but the oscillations did not last long as the generator tends to align to their reference machine. It could be noticed from this subplot that the reference machine (Majuba gen4) was stable throughout the fault period as its value was 0^0. Thus, the systems regain their stable state as the oscillation amplitude was damped out as simulation time increases. Figure 6.42 represent the generator speed. Slight increase in speed with little oscillations was recorded but maintained a new steady state operating range as the system get restored back to their stable operating condition.

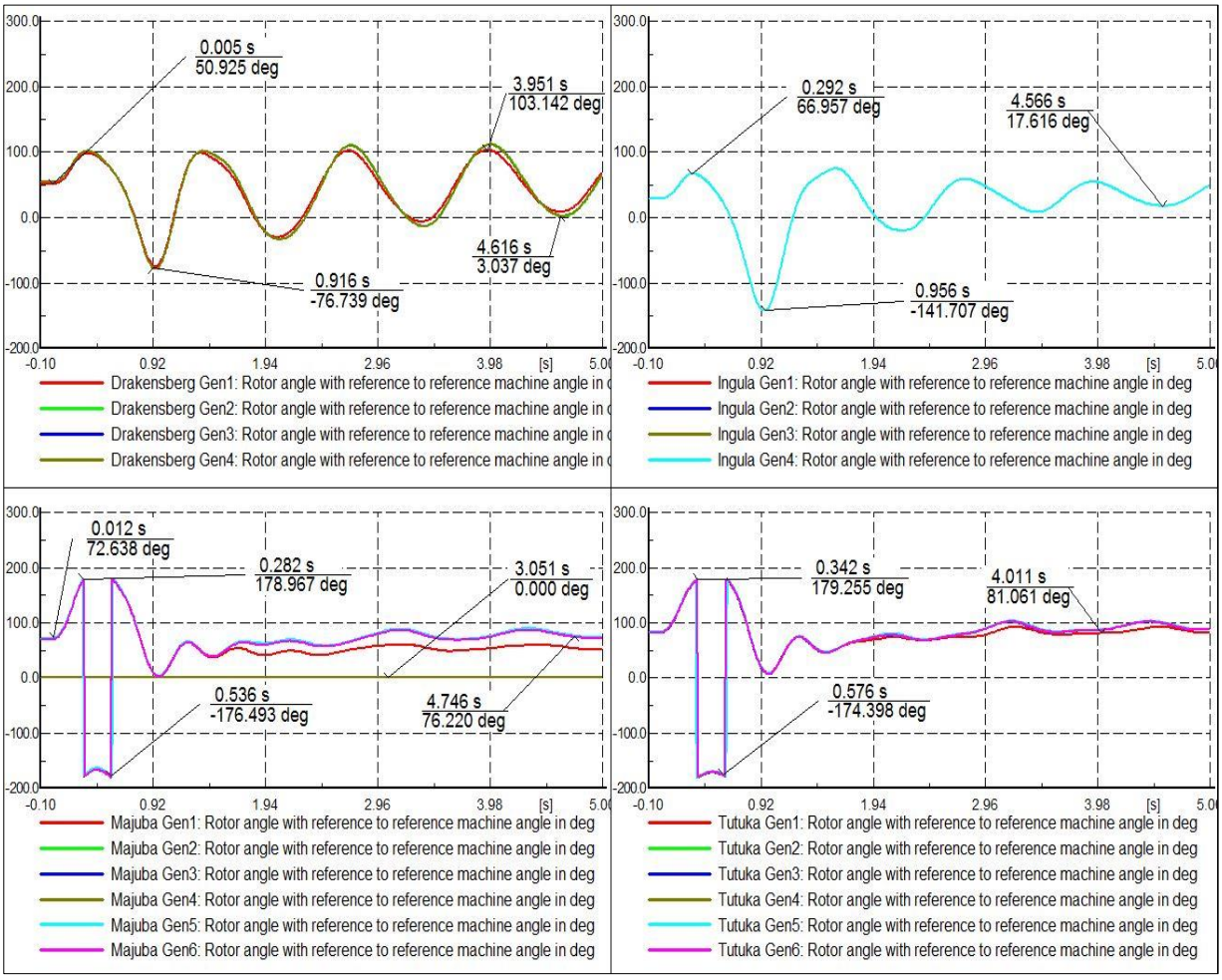

Figure 6.41: Generator rotor angle with respect to the reference machine

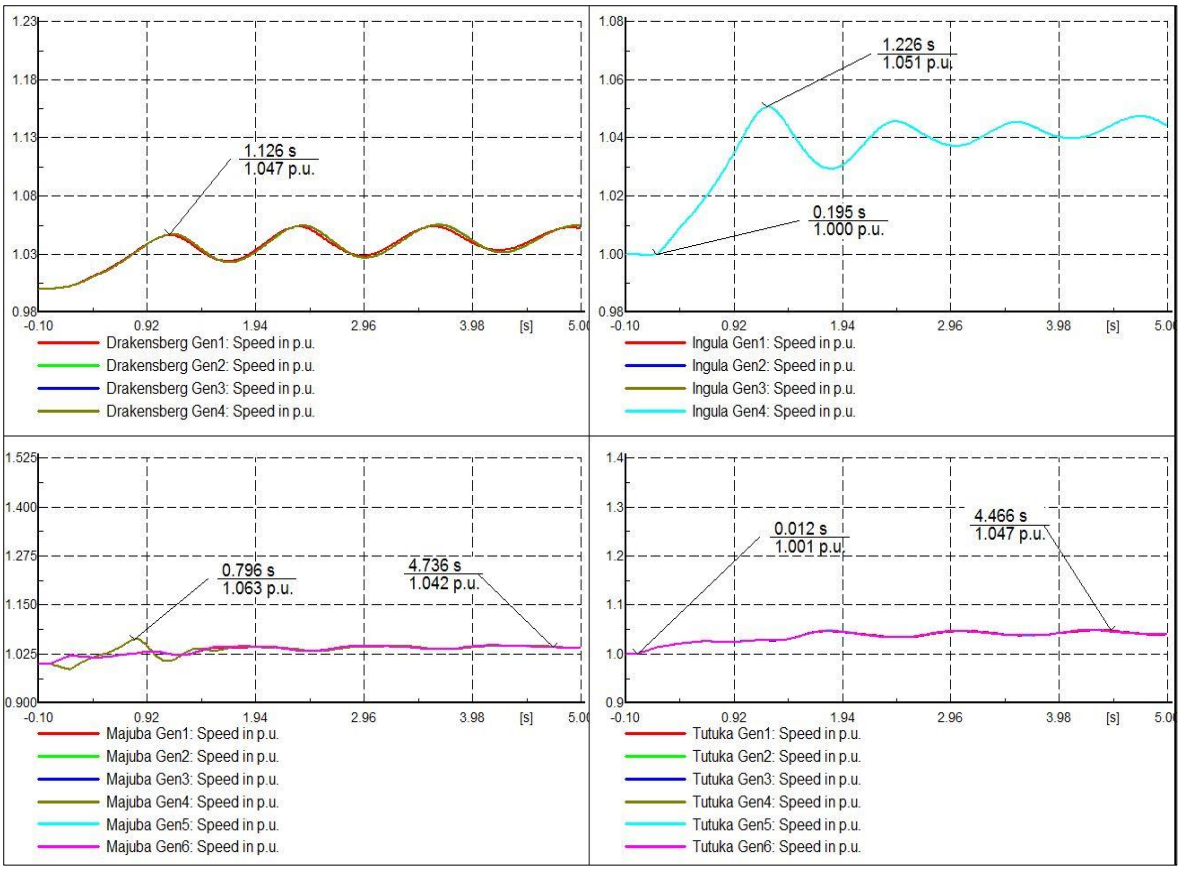

Figure 6.42: Load active and reactive power

6.6. System Performance with 800kV HVDC

800kV HVDC is a system with 5000MW capability. With this voltage and power rating, more power can be transfer into the Eastern grid with little line losses, reduced ROW compared to its contemporary 765kV HVAC lines. Upgrading from a 600kV scheme to 800kV scheme requires a modification and upgrading of the converter stations, transformer rating, transmission tower configuration, insulators, ROW as well as the different compensating devices used. Finally, the converter controller, which mainly is the heartbeat of the converter stations, needs some modification in the VDCOL rating as well as the pre-set voltage and current order. The effectiveness of this HVDC scheme will bring about a stable system that is immune to different system fault/disturbances.

The 800kV, 5000MW was used on the Eastern grid to convey power from the same power pool at Massa substation in Limpopo province to Hector substation in KwaZulu-Natal province. During the usage of 800kV line on the Eastern grid, the power was limited to 2500WM due to limited load on the network, but the HVDC scheme was modeled to have a capability up to 5000MW rated power. Different system performance analysis was thereby carried out on this network to determine its performance during the deployment of this scheme. It was found out that most of the major waveforms were the same as that of 600kV HVDC only different in its critical clearing/isolating time as this time records small improvement. Also during the steady load flow analysis, more improvement

was also noticed on the network parameters. Table 6.3 and 6.4 give a summarized result for the RMS simulation time for a three-phase fault on busbar and transmission line respectively.

Table 6.3: Busbar critical clearing time

Busbar (0Ω fault reactance)	**CCT of Busbar**		
	HVAC line	600kV HVDC line	800kV HVDC line
Majuba 400	80	190	200
Tutuka 400	100	240	250
Pegasus 400	150	500	510
Athene 400	200	1300	1400

Table 6.4: Transmission line critical isolation time and critical clearing time

Transmission lines (5Ω fault Reactance)	CIT (ms)			CCT (ms)		
	HVAC line	600kV HVDC line	800kV HVDC line	HVAC line	600kV HVDC line	800kV HVDC line
Majuba-Umfolozi 400	0	310	320	50	350	360
Majuba-Pegasus 400	0	280	290	70	350	360
Pegasus-Tutuka 400	0	410	420	80	450	460
Ingula-Majuba 400	10	280	300	100	350	360

6.7. 1000kV HVDC Network

1000kV is a next anticipated level of high power transmission over a long distance. Adopting such high voltage level requires more considerate studies to the field-testing with respect to the corona discharge from electric/magnetic field effect, insulation strength and pollution test. EPRI and other international bodies did major work on this research up to ultra-high voltage level of +1200kV. As much as the benefits that it offers in high power transmission due to strong growth in load demand, more emphasis need to be made on the current performance of any already installed HVDC scheme in the location where it is going to be used. Also, to look into the economic possibilities of constructing such high voltage transmission lines considering the insulation level, surge resistance, etc., furthermore, type and nature of the converter station, impacts on the environment as a result of audible noise couple with radio interference needs to be considered too. Finally, the unforeseen circumstances as regards new challenges in introducing ultra-high voltage level and above need to be well phantom into the design of such system. Example of these are, availability of testing facilities, sizing/appearance of the converter station, air clearance as a result of stressed dc voltage and switching surges, creepage distance especially in some highly polluted areas, and above all, the effect of loss of power to fault or outage event are all needed to be examined before implementation. More research have to be carried out to measure the safety of the voltage level in obedience to South Africa grid code and standard [21, 22]. However, this project study only use 600kV and 800kV voltage level due to less load forecast on Eskom TDP 2016-2025.

6.8. Cahora-Bassa HVDC Scheme

Cahora-Bassa HVDC link transmits 1,920 MW of power from hydropower plant located in Zambezi River, north of Mozambique to Johannesburg, South Africa. The rectifier station, located at Songo station of Mozambique is connected to the inverter station located at Apollo station using a 1414km, ±533kV bipolar lines. 64.2% of the transmission length is located in Mozambican territory while the remaining 35.8% resides in South Africa. An approximate of 7,000 towers span averagely over 426 meters of the transmission network. Reinforced towers with earth return are provided using buried graphite electrodes located at considerable distance from the converter station. Smoothing reactors, surge arrester, and capacitors bank are provided at each of the converter station to have a stable system. The inverter side of this scheme was refurbished in 2008, equipping it with 5'' electrically triggered thyristor valve capable of withstanding 3.3KA, 8.5 kV switching capacity [141]. Figure 6.43 shows the detailed diagram for Cahora-Bassa HVDC link as modelled on DIgSILENT. This diagram shows the hydropower plant, low-frequency/high-frequency filter and capacitor bank in Songo rectifier station. Inverter station located at Apollo has the equivalent load (external grid) and different compensating devices attached to its substation.

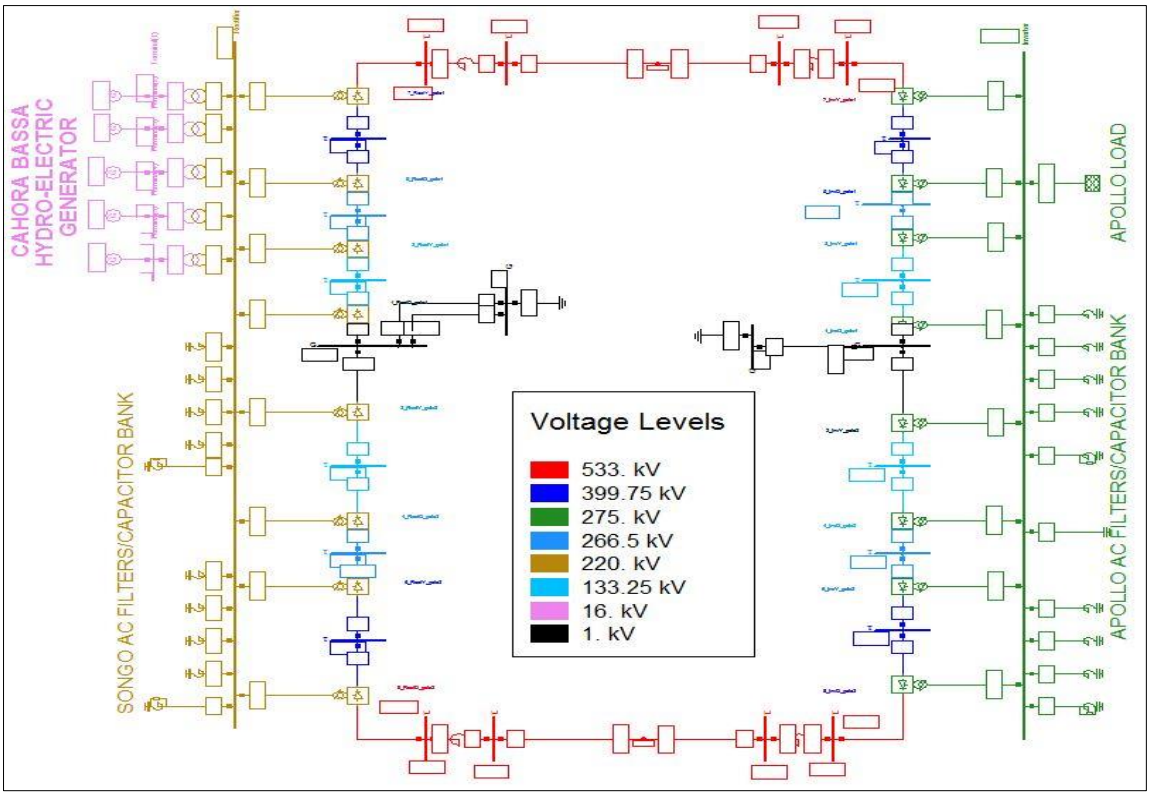

Figure 6.43: Detailed network diagram of Cahora-Bassa HVDC scheme

6.8.1. Performance analysis

The performance analysis used for Cahora-Bassa is to analyse the harmonics and voltage distortion during a three-phase short circuit fault. Fault at inverter side of the converter has more impact on the HVDC link than rectifier station fault, the more reason for frequent commutation failure occurrence

at inverter station. Thus, a three phase short circuits with zero fault reactance was applied at the inverter AC busbar for t =200ms, using electromagnetic EMT simulation tool which was ran for 1.00 seconds simulation time. The busbar voltage and converter current were represented in a graph. This graph was later zoomed upon to investigate different harmonics/distortion on this waveform of the converter current and busbar voltage. Figure 6.44a represents AC busbar voltage of both converter station during AC system fault. The rectifier (Songo) station witness reduction in voltage during the fault, whiles the inverter (Apollo) station experienced long interruption due to a fault. Converter AC current rises in Figure 6.45a while inverter station suffers commutation failure. Effect of controller in aiding HVDC system during system fault has been earlier discussed in chapter 3. Distortion in current/voltage waveform due to a fault in Cahora-Bassa HVDC scheme will be analyse in this section. Though the system regains its normal operating condition after successful clearing of the fault, but the AC voltage waveform, which was expected to be perfect sinusoidal has few distortions as seen in Figure 6.44b. Furthermore, the current waveform of an LCC HVDC is more or less like a trapezoid form rather than a perfect sinusoidal shape. This can be seen in Figure 6.45b.

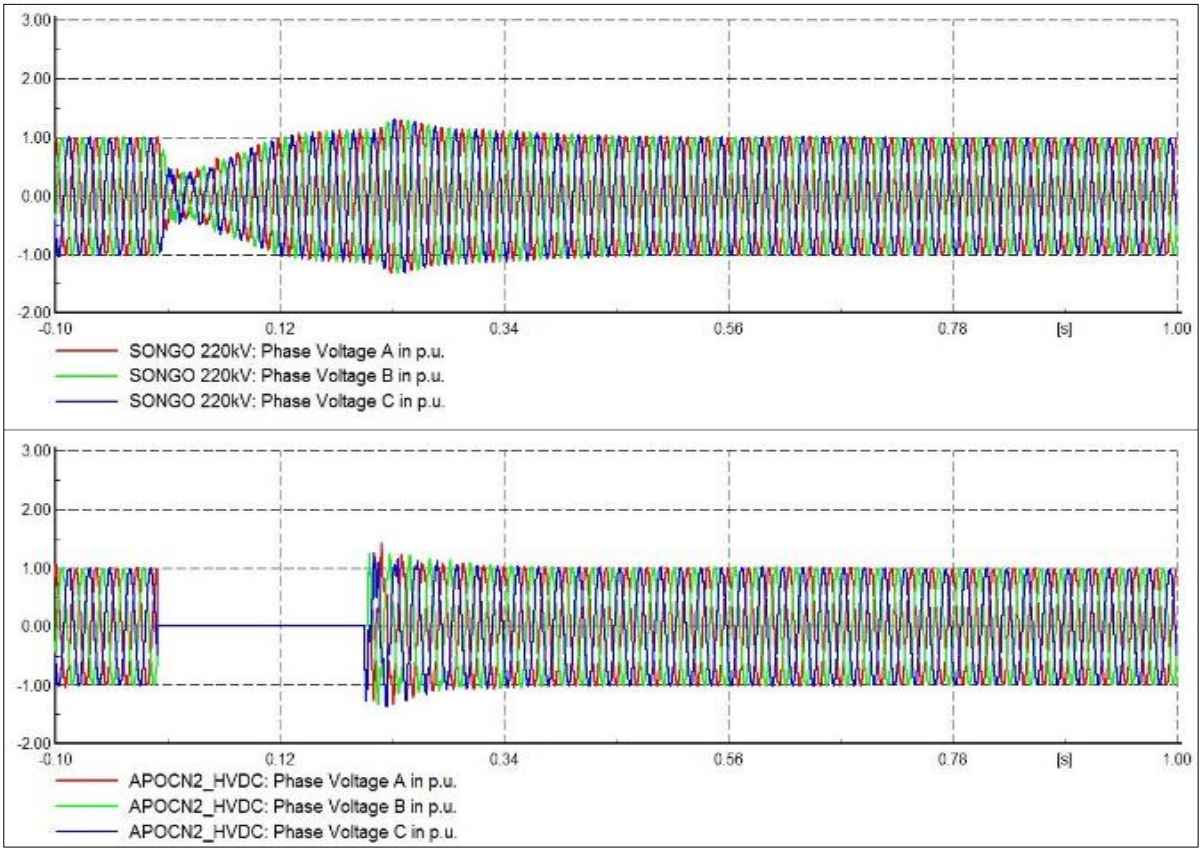

Figure 6.44a: AC busbar voltage of LCC-HVDC

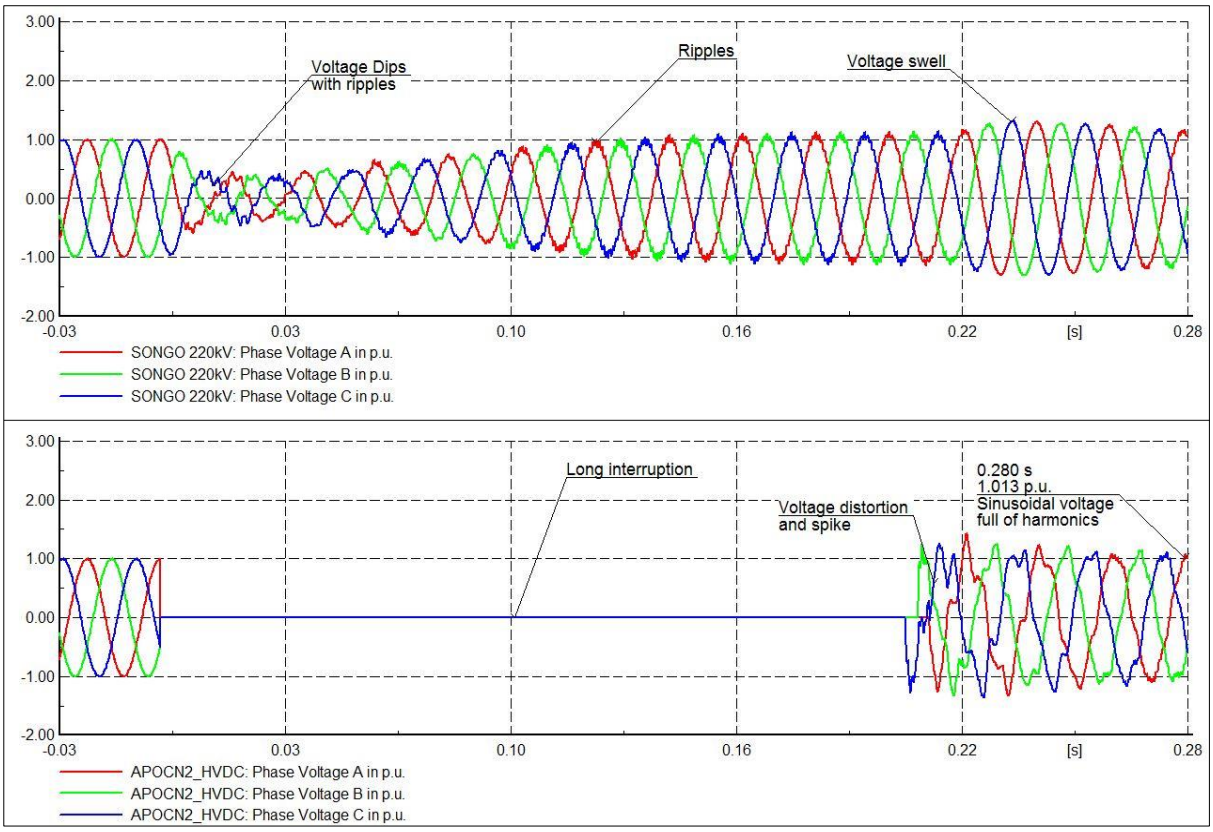

Figure 6.44b: Zoomed voltage waveform between -0.03 to 0.28-simulation time

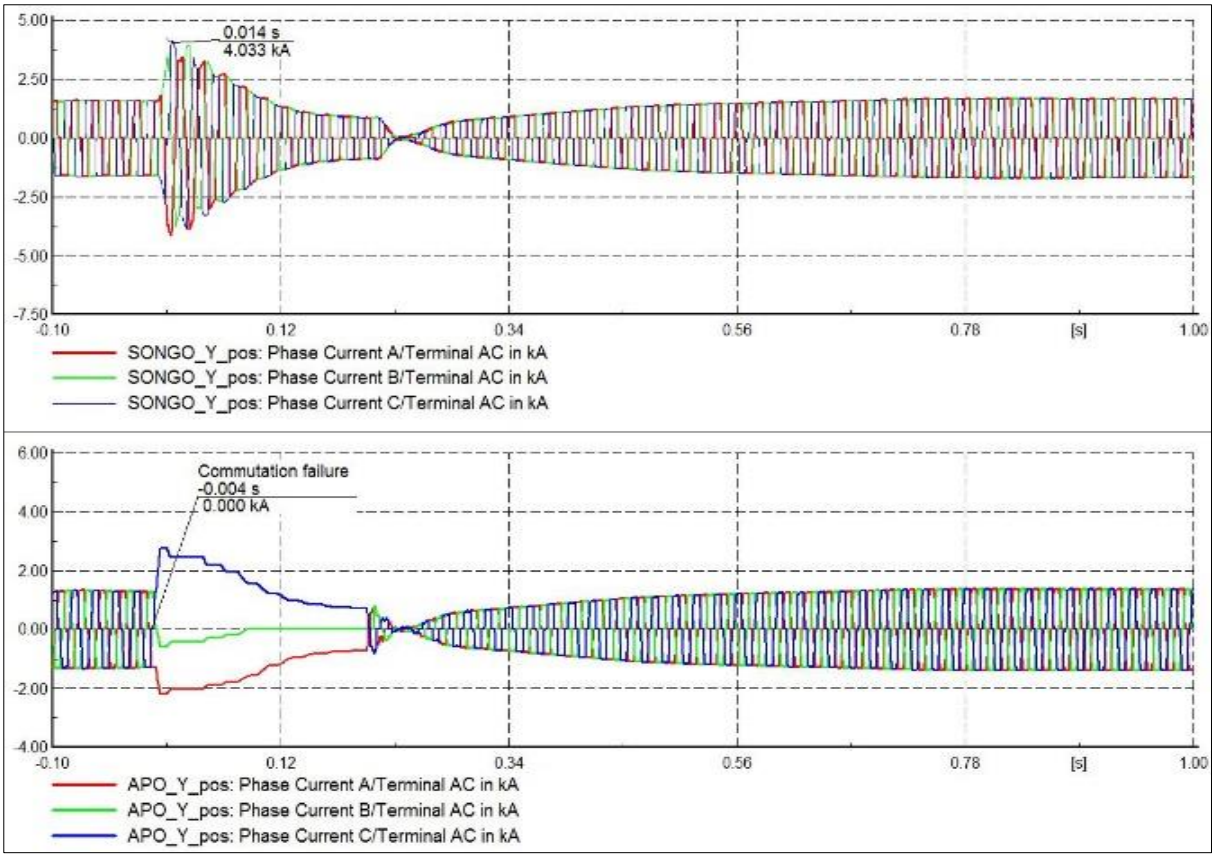

Figure 6.45a: LCC-HVDC converter current

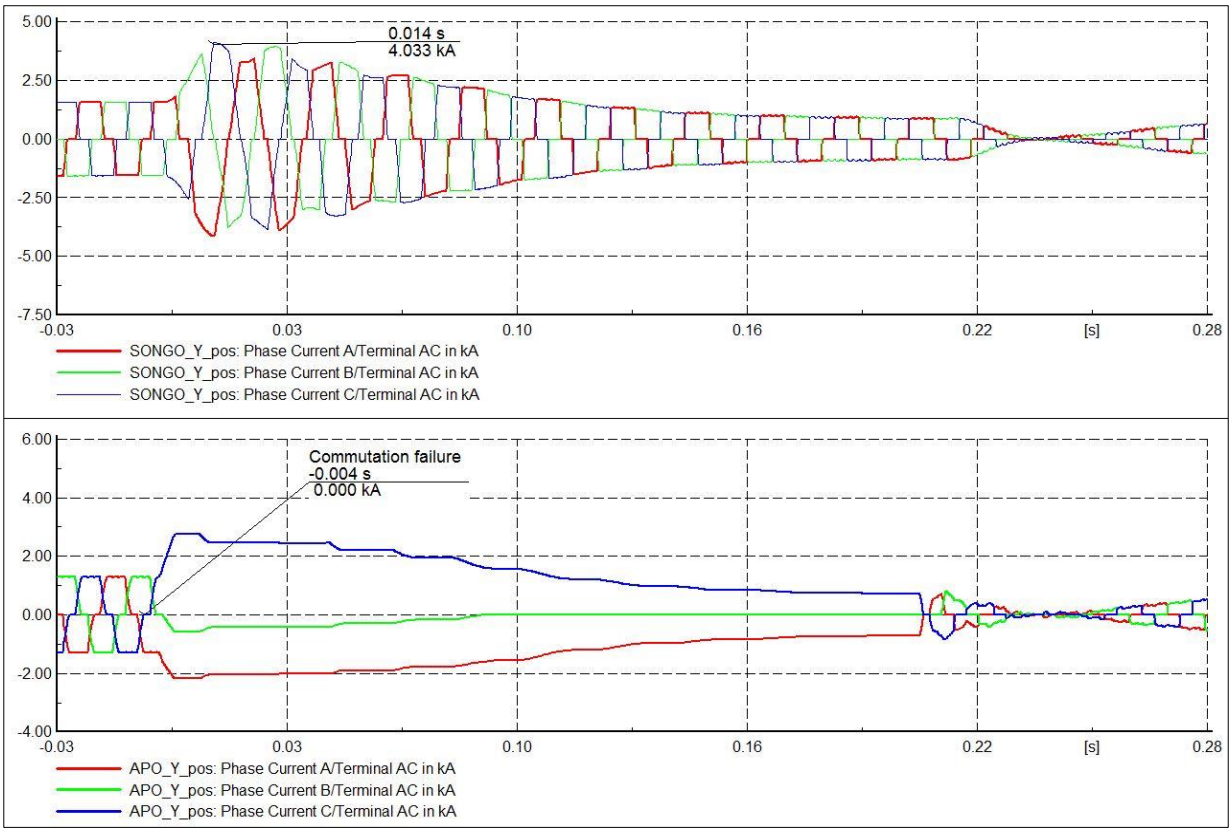

Figure 6.45b: Zoomed converter current between -0.03 to 0.28 simulation time

6.8.2. Re-engineering using VSC-HVDC

Voltage source converter uses IGBT technology. It creates its own AC voltages in case of black start thus helping the current be switched on and off at any time independent of the AC voltage. Its converters operate at a high frequency with PWM that allows simultaneous adjustment of the amplitude and phase angle of converter while keeping the voltage constant. It has a high degree of flexibility with an inbuilt capability to control both its active and reactive power, which makes it more useful in urban power network area. Most new VSC-HVDC technology converter stations use multi-level converter circuits proposed in 2003, at the University of Bundeswehr in Munich, Germany, by Prof. Rainer Marquardt.

For proper effectiveness and good power controllability, a re-engineering of Cahora-Bassa HVDC scheme with the use ±500kV, 1500MW VSC-HVDC was implemented using DIgSILENT PowerFactory according to Figure 6.46. Three phase short circuit was also applied at AC busbar of the inverter station and cleared at t=200ms. This is to compare the effect of fault analysed during LCC-HVDC to VSC-HVDC system by looking into the harmonics/distortion generated after fault and to look into how perfect sinusoids the waveforms during this fault condition.

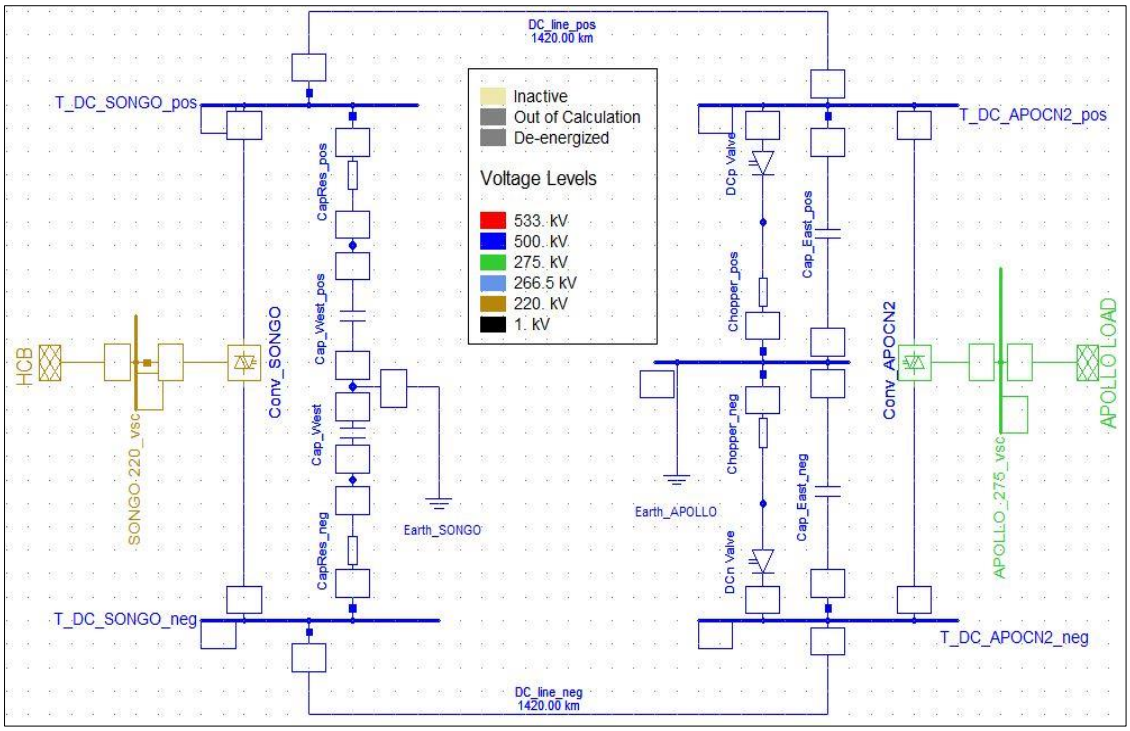

Figure 6.46: VSC-HVDC model for new Cahora-Bassa network

Figure 6.47a shows Songo and Apollo busbars voltages, which were zoomed in Figure 6.47b between -0.03- 0.28 seconds of the simulation time. Unlike the LCC-HVDC, the Apollo voltage waveform suffers no reduction in bus voltage during a fault, as it can be seen that it maintained an amplitude ±1.00p.u. peak-to-peak voltage. The long interruption occurred at Apollo station during fault condition but the retained back its perfect ±1.00p.u. peak-to-peak sinusoid voltage waveform after a fault. A conclusion can thus be reached that VSC-HVDC provides more stability enhancement to AC system than its conventional LCC counterpart does.

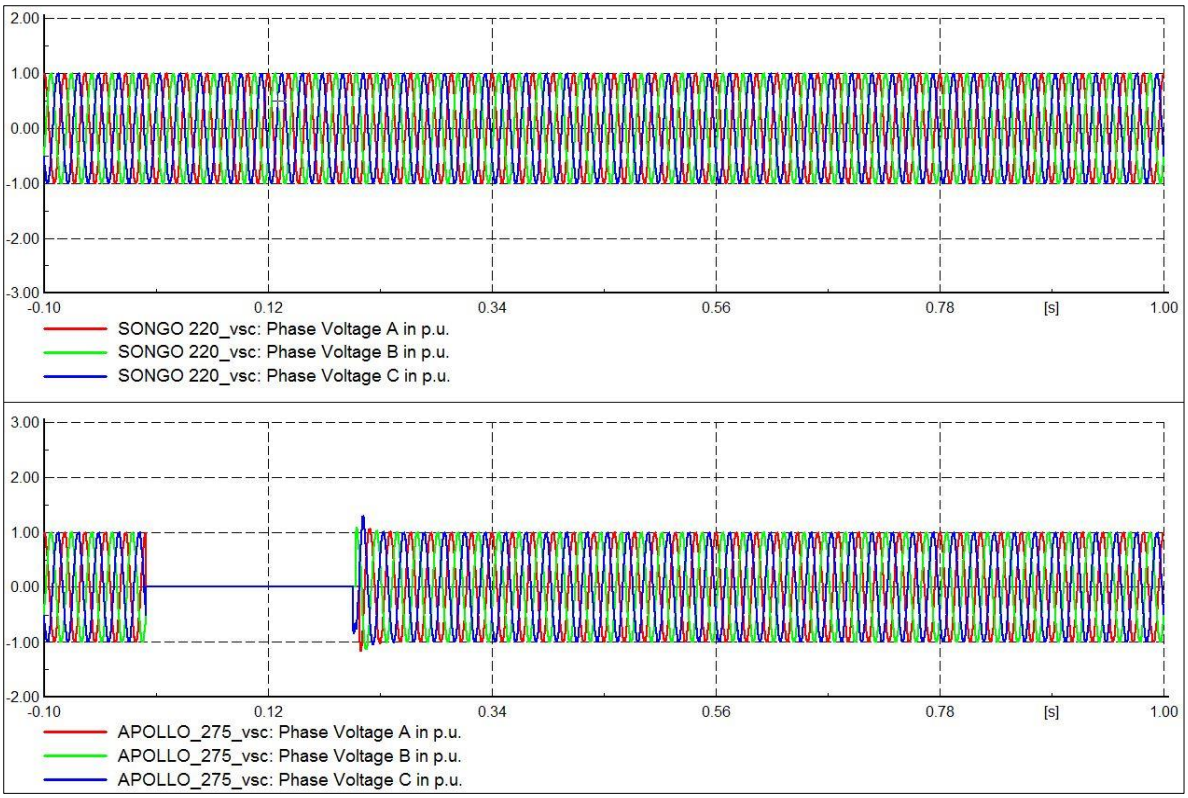

Figure 6.47a: AC busbar voltage of VSC-HVDC

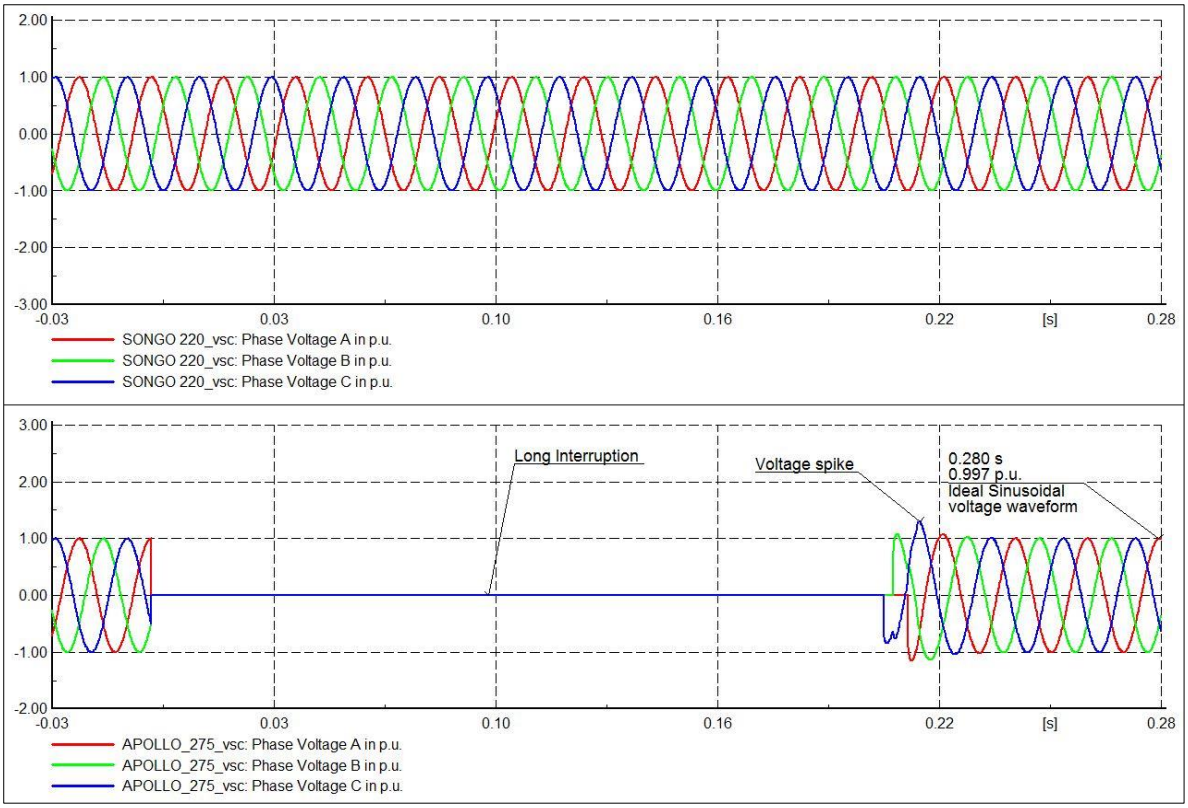

Figure 6.47b: Zoomed busbar voltage between -0.03 to 0.28-simulation time

Converter current can be seen in Figure 6.48a which was zoomed in Figure 6.48b. There was no case of commutation failure recorded during at the inverter end during fault condition. Only slight increase of current spike at the instant of when fault occurs to when the fault was cleared. The systems

maintained back its perfect sinusoids waveform after fault, unlike LCC scheme that still have to builds its converter current. It could also be noticed that VSC-HVDC produced a perfect sinusoidal current waveform compared to a trapezoidal waveform of LCC.

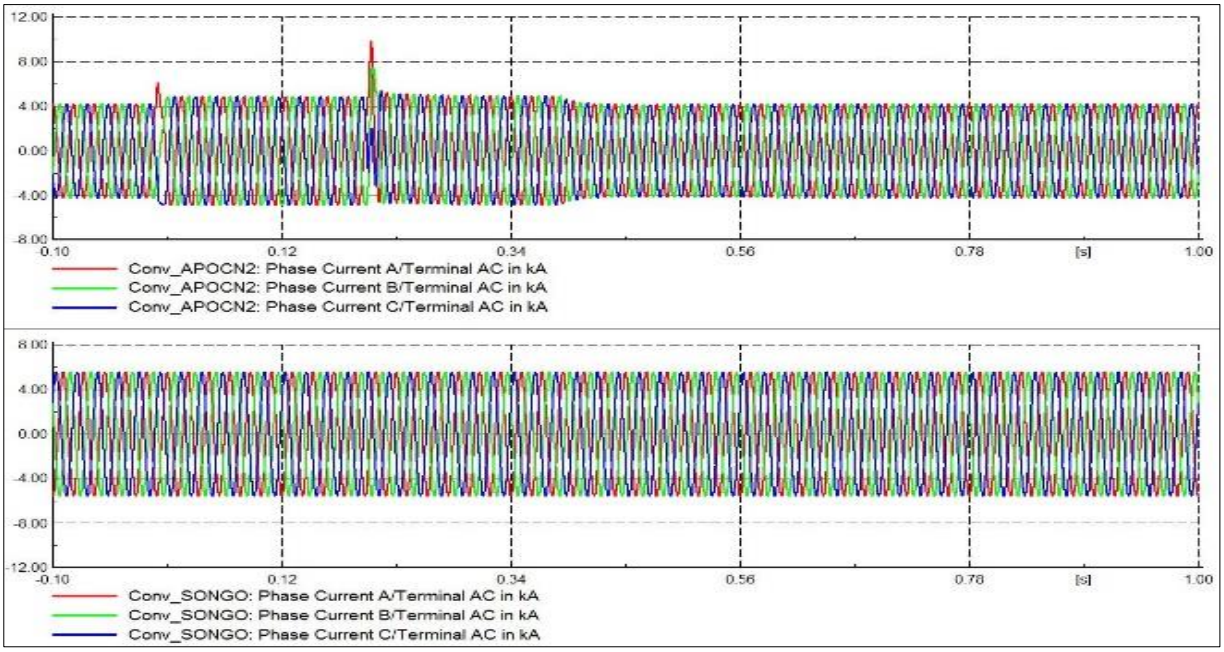

Figure 6.48a: VSC-HVDC converter current

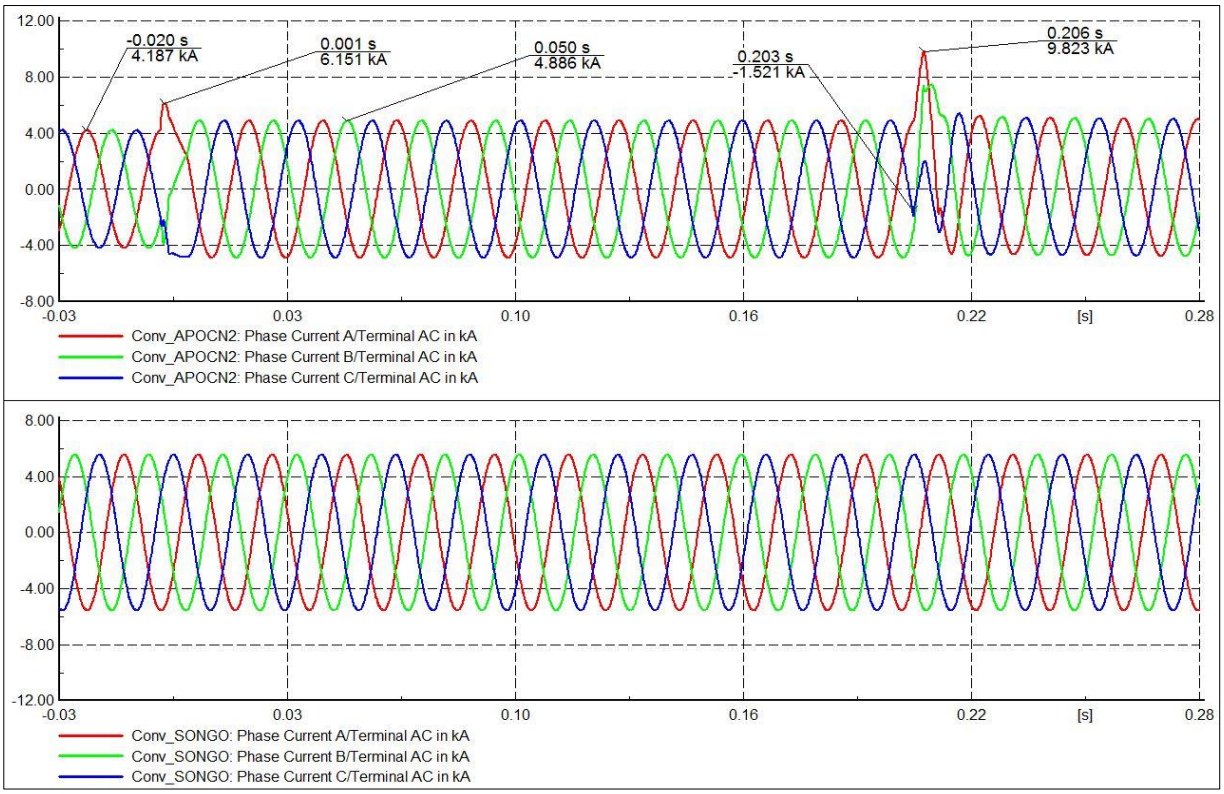

Figure 6.48b: Zoomed converter current between -0.03 to 0.28 simulation time

CHAPTER 7: ECONOMIC AND FINANCIAL ANALYSIS OF HVAC/HVDC LINES

7.1. Transmission Line Components and Specifications

Transmission network takes an important part of power systems operation as it serves as interlink between the source and load. The main objective of any electric power systems is successful transmission of power from generating end to the consumer. Achieving this requires a transmission medium that can be through either conductors or underground cables. Transmission networks are mostly at 3-phase, 50Hz AC (60Hz in the USA), but few networks nowadays integrate DC systems into their main transmission network due to its effectiveness and bulk power capability couple with reduced ROW. Transmission cables or conductors are rated most times at high voltage with low current in order to reduce the I^2R loss on the cable/conductor. Installation of diferrent transmission line depends on many factors such as; the voltage of the line, site terrain, the population density of the land as well as different country's standards. Figure 7.1 shows a 765kV guyed-V suspension tower and its skeletal diagram. The most important part of a transmission line is the tower and the conductors/cables used to convey the power generated. Other small parts such as the insulators, earth wires, spacers, and isolators also have crucial roles in transmission system. Information data is conveyed to different substation or power station on transmission line via an optical ground wire (OPGW).

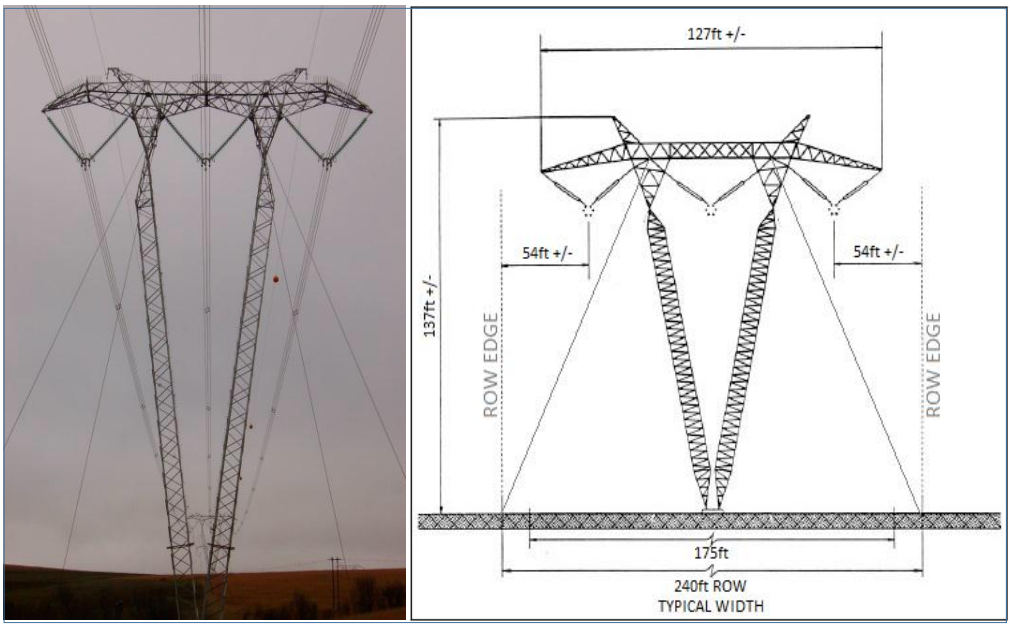

Figure 7.1: 765kV Guyed V suspension tower

Due to transmission line congestion because of an increase in load demand coupled with transmission line reactance, the receiving end voltage of a transmission line always deviates either above or below the nominal rated voltage of the line. Much voltage discrepancies may result in damage to power

utility equipment or consumer appliances. This deviation normally occurs along a long transmission line. Thus, in the case of South Africa network, necessary voltage requirement by the South African government called the grid code must always be obeyed.

Increasing transmission line capacity can be done by either upgrading the existing transmission infrastructures or construction of new transmission facilities. Either way, the cost analysis involved are major factors that determine which measure needs to be adopted. Few component of transmission lines are [142, 143]:

- **Tower**: the tower gives support to the conductors as well as physical and electrical isolation to the conductors carrying power. It isolate the conductors from their surroundings and from each other. Transmission tower specification is based on voltage and MVA rating. Its construction ranges in terms of different geometry, the span between one tower to another, the number of circuits on the tower, and the circuits configuration. Each tower geometry varies with site. Therefore, several geometries may exist along one transmission path. Minimum clearance between phases, and phase-to-earth are always stipulated for every geometry used based on the line voltage rating. An example is the case of 765kV Guyed V suspension tower in Figure 7.1 and different transmission tower specification of Figure 7.2. Conductors are supported onto a transmission tower with the help of insulators. Insulator design depends on the function of the tower. Lightning rods are always used for each tower to provide an earth return in case of lightning. Other parts of towers are cross arm, flanges etc.

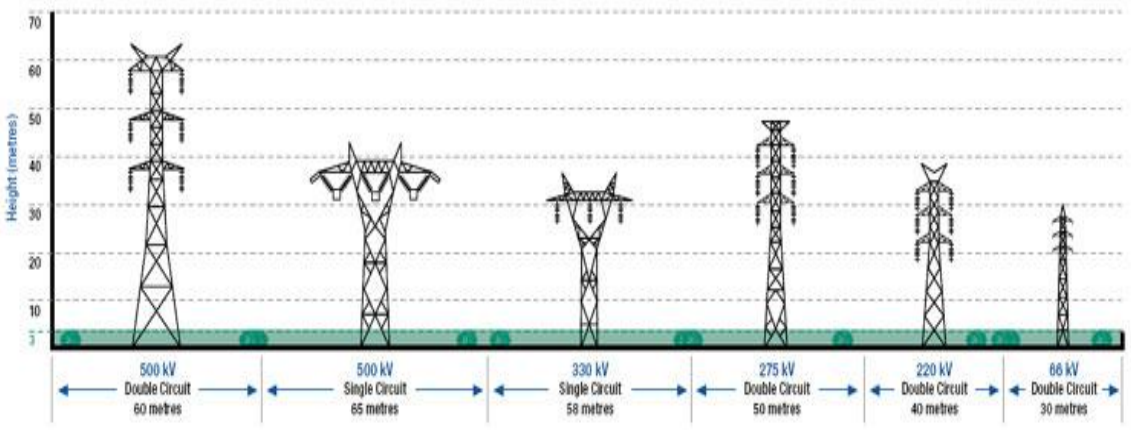

Figure 7.2: Transmission tower specification

- **Cables/Conductors**: these are the transmission medium, the carrier of electric power from generating end to the consumer. Cable is a term used for underground conduits wiring while conductors are suspended on an overhead tower. Several factors need to be considered in the choice of the conductor to use for any particular transmission line project. Factors like capacity and economy loading of the line, mechanical demands and corrosion resistance of the conductor. A variety of conductor construction and composition are presently in use in

order to meet the different condition. Copper was initially used due to its high electrical conductivity but suffer a setback in terms of weight. Aluminium was later introduced because of its reduced weight to strength ratio though less conductivity compares to copper. Aluminium conductor steel reinforced ACSR as well as aluminium conductor composite ACCR and reinforced High Tensile Low Sag HTLS, are another means of increasing strength to weight ratio of transmission lines because they provide a high strength, good electric conductivity with lighter weight.

- **Substation**: this comprises of transformers, circuits breakers, isolators, switches, relays and different compensating devices to help keep the system stable and to reduce fault. Voltage transmitted along a transmission line always exceeds consumers' needs, therefore, the need for transformation from a high voltage to medium one or low voltage. Most consumer equipment operates at hundreds of volt, but that of the transmission line is in thousands of volts. Fault protection will be extremely expensive if such thousands of volts were used by power consumer. The transformation from a higher voltage to a lesser voltage in a substation marks the end of the transmission line. There is possibility of having more than one substation along a transmission line as all HVAC system have distance limitation which requires introduction of compensating device. This is to maintain a fixed transmission voltage along the line. In the case of HVDC system, substations are also needed to accommodate AC to DC converters. Figure 7.3 shows Eskom Kusile 400kV substation.

Figure 7.3: Kusile 400kV substation (Eskom)

- **ROWs**: can be termed as the allowable clearance or safety margin between the transmission line and the nearby surrounding structures and vegetation. It is nearly passive but important part of transmission because it helps gives an access and inspection for the tower, conductors,

and other transmission line component. Inadequate ROW can result in a life-threatening situation during repairs or maintenance.

7.2. Cost of Transmission System

Transmission system comprises of all associate component used in power transmission from generating end to the consumer. Transmission system starts after stepping up generator low voltage to a higher voltage of above 130kV and ends when the higher voltage was stepped down to 110kV or less. For an AC system, possibility of having more than one substation along a transmission line exits. Therefore, power utility always weighs the cost of all installation on their network before embarking on the project [144]. It is required to carry out different research and planning on voltage level to adopt, transmission path, number of substation base on the kilometres of the line, the terrain of the network path, the cable/conductor to use, transmission tower to use, rating of the cable/conductor, foreseeable expansion strategy in case of congestion, etc. All these matter most in transmission system planning. Since any option of focus is directly proportional to construction cost. Hence, the need to assess the financial implication of all this planning. This study made use of transmission line and substation cost documents submitted to Western Electric Coordinating Councils (WECC) [145]. Therefore, the costing is subjected to different factors such as inflation, equipment manufacturer/contractor, country etc. thus the cost cannot be termed as being accurate, but to give a preamble and an approximate cost of each component used for power system transmission.

7.2.1. Overheard line transmission cost

The transmission cost calculation of an overhead line will be derived from the following factors;

- The voltage levels shall be limited to 500kV HVAC (double circuit) and 600kV HVDC both with power carrying capability of 3000MW.
- Baseline cost of $3,071,750 for 500kV double circuits and $1,613,200 for 600kV bipolar HVDC line shall be used for the approximate price of a transmission line.
- Conductor type shall either be ACSR (1.0 multiplier) or aluminium conductor steel support (ACSS with 1.08 multiplier).
- Transmission tower shall be limited to either lattice (1.0 multiplier) or a tubular steel (1.50 multiplier) Structure type.
- The transmission length from Massa substation to Hector substation will be 808miles (1300km). HVAC line is assumed to have four substation (two new and two re-conducted substations) in-between this transmitting distance while that of HVDC will only have two substation signifying the converter station.

- The terrain factors displayed on Table 7.1 explain different terrain multiplying factor along Limpopo-KwaZulu Natal corridor. The transmission distance over each terrain was assumed for this study, an accurate distance over each terrain would require fieldwork and better assessment of this transmission corridor.

Table 7.1: Terrain factor multiplier

TERRAIN	WECC (Multiplier factor)	DISTANCE OVER TERRAIN (miles)
Desert	1.05	70.0
Scrub / Flat	1.00	178.0
Farmland	1.00	208.0
Forested	2.25	85.0
Rolling Hill (2-8% slope)	1.40	78.0
Mountain (8% slope and above)	1.75	69.3
Wetland	1.20	26.0
Urban/Suburban	1.4	95.2

- Right of way width and its cost per acre was also estimated for both HVAC and HVDC line as shown in Table 7.2. Bureau Land Management (BLM) for land rental cost is also another factor to consider in allocating cost on ROW. The cost ROW per acres varies with BLM zones. Rental cost of $17/acre-year with total capital cost of $171/acre will also be assumed for this study. Possibility of having different zone on a transmission path also exist. This will not be consider in this study.

Table 7.2: ROW widths by voltage levels

	500kV DOUBLE CIRCUIT	600kV DC BIPOLE
ROW (ft.)	200	225
Acres/mile	24.23	27.27

Note that: $$Acres/miles = \frac{ROW \times 5280\ ft.mile^{-1}}{43560 sq.ft.Acre^{-1}}$$

Thus, the total transmission line cost will be calculated with equation [145].

$$T_C = \left[B_C \times C_M \times S_M \times R_M \times T_M\right] + \left[ROW\left(acres/mile\right) \times B_{LM}\left(cost/acre\right) \times D_{mi}\right] \quad 7.1$$

Tc - Total transmission line cost

B_C - Baseline cost

C_M	-	Conductor type multiplier
S_M	-	Tower structure type multiplier
R_M	-	Re-conductor multiplier
T_M	-	Terrain multiplier
ROW	-	Right of way in acres/mile
B_{LM}	-	Land cost/acre from BLM
D_{mi}	-	Distance in miles

7.2.2. Substation cost

Substation cost are calculated with respect to the following factors:

- Baseline cost of a substation cover the cost of land, building, substation fencing and any other cost of labour that are not electrical component.
- Ring bus (with 1.0 multiplier) setup was assumed for circuits breaker, line and transformer interconnection in this substation.
- Transformer cost per MVA based on step-up or step-down voltage will also be estimated with (Table 7.3):

Table 7.3: Transformer capital costs

TRANSFORMER COST ($/MVA)	230 kV SUBSTATION	345 kV SUBSTATION	500 kV SUBSTATION
115/500 kV XFMR	-	-	$10,350
138/500 kV XFMR	-	-	$10,350
230/500 kV XFMR	$11,400	-	$11,400
345/500 kV XFMR	-	$13,450	$13,450

- The cost of providing reactive power support based on three major reactive component of shunt reactor, series capacitor, or static VAR compensator (SVC) was given in Table 7.4. It should be noted that each reactive power component has its own capacity, weakness, complexity and size.

Table 7.4: Reactive compensator capital costs

EQUIPMENT FOR 500kV SUBSTATION	($/MVAR)
Shunt Reactor	$20,700
Series Capacitor	$10,350
SVC	$88,000

- HVDC converter station cost for 600kV, 3000MW capacity was calculated to be $506,779,350. This cost covers all different component in both converter (rectifier and inverter) station as well as the cost emanated from AC filters and different capacitor banks used for reactive power compensation.

Thus, the total substation cos will be calculated with equation [145].

$$S_{TIC} = \begin{bmatrix} S_{BC} + \left(LX_{BC} \times LX_n \times RB_M\right) + \left(X_{cost/MVA} \times X_R \times X_n\right) + \left(SVC_{cost/MVA} \times SVC_n\right) \\ + \left(SC_{cost/MVA} \times SC_n\right) \times \left(SR_{cost/MVA} \times SR_n\right) + \left(DC_C\right) \end{bmatrix} \quad 7.2$$

S_{TIC}	-	Total individual substation cost
S_B	-	Substation Base Cost
LX_{BC}	-	Line/transformer position base cost
LX_n	-	Number of line/transformer positions
RB_M	-	Ring bus Multiplier
$X_{cost/MVA}$	-	Transformer cost per MVA
X_R	-	Transformer MVA rating
X_n	-	Number of transformer
$SVC_{cost/MVA}$	-	SVC cost per MVA
SVC_n	-	Number of SVC
$SC_{cost/MVA}$	-	Series capacitor cost per MVA
SC_n	-	Number of series capacitor
$SR_{cost/MVA}$	-	Shunt reactor cost per MVA
SR_n	-	Number of shunt reactor
DC_c	-	Cost of HVDC converter station

Four substation were assumed for the 500kV double circuit transmission network. Two of which are new substation with 120MVA reactive power support and two re-conducted substation with no reactive power support. These substations were assumed to be between Massa and Hector substation, separated by 808 miles (1300km) transmission lines. The total losses, the total cost of transmission with the substation cost can be seen in Table 7.5.

HVDC 600kV estimated cost is highlighted in Table 7.6; it comprises of the transmission line cost, right of way cost, converter station cost and the transmission losses.

Allowance for Fund Used during Construction and Overhead Cost (AFUDC) was calculated as a percentage of the total transmission cost. This is to estimate a realistic project cost implementation. This cost is added to transmission and substation cost to generate the total project cost. This AFUDC

cost was given based on different survey carried out by WECC to develop a recommended value. The total project cost was finally converted to South African Rand on a scale of R15.50 to $1.

Table 7.5: 500kV double circuit transmission cost

Project Cost Results	**Per Mile**	**Total**
Line Cost ($)	6 055 015.99	4 901 535 445.85
ROW Cost ($)	5 162.42	4 178 976.00
New Substation #1 ($)	N/A	11 939 454 171.54
New Substation #2 ($)	N/A	71 473 429 955.55
Re-conducting Substation #1 ($)	N/A	38 080 611.66
Re-conducting Substation #2 ($)	N/A	40 513 566.66
AFUDC/Overhead Cost ($)	1 060 531.22	15 469 508 727.27
Total cost in USD ($)	**7 120 709.63**	**103 866 701 454.53**
Total cost in ZAR (R)	**110 370 999.27**	**1 609 933 872 545.25**
Average Losses (MW)	**174.76**	

Table 7.6: 600kV transmission cost

Project Cost Results	**Per Mile**	**Total**
Line Cost ($)	3 179 954.81	2 574 173 418.18
ROW Cost ($)	4 646.17	3 761 078.40
HVDC Converter station ($)	N/A	598 472 868.63
AFUDC/Overhead Cost ($)	557 305.17	555 871 288.91
Total costs USD ($)	**3 741 906.16**	**3 732 278 654.12**
Total cost in ZAR (R)	**57 999 545.42**	**57 850 319 138.80**
Average Losses (MW)	**92.84**	

7.3. ECONOMIC ANALYSIS OF HVAC/HVDC

Economic analysis of a transmission network largely discusses the proximity of power transmission lines with regards to any health or physical impact, both beneficiary or adverse effect of conveying power from one location to another. Non-environmental friendly system is a danger trap to society no matter what advantage they may offer. Different engineering project are sometimes scrapped out or decommissioned due to health challenges that they may posed. Although, this adverse effect might likely not be known at point of construction or probably with negligible impact, but became more apparent and consistence with time. Equipment ageing is also one major factor to consider. Contemplating which means of power transfer (either AC or DC) or perhaps which transmission path/route needs be taken during project planning requires a careful investigation of AC and DC lines environmental effect before implementation. Thus, the importance of the research carried out on both HVAC and HVDC transmission lines by [146] which highlight the environmental effect of both transmission lines based on the following listed points.

7.3.1. Electric and magnetic field effect

Electric field produced by HVDC line are originated from the line voltage electrostatic effect and corona spaced discharge. This create few charges between the lines and ground or nearby surroundings. Research carried out in IREQ, Canada and several other scientific centre like NIIPT in Russia showed that electric field discharge from humans to bushes or nearby vegetation which are frequently felt under HVAC lines are not easily detected under HVDC transmission. It discharges 100 times per second in AC lines. Also while using the NIIPT experimental line section, ionic current measurements that streamed through a human standing under capacitive current from a HVAC line at a voltage of 1150 kV and human standing under ±1000 kV HVDC line were investigated. The results showed that the ratio of the current felt under both lines are around 1:100 (HVAC line with 0.2 mA versus HVDC line with 2-3 μA). To show that HVDC line electrostatic field are limited and less hazardous unlike HVAC line, a human standing under HVDC line usually does perceive an electrostatic effect beyond a sensational hair movement. Results of measurement also show that HVDC line in good weather condition has an ion current which can lead to more concentration of positive in the air ranging from 10^3-10^4 levels to 10^6-10^7 per cubic inch. This value deteriorates during precipitation or bad weather. An ion current density higher than 10^5 per cubic inch are considered harmful to human health as a result of long exposure of the human lungs.

Magnetic field effect of transmission line on human has been less researched than electric field effect. Still, several assessments on AC power transmission gives a maximum value ranging from 10 to 50μT magnetic field strength around the AC lines, while several meters away to each residential houses feel less magnetic field, normally less than 1μT (BPA 1996). In contrast to the convectional AC line with magnetic field that varies continuously in polarity and strength, DC lines generate a relatively constant yet not perceivable magnetic field effect. Hence, reason for no guidelines linking the designing of DC lines with respect to magnetic field effect. Figure 7.4 shows the electric field strength of 1000kV UHV AC transmission line while Figure 7.5 represent ±800kV HVDC line.

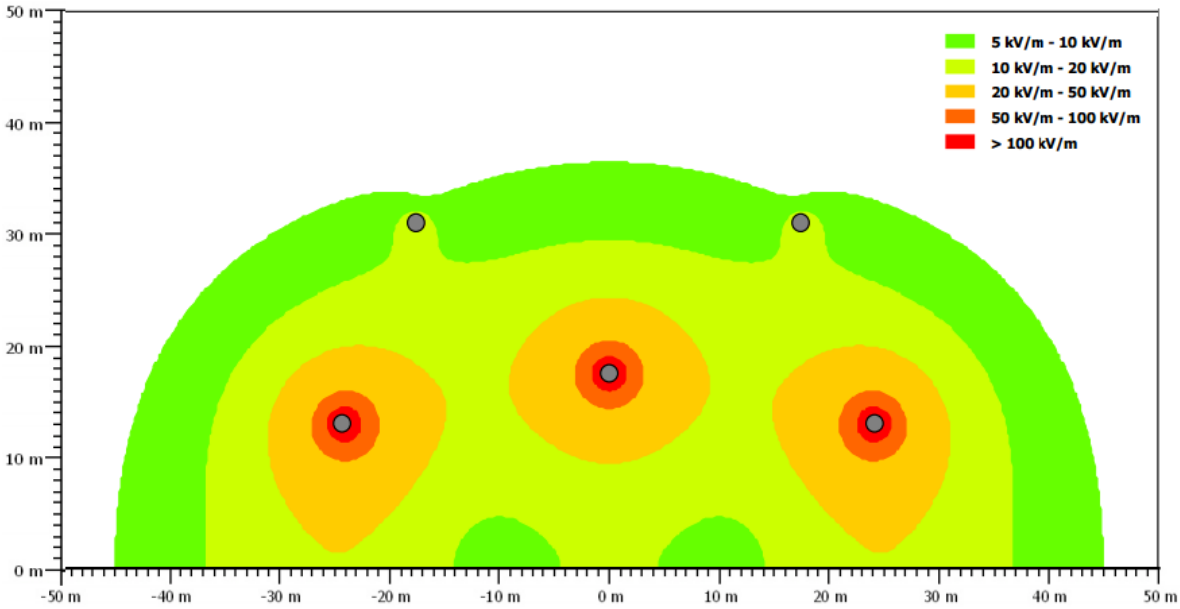

Figure 7.4: Sectional view of electric view strength of an AC line [59]

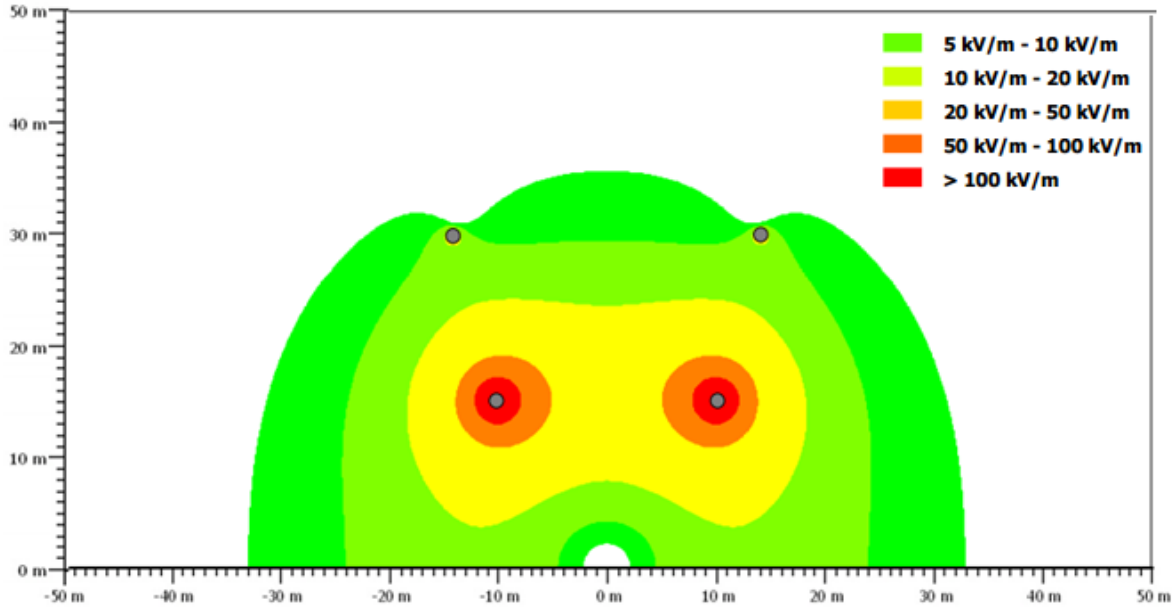

Figure 7.5: Sectional view of electric field strength of a DC line [59]

7.3.2. Radio interference effect

Transmission lines corona discharge on power carrying conductor always result in generation of radio interference along conductor path. Three phases for single circuits or six for double circuits of HVAC line generate corona discharge while HVDC conductors being two generate less corona discharge. Difference atmospheric weather conditions have effect on the level of induced radio interference for both AC and DC lines. During rainy season, AC lines contribute up to 10dB increase in radio noise, while DC lines are limited to adequate level of 4-6dB radio noise. This is majorly achieved in DC lines by restricting the electric field gradient of the line to about 64kV/inch. Visible effect of corona discharge on 765kV transmission line can be seen on Figure 7.6.

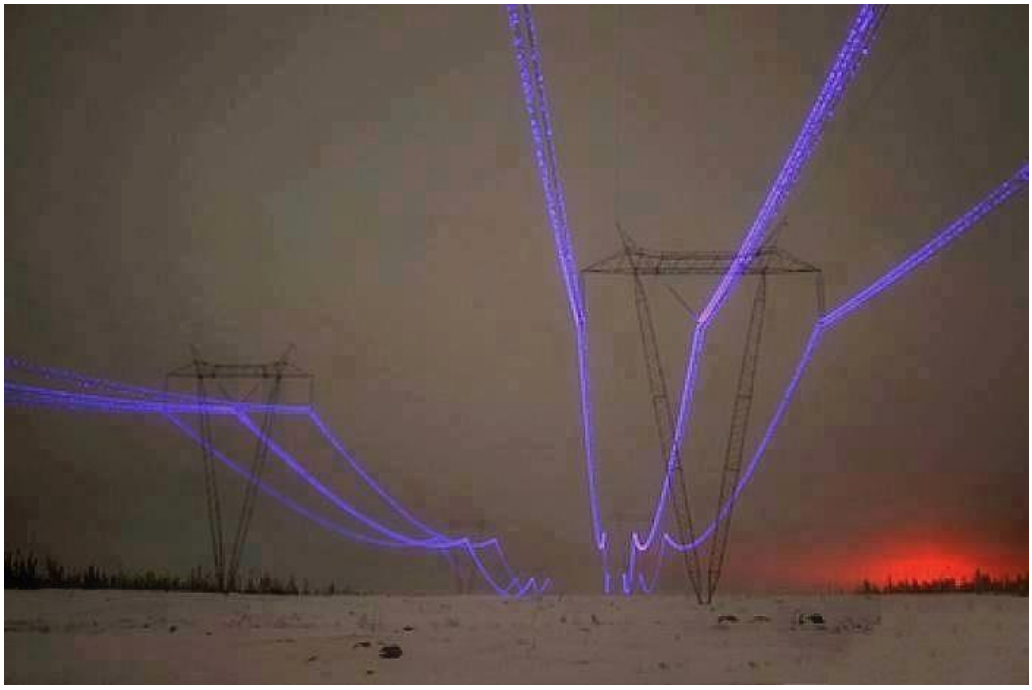

Figure 7.6: Corona effect on 750kV transmission line (Electrical Engineering World)

7.3.3. Audible noise effect

HVDC converter and the converter transformer usually contribute to audible noise in HVDC system. This noise can be minimized by surrounding the transformer and the converters with screen. DC transmission line generate a broadband noise of high frequency. Foul weather condition contributes more to this audible noise but not prevalent compared to audible noise in AC lines. Audible noise along transmission line path that are nearer to residential areas are always restricted to 50dB during the day and 40dB at night. The same measures used in addressing audible noise in AC lines are also practicable in DC lines.

7.3.4. Step voltage and ground current

HVDC systems requires a complex grounding systems particularly in bipolar DC lines with no metallic return. Ground current are mostly associated with monopolar HVDC systems. During an emergency or outage in one pole of a bipolar system, power is hence transfer using the available pole. During this period, it is thus required to provide a current return path using either earth or separate conductor (metallic return). Metallic return does not produce leakage current compared to earth/ground return, but create additional cost due to conductor used. When the current return path is through earth, many concerns are always made to nearby buried conductors such as pipelines, water pipes or telecommunication cables along the current path. This pose some dangers to people living around such installation as this buried conductor can also serve as current return path, which are capable of causing electrocution or shock. The current path can also cause some corrosion around the buried conductors. Thus, the grounding installations required additional designs to incorporate dangerous steps voltage and corrosion to nearby buried conductors. Rapid corrosion can be avoided

to nearby buried infrastructure around earth return path with the use of cathode protection. Usually, dissymmetry estimate current of 1–3% of the nominal value passes through the ground continuously due to changes in current flow between the two poles of HVDC system.

7.3.5. Environmental effect of underground cables

Restriction in ROW as a result of densely populated area or oceanic area bring about the use of underground cable for power transmission. Underground cables installation basically involves permitting, working around traffic and other surface activity, trenching, laying cable, bringing in thermal sands, and avoiding other underground utilities, such as gas pipelines and telecommunication cables, because of generated heat or electromagnetic fields [147].

Construction of underground transmission lines often have harmful impacts to soils and associated resources than construction of overhead lines as it requires diggings of the entire length of the line, resulting in large areas of disturbance from the excavation and associated activities. Archaeological and cultural resources could also be affected due to the soil disturbance. Socioeconomic impacts could be greater for an underground line due to greater construction costs. Although greater number of resource areas such as the land use impacts would be largely reduced compared to overhead lines transmission but lack visual impacts or inspection safe some places with aboveground support facilities. Underground transmission lines are mostly preferred to overhead lines in that bird strikes are eliminated; ROW clearance and maintenance are greatly reduced; health and safety impacts are minimized as a result of reduction in transmission line fault due to accidents or acts of nature on the line. TV and radio interference are also reduced. Underground lines contribute higher to economic activity resulting from construction of the lines compared to overhead lines.

Sealing end compounds (SECs) are areas where underground fluid-filled conductors are joined to overhead lines, which use different conductors. SECs provide sealing of the pressurized oil system of buried fluid-filled lines. Insulation requirements requires a minimum of air clearance for the connected overhead line. Therefore, a sizable area is for the SECs, typically 2,376 square yards (88 yards × 27 yards) for a 400-kV line. Overhead line towers are incorporated to complete the facilities connection.

Reactive compensators are required because of the increased impedance due to thicker conductors used in underground lines for lower resistive heat production. The facilities are located every 12.4 miles on a 400-kV line and are collocated at substations, if possible. These facilities are not required for DC lines, which is one reason DC is used in undersea applications.

CHAPTER 8: CONCLUSION AND RECOMMENDATION

8.1. Conclusion

The reason for HVDC transmission system was first discussed in this research investigation. Different HVDC systems topology and configurations were also discussed. HVDC technologies, advantages, application and advantages between converter technologies were analyzed.

HVDC systems were modelled using CIGRE benchmark. Fault type and different control actions were analysed on the models. The practical application was implemented on a bipolar HVDC system. Three-phase fault was simulated on AC side of both converter station, and each control, signals were plot out using EMT simulation. It was then confirmed from the simulation plot that fault at the inverter stations has high impact than the rectifier station fault. This was observed from a commutation failure that was recorded during a fault at the inverter AC bus. However, the system maintained back their steady state operating point after the fault was cleared. This was achieved with the help of a rugged controller that helps in coordinating the system performance and operation.

The impact of HVDC scheme on AC systems short-term voltage stability study was also investigated. It was found out that HVDC systems help in enhancing voltage stability than the AC line, in that it helps to improve the critical clearing/ isolating time for disturbances on the systems. The effect of VDCOL in HVDC link during systems disturbance was also analysed.

Technical performance and stability analysis was then carried out on modified Eskom network. HVAC transmission line of 400kV double circuit was compared with a bipolar 600kV HVDC line. Generator and transformer utilization/loading, busbars voltage profile as well as transmission losses from NRLF analysis on DIgSILENT were displayed on a bar-subplot. Static analysis with the use of P-V curve was carried out to investigate the loading of the network. Increment in Athene load versus selected busbar voltage profile was carried out using PV script. Using AC lines brings about limited power flow into the Athene substation before the bus voltage fell below 0.95p.u. This plot witness a slight improvement when the tap changers was switched on. However, HVDC line gives the best operating performance as more power could be transmitted with minima losses. This attest to the benefit of HVDC scheme when there is sudden increment load demand. Then, a dynamic analysis with the use of RMS simulation tab was carried out to investigate the critical clearing/isolating time of fault on different elements (busbars and transmission lines) of the network. From the results obtained, it was found that Majuba 400kV busbar and Majuba_Umfolozi transmission line are the least stable lines and bus of the Eastern grid. Prolonged fault on these network elements caused system collapse on the entire grid. The effectiveness of HVDC scheme as better alternatives for bulk power

transmission was then proposed. These means of power transfers gives a better safety margin for system operations. Result obtained from this research study also validate those analyses, as all parameters are in acceptable limit unlike the AC lines. Harmonic and distortion analysis was finally carried out on ±533kV Cahora-Bassa HVDC scheme; this was to investigate few limitations of LCC-HVDC concerning harmonic distortion, imperfect current waveform, and frequent occurrence of commutation failure at the inverter side of the converter station. A better means of power transfer with enhanced system stability couple with a perfect sinusoidal waveform was suggested with the use of VSC-HVDC technology.

Implementation of any new technology directly depends on its cost as well as its environmental impact on the users. A project with high inherent risk will suffer much setback even if at a reduced implementation cost and vice versa. Therefore, this research study finally weighs different environmental opinion on the implementation of the proposed option of bulk power transmission. The cost of implementation was calculated using different assumption and mathematic spreadsheet provided by WECC. It was thus found out that HVDC scheme is not only environmental friendly but also cost effective to implement than convectional HVAC line. It also offer reduced transmission losses compared to HVAC transmission system.

Different FACTs devices and a well-modelled generator controller helps in enhancing voltage stability of a system but it cannot be compared to the benefit that HVDC systems offers. This benefits includes; little line losses, long distance bulk power transfer, immunity to cascading effect, bi-direction power transfer, small right of way, asynchronous interconnection etc. although, the cost of constructing a converter station might be a little expensive for now, but the cost saved by transmission line construction with associated losses in DC systems outweigh the latter. Even with the emergence of new power electronic converter and well-rugged controller, this will eventually make HVDC system the best mode to transmit power due to high efficiency and economics of transmission that it offers. The strategies for improving power system stability on Eskom network are thus proposed with the use of HVDC lines. Adoption of this method into Eskom eastern grid will bring a far better improved means of power transfer.

8.2. Recommendation

Advantages of using LCC-HVDC and VSC HVDC system was investigated in this study. LCC-HVDC allow transmission of bulk power over a long distance using both underground and overhead lines but limited stability margin with frequent commutation failure. VSC-HVDC proffer solution to the aforementioned setbacks due to modern power electronics technology with high switching frequency of its converter. However, it suffer setback in transmitting bulk power due to its low current and voltage rating. Based on this observation, the author would want a further research to be carried out on the control co-ordination of hybrid multi-terminal HVDC systems. Hybrid HVDC uses combined LCC and VSC HVDC technology in one bipolar system. This technology will make use of

bulk power transmission of LCC system, and high power controllability with enhanced system stability of VSC system. More research must be carried out on modelling of both LCC and VSC controller, and such knowledge should be transferred to the modelling of hybrid multi-terminal HVDC system. Finally, effect of high penetration of renewable energy such as wind and Photo Voltaic (PV) system on overall system stability of Eskom Eastern grid using this Hybrid HVDC system should be analysed.

REFERENCES

[1] T. Halder, "Comparative Study of HVDC and HVAC for a Bulk Power Transmission," in *IEEE International Conference Power, Energy and Control (ICPEC)*, Sri Rangalatchum Dindigul, 2013, pp. 139-144.

[2] S. Kulshrestha, S. Yadav, and A. Gupta, "An Index For Dissection of Voltage Stability and Reactive Power Remuneration of Distribution Network Based on Synthesis Load Model," in *International Conference On Recent Trends In Engineering Science And Management*, New Delhi, India, 2015.

[3] P. S. Virk and V. K. Garg, "Power System Stability Improvement of Long Transmission Line System by Using Static Var Compensator (SVC)," *International Journal of Engineering Research and Applications* vol. 3, pp. 01-03, Oct 2013.

[4] P. Kundur, J. Paserba, V. Ajjarapu, G. Andersson, A. Bose, C. Canizares, *et al.*, "Definition and classification of power system stability IEEE/CIGRE joint task force on stability terms and definitions," *IEEE Transactions on Power Systems*, vol. 19, pp. 1387-1401, 2004.

[5] S Mwale and I. E. Davidson, "Power deficits and outage planning in South Africa," *Journal of Energy Challenges and Mechanics*.2014.

[6] S Mwale and I. E. Davidson, "SADC Power Grid Reliability - A Steady-state Contingency Analysis and Strategic HVDC Interconnections Using the N-1 Criterion," *Journal of Energy Challenges and Mechanics*. 2014.

[7] Le Tang and ABB, "HVDC Technologies & ABB Experience," *presented at the Directorate of Energy Workshop Applications for High-Voltage Direct Current Transmission Technologies*, 2013.

[8] P. E. Joe Mooney, "Electrical Consideration for HVDC Transmission Lines" Power Engineers presentation," *presented at the POWER Engineers workshop*, 2009.

[9] L. A. Koshcheev, "Basic Principles of Interstate Electrical Power Links Organization in Northeast Asia Region," in *Power Grid Interconnection in Northeast Asia Workshop*, Beijing, China, 2001.

[10] P. A. David, "Heroes, Herds and Hysteresis in Technological History: Thomas Edison and 'The Battle of the Systems' Reconsidered," *Journal of Industrial and Corporate Change*, vol. 1, pp. 129-180, 1992.

[11] R. M. Black, *The History of Electric Wires and Cables*. London, UK: IET, Peter Peregrinus Ltd., 1983.

[12] R. Munson, *From Edison to Enron: the Business of Power and What it Means for the Future of Electricity*. Northeast-Midwest Institute: Praeger Publishers, 2005.

[13] G. D. Kamalapur, V. R. Sheelavant, S. Hyderabad, A. Pujar, S. Baksi, and A. Patil, "HVDC Transmission in India," *IEEE Potentials*, vol. 33, pp. 22-27, 2014.

[14] P. David, "The hero and the herd in technological history: Reflections on Thomas Edison and the battle of the systems," *Favorites to Fortune*, pp. 72-119, 1991.

[15] S. N. Singh, "Technology for Generation,Transmission and Distribution -Status and Performance Indicators," *presented at the 3rd Capacity Building Programme for Officers of Electricity Regulatory Commissions*, Indian Institute of Technology Kanpur, August, 2010.

[16] F. Nozari and H. S. Patel, "Power electronics in electric utilities: HVDC power transmission systems," *Proceedings of the IEEE*, vol. 76, pp. 495-506, 1988.

[17] M. Bahrman and B. Johnson, "The ABCs of HVDC transmission technologies," *IEEE Power and Energy Magazine*, vol. 2, pp. 32-44, 2007.

[18] D. Tiku, "dc Power Transmission: Mercury-Arc to Thyristor HVdc Valves [History]," *IEEE Power and Energy Magazine,*, vol. 12, pp. 76-96, 2014.

[19] K. Singh, H. S. Saini, H. S. Sandhu, and A. Faridkot, "Methodology of HVDC Transmission System," *International Journal For Technological Research In Engineering*, vol. 2, Jan 2015.

[20] L. Englund, M. Lagerkvist, and R. Dass, "HVDC superhighways for China," *ABB Review*, vol. 4, 2003.

[21] R. Nayak, R. Sasmal, Y. Sehgal, M. Rashwan, and G. Flisberg, "Technical feasibility and research & development needs for±1000 kV and above HVDC system," *CIGRE B4-105_2010*, 2010.

[22] L. Zehong, G. Liying, W. Zuli, Y. Jun, Z. Jin, and L. Licheng, "R&D Progress of±1100kV UHVDC Technology," *CIGRE, Paris*, 2012.

[23] C. R. Bayliss and B. J. Hardy, "Chapter 26 - High Voltage Direct Current Transmission," in *Transmission and Distribution Electrical Engineering (Fourth Edition)*, C. R. Bayliss and B. J. Hardy, Eds., ed Oxford: Newnes, 2012, pp. 1027-1057.

[24] M. H. Okba, M. H. Saied, M. Z. Mostafa, and T. M. Abdel-Moneim, "High voltage direct current transmission - A review, part I," in *Energytech, 2012 IEEE*, 2012, pp. 1-7.

[25] L. C. Azimoh, K. A. Folly, and S. P. Chowdhury, "Mitigations of voltage instability in power systems," in *Electrical Power & Energy Conference (EPEC), 2009 IEEE*, 2009, pp. 1-6.

[26] C. Chih-Ju, H. Chia-Yu, W. Yuan-Kang, and L. Ching-Yin, "Study on voltage stability of island grid supplied by large grid with long submarine cables considering different load patterns," in *Utility Exhibition on Power and Energy Systems: Issues & Prospects for Asia (ICUE), 2011 International Conference and*, 2011, pp. 1-10.

[27] C. Nguyen-Mau, K. Rudion, and Z. A. Styczynski, "HVDC application for enhancing power system stability," in *Science and Technology, 2011 EPU-CRIS International Conference on*, 2011, pp. 1-6.

[28] O. E. Oni, K. N. Mbangula, and I. E. Davidson, "Voltage Stability Improvement of a Multi-Machine System using HVDC," in *Power Systems Conference* Clemson University, 2016.

[29] O. E. Oni, K. N. Mbangula, and I. E. Davidson, "Dynamic Voltage Stability Studies using a Modified IEEE 30-Bus System," presented at the 16th IEEE international Conference on Environment and Electrical Engineering, Florence, Italy, 2016.

[30] L. Yan and C. Zhe, "Transient voltage stability analysis and improvement of a network with different HVDC systems," in *Power and Energy Society General Meeting, 2011 IEEE*, 2011, pp. 1-8.

[31] O. Swaitti, "Assessing the Impacts of Increasing Penetration of HVDC Lines on Power System Reliability," Master of Science, School of Electrical Engineering, Royal Institute of Technology (KTH), Stockholm,Sweden, 2007.

[32] K. Meah and S. Ula, "Comparative Evaluation of HVDC and HVAC Transmission Systems," in *IEEE Power Engineering Society General Meeting*, Tampa, Florida, 2007, pp. 1-5.

[33] J.C Molburg, J.A Kavicky, and K. C. Picel, "The Design, Construction, and Operation of Long Distance High-Voltage Electricity Transmission Technologies," The Decision and Information Science Division, Argone National Laboratory. Nov, 2007.

[34] R. T. Pinto, "Multi-Terminal DC Networks System Integration, Dynamics and Control," Electrical Engineering, Delft University of Technology, Netherlands, 2014.

[35] Siemens, "High Voltage Direct Current Transmission – Proven Technology for Power Exchange," Power Transmission Division, 2011.

[36] N. Flourentzou, V. G. Agelidis, and G. D. Demetriades, "VSC-Based HVDC Power Transmission Systems: An Overview," *IEEE Transactions on Power Electronics*, vol. 24, pp. 592-602, 2009.

[37] J. Luo, J. Yao, D. Wu, C. Wen, S. Yang, and J. Liu, "Application research on VSC-HVDC in urban power network," in *IEEE Power Engineering and Automation Conference (PEAM)*, Wuhan, China, 2011, pp. 115-119.

[38] T. Magg, M. Manchen, E. Krige, J. Wasborg, and J. Sundin, "Connecting Networks with VSC HVDC in Africa: Caprivi Link Interconnector," in *IEEE PES PowerAfrica Conference and Exposition*, Johannesburg, South Africa, 2012

[39] O. E. Oni, K. N. Mbangula, and I. E. Davidson, "A Review of LCC-HVDC and VSC-HVDC Technologies and Applications," presented at the 16th IEEE international Conference on Environment and Electrical Engineering, Florence, Italy, 2016.

[40] S. Achenbach, V. Barry, C. H. Bayfield, and P. F. Coventry, "Increasing the GB electricity transmission networks' power transfer capability between North and South — The Western HVDC Link," in *AC and DC Power Transmission (ACDC 2012), 10th IET International Conference on*, 2012, pp. 1-4.

[41] C.-K. Jung, H.-S. Park, and J.-W. Kang, "Insulation Design and Reliability Evaluation of +/- 80kV HVDC XLPE Cables," *Journal of Electrical Engineering & Technology*, vol. 9, pp. 1002-1008, May 2014.

[42] N. M. Kirby, "HVDC system solutions," in *Transmission and Distribution Conference and Exposition (T&D), 2012 IEEE PES*, 2012, pp. 1-3.

[43] M. Marzinotto and G. Mazzanti, "The statistical enlargement law for HVDC cable lines part 2: application to the enlargement over cable radius," *IEEE Transactions on Dielectrics and Electrical Insulation*, vol. 22, pp. 202-210, 2015.

[44] N. M. Kirby, "HVDC System Solutions," in *IEEE PES, Transmission and Distribution Conference and Exposition (T&D)*, Orlando, Florida, 2012, pp. 1-3.

[45] H. Rahman and B. H. Khan, "Power Upgrading of Transmission Line by Combining AC–DC Transmission," *IEEE Transactions on Power Systems*, vol. 22, pp. 459 - 466, 2007.

[46] J. Liang, O. Gomis-Bellmunt, J. Ekanayake, N. Jenkins, and W. An, "A multi-terminal HVDC transmission system for offshore wind farms with induction generators," *International Journal of Electrical Power & Energy Systems*, vol. 43, pp. 54-62, 12// 2012.

[47] D. Van Hertem and M. Delimar, "6 - High Voltage Direct Current (HVDC) electric power transmission systems," in *Electricity Transmission, Distribution and Storage Systems*, Z. Melhem, Ed., ed: Woodhead Publishing, 2013, pp. 143-173.

[48] H. Huang and V. Ramaswami, "Design of UHVDC Converter Station," in *Transmission and Distribution Conference and Exhibition: Asia and Pacific, 2005 IEEE/PES*, 2005, pp. 1-6.

[49] B. Beilstein, R. Germick, J. Haney, A. Joss, M. Murphy, and S. You, "HVDC Technology: Review and Prospect."

[50] S. Shah, R. Hassan, and S. Jian, "HVDC transmission system architectures and control - A review," in *Control and Modeling for Power Electronics (COMPEL), 2013 IEEE 14th Workshop on*, 2013, pp. 1-8.

[51] G. Chunyi, Z. Chengyong, and C. Xiuyu, "Analysis of dual-infeed HVDC with LCC inverter and VSC rectifier," in *PES General Meeting | Conference & Exposition, 2014 IEEE*, 2014, pp. 1-4.

[52] R. L. Sellick, x030A, and M. kerberg, "Comparison of HVDC Light (VSC) and HVDC Classic (LCC) site aspects, for a 500MW 400kV HVDC transmission scheme," in *AC and DC Power Transmission (ACDC 2012), 10th IET International Conference on*, 2012, pp. 1-6.

[53] S. Foster, X. Lie, and B. Fox, "Control of an LCC HVDC system for connecting large offshore wind farms with special consideration of grid fault," in *Power and Energy Society General Meeting - Conversion and Delivery of Electrical Energy in the 21st Century, 2008 IEEE*, 2008, pp. 1-8.

[54] P. Manohar, V. Kelamane, D. Kaushik, and W. Ahmed, "Improved controls for LCC-VSC hybrid HVDC system," in *Circuits, Controls and Communications (CCUBE), 2013 International conference on*, 2013, pp. 1-5.

[55] H. Liu and J. Sun, "Modeling and analysis of DC-link harmonic instability in LCC HVDC systems," in *Control and Modeling for Power Electronics (COMPEL), 2013 IEEE 14th Workshop on*, 2013, pp. 1-9.

[56] M. Daryabak, S. Filizadeh, J. Jatskevich, A. Davoudi, M. Saeedifard, V. K. Sood, *et al.*, "Modeling of LCC-HVDC Systems Using Dynamic Phasors," *Power Delivery, IEEE Transactions on*, vol. 29, pp. 1989-1998, 2014.

[57] H. Rao, B. Luo, X. Li, Z. Cai, and L. Li, "Development of Â± 800kV UHVDC Transmission Technology in China," in *High Voltage Engineering and Application, 2008. ICHVE 2008. International Conference on*, 2008, pp. 1-7.

[58] J. Cao and J. Cai, "HVDC in China," in *2013 HVDC and FACTS Conference, Palo Alto, CA, USA*, 2013.

[59] L. Xianzhang, "Practice of HVDC Transmission in China," State Grid corporation of China, October 2011.

[60] K. Zha, j. Wen, X. Yang, G. Chong, and G. Tang, "Upgrade Study of High Power Electronics Laboratory for Â±800kV UHVDC Valves," in *Power System Technology and IEEE Power India Conference, 2008. POWERCON 2008. Joint International Conference on*, 2008, pp. 1-6.

[61] W. Hammer, "Dynamic Modeling of Line and Capacitor Commutated Converters for HVDC Power Transmission," Doctor of Technical Sciences, Power Systems Laboratory, Swiss Federal Institute of Technology. Zurich, 2003.

[62] Y. Jiang-Hafner, H. Duchen, M. Karlsson, L. Ronstrom, and B. Abrahamsson, "HVDC with Voltage Source Converters-A Powerful Standby Black Start Facility," in *IEEE PES Transmission and Distribution Conference and Exposition*, Chicago, Illinois, 2008, pp. 1-9.

[63] K. Sivanagamani and P. B. Reddy, "Simulation of VSC Based HVDC Transmission System under Fault Conditions," *International Journal of Science Engineering and Advance Technology,* vol. 2, pp. 1049-1055, 2015.

[64] K. Friedrich, "Modern HVDC PLUS application of VSC in Modular Multilevel Converter Topology," in *IEEE International Symposium on Industrial Electronics*, Bari, Italy, 2010, pp. 3807-3810.

[65] B. Jacobson, P. Karlsson, G. Asplund, L. Harnefors, and T. Jonsson, "VSC-HVDC transmission with cascaded two-level converters," *International Journal for water and Energy,* vol. 57b, 2010.

[66] Z. Lu and D. Jovcic, "Comparison of L-VSC and LCL-VSC converter for HVDC transmission," in *IEEE Power Electronics and Motion Control Conference (EPE/PEMC)*, Novi Sad, Serbia, 2012, pp. DS3b.5-1-DS3b.5-7.

[67] Y. Zhaoqiang and W. Hairong, "The Research on the VSC-HVDC Control System Structure," in *Asia-Pacific Power and Energy Engineering Conference*, Shanghai, China, 2012, pp. 1-4.

[68] C. Xia, H. Yunhe, and W. Jinyu, "Fault Characteristics Analysis of Two HVDC Technologies for Wind Power Integration," in *IEEE PES Innovative Smart Grid Technologies Conference*, Washington, DC, 2014, pp. 1-6.

[69] S. M. Yousuf and M. S. Subramaniyan, "HVDC and Facts in Power System," *International Journal of Science and Research,* vol. 2, 2013.

[70] P. Manohar, V. Kelamane, D. Kaushik, and W. Ahmed, "Improved Controls for LCC-VSC Hybrid HVDC System," in *International conference on Circuits, Controls and Communications*, Bengaluru, India, 2013, pp. 1-5.

[71] M. Callavik, P. Lundberg, and O. Hansson, "NORDLINK Pioneering VSC-HVDC interconnector between Norway and Germany," presented at the ABB Power systems, Germany, 2015.

[72] V. Gelman, "Insulated-Gate Bipolar Transistor Rectifiers: Why They Are Not Used in Traction Power Substations," *IEEE Vehicular Technology Magazine,* vol. 9, pp. 86-93, 2014.

[73] O. Abarrategui, D. M. Larruskain, I. Zamora, V. Valverde, G. Buigues, and A. Iturregi, "VSC-based HVDC System Capability to Ride Through Faults," in *International Conference on Renewable Energy and Power Quality*, La corula, Spain, 2015.

[74] G. Tang and Z. Xu, "A LCC and MMC hybrid HVDC topology with DC line fault clearance capability," *International Journal of Electrical Power & Energy Systems,* vol. 62, pp. 419-428, 11// 2014.

[75] Bakhda Jay S, Patel Tejas V., and A. Deshpande, "Simulation and Modelling of VSC Based HVDC Transmission Line," *Intenational Journal of Research in Elecronics and Communication,* vol. 1, pp. 41-45, April-June 2014.

[76] F. Shewarega and I. Erlich, "Simplified Modeling of VSC-HVDC in Power System Stability Studies," in *International Federation of Automatic Control*, Cape Town, South Africa, 2014.

[77] C. C. Davidson and D. Trainer, "Innovative Concepts for Hybrid Multi-Level Converters for HVDC Power Transmission," in *9th IET International Conference on AC and DC Power Transmission*, London, 2010, pp. 1-5.

[78] R. Marquardt, "Modular Multilevel Converter: An Universal Concept for HVDC-Networks and Extended DC-Bus-Applications," in *IEEE Power Electronics Conference (IPEC),* , Sapporo, 2010, pp. 502-507.

[79] T. Guangfu, H. Zhiyuan, and P. Hui, "R&D and application of voltage sourced converter based high voltage direct current engineering technology in China," *Journal of Modern Power Systems and Clean Energy*, vol. 2, pp. 1-15, 2014.

[80] P. Hurtuk, R. Radvan, and M. Frivaldský, "Investigation of Possibilities to Increasing Efficiency of Full Bridge Converter Designed for Low Output Voltage and High Output Current Applications," in *IEEE ELEKTRO*, Rajeck Teplice, Slovakia, 2012, pp. 129-132.

[81] R. Marquardt, "Modular Multilevel Converter Topologies with DC-Short Circuit Current Limitation," in *IEEE 8th International Conference on Power Electronics and ECCE Asia*, Jeju, 2011, pp. 1425-1431.

[82] M. Buschendorf, J. Weber, and S. Bernet, "Comparison of IGCT and IGBT for the use in the Modular Multilevel Converter for HVDC Applications," in *9th International Multi-Conference on Systems, Signals and Devices (SSD)*, Chemnitz, Gemany, 2012, pp. 1-6.

[83] W. Li and X. He, "Review of nonisolated high-step-up DC/DC converters in photovoltaic grid-connected applications," *Industrial Electronics, IEEE Transactions on,* vol. 58, pp. 1239-1250, 2011.

[84] E. Najafi and A. H. M. Yatim, "Design and implementation of a new multilevel inverter topology," *Industrial Electronics, IEEE Transactions on,* vol. 59, pp. 4148-4154, 2012.

[85] S. Tamai, "High Power Converter Technologies for Saving and Sustaining Energy," in *26th International Symposium on Power Semiconductor Devices & IC's (ISPSD)*, Waikoloa, Hawaii, 2014, pp. 12-18.

[86] G. P. Adam, S. J. Finney, and B. W. Williams, "Hybrid converter with ac side cascaded H-bridge cells against H-bridge alternative arm modular multilevel converter: steady-state and dynamic performance," *Generation, Transmission & Distribution, IET,* vol. 7, pp. 318-328, 2013.

[87] G. P. Adam, I. A. Abdelsalam, K. H. Ahmed, and B. W. Williams, "Hybrid Multilevel Converter With Cascaded H-bridge Cells for HVDC Applications: Operating Principle and Scalability," *Ieee Transactions on Power Electronics,* vol. 30, pp. 65-77, Jan 2015.

[88] G. P. Adam, K. H. Ahmed, and B. W. Williams, "Mixed Cells Modular Multilevel Converter," in *23rd International Symposium on Industrial Electronics (ISIE)*, Istanbul, Turkey, 2014, pp. 1390-1395.

[89] G. P. Adam, O. Anaya-Lara, G. M. Burt, D. Telford, B. W. Williams, and J. R. McDonald, "Modular multilevel inverter: pulse width modulation and capacitor balancing technique," *IET Power Electronics,* vol. 3, pp. 702-715, 2010.

[90] A. Rasic, U. Krebs, H. Leu, and G. Herold, "Optimization of the Modular Multilevel Converters Performance Using the Second Harmonic of the Module Current," in *13th European Conference on Power Electronics and Applications*, Barcelona, Spain, 2009, pp. 1-10.

[91] G. P. Adam, S. J. Finney, B. W. Williams, and A. Massoud, "Quasi two-level operation of a five-level inverter," *Przeglad Elektrotechniczny,* vol. 83, pp. 120-125, 2007.

[92] G. P. Adam, S. J. Finney, O. Ojo, and B. W. Williams, "Quasi-two-level and three-level operation of a diode-clamped multilevel inverter using space vector modulation," *IET Power Electronics,* vol. 5, pp. 542-551, 2012.

[93] G. P. Adam and I. E. Davidson, "Robust and Generic Control of Full-Bridge Modular Multilevel Converter High-Voltage DC Transmission Systems," *IEEE Transactions on Power Delivery,* vol. 30, pp. 2468 - 2476, 2015.

[94] S. Qiang, L. Wenhua, L. Xiaoqian, R. Hong, X. Shukai, and L. Licheng, "A Steady-State Analysis Method for a Modular Multilevel Converter," *Power Electronics, IEEE Transactions on,* vol. 28, pp. 3702-3713, 2013.

[95] R. K. Antar, B. M. Saied, and R. A. Khalil, "Using Seven-Level Cascade H-Bridge Inverter with HVDC System to Improve Power Quality," in *First National Conference for Engineering Sciences*, Baghdad, Iraq, 2012, pp. 1-7.

[96] Y. Cheng, C. Qian, M. L. Crow, S. Pekarek, and S. Atcitty, "A comparison of diode-clamped and cascaded multilevel converters for a STATCOM with energy storage," *Industrial Electronics, IEEE Transactions on,* vol. 53, pp. 1512-1521, 2006.

[97] J.-S. Lai and F. Z. Peng, "Multilevel converters-a new breed of power converters," *Industry Applications, IEEE Transactions on,* vol. 32, pp. 509-517, 1996.

[98] M. Marchesoni and P. Tenca, "Diode-clamped multilevel converters: a practicable way to balance DC-link voltages," *Industrial Electronics, IEEE Transactions on,* vol. 49, pp. 752-765, 2002.

[99] Z. Pan, F. Z. Peng, K. Corzine, V. R. Stefanovic, J. M. Leuthen, and S. Gataric, "Voltage balancing control of diode-clamped multilevel rectifier/inverter systems," *Industry Applications, IEEE Transactions on,* vol. 41, pp. 1698-1706, 2005.

[100] G. P. Adam, S. J. Finney, A. M. Massoud, and B. W. Williams, "Capacitor balance issues of the diode-clamped multilevel inverter operated in a quasi two-state mode," *Industrial Electronics, IEEE Transactions on,* vol. 55, pp. 3088-3099, 2008.

[101] S. G. Lee, D. W. Kang, Y. H. Lee, and D. S. Hyun, "The Carrier-Based PWM Method for Voltage Balance of Flying Capacitor Multilevel Inverter," in *IEEE 32nd Annual Power Electronics Specialists Conference. PESC*, Vancouver, BC, 2001, pp. 126-131.

[102] M. F. Escalante, J.-C. Vannier, and A. Arzandé, "Flying capacitor multilevel inverters and DTC motor drive applications," *Industrial Electronics, IEEE Transactions on,* vol. 49, pp. 809-815, 2002.

[103] B. P. McGrath and D. G. Holmes, "Analytical modelling of voltage balance dynamics for a flying capacitor multilevel converter," in *Power Electronics Specialists Conference, 2007. PESC 2007. IEEE*, 2007, pp. 1810-1816.

[104] A. Shukla, A. Ghosh, and A. Joshi, "Improved multilevel hysteresis current regulation and capacitor voltage balancing schemes for flying capacitor multilevel inverter," *Power Electronics, IEEE Transactions on,* vol. 23, pp. 518-529, 2008.

[105] B. S. Riar and U. K. Madawala, "Decoupled Control of Modular Multilevel Converters Using Voltage Correcting Modules," *Power Electronics, IEEE Transactions on,* vol. 30, pp. 690-698, 2015.

[106] P. D. Judge, M. M. C. Merlin, P. D. Mitcheson, and T. C. Green, "Power Loss and Thermal Characterization of IGBT Modules in the Alternate Arm converter," in *IEEE Energy Conversion Congress and Exposition*, Denver, Colorado, 2013, pp. 1725-1731.

[107] G. P. Adam, K. H. Ahmed, S. J. Finney, K. Bell, and B. W. Williams, "New Breed of Network Fault-Tolerant Voltage-Source-Converter HVDC Transmission System," *IEEE Transactions on Power Systems,* vol. 28, pp. 335-346, Feb 2013.

[108] M. Glinka and R. Marquardt, "A new AC/AC multilevel converter family," *IEEE Transactions on Industrial Electronics,* vol. 52, pp. 662-669, 2005.

[109] A. Lesnicar and R. Marquardt, "An Innovative Modular Multilevel Converter Topology Suitable for a Wide Power Range," in *IEEE Power Tech Conference Proceeding*, Bologna, 2003, p. 6.

[110] S. Kenzelmann, A. Rufer, M. Vasiladiotis, D. Dujic, F. Canales, and Y. R. De Novaes, "A versatile DC-DC converter for energy collection and distribution using the Modular Multilevel Converter," in *Proceedings of the 14th European Conference on Power Electronics and Applications (EPE)*, Birmingham, 2011, pp. 1-10.

[111] C. M. Franck, "HVDC Circuit Breakers: A Review Identifying Future Research Needs," *Ieee Transactions on Power Delivery,* vol. 26, pp. 998-1007, Apr 2011.

[112] D. Schmitt, Y. Wang, T. Weyh, and R. Marquardt, "DC-Side Fault Current Management in Extended Multiterminal-HVDC-Grids," in *9th International Multi-Conference on Systems, Signals and Devices (SSD)*, Chemnitz, Germany, 2012, pp. 1-5.

[113] S. Debnath, J. Qin, B. Bahrani, M. Saeedifard, and P. Barbosa, "Operation, Control, and Applications of the Modular Multilevel Converter: A Review," *Ieee Transactions on Power Electronics*, vol. 30, pp. 37-53, Jan 2015.

[114] I. A. Gowaid, G. P. Adam, S. Ahmed, D. Holliday, and B. W. Williams, "Analysis and Design of a Modular Multilevel Converter With Trapezoidal Modulation for Medium and High Voltage DC-DC Transformers," *IEEE Transactions on Power Electronics*, vol. 30, pp. 5439-5457, 2015.

[115] A. Nami, J. Liang, F. Dijkhuizen, and G. D. Demetriades, "Modular Multilevel Converters for HVDC Applications: Review on Converter Cells and Functionalities," *Ieee Transactions on Power Electronics*, vol. 30, pp. 18-36, Jan 2015.

[116] G. P. Adam, S. J. Finney, K. Bell, and B. Williams, "Transient Capability Assessments of HVDC Voltage Source Converters," in *IEEE Power and Energy Conference*, Illinois 2012, pp. 1-8.

[117] D. A. N. Jacobson, P. Wang, M. Mohaddes, M. Rashwan, and R. Ostash, "A Preliminary Look at the Feasibility of VSC HVDC in Manitoba," in *IEEE Electrical Power and Energy Conference (EPEC)*, Manitoba, Canada, 2011, pp. 80-85.

[118] G. F. Reed, H. A. Al Hassan, M. J. Korytowski, P. T. Lewis, and B. M. Grainger, "Comparison of HVAC and HVDC solutions for offshore wind farms with a procedure for system economic evaluation," in *Energytech, 2013 IEEE*, 2013, pp. 1-7.

[119] O. Heyman, L. Weimers, and M.-L. Bohl, "HVDC-A key solution in future transmission systems," in *World Energy Congress-WEC*, 2010, pp. 12-16.

[120] P. Thepparat, D. Retzmann, E. Ogee, and M. Wiesinger, "Smart transmission system by HVDC and FACTS," in *PowerTech (POWERTECH), 2013 IEEE Grenoble*, 2013, pp. 1-6.

[121] P. Buijs, D. Bekaert, S. Cole, D. Van Hertem, and R. Belmans, "Transmission investment problems in Europe: Going beyond standard solutions," *Energy Policy*, vol. 39, pp. 1794-1801, 3// 2011.

[122] NERSA, "The South African Grid Code-The Network Code, ," *ed*, 2010.

[123] DIgSILENT, "PowerFactory 15.1 Detailed Product Information," *DIgSIELNT Gmbh, Gomarigen* 2014.

[124] R. B. Roy and M. R. Amin, "Analysis of proposed controlling topology of the HVDC link between Bangladesh and India," in *Strategic Technology (IFOST), 2014 9th International Forum on*, 2014, pp. 390-395.

[125] L. Risheng, S. Bozhko, and G. Asher, "Frequency Control Design for Offshore Wind Farm Grid With LCC-HVDC Link Connection," *Power Electronics, IEEE Transactions on*, vol. 23, pp. 1085-1092, 2008.

[126] P. Kundur, N. J. Balu, and M. G. Lauby, *Power system stability and control* vol. 7: McGraw-hill New York, 1994.

[127] J. Paulinder, "Operation and Control of HVDC Links Embedded in AC Systems," Licentiate of Engineering, Department of Electric Power Engineering, Chalmers University of Technology, Geteborg, Sweden, 2003.

[128] D. Kong, "Advanced HVDC Systems for Renewable Energy Integration and Power Transmission: Modelling and Control for Power System Transient Stability," Doctor of Philosophy, School of Electronic, Electrical and Computer Engineering, University of Birmingham, Birmingham, 2013.

[129] A. Gavrilovic, "AC/DC System Strength as Indicated by Short Circuit Ratios," in *International Conference on AC and DC Power Transmission*, London, 1991, pp. 27-32.

[130] R. Thallam, "Review of the Design and Performance Features of HVDC Systems Connected to Low Short Circuit Ratio AC Systems," *IEEE Transactions on Power Delivery*, vol. 7, pp. 2065-2073, 1992.

[131] B. Gao, G. Morison, and P. Kundur, "Voltage stability evaluation using modal analysis," *Power Systems, IEEE Transactions on*, vol. 7, pp. 1529-1542, 1992.

[132] C. W. Taylor, *Power system voltage stability*: McGraw-Hill, 1994.

[133] T. Van Cutsem and C. Vournas, *Voltage stability of electric power systems* vol. 441: Springer Science & Business Media, 1998.

[134] P. Sauer and M. Pai, "Power System Steady-State Stability and the Load-Flow Jacobian," *IEEE Transactions on power systems*, vol. 5, pp. 1374-1383, 1990.

[135] H. Le Nguyen, "Newton-Raphson method in Complex Form [Power System Load Flow Analysis]," *IEEE Transactions on Power Systems*, vol. 12, pp. 1355-1359, 1997.

[136] V. Ajjarapu and C. Christy, "The continuation power flow: a tool for steady state voltage stability analysis," *IEEE Transactions on Power Systems*, vol. 7, pp. 416-423, 1992.

[137] H. Li, Y. Jin, A. Zhang, X. Shen, C. Li, and B. Kong, "An Improved Hybrid Load Flow Calculation Algorithm for Weakly-Meshed Power Distribution System," *International Journal of Electrical Power & Energy Systems*, vol. 74, pp. 437-445, 2016.

[138] S. Johansson, "Long-term Voltage Stability in Power Systems: Alleviating the Impact of Generator Current Limiters," Doctor of Philosophy, Department of Electric Power Engineering, Chalmers University of Technology, Göteborg, Sweden, 1998.

[139] Eskom. (2016). *Transmission Development Plan Brochure for 2016-2025* Available: http://www.eskom.co.za/Whatweredoing/TransmissionDevelopmentPlan/Documents/TransDevPlan2016-2025Brochure.pdf

[140] Eskom. (2015). *Transmission Development Plan 2016 – 2025 Public Forum*. Available: http://www.eskom.co.za/Whatweredoing/TransmissionDevelopmentPlan/Documents/2016-2025TDP__Oct2015Rev5.pdf

[141] P. Goosen, C. Reddy, B. Jonsson, T. Holmgren, O. Saksvik, and H. Bjorklund, "Upgrade of the Apollo HVDC Converter Station," in *Cigre 6th Southern Africa Regional Conference*, Cape Town, South Africa, 2009.

[142] Matthew H. Brown and R. P. Sedano, "Electricity Transmission: A Primer," a Report by Department of Energy and National Council on Electricity Policy, U.S, 2004.

[143] NRECA, "Design Manual for High Voltage Transmission Lines," a report by Department of Agrictulture, Rural Utilities Service, Electric Staff Division. U.S. 2009.

[144] J. Yli-Hannuksela, "The Transmission Line cost Calculation," Bachelor Degree, Department of Electrical Engineering, University of Applied Sciences, Wärtsilä Power Plants. Vaasa, Finland, 2011.

[145] Black and Veatch, "Capital Costs for Transmission and Substation," a report for Western Electricity Coordinating Council WECC, Transmission Expansion Planning. 2014.

[146] L. Koshcheev, "Environmental characteristics of HVDC overhead transmission lines," in *3rd workshop on Power Grid Interconnection in Northeast Asia, Vladivostok, Russia*, 2003.

[147] A. Malozemoff, J. Maguire, B. Gamble, and S. Kalsi, "Power Applications of High-Temperature Superconductors: Status and Perspectives," *IEEE Transactions on Applied Superconductivity*, vol. 12, pp. 778-781, 2002.

APPENDIX

HVDC terms definition

- **Firing delay angle α:** is the interval between the moments the commutation voltage becomes positive and the actual firing (R).
- **Overlap angle μ**: is the interval between the firing of the incoming valve and the cessation of the current in the outgoing valve (R).
- **Advance angle β:** is the interval between the firing of the incoming valve and the moment the commutation voltage is going negative (I).
- **Extinction angle γ:** is the interval between cessation of the current in the outgoing valve and the moment the commutation voltage is going negative (I).

APP 1: ±600kV Bipolar HVDC Scheme Modelling details

a. Voltage Dependent Current Order Limiter (VDCOL) Modelling

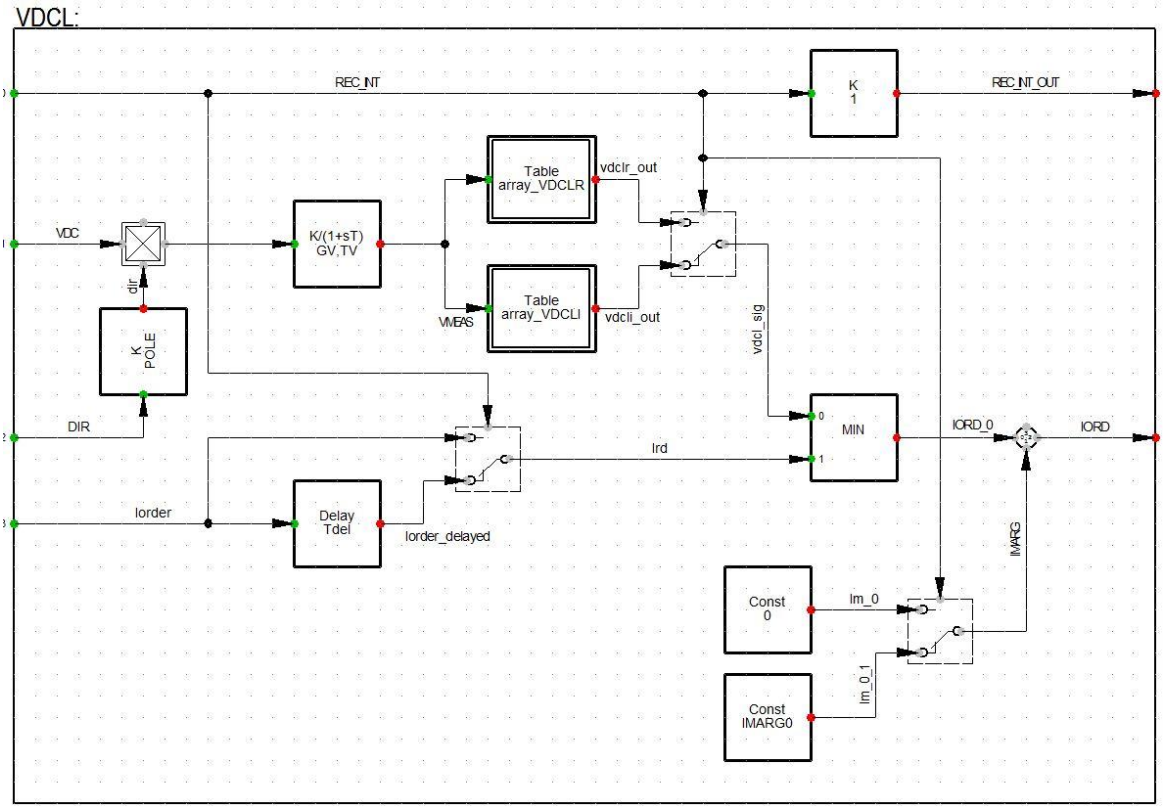

Figure 0.1: Voltage Dependent Current Order Limiter controller block (VDCOL)

- **DIgSILENT Simulation Language for VDCOL Controller**

inc(REC_INT)=REC_INT_OUT

inc(DIR)=POLE*select(VDC>0,1,-1)

inc(Iorder)=select(REC_INT,IORD,IORD-IMARG0)

inc(xV)=GV*abs(VDC)

Table 0.1: VDCOL ARRAY

	VDCOLI_x	VDCOLI_y	VDCOLR_x	VDCOLR_y
size	5.	0.	4.	0.
1	0.	0.2	0.	0.3
2	0.1	0.2	0.1	0.3
3	0.9	0.9	0.8	1.
4	1.1	1.1	1.8	1.8
5	2.2	2.2	1.8	1.8

Table 0.2: VDCOL controller parameters

	Negative pole	Positive pole
GV	1.	1.
TV	0.1	0.1
POLE	-1.	1.
Tdel	0.07	0.07
IMARG0	-0.1	-0.1

b. Power Controller

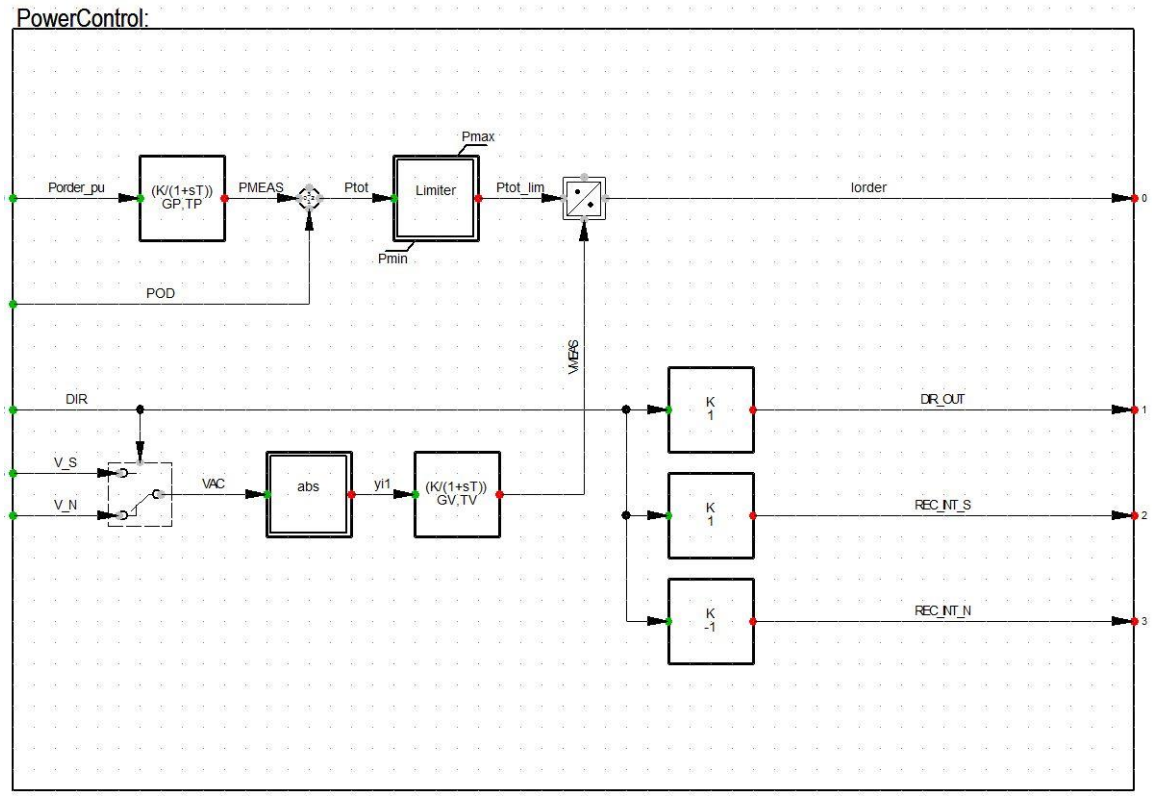

Figure 0.2: HVDC overall power control Block

- **DIgSILENT Simulation Language for Power Control**

inc(DIR)=DIR_OUT

inc(xV)=abs(GV*VAC)

inc(POD)=0

inc(PMEAS)=Iorder*abs(GV*VAC)

inc(Porder_pu)=PMEAS/GP

inc(xP)=PMEAS

Table 0.3: Power controller parameters

	Negative pole	Positive pole
GP	1	1
TP	0.03	0.03
GV	1	1
TV	5	7
Pmin	-2	-2
Pmax	2	2

c. Extinction Angle Control (gamma control)

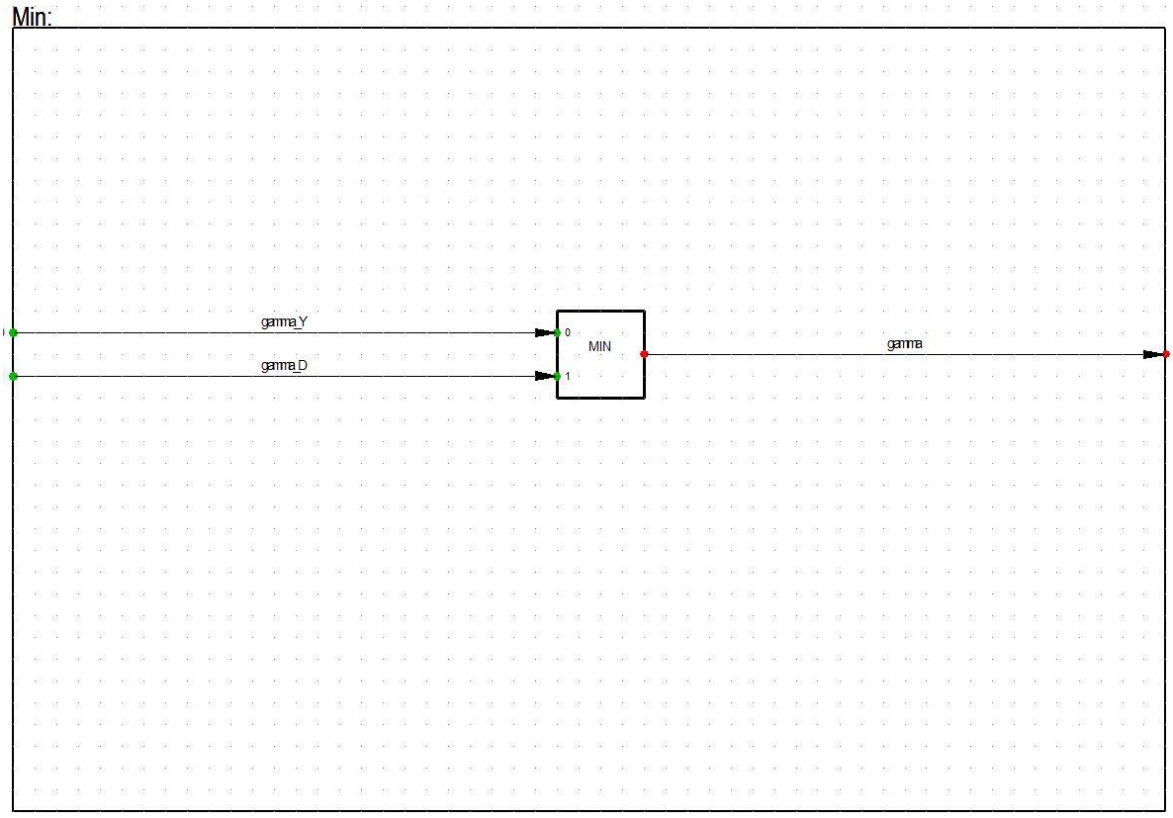

Figure 0.3: Extinction angle control block (gamma control)

- **DIgSILENT Simulation Language for Extinction Angle Control**

inc(gamma)=min(gamma_Y,gamma_D+0.000001)

d. Converter Firing Angle Control

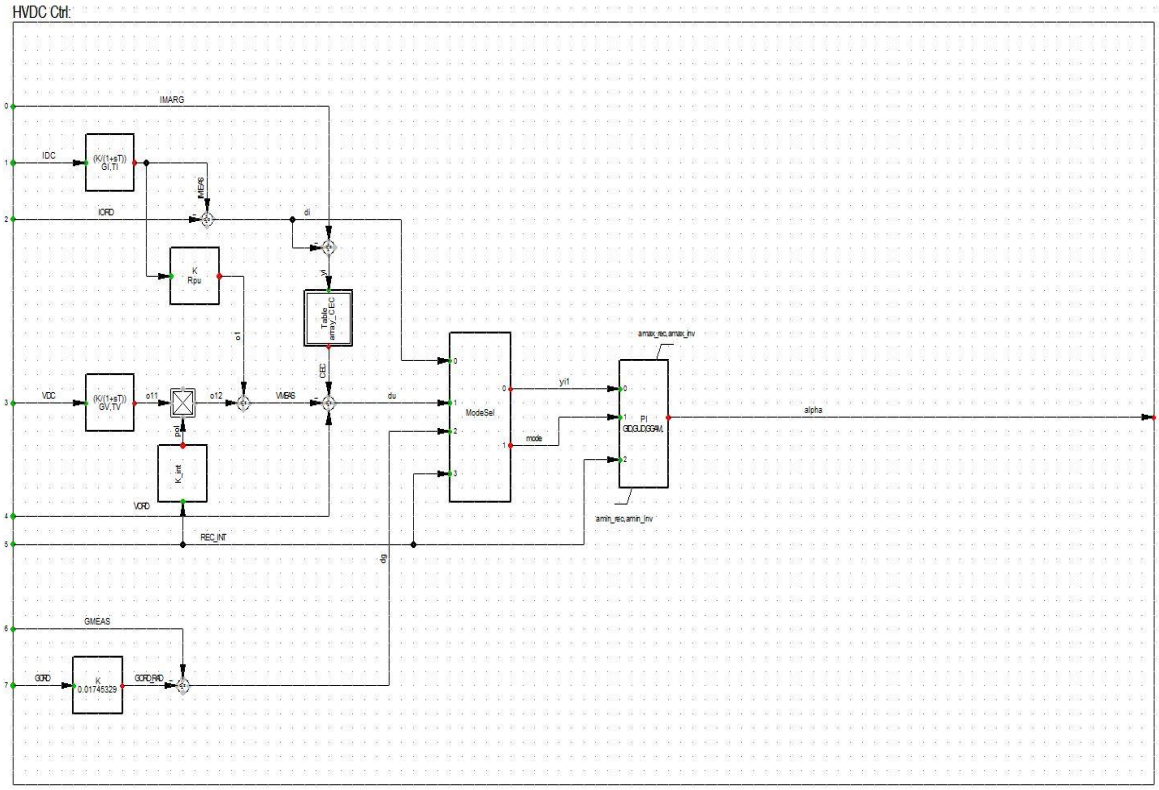

Figure 0.4: HVDC firing angle control block (alpha controller)

- **DIgSILENT Simulation Language for Firing Angle Control**

inc(REC_INT)=select(alpha>pi()/2,-1,1)

inc(du0)=VORD0-VMEAS-CEC

inc(dg0)=GMEAS-0.01745329*GORD0

inc(mode)=select(REC_INT=1,1,select(du0<dg0,2,3))

inc(xpi)=alpha

inc(xamax)=Grad*select(REC_INT=1,amax_rec,amax_inv)

inc(xamin)=Grad*select(REC_INT=1,amin_rec,amin_inv)

inc(xgpg)=select(mode=1,GID,select(mode=2,GUD,GGAM))

inc(xI)=GI*IDC

inc(xV)=GV*VDC

inc(IMARG)=select(REC_INT=1,0,IMARG0)

inc(IORD)=select(REC_INT=1,GI*IDC,GI*IDC+IMARG0)

inc(VORD)=select(mode=2,VMEAS-CEC,VORD0)

inc(GORD)=select(mode=3,GMEAS/0.01745329,GORD0)

inc0(VDC)=VORD0/GV

inc(INV)=VDC/abs(VDC)/REC_INT

Table 0.4: Firing angle control CEC array

Size	CEC_x	CEC_y
	4.	0.
1	-0.1	0.
2	0.01	0.
3	0.1	0.1
4	0.2	0.1

Table 0.5: Firing angle control parameter

	Negative pole	**Positive pole**
GI	1.	1.
TI	0.01	0.01
GV	1.	1.
TV	0.01	0.01
Rpu	0.1481482	0.1481482
GID	0.25	0.25
GUD	1.	1.
GGAM	0.5	0.5
TID	0.02	0.02
TUD	0.02	0.02
TGAM	0.04	0.04
IMARG0	-0.1	-0.1
GORD0	22.	25.
VORD0	1.2	1.2
amin_rec	3.	3.
amin_inv	90.	90.
amax_rec	120.	120.
amax_inv	165	165.

e. HVDC Overall Control Model

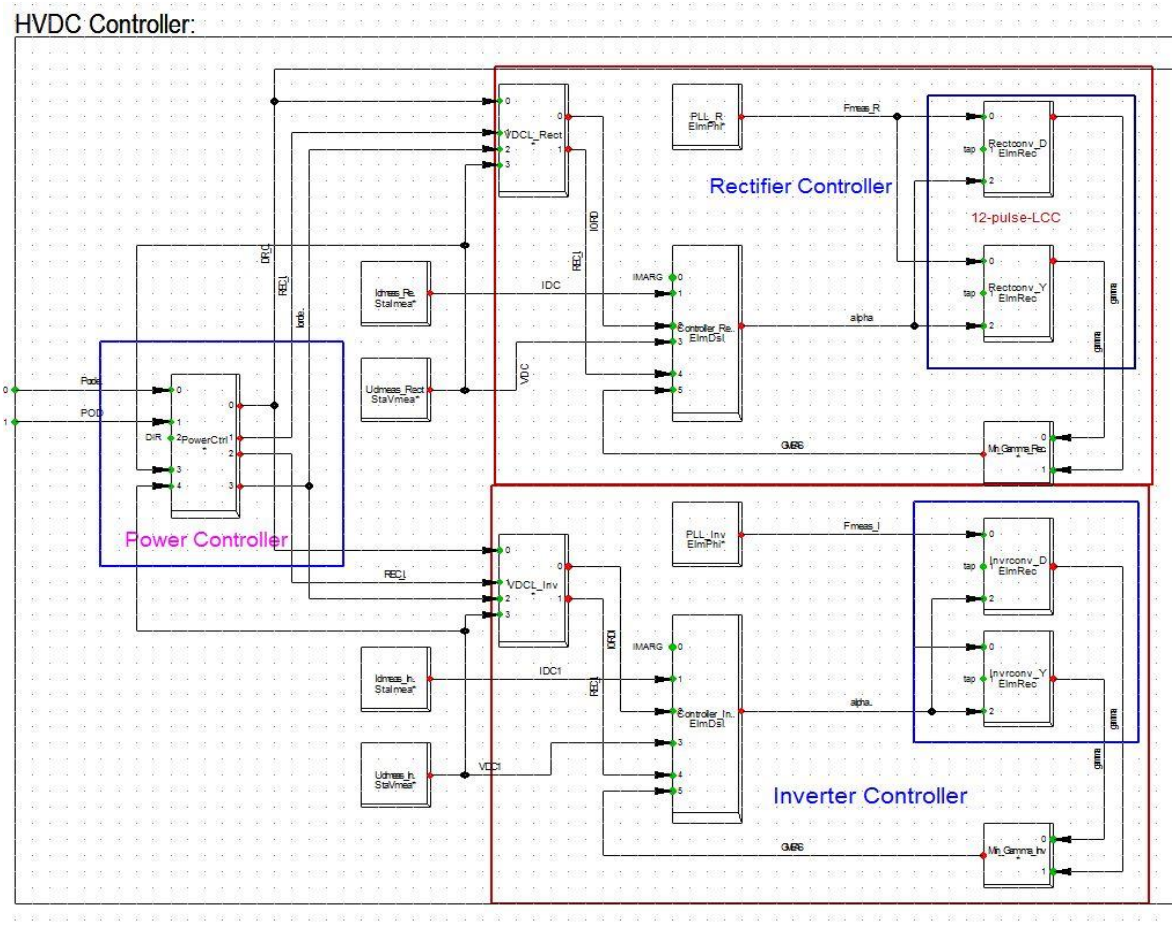

Figure 0.5: Overall HVDC composite model

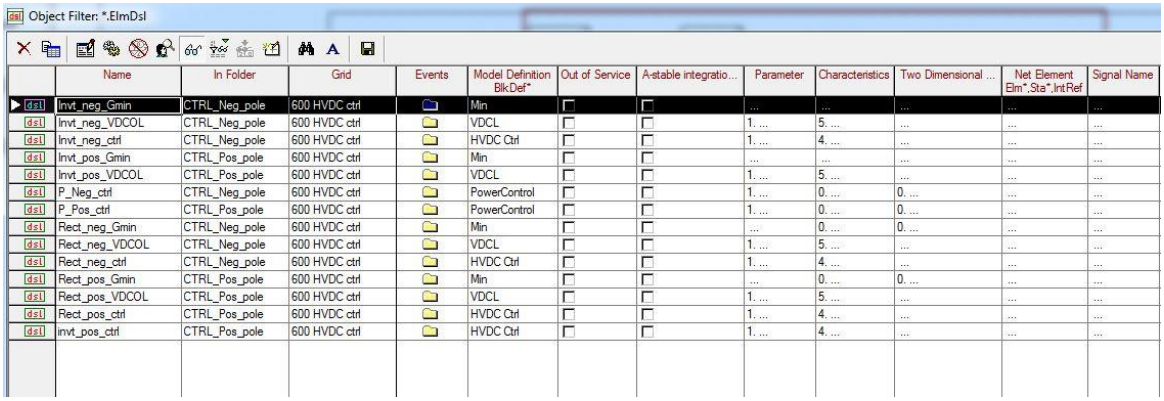

Name	In Folder	Grid	Events	Model Definition BlkDef*	Out of Service	A-stable integratio...	Parameter	Characteristics	Two Dimensional ...	Net Element Elm*,Sta*,IntRef	Signal Name
Invt_neg_Gmin	CTRL_Neg_pole	600 HVDC ctrl		Min			...	...	...	...	...
Invt_neg_VDCOL	CTRL_Neg_pole	600 HVDC ctrl		VDCL			1. ...	5. ...	...	...	...
Invt_neg_ctrl	CTRL_Neg_pole	600 HVDC ctrl		HVDC Ctrl			1. ...	4. ...	...	...	...
Invt_pos_Gmin	CTRL_Pos_pole	600 HVDC ctrl		Min			...	...	...	...	...
Invt_pos_VDCOL	CTRL_Pos_pole	600 HVDC ctrl		VDCL			1. ...	5. ...	...	...	...
P_Neg_ctrl	CTRL_Neg_pole	600 HVDC ctrl		PowerControl			1. ...	0. ...	0. ...	...	...
P_Pos_ctrl	CTRL_Pos_pole	600 HVDC ctrl		PowerControl			1. ...	0. ...	0. ...	...	...
Rect_neg_Gmin	CTRL_Neg_pole	600 HVDC ctrl		Min			...	0. ...	0. ...	...	...
Rect_neg_VDCOL	CTRL_Neg_pole	600 HVDC ctrl		VDCL			1. ...	5. ...	...	...	...
Rect_neg_ctrl	CTRL_Neg_pole	600 HVDC ctrl		HVDC Ctrl			1. ...	4. ...	...	...	...
Rect_pos_Gmin	CTRL_Pos_pole	600 HVDC ctrl		Min			...	0. ...	0. ...	...	...
Rect_pos_VDCOL	CTRL_Pos_pole	600 HVDC ctrl		VDCL			1. ...	5. ...	...	...	...
Rect_pos_ctrl	CTRL_Pos_pole	600 HVDC ctrl		HVDC Ctrl			1. ...	4. ...	...	...	...
invt_pos_ctrl	CTRL_Pos_pole	600 HVDC ctrl		HVDC Ctrl			1. ...	4. ...	...	...	...

Figure 0.6: HVDC Common model as set up in DIgSILENT PowerFactory

Table 0.6: DC reactor parameters

Line name	Nom. V kV	Rated MVA	System type	Irated kA	Inductance mH
Neg_Reactor_I	600	1500	DC	2.5	650.8
Neg_Reactor_R	600	1500	DC	2.5	650.8
Pos_Reactor_I	600	1500	DC	2.5	650.8
Pos_Reactor_R	600	1500	DC	2.5	650.8

Table 0.7: AC/DC filters and capacitors banks

Name	Volt (kV)	System type	MVA rating	Frequency (Hz)	Quality factor	Parallel Res. (Ω)
HighFreq Filter_I	275	AC	200.2341	600.4499	0	37.03
HighFreq Filter_I(1)	400	AC	202.2341	600.4499	0	37.03
HighFreq Filter_R	400	AC	200.2342	600.8372	0	83.32
HighFreq Filter_R(1)	275	AC	200.2342	600.8372	0	83.32
LowFreq Filter_I	275	AC	245.9506	80.0458	5.00906	116.36
LowFreq Filter_I(1)	400	AC	200.9506	80.0458	5.00906	116.36
LowFreq Filter_R	400	AC	200.9702	80.0103	5.011137	261.87
LowFreq Filter_R(1)	275	AC	245.9702	80.0103	5.011137	261.87
Neg_ShuntCapDC	600	DC	2042.035	0	0	0
Pos_ShuntCapDC	600	DC	2042.035	0	0	0
Shunt Cap_I	275	AC	70.0083	0	0	0
Shunt Cap_I(1)	400	AC	70.0083	0	0	0
Shunt Cap_R	400	AC	70.9668	0	0	0
Shunt Cap_R(1)	275	AC	70.9668	0	0	0

Table 0.8: Thyristors type data

Name	Vac (kV)	Vdc (kV)	P_{rated} (MW)	I_{DC} (kA)	Nom. turns ratio	α-nom.	min. turns ratio p.u.	max turns ratio p.u.
6-Pulse Inverter	275.6	301.55	904.6542	3	0.83888	15	0.9	1.3
6-Pulse Rectifier	400.9	309.86	929.5867	3	0.592586	15	0.7	1.4

Table 0.9: HVDC converter parameters

Name	control xtics	Vset p.u.	Pset (MW)	Iset (kA)	γ (deg)	α-min (deg)	α-max (deg)	γ-min (deg)	winding ratio p.u	commutation reactance
Inv_neg_D	EXT	-0.994	1	1	20	3	180	10	0.95	13.4445
Inv_neg_Y	Vdc	-0.99	1	1	20	3	180	10	0.95	13.4445
Inv_pos_D	EXT	-0.994	1	1	20	3	180	10	0.95	13.4445
Inv_pos_Y	Vdc	-0.99	1	1	20	3	180	10	0.95	13.4445
Rect_neg_D	EXT	1	800	2	15	3	180	15	0.95	13.4445
Rect_neg_Y	I	1	600	1.7	15	3	180	15	0.95	13.4445
Rect_pos_D	EXT	1	800	2	15	3	180	15	0.95	13.4445
Rect_pos_Y	I	1	600	1.7	15	3	180	15	0.95	13.4445

Table 0.10: DC line parameters

Name	Length (km)	R' 20^0 Ω/km	R' 80^0 Ω/km	alpha 1/k	B' uS/km	C' uF/km	I kA	Z1 (Ω)
Neg_LineDC_I	650	0.01	0.012418	0.00403	3.414	0.0108671	3	6.5
Neg_LineDC_R	650	0.01	0.012418	0.00403	3.414	0.0108671	3	6.5
Pos_LineDC_I	650	0.01	0.012418	0.00403	3.414	0.0108671	3	6.5
Pos_LineDC_R	650	0.01	0.012418	0.00403	3.414	0.0108671	3	6.5

APP 2: IEEE 30-bus system DATA

600kV Monopolar HVDC Data

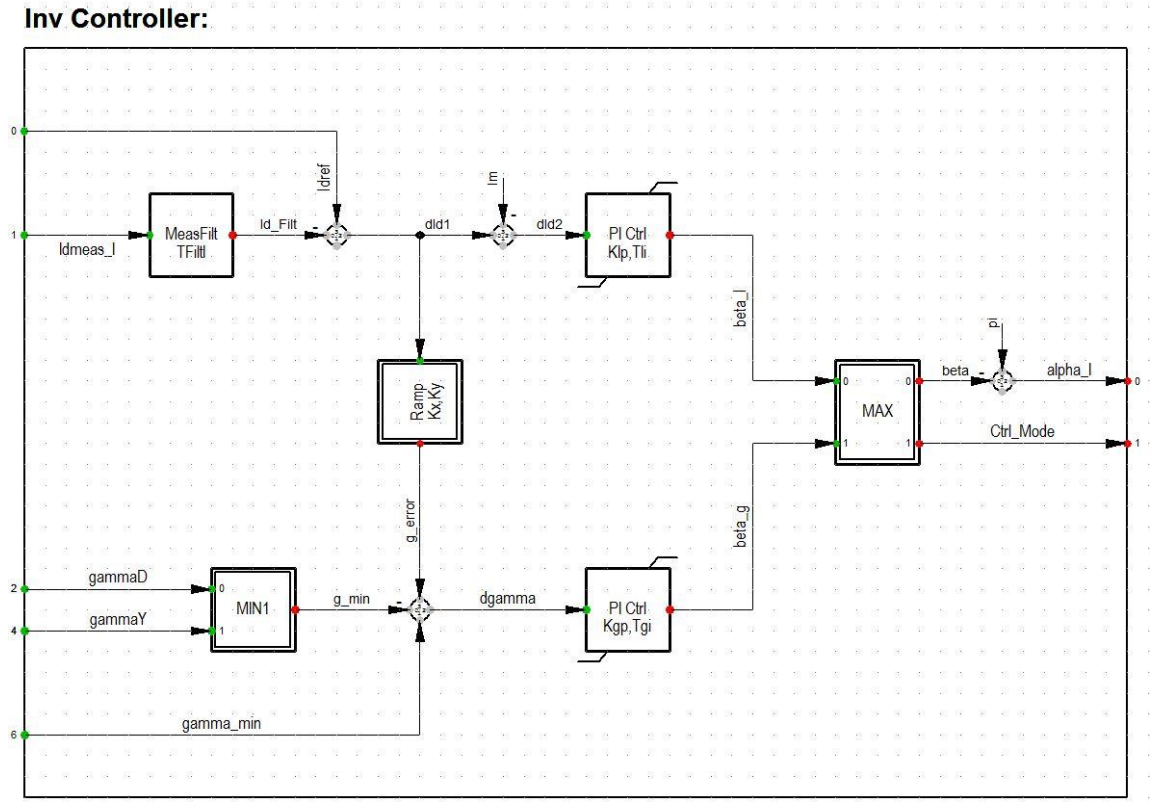

Figure 0.7: Inverter control block

- **DIgSILENT simulation language for Inverter control block**

inc(xg)=pi()-alpha_I

inc(xI)=bI_max

inc(gamma_min)=select(gammaD>gammaY,gammaY,gammaD)

inc(Idref)=Idmeas_I

inc(xFiltI)=1

inc0(gammaD)=99999.

inc0(gammaY)=99999.

vardef(gamma_min)='rad';'Minimum Extinction Angle'

vardef(Kgp)='p.u.';'Proportional Gain Gamma Controller'

vardef(Tgi)='s';'Integral Time Constant Gamma Controller'

vardef(alpha_g_max)='rad';'Maximum Firing Angle (Gamma Ctrl)'

vardef(alpha_g_min)='rad';'Minimum Firing Angle (Gamma Ctrl)'

vardef(KIp)='p.u.';'Proportional Gain Current Controller'

vardef(TIi)='s';'Integral Time Constant Current Controller'

vardef(alpha_I_max)='rad';'Maximum Firing Angle (Id Ctrl)'

vardef(alpha_I_min)='rad';'Minimum Firing Angle (Id Ctrl)'

vardef(Imargin)='p.u.';'Current Margin'

vardef(Kx)='p.u.';'x-Edge of Ramp Function'

vardef(Ky)='p.u.';'y-Edge of Ramp Function'

vardef(TFiltI)='s';'Filter Time Constant of Id-Measurement'

Table 0.11: Inverter control Block parameters

Controller Signals	Inverter Control
Kgp Proportional Gain Gamma Controller (p.u.)	0.1
Tg Integral Time Constant Gamma Controller (s)	0.01
Kip Proportional Gain Current Controller (p.u.)	0.1
Tii Integral Time Constant Current Controller (s)	0.01
Imargin Current Margin (p.u.)	0.1
TFiltI Filter Time Constant of Id-Measurement (s)	0.0012
Kx x-Edge of Ramp Function (p.u.)	0.1
Ky y-Edge of Ramp Function (p.u.)	0.3
alpha_g_min Minimum Firing Angle Gamma Ctrl (rad)	90
alpha_I_min Minimum Firing Angle Id Ctrl rad	70
alpha_g_max Maximum Firing Angle Gamma Ctrl (rad)	150
alpha_I_max Maximum Firing Angle Id Ctrl (rad)	150

Rect Controller:

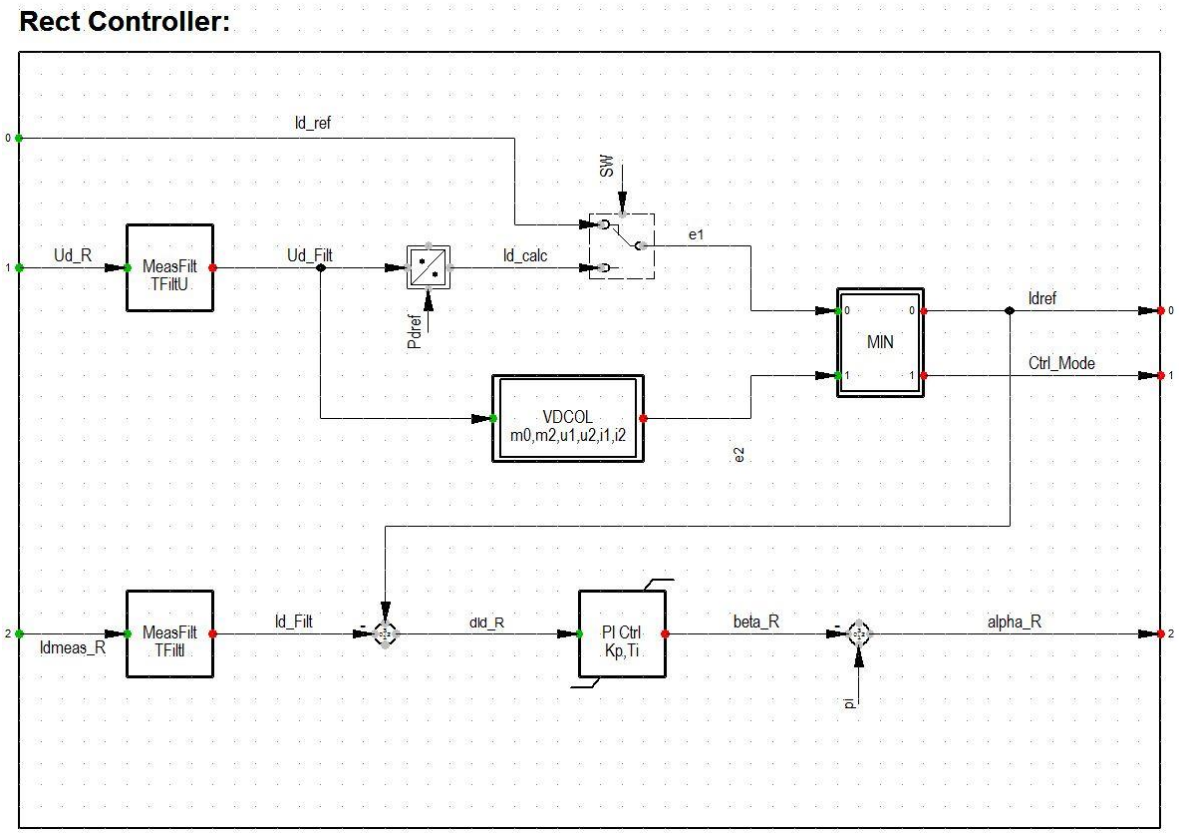

Figure 0.8: Rectifier control block diagram

- **DIgSILENT simulaton language for Rectifier control block**

inc(xi)=pi()-alpha_R

inc(Id_ref)=Idmeas_R

inc(xFiltU)=1

inc(xFiltI)=1

inc0(Ud_R)=1

inc0(Idref)=Idmeas_R

vardef(Kp)='p.u.';'Proportional Gain'

vardef(Ti)='s';'Integral Time Constant'

vardef(alpha_max)='rad';'Maximum Firing Angle'

vardef(alpha_min)='rad';'Minimum Firing Angle'

vardef(Pd)='p.u.';'DC Power Setpoint'

vardef(P_I)='ON/OFF';'Current/Power Control, Pd=1/Id=0'

vardef(TFiltU)='s';'Filter Time Constant Ud-Measurement'

vardef(TFiltI)='s';'Filter Time Constant Id-Measurement'

alpha_deg = alpha_R/pi()*180

beta_deg = beta_R/pi()*180

Idref_kV = Idref*2

Table 0.12: Rectifier control block parameters

Controller Signals	Rectifier Control
Kp Proportional Gain (p.u.)	1.1
Ti Integral Time Constant (s)	0.01
P_I Current/Power Control, Pd=1/Id=0 (ON/OFF)	0
Pd DC Power Setpoint p.u	1.1
TFiltU Filter Time Constant Ud-Measurement (s)	0.03
TFiltI Filter Time Constant Id-Measurement (s)	0.0013
m0	0
m2	1
u1	0.4
u2	0.8
i1	0.55
i2	0.9
alpha_min Minimum Firing Angle (rad)	5
alpha_max Maximum Firing Angle (rad)	150

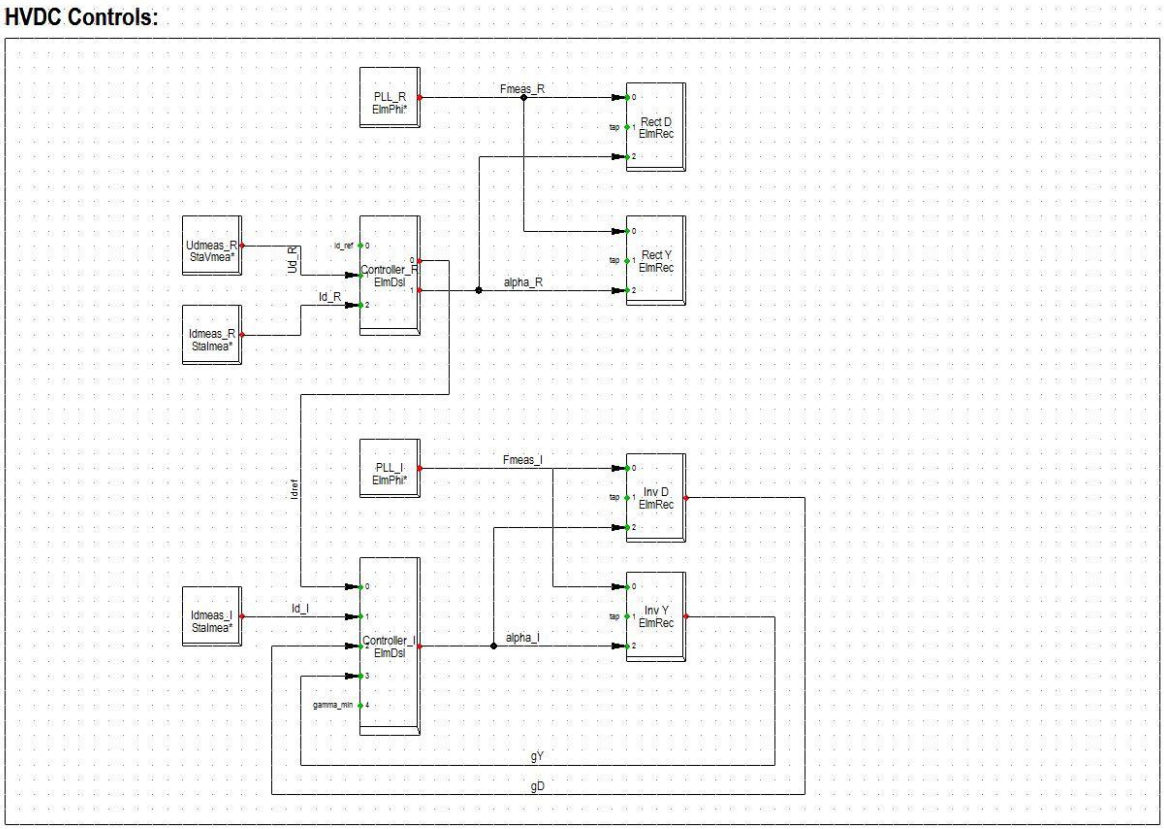

Figure 0.9: Overall composite model for monopolar HVDC scheme

Table 0.13: HVDC line parameters

Line Name	length (km)	I rated kA	Nom. V. (kV)	R' 20^{0}C Ω/km	x'	L'	R 80^{0}C Ω/km
LineDC_R	350	2.8	600	0.01	0.1	0.31831	0.012418
LineDC_I	350	2.8	600	0.01	0.1	0.31831	0.012418

Table 0.14: HVAC line parameters

Line Name	Length (km)	I kA	Nom. V. (kV)	R' 20^{0}C Ω/km	x'	L'	B'	C'
line 1_2	105	1	400	0.0452	0.3	0.95493	4.426979	0.014092
Line13_14	55	1	400	0.057	0.3	0.95493	4.181989	0.013312
Line 9_13	17	1.3	400	0.1243	0.3	0.95493	3.5162	0.011192
Line 8_9	45	1	400	0.0169	0.3	0.95493	3.932318	0.012517
Line 8_3	75	1.3	400	0.057	0.3	0.95493	5.409538	0.017219
Line 8_27	400	1	400	0.0581	0.3	0.95493	2.937006	0.009349
Line 8_13	65	1	400	0.057	0.3	0.95493	2.49671	0.007947
Line 7_8	30	1	400	0.0936	0.3	0.95493	3.120888	0.009934
Line 7_27	340	1	400	0.0192	0.3	0.95493	3.99342	0.012711
Line 6_5	10	1.2	400	0.1	0.3	0.95493	5.201479	0.016557
Line 4_8	155	1	400	0.034	0.3	0.95493	5.201479	0.016557
Line 4_5	12	1	400	0.0231	0.3	0.95493	2.559128	0.008146
Line 4_2	156	1	400	0.0243	0.3	0.95493	3.8699	0.012318
Line 4_11	128	1	400	0.0243	0.3	0.95493	3.8699	0.012318
Line 3_1	40	1.4	400	0.011	0.3	0.95493	4.181989	0.013312
Line 2_6	75	1	400	0.057	0.3	0.95493	4.406173	0.014025
Line 29_30	60	1.2	400	0.1243	0.3	0.95493	3.517516	0.011197
Line 28_30	110	1.3	400	0.0243	0.3	0.95493	2.60074	0.008278
Line 28_29	150	1.2	400	0.1243	0.3	0.95493	3.517516	0.011197
Line 27_28	300	1	400	0.0181	0.3	0.95493	5.617597	0.017881
Line 25_28	75	1.3	400	0.057	0.3	0.95493	2.517516	0.008014
Line 25_26	60	1.3	400	0.057	0.3	0.95493	2.517516	0.008014
Line 23_24	85	1	400	0.057	0.3	0.95493	3.120888	0.009934
Line 22_24	180	1.2	400	0.1243	0.3	0.95493	3.517516	0.011197
Line 21_25	50	1.5	400	0.057	0.3	0.95493	2.49671	0.007947
Line 20_21	150	1	132	0.0231	0.3	0.95493	4.614233	0.014688
Line 1_8	120	1.3	400	0.0192	0.3	0.95493	4.161183	0.013245
Line 19_20	32	1.2	400	0.1243	0.3	0.95493	3.517516	0.011197
Line 16_22	180	1.2	400	0.1243	0.3	0.95493	3.517516	0.011197
Line 15_18	123	0.1	11	0.0747	0.3	0.95493	4.452466	0.014173
Line 14_23	150	1.2	400	0.1243	0.3	0.95493	3.517516	0.011197
Line 14_17	15	0.7	400	0.0231	0.3	0.95493	3.745065	0.011921
Line 13_17	70	1.3	400	0.057	0.3	0.95493	2.517516	0.008014
Line 11_22	300	1	400	0.0581	0.3	0.95493	2.937006	0.009349
Line 11_16	60	0.7	400	0.0231	0.3	0.95493	3.745065	0.011921

Line 11_12	18	1	400	0.057	0.3	0.95493	3.120888	0.009934

- **Synchronous Machine Controller Data**

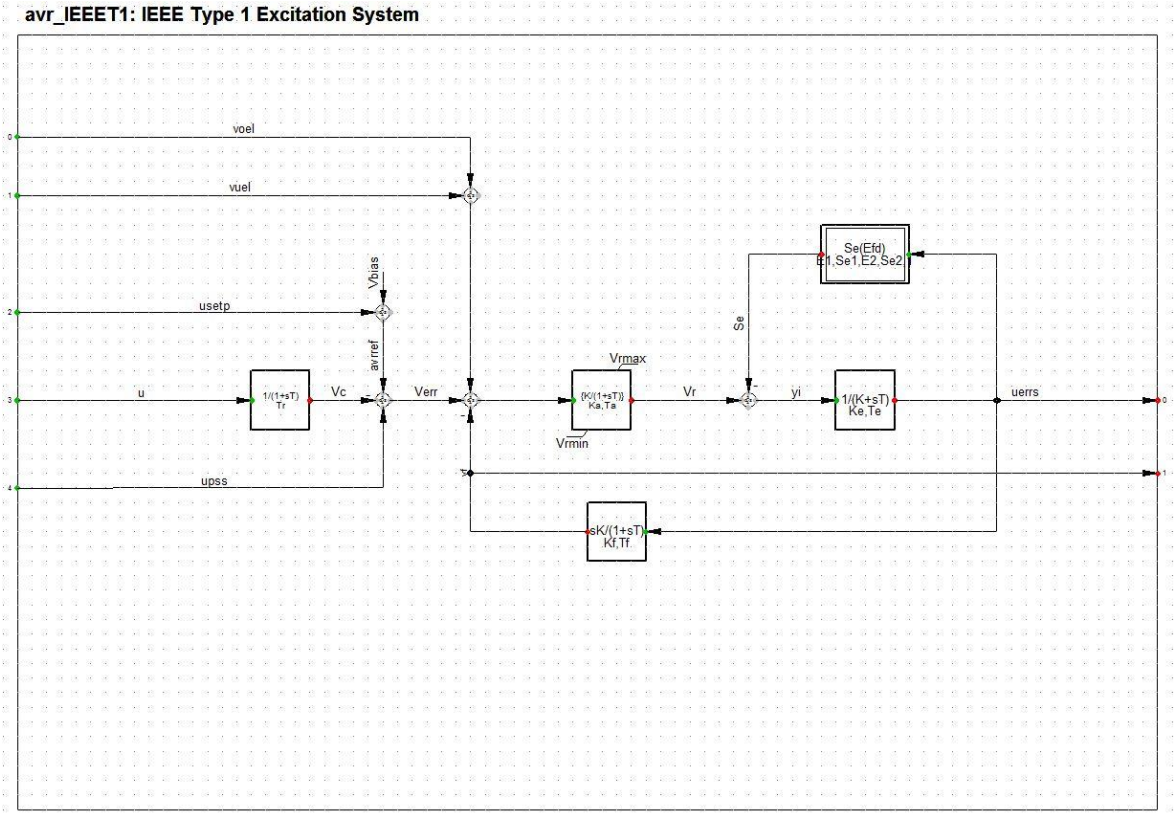

Figure 0.10: Avr_IEEET1- IEEE type 1 excitation system

- **DIgSILENT simulation language for Avr_IEEET1- IEEE type 1 excitation system**

inc(upss) = 0

inc(vuel) = 0

inc(voel) = 0

!inc(usetp) = xa/Ka+u

inc(usetp) = u

inc(Vbias) = xa/Ka-(vuel+voel)

inc(xr) = u

inc(xe) = uerrs

inc(xf) = uerrs

inc(xa) = xe*Ke1+Se

inc(Y_max)=select(Vrmax<=0,select(Ke>0,(Se2+Ke)*E2,(Se2)*E2),Vrmax)

inc(Y_min)=select(Vrmax<=0,-Y_max,Vrmin)

inc(Ke1)=select(Ke=0,Y_max/uerrs/10-Se,Ke)

inc(vf) = 0.0

vardef(Tr) ='s';'Measurement Delay'

vardef(Ka) ='pu';'Controller Gain'

vardef(Ta) ='s';'Controller Time Constant'

vardef(Vrmax) ='pu';'Controller Output Maximum'

vardef(Vrmin) ='pu';'Controller Output Minimum'

vardef(Ke) ='pu';'Exciter Constant'

vardef(Te) ='s';'Exciter Time Constant'

vardef(Kf) ='pu';'Stabilization Path Gain'

vardef(Tf) ='s';'Stabilization Path Time Constant'

vardef(E1) ='pu';'Saturation Factor 1'

vardef(E2) ='pu';'Saturation Factor 3'

vardef(Se1) ='pu';'Saturation Factor 2'

vardef(Se2) ='pu';'Saturation Factor 4'

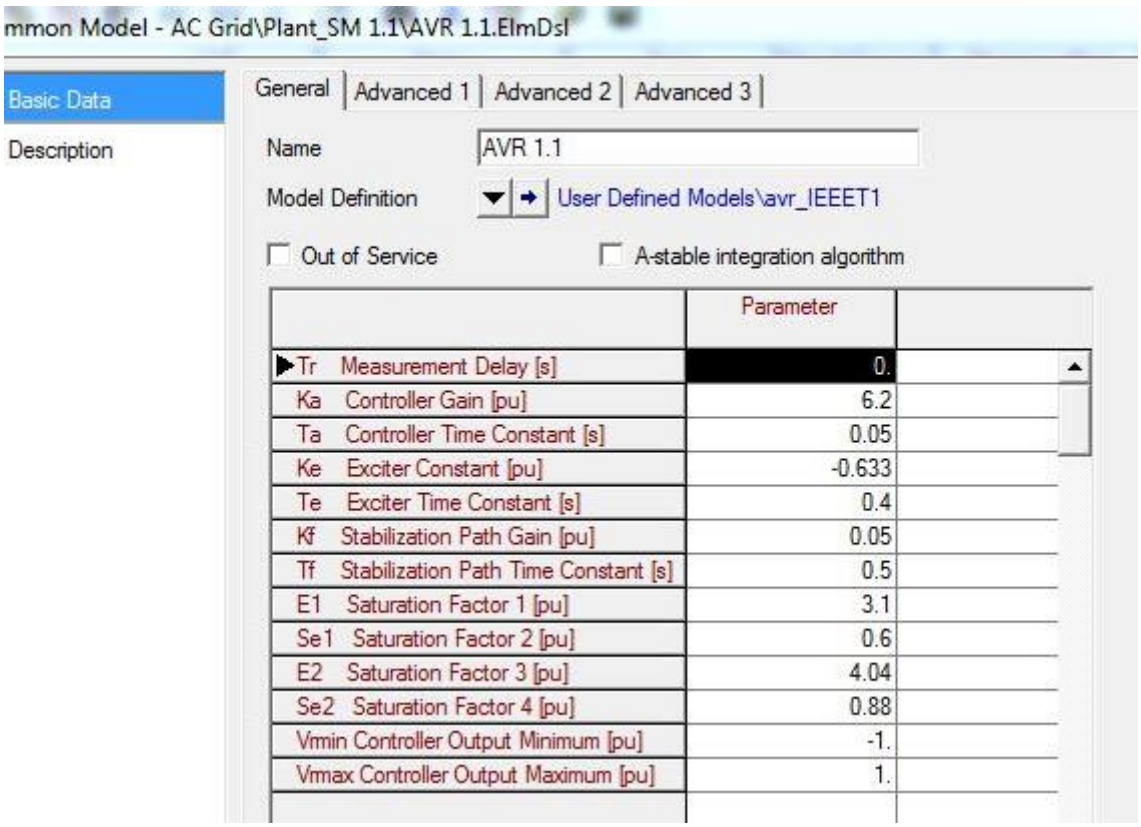

Figure 0.11: Avr_IEEET1- IEEE type 1 excitation system Parameters

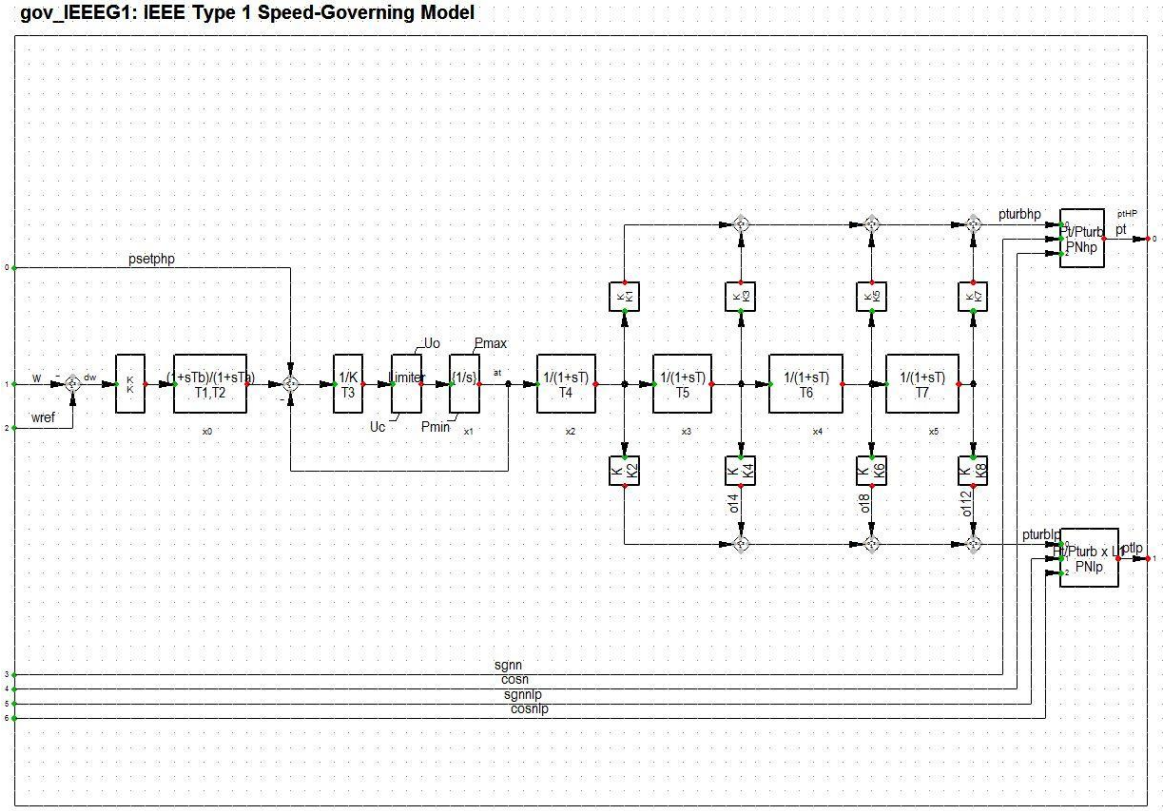

Figure 0.12: Gov_IEEEGI – IEEE type 1 speed governing model

- **DIgSILENT simulation language for Gov_IEEEGI – IEEE type 1 speed governing model**

inc(Plp) =select(PNlp>0.0,ptlp*sgnnlp*cosnlp/PNlp,ptlp)

inc(Php) =select(PNhp>0.0,pt*sgnn*cosn/PNhp,pt)

inc(L1) = select(K2+K4+K6+K8 > 0.00001,(Plp)/ ((Php)*(K2+K4+K6+K8) / (K1+K3+K5+K7)),0.0)

inc(x0) =0.0

inc(wref) =w

inc(psetphp)=pturbhp/(K1+K3+K5+K7)

inc(x1) =psetphp

inc(x2) =psetphp

inc(x3) =psetphp

inc(x4) =psetphp

inc(x5) =psetphp

inc0(ptlp) =0.0

inc0(cosnlp)=1.0

inc0(sgnnlp)=1.0

vardef(K) ='p.u.';'Controller Gain'

vardef(T1) ='s';'Governor Time Constant'

vardef(T2) ='s';'Governor Derivative Time Constant'

vardef(T3) ='s';'Servo Time Constant'

vardef(Uo) ='p.u./s';'Valve Opening Time'

vardef(Uc) ='p.u./s';'Valve Closing Time'

vardef(Pmax)='p.u.';'Maximum Gate Limit'

vardef(Pmin)='p.u.';'Minimum Gate Limit'

vardef(T4) ='s';'High Pressure Turbine Time Constant'

vardef(K1) ='p.u.';'High Pressure Turbine Factor'

vardef(K2) ='p.u.';'High Pressure Turbine Factor'

vardef(T5) ='s';'Intermediate Pressure Turbine Time Constant'

vardef(K3) ='p.u.';'Intermediate Pressure Turbine Factor'

vardef(K4) ='p.u.';'Intermediate Pressure Turbine Factor'

vardef(T6) ='s';'Medium Pressure Turbine Time Constant'

vardef(K5) ='p.u.';'Medium Pressure Turbine Factor'

vardef(K6) ='p.u.';'Medium Pressure Turbine Factor'

vardef(T7) ='s';'Low Pressure Turbine Time Constant'

vardef(K7) ='p.u.';'Low Pressure Turbine Factor'

vardef(K8) ='p.u.';'Low Pressure Turbine Factor'

vardef(PNhp) ='MW';'HP Turbine Rated Power(=0->PNhp=PgnnHp)'

vardef(PNlp) ='MW';'LP Turbine Rated Power(=0->PNlp=Pgnnlp)'

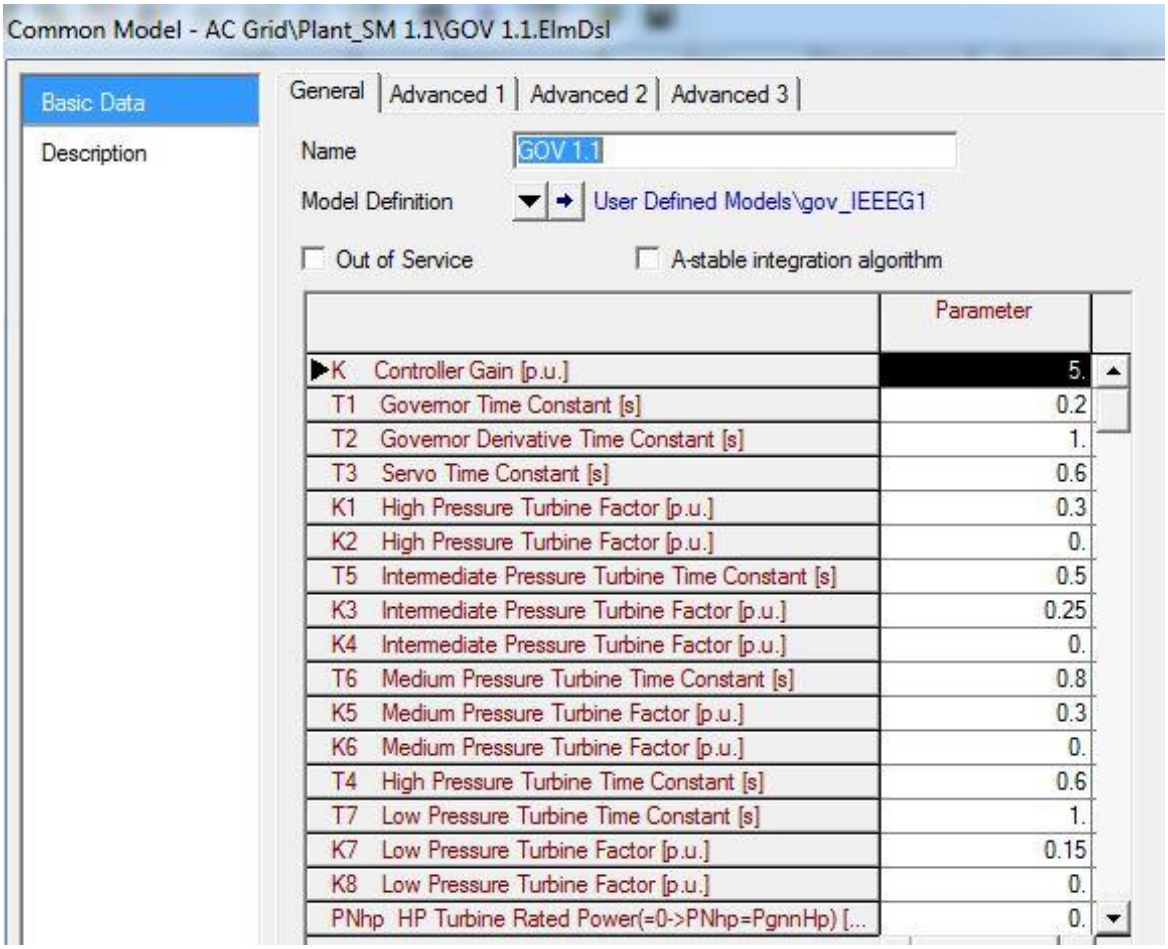

Figure 0.13: Gov_IEEEGI – IEEE type 1 speed governing model parameters

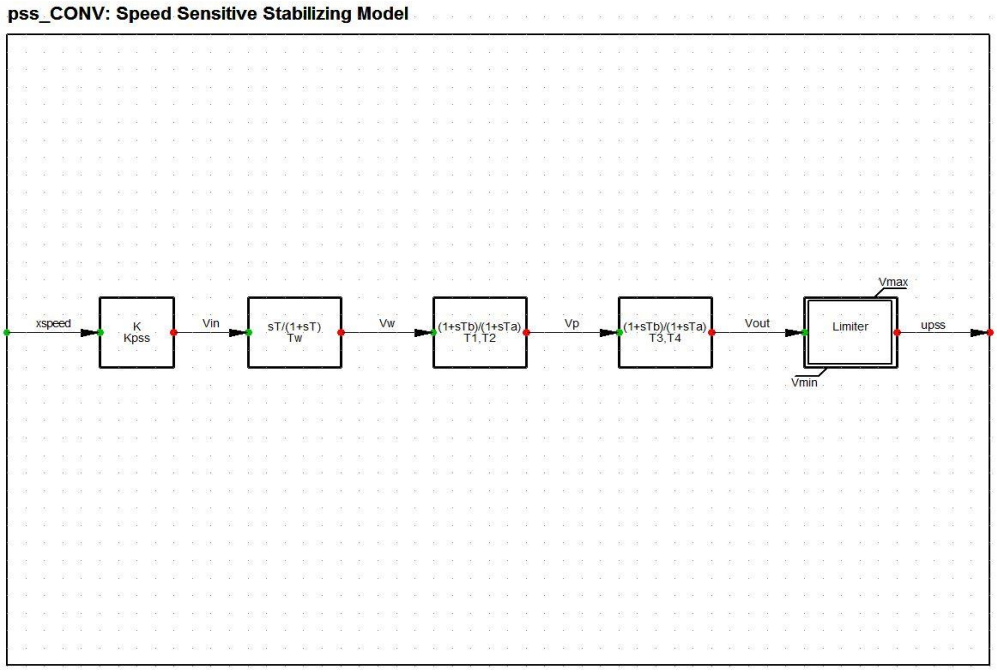

Figure 0.14: PSS_CONV – speed sensitive stabilizing model

- **DIgSILENT simulation language for PSS_CONV – speed sensitive stabilizing model**

inc(xw) =xspeed*Kpss

inc(x2) =0

inc(x3) =0

inc(upss) =0

vardef(Kpss) ='pu';'Stabilizer Gain'

vardef(Tw) ='s';'Washout integrate time constant'

vardef(T1) ='s';'First Lead/Lag derivative time constant'

vardef(T2) ='s';'First Lead/Lag delay time constant'

vardef(T3) ='s';'Second Lead/Lag derivative time constant'

vardef(T4) ='s';'Second Lead/Lag delay time constant'

vardef(Vmax) ='pu';'Signal pss maximum'

vardef(Vmin) ='pu';'Signal pss minimum'

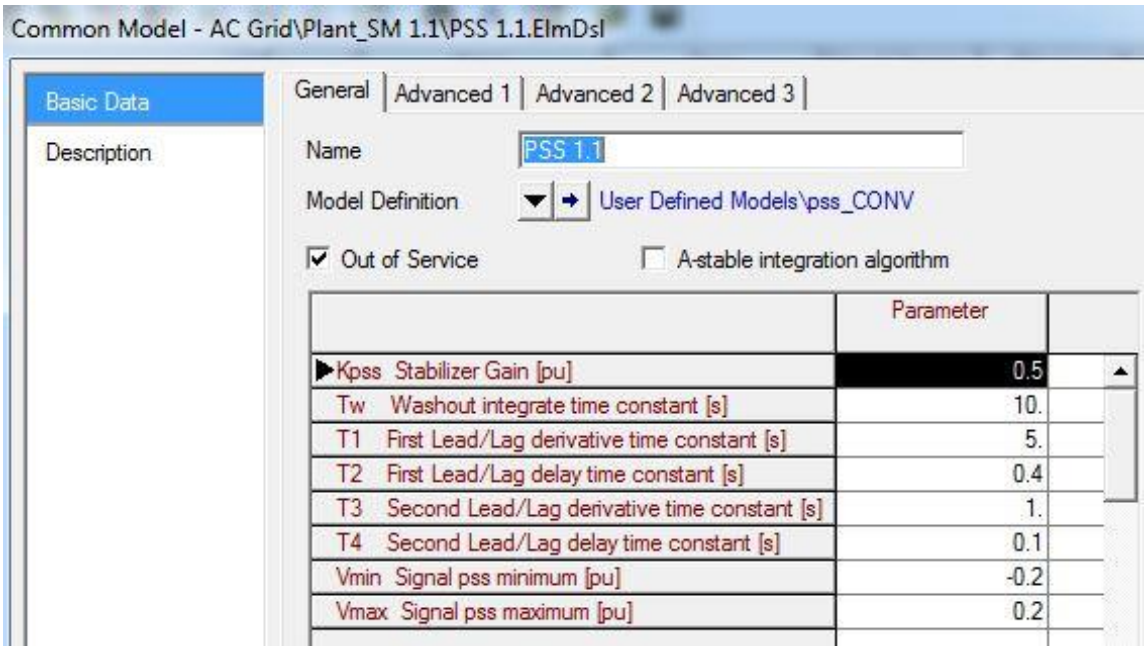

Figure 0.15: PSS_CONV – speed sensitive stabilizing model parameters

SYM Frame_no droop: Synchronous Machine Signal Interconnections

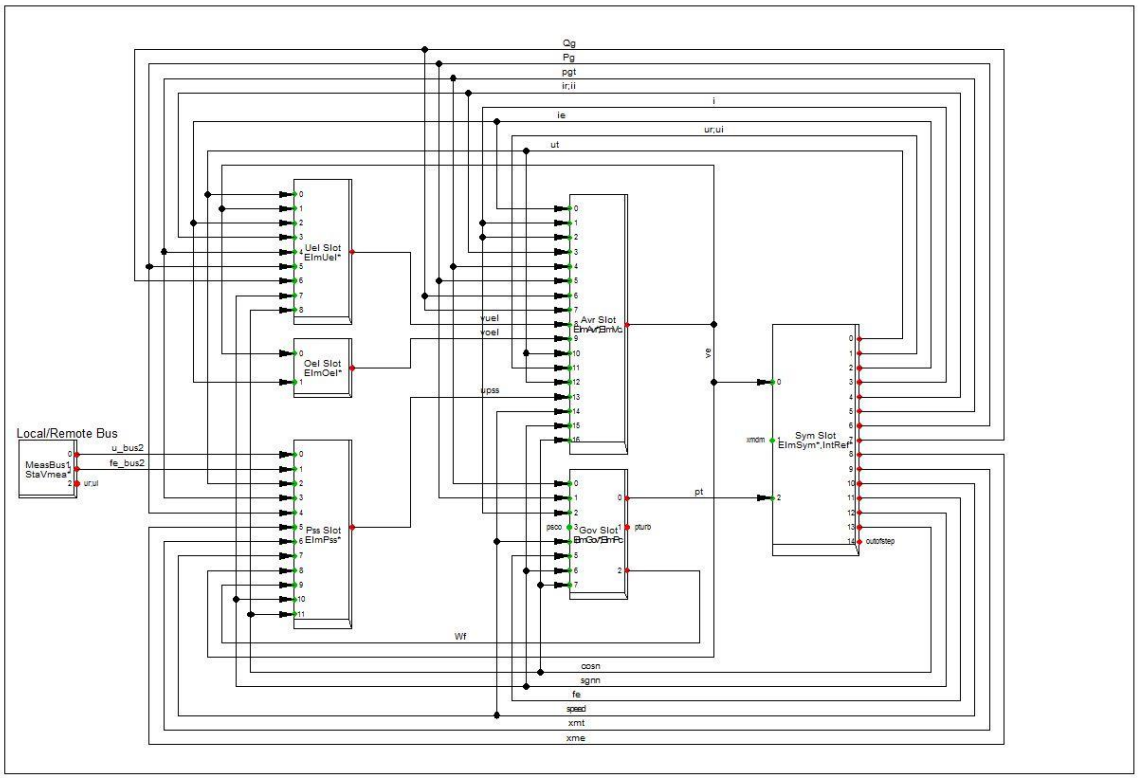

Figure 0.16: Synchronous machine signal interconnect on DIgSILENT

Table 0.15: Synchronous machine data

Machine Name	App. power MVA	Nom. V kV	power factor	P (MW)	Q Mvar	Vset p.u.	power factor
SM 1.1	850	20	0.9	700	5	1	0.9999744
SM 1.2	850	20	0.9	700.5651	0	0.99	1
SM 2	850	20	0.9	319.7674	0	1	1
SM 3	500	16.5	0.85	406.9767	0	1.03	1
SM 4.1	850	20	0.9	720.6294	5	1	0.9999759
SM 4.2	850	20	0.9	720.3079	0	1	1
SM 5	500	16.5	0.85	387.5969	0	1.01	1
SM 6	500	16.5	0.89	385.6589	5	1.01	0.999916

Table 0.16: Synchronous machine type

SM Type	H_Sgn (s)	xl p.u	xd p.u.	xq p.u.	Td' (s)	Tq' (s)	Td'' (s)	Tq'' (s)	xd' p.u.	xq' p.u.	xd'' p.u.	xq'' p.u.	x0 p.u
SM 1.1	3	0.3	2.2	2.2	2.1	0.28	0.02	0.008	0.6	0.8	0.4	0.4	0.1
SM 1.2	3	0.3	2.2	2.2	2.1	0.28	0.02	0.008	0.6	0.8	0.4	0.4	0.1
SM 2	3	0.3	2.2	2.2	2.1	0.28	0.02	0.008	0.6	0.8	0.4	0.4	0.1
SM 3	4	0.1	2	2	1	1	0.05	0.05	0.3	0.3	0.2	0.2	0.1
SM 4.1	3	0.3	2.2	2.2	2.1	0.28	0.02	0.008	0.6	0.8	0.4	0.4	0.1
SM 4.2	3	0.3	2.2	2.2	2.1	0.28	0.02	0.008	0.6	0.8	0.4	0.4	0.1
SM 5	4	0.1	2	2	1	1	0.05	0.05	0.3	0.3	0.2	0.2	0.1
SM 6	4	0.15	1.3	2	1	1	0.05	0.05	0.3	0.3	0.2	0.2	0.18

Table 0.17: Transformer parameters

Transformer Name	MVA Rating	LV kV	HV kV	shc volt (%)	x1 (p.u.)	x0 (p.u.)	vector group	uk (%)
Trxfrm 1.1	850	400	20	14.44	0.1444	0.1444	YNd1	14.44
Trxfrm 1.2	850	400	20	14.44	0.1444	0.1444	YNd1	14.44
Trxfrm 11_15	400	400	11	12.6	0.126	0.126	YNd1	12.6
Trxfrm 13_18	400	400	11	12.6	0.126	0.126	YNd1	12.6
Trxfrm 13_19	400	400	132	11.82	0.1182	0.1182	YNyn0	11.82
Trxfrm 2	850	400	20	14.44	0.1444	0.1444	YNd1	14.44
Trxfrm 21_22	850	400	20	14.44	0.1444	0.1444	YNd1	14.44
Trxfrm 3	600	400	16.5	14.88	0.1488	0.1488	YNd1	14.88
Trxfrm 4.1	850	400	20	14.44	0.1444	0.1444	YNd1	14.44
Trxfrm 4.2	850	400	20	14.44	0.1444	0.1444	YNd1	14.44
Trxfrm 5	600	400	16.5	14.88	0.1488	0.1488	YNd1	14.88
Trxfrm 6	600	400	16.5	14.88	0.1488	0.1488	YNd1	14.88

Table 0.18: Transformer tap changers parameter

Transformer Name	tap changers					
	tap side	add. Volt/tap	phase of du (deg)	neutral tap	min tap	max tap
Trxfrm 1.1	HV	1.25	180	0	-5	5
Trxfrm 1.2	HV	1.25	180	0	-5	5
Trxfrm 11_15	HV	1.25	180	0	-5	5
Trxfrm 13_18	HV	1.25	180	0	-5	5
Trxfrm 13_19	HV	1.1	180	0	-3	3
Trxfrm 2	HV	1.25	180	0	-5	5
Trxfrm 21_22	HV	1.25	180	0	-5	5
Trxfrm 3	HV	1.1	180	0	-4	4
Trxfrm 4.1	HV	1.25	180	0	-5	5
Trxfrm 4.2	HV	1.25	180	0	-5	5
Trxfrm 5	HV	1.1	180	0	-4	4
Trxfrm 6	HV	1.1	180	0	-4	4

APP 3: Eskom Eastern Grid Generator Data

Table 0.19: Generator Data for Eskom Eastern grid

Gen Name	Act. Power MW	Reactive Power Mvar	App Power MVA	App Power Rated	Power factor
Avon Gen1	100	0	100	186	1
Avon Gen2	110	0	110	186	1
Avon Gen3	100	0	100	186	1
Avon Gen4	120	0	120	186	1
Drakensberg Gen1	220	0	220	280	1
Drakensberg Gen2	220	0	220	280	1
Drakensberg Gen3	220	0	220	280	1
Drakensberg Gen4	220	0	220	280	1
Ingula Gen1	80	26.29475	84.21053	373.2	0.9499999
Ingula Gen2	80	26.29475	84.21053	373.2	0.9499999
Ingula Gen3	80	26.29475	84.21053	373.2	0.9499999
Ingula Gen4	80	26.29475	84.21053	373.2	0.9499999
Majuba Gen1	400	0	400	739	1
Majuba Gen2	400	0	400	739	1
Majuba Gen3	400	0	400	739	1
Majuba Gen4	0	0	0	739	0
Majuba Gen5	400	0	400	739	1
Majuba Gen6	400	0	400	739	1
Southwest Gen	120	0	120	373.2	1
Tutuka Gen1	420	0	420	666	1
Tutuka Gen2	420	0	420	666	1
Tutuka Gen3	420	0	420	666	1
Tutuka Gen4	420	0	420	666	1
Tutuka Gen5	420	0	420	666	1
Tutuka Gen6	420	0	420	666	1

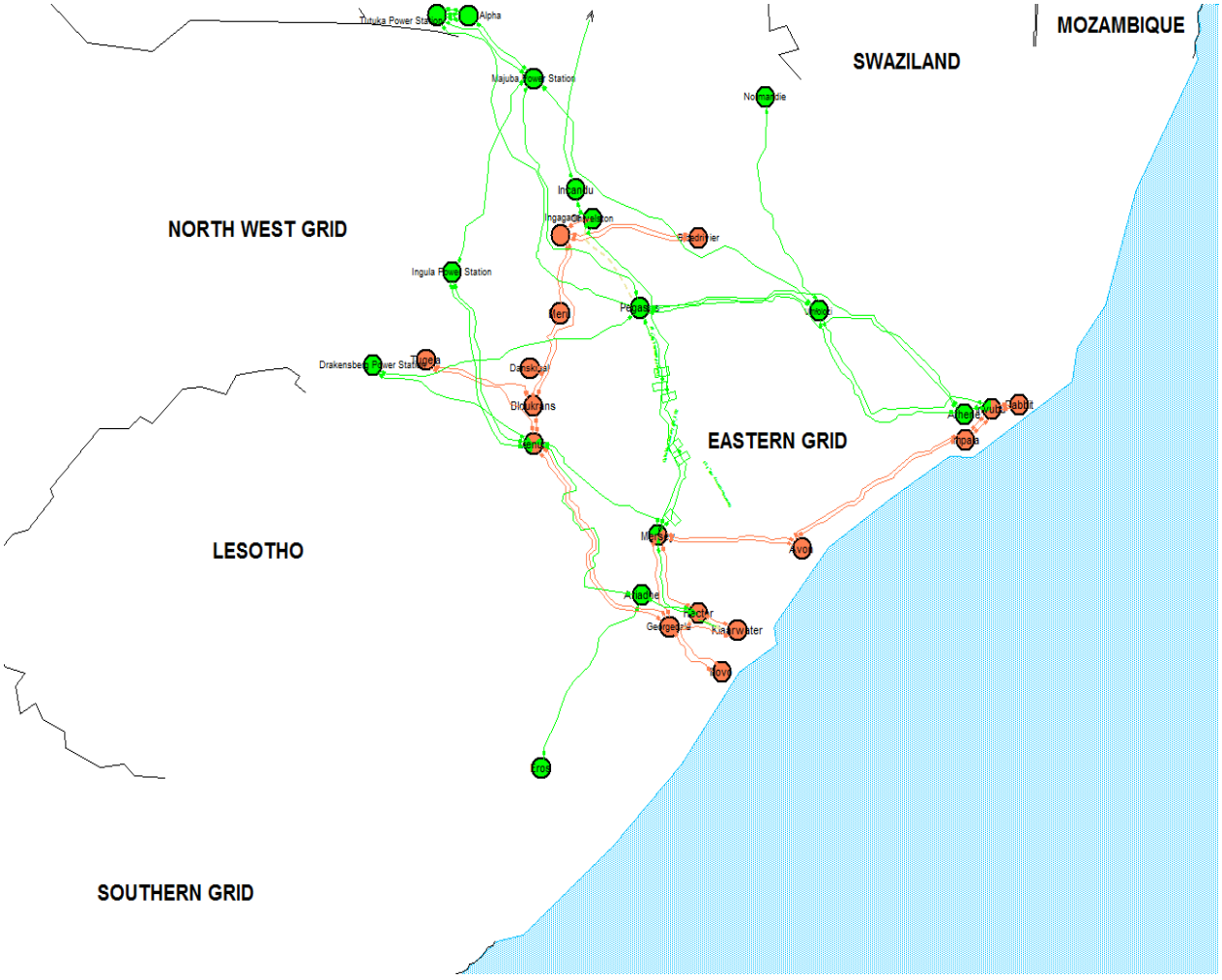

Figure 0.17: Eastern grid overview diagram